Title	Burst-mode electronic dispersion compensation in long reach PONs
Authors	Porto, Stefano
Publication date	2014
Original Citation	Porto, S. 2014. Burst-mode electronic dispersion compensation in long reach PONs. PhD Thesis, University College Cork.
Type of publication	Doctoral thesis
Rights	© 2014, Stefano Porto. - http://creativecommons.org/licenses/by-nc-nd/3.0/
Download date	2025-08-18 08:03:43
Item downloaded from	https://hdl.handle.net/10468/2035

Burst-Mode Electronic Dispersion Compensation in Long Reach PONs

by

Stefano Porto

A Thesis Submitted to
The National University of Ireland, Cork
for the degree of

Doctor of Philosophy (Ph.D.)

Photonics Systems Group, Tyndall National Institute
Department of Electrical and Electronic Engineering
National University of Ireland
Ireland

University College Cork, Ireland
Coláiste na hOllscoile Corcaigh

September 2014

Research Supervisor: Prof. Paul D. Townsend
Research Co-Supervisor: Dr. Peter Ossieur
Head of the Department: Prof. Nabeel Riza

Acknowledgements

There are a number of exceptional people who have supported me throughout this exciting, rewarding, and at times difficult journey. I would like to express my deepest and sincere gratitude to all of them for making this PhD work possible.

First and foremost, I would like to thank my supervisor Prof. Paul Townsend for giving me the very unique opportunity of joining the Photonic Systems Group at Tyndall. In spite of his very busy schedule, he was always there to listen and to provide me with advice and technical guidance.

I would also like to thank my co-supervisor Dr. Peter Ossieur for his invaluable contribution to this work, continuous support, and for giving me the chance to experiment with his state-of-the-art technologies.

Furthermore, I am very grateful to Dr. Cleitus Antony. Under his day-to-day guidance and constructive criticism I did not only focus on the technical aspects of my research topic but on research methodology in general.

I am also indebted to Dr. Giuseppe Talli, whose support and advice at all times helped me in resolving many practical problems.

I cannot forget to mention all the present and former members of the access group, in particular Alan Naughton, Daniel Carey, Caroline Lai, Daniel Brunina and Denis Kelly for all their valuable contribution to some setups, for the useful discussions, or simply for the help offered when required. Special thanks must be extended also to other members of the Photonic Systems Group, in particular to Bob Manning, Rod Webb, and Fatima Gunning for the enjoyable discussions and for sharing lab equipment when necessary as well as valuable notes and lecture material. Thanks also to Martina Connolly for promptly dealing with administrative matters and for always helping out when needed.

Moreover, I am grateful to Marc Rensing and Nicola Pavarelli from the Photonics Packaging Group for the invaluable help provided with the assembly and packaging of the LBMRx.

Of course this journey was not only about science and I cannot forget to thank all the people with whom I spent most of my enjoyable time inside and outside work. Moving to another country is not easy when you have to leave behind your family and friends. A number of people, however, have made this process much easier. Among all, I would like to thank Alan, Nicola and Dave in particular for the great time spent together. Thanks also to BK, Caroline, Cleitus, Cristian, Dan, Daniel, DW, Giuseppe, Kasia, Liam, Mark, Naoise, Peter, Shane, Steve and many more for making my time in Tyndall very enjoyable. In general, my sincere thanks go to all the 'Irish lads' I have met over the last number of years, as they always made me feel welcome and well integrated.

On a personal note, I would like to express my deep gratitude to my parents for the inspiring education they provided me, for the many sacrifices they have made for me over the years, for their constant love, support, and encouragement to pursue my dreams. Thanks also to my sister and to the rest of my family. Even though I am far away from home, I could always rely on them and on their support.

Finally, a special thanks goes to my girlfriend and life companion Anna who has been the most important and valuable source of support. I want to thank Anna for sharing this adventure with me and for the unconditional love, patience and understanding for which I will always be indebted.

Stefano Porto
Cork, July 18th, 2014.

Abstract

Long reach passive optical networks (LR-PONs), which integrate fibre-to-the-home with metro networks, have been the subject of intensive research in recent years and are considered one of the most promising candidates for the next generation of optical access networks. Such systems ideally have reaches greater than 100km and bit rates of at least 10Gb/s per wavelength in the downstream and upstream directions. Due to the limited equipment sharing that is possible in access networks, the laser transmitters in the terminal units, which are usually the most expensive components, must be as cheap as possible. However, the requirement for low cost is generally incompatible with the need for a transmitter chirp characteristic that is optimised for such long reaches at 10Gb/s, and hence dispersion compensation is required.

In this thesis electronic dispersion compensation (EDC) techniques are employed to increase the chromatic dispersion tolerance and to enhance the system performance at the expense of moderate additional implementation complexity. In order to use such EDC in LR-PON architectures, a number of challenges associated with the burst-mode nature of the upstream link need to be overcome. In particular, the EDC must be made adaptive from one burst to the next (burst-mode EDC, or BM-EDC) in time scales on the order of tens to hundreds of nanoseconds.

Burst-mode operation of EDC has received little attention to date. The main objective of this thesis is to demonstrate the feasibility of such a concept and to identify the key BM-EDC design parameters required for applications in a 10Gb/s burst-mode link. This is achieved through a combination of simulations and transmission experiments utilising off-line data processing. The research shows that burst-to-burst adaptation can in principle be implemented efficiently, opening the possibility of low overhead, adaptive EDC-enabled burst-mode systems.

Statement of Originality

I hereby certify that I am the sole author of this thesis. Except where indicated, all the work presented in this thesis is solely attributed to the author. The author participated in the design and implementation of all experiments except where explicitly stated. Precise details of collaborators may be ascertained from the list of co-authors in the List of Publications.

I certify that, to the best of my knowledge, my thesis does not infringe upon anyone's copyright nor violate any proprietary rights and that any ideas, techniques, quotations, or any other material from the work of other people included in my thesis, published or otherwise, are fully acknowledged in accordance with the standard referencing practices.

I declare that this is a true copy of my thesis and has not been submitted for another degree to any other University or Institution.

Contents

Contents

Chapter 1

Introduction

The application of optical fibres in the field of telecommunications was made possible in the early 1970s thanks to the progress in silica fibre-optic production technologies along with the development of compact and more efficient semiconductor laser diodes. Since then, the use of and demand for optical fibre have grown tremendously, and some view this as the beginning of the 'information age' comparing today's social revolution of information accessibility to last century's industrial revolution, in terms of scope and impact [1]. While 20 years ago people around the world could communicate in real-time only through the phone, today it is possible to transmit voice, data, and video at the speed of light along a strand of glass thinner than a human hair. Optical fibre technology rapidly enabled a fast and reliable delivery of the services upon which all people depend in today's world. Indeed, everyone expects to be seamlessly, instantly, and continuously connected to the network using a myriad of devices such as smart phones, computers, hand-held devices, high definition TV, game systems, GPS, e-book readers, and others. If today's generation had to be described using one word, that word would be 'connected'. None of this would be possible without optical fibre. Currently more than 1.8 billion kilometres of optical fibre is deployed around the world [1], connecting people, businesses, communities, countries, and continents.

While today's core and metro networks (hence the majority of the Internet's physical distance) are dominated by optical fibre, the access network is still mostly based on copper or wireless technologies. To keep up with increasing bandwidth demands, however, telecoms operators are gradually migrating to fibre-based networks, which promise to deliver significantly higher speeds. The actual level of

penetration of fibre in the access network varies between countries. Figure 1.1 shows the data collected by the Organisation for Economic Co-operation and Development (OECD) for the number of fibre connections as a percentage of total broadband connections among OECD countries reporting fibre subscribers as of June 2013 [2].
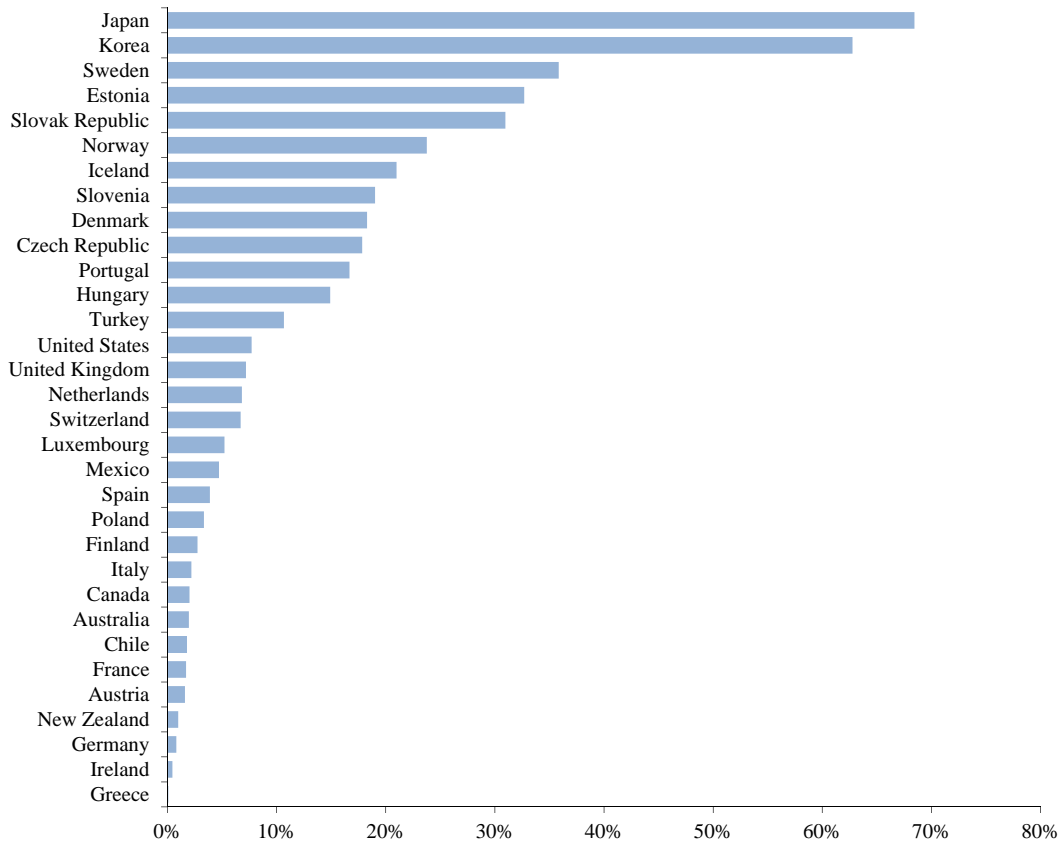
Figure 1.1: Percentage of fibre connections in total broadband subscriptions (June 2013).

The reason why the percentage of fibre connections in most of the countries reported in Fig. 1.1 is still relatively modest is due to the fact that migration to an all-fibre network infrastructure requires major investment and takes considerable time to complete. In fact, in some countries there is still a lack of applications to take full advantage of the high bandwidth offered by the fibre and as a consequence there is limited near or medium term demand for high-speed residential services to justify such investments in new technology. This pushed most operators to opt against providing immediate fibre-to-the-home (FTTH) or fibre-to-the-building (FTTB) solutions and opting, instead, for an incremen-

tal network upgrade to maximally reuse the already existing infrastructures. In the short term, therefore, access to high-speed broadband services will still be provided by copper-based solutions [3]. However, looking at the trend in Fig. 1.1 of countries like Japan and Korea where FTTH/B is already the leading access technology [4], it is clear that fibre-optic access infrastructure is no longer a matter of if, but when. Indeed, copper-based and wireless technologies will not be able to support the continuously growing demand for higher bit-rates due to physical media constraints which eventually limit the performance either in terms of bandwidth or physical reach.

1.1 Context of the Study

The most promising and high-performance architecture to drive FTTH is arguably the passive optical network (PON). A PON is a point-to-multipoint fibre network architecture in which optical splitters are used to enable a single optical fibre to serve multiple users. The term passive derives from the fact that in a conventional PON there are no powered components deployed in the field. Although PONs are undeniably cost-effective architectures thanks to their ability to share network costs among a number of customers, the cost reduction offered by PONs alone is still not enough to guarantee the margins and hence the profitability expected by operators [5]. This is mainly due to the high cost of optical components along with the fact that conventional metro/core networks are built upon a large base of power-hungry (thus expensive) electronic equipment. This means that, in order to further reduce costs, metro and core networks will also need upgrading.

One potential solution in order to address this problem is to simplify the current network architecture. This could be achieved, for instance, by combining the access and metro networks into a single, integrated, all-optical system by using optical amplification. The concept of increasing the reach and/or split of a PON via intermediate equipment is known as long-reach PON (LR-PON). LR-PONs are a very cost-effective solution as the CAPEX and the OPEX of the network are lower mainly due to the fact that the number of equipment interfaces, network elements, and nodes are reduced, and moreover, the network management complexity is also simplified [6]. In conventional PON architectures such as Ethernet PON (E-PON) from IEEE [7] and the Gigabit PON (G-PON)

from ITU-T [8], the maximum logical reach can typically be increased from 20km up to 60km by using an intermediate reach-extender. However, for more advanced network architectures [9, 10, 11] this target reach can be increased significantly up to 100km or beyond. Note that another objective of such next generation access networks is to achieve bit rates of at least 10Gb/s per wavelength in the downstream and upstream directions [12].

It is clear that with increasing bit rates, reaches, and more generally with increasing complexity of the optical layer, signal distortions are also increasing, whereas the component and system tolerances are typically decreasing. In particular, for the single channel applications that this thesis is focusing on, chromatic dispersion (CD) can pose severe limitations to the system performance. Considering also that the low cost transmitter targeted for use in each optical network unit (ONU) might not have a chirp characteristic that is optimised for such reaches at 10Gb/s, some sort of dispersion compensation is required. Multiple techniques have been proposed and implemented both in the electrical and optical domain in order to compensate/mitigate for CD [13]. Among these, for example, the system impact of CD could be reduced by means of dispersion compensating fibres (DCFs) or dispersion compensating gratings (DCGs) in the optical domain, or else by means of linear/quasi-linear equalisers, Volterra equalisers, or maximum-likelihood sequence estimation (MLSE) equalisers in the electrical domain.

The main advantage offered by optical compensators over electronic techniques is that they operate prior to square-law photodetection, and can therefore make use of the full optical field information (amplitude and phase) rather than of the optical intensity only, resulting in significantly better performance. However, these methods are relatively expensive and moreover they are typically static in nature and hence they cannot respond to time-dependent variations of the signal impairments. On the other hand, electronic equalisers can be much cheaper once they have entered large volume production and, in principle, they could also be made adaptive. Therefore, the advantages offered by these techniques over optical compensators can justify the loss in performance associated with direct detection and the loss of phase information.

In this thesis work a subset of the aforesaid electronic equalisation techniques, namely feedforward equalisers (FFEs) and decision feedback equalisers (DFEs), is studied to demonstrate that their use in next generation PONs can efficiently mitigate the effect of CD as well as other types of impairments.

1.2 Objectives and Overview of the Thesis

In conventional PON systems all the users time-share the same wavelength and fibre infrastructure. While in the downstream direction transmitters and receivers operate in continuous-mode as data packets (referred to as bursts) are broadcast to all ONUs, in the upstream direction only one burst from a single ONU can be transmitted at a given time in order to avoid collision. This type of communication is known as burst-mode transmission. The fundamental difference between burst-mode and conventional continuous-mode transmission is that even if all bursts are launched from each ONU at the same average optical power, each will experience a different amount of fibre and number of splitters enroute to the OLT and hence will arrive with varying power levels depending on the individual path loss. Recently, there has been increasing interest in supporting larger differential reaches[1], as evident in latest updates to the ITU-T GPON and XGPON standards which now support a 40km differential reach rather than the conventional 20km [14]. As a consequence, the burst-to-burst amplitude variation in the upstream signal can be greater than 20dB ($\times 100$) [15, 16]. Furthermore, due to such differential reaches, consecutive bursts may undergo different amounts of dispersion. This means that if an equaliser is employed to mitigate the effect of dispersion, it must also be adaptive on a burst-by-burst basis. While a number of adaptive electronic equalisers are already commercially available, they are typically characterised by slow adaptation rates (in the order of seconds or even minutes [13]). This is clearly unacceptable for the LR-PONs applications of interest in this work, where adaptation should be achieved in the order of tens or hundreds of nanoseconds to support PON time sharing protocols. It is clear that a number of major challenges posed by the next generation PONs arise from the requirement for high speed ($\geq$10Gb/s) technologies which must operate in burst-mode. These involve burst-mode transmitters/receivers, burst-mode optical amplifiers, and ultimately the burst-mode electronic equalisers that this thesis is focusing on.

Indeed, the main objective of this thesis is to demonstrate the feasibility of a burst-mode electronic dispersion compensator (BM-EDC) based on FFE/DFE structures, and to obtain its main design parameters through simulations as well

---

[1]The difference between the maximum and minimum fibre length of the ONUs to the central office.

as off-line processing of lab-data obtained from an emulated 10Gb/s burst-mode link. Note that the hardware implementation of an EDC chip requires that the amplitude of the incoming signal remains constant with time and also that the pulse shapes are preserved, which in a continuous mode link is achieved using a linear variable gain amplifier [17]. In a burst-mode link, a linear burst-mode receiver (LBMRx) is then required, which amplifies linearly the incoming packets such that they all have the same amplitude. Our group at Tyndall National Institute recently developed the first receiver of this type [18]. Therefore, another key aspect of this thesis is the study and characterisation of this state of the art 10Gb/s LBMRx that would accompany the BM-EDC. This involves the development of novel characterisation techniques and test-beds, as the conventional continuous-mode methods alone cannot be fully applied. All the work described in this thesis was carried out within the Photonics Systems Group, Tyndall National Institute and Department of Physics/Electrical and Electronic Engineering, University College Cork, Cork, Ireland. This activity was funded by Science Foundation Ireland (SFI) under grants 06/IN/I969, 10/CE/I1853 and 12/IA/1270, the European Commission Seventh Framework Programme for Research (FP7) project DISCUS, and Enterprise Ireland under grant CF2011 1009.

Outline of the thesis and key results:

This thesis presents a study of electronic equalisation for 10Gb/s direct-detection LR-PONs. In particular, the fundamental limitations due to chromatic dispersion and their practical impact on the equaliser design are explored. The main achievements are in overcoming all the physical layer challenges associated with the burst-mode nature of the transmission in these network architectures. This work has resulted in a number of papers published in renowned journals and international conferences (see List of Publications for details). Note however that the thesis mainly focuses on research described in eight of the published papers, which is reproduced here together with addition information and analysis. This document is organised as follows.

The context and objectives of this work, along with some of the key challenges to be addressed, have been discussed in Chapter 1.

In Chapter 2 the physical background of fibre-optic based transmission systems is briefly presented. The fundamental impairments that affect such systems have been taken into account, with particular focus on chromatic dispersion.

The noise mechanisms used to stress the system under test, along with the performance evaluation methods used in this work are also discussed in detail.

Chapter 3 reviews the state-of-the-art technologies in optical access, focusing on the PON architectures that are believed to be the most promising candidates for the mass market. In order to achieve long-reaches, optical amplification cannot be avoided, and must be employed at the local exchange as well as in the metro/core node. Several technology options are discussed, and a novel potential solution for a semiconductor optical amplifier (SOA) based reach-extender is presented and analysed experimentally in detail. This study resulted in two publications ([C1] and [J3], see List of Publications).

Chapter 4 provides a review of linear and quasi-linear electronic adaptive equalisers (with adaptation based upon the least mean squares, or LMS, algorithm). For the first time, to the best of our knowledge, the analysis of these equalisers is extended specifically with a view to optimisation for applications in LR-PONs. Indeed, a detailed characterisation of the FFE and DFE (simulated) performance is presented in order to understand how such electronic equalisation techniques can be used to mitigate the intersymbol interference due to chromatic dispersion, and to extract a number of key design parameters such as optimum number of taps, tap delay, step-size, training length, etc., to mention a few.

In Chapter 5, the performance of the FFE/DFE architectures used to compensate for chromatic dispersion is discussed when other degrading effects, such as non-optimal transmitter and receiver bandwidths or the presence of patterning introduced by a saturated SOA, are also involved. A detailed numerical analysis is carried out in order to determine whether the same equaliser can also mitigate for such effects without losing its effectiveness in compensating chromatic dispersion. This chapter also investigates whether the FFE/DFE exhibits a loss in performance when used in beat noise limited systems rather than thermal noise limited systems (or vice-versa). The impact of such different noise mechanisms on the equaliser design are taken into account, with focus on the optimisation of the DFE slicing-threshold.

Chapter 6 can be divided into two main parts. The first one presents a detailed characterisation of the world's first 10Gb/s LBMRx employed to enable the use of a BM-EDC module. The processes followed in order to assemble and package this prototype device are also illustrated. In the second part, the findings obtained from the simulations presented in Chapters 4 and 5 are verified

using transmission experiments and offline processing in an emulated (lab-based) 10Gb/s LR-PON upstream link. The requirements on the BM-EDC in terms of adaptation speed are also derived. To the best of our knowledge, this work led to the first demonstration of 10Gb/s burst-mode transmission using a LBMRx and a BM-EDC (emulated using offline processing). The findings obtained from the work presented in Chapters 4, 5, and 6 resulted in three high impact conference publications ([C7], [C8], and [C9] in List of Publications) and a journal publication (invited , [J7] in List of Publications). All the work related to the characterisation and test of the LBMRx chip contributed to a number of publications, among which a conference paper (post-deadline paper, [C2] in List of Publications) and a journal paper ([J2] in List of Publications).

Finally, Chapter 7 concludes the thesis with a brief summary of all important achievements and some suggestions for potential future work in this area.

Chapter 2

Transmission Impairments and Performance Measurements in Fibre Optic Systems

In general, the impairments in fibre optic systems can be classified into three categories: linear distortions, nonlinear effects, and noise. These three categories of impairments can accumulate along the fibre and can influence each other. The interaction between these phenomena may lead to deterministic as well as stochastic impairments. The major linear effects include fibre loss, group velocity dispersion (GVD), polarisation mode dispersion (PMD), adjacent channel crosstalk, and filter-induced distortion. The main nonlinear effects, on the other hand, include self-phase modulation (SPM), cross phase modulation (XPM), four-wave mixing (FWM), stimulated Brillouin scattering (SBS), and stimulated Raman scattering (SRS). In Section 2.1 each of these linear and nonlinear impairments is briefly discussed.

Optical amplifiers can be used in order to compensate for the fibre propagation losses in long distance links and branching losses in access networks avoiding costly optical-electrical-optical (OEO) regeneration. Some general concepts common to all optical amplifiers, such as gain saturation and signal degradation due to amplifier noise, are described in Section 2.2.

Section 2.3 deals with various noise sources that limit the signal-to-noise ratio in optical receivers, with focus on thermal noise, shot noise, and beat noise.

Finally, Section 2.4 is devoted to the system performance evaluation methods

used in this thesis. The difference in behaviour of a thermal noise limited system when compared to a beat noise limited system is also discussed.

2.1 Fibre Impairments

The optical fibre is often seen as a perfect transmission medium with almost limitless bandwidth, but in practice the propagation through the fibre is affected by several limitations, in particular for high bit-rates and when the transmission distance is increased as in multi-span amplified systems. Indeed, when short optical pulses propagate through a fibre, both dispersive and nonlinear effects influence their shape and spectra. In order to better understand these phenomena, it is necessary to consider the theory of electromagnetic wave propagation in dispersive nonlinear media and examine the wave equation that describes light propagation in optical fibres. After making several simplifying approximations [19], it is possible to obtain the propagation equation of short optical pulses in single mode fibres as a function of the mode propagation constant $\beta(\omega)$, which determines how the phase of a pulse of light at a given frequency varies along the propagation direction. First, in order to simplify the mathematical treatment, it is useful to expand $\beta(\omega)$ in a Taylor series around the carrier frequency ω_0 at which the pulse spectrum is centred:

$$\beta(\omega) = n(\omega)\frac{\omega}{c} = \beta_0 + (\omega - \omega_0)\beta_1 + \frac{1}{2}(\omega - \omega_0)^2\beta_2 + \frac{1}{6}(\omega - \omega_0)^3\beta_3 + ..., \quad (2.1.1)$$

where $n(\omega)$ is the refractive index, and $\beta_m = (d^m\beta/d\omega^m)_{\omega=\omega_0}$. Note that such an expansion in a Taylor series is a valid approximation as there is only interest in relatively small deviations around the carrier frequency (slowly varying envelope approximation [20]). Equation (2.1.1) represents the local variation of the mode-propagation constant due to the fibre and the β coefficients are defined as follows:

$$\beta_0 \equiv \beta(\omega)\big|_{\omega=\omega_0} = n(\omega_0)\frac{\omega_0}{c} = \frac{\omega_0}{\nu_p(\omega_0)} \equiv \frac{\omega_0}{\text{phase velocity}}, \quad\quad (2.1.2a)$$

$$\begin{aligned} \beta_1 \equiv \frac{d\beta}{d\omega}\bigg|_{\omega=\omega_0} &= \frac{1}{c}\left(n(\omega) + \omega\frac{dn(\omega)}{d\omega}\right)\bigg|_{\omega=\omega_0} \\ &= \frac{n_g(\omega)}{c}\bigg|_{\omega=\omega_0} = \frac{1}{\nu_g(\omega_0)} \equiv \frac{1}{\text{group velocity}}, \end{aligned} \quad (2.1.2b)$$

$$\beta_2 \equiv \left.\frac{d^2\beta}{d\omega^2}\right|_{\omega=\omega_0} = \frac{1}{c}\left.\left(2\frac{dn(\omega)}{d\omega} + \omega\frac{d^2n(\omega)}{d\omega^2}\right)\right|_{\omega=\omega_0}$$

$$= \left.\frac{d}{d\omega}\left(\frac{1}{\nu_g(\omega)}\right)\right|_{\omega=\omega_0} \equiv GVD, \tag{2.1.2c}$$

$$\beta_3 \equiv \left.\frac{d^3\beta}{d\omega^3}\right|_{\omega=\omega_0} = \frac{1}{c}\left.\left(3\frac{d^2n(\omega)}{d\omega^2} + \omega\frac{d^3n(\omega)}{d\omega^3}\right)\right|_{\omega=\omega_0} \equiv TOD, \tag{2.1.2d}$$

where the quantity $n_g(\omega)$ in Eq. (2.1.2b) is called the group index. The first term in Eq. (2.1.1) is related to the carrier phase velocity ν_p as shown in Eq. (2.1.2a) and it adds a constant phase shift that has no effect on the shape of the pulse [21]. The physical meaning of the group velocity dispersion (GVD) and the third order dispersion (TOD) used in Eqs. (2.1.2c) and (2.1.2d) is discussed in the remainder of this section.

If the input electric field is assumed to propagate in the z-direction, under the aforesaid assumptions and after introducing the slowly varying amplitude $A(z,t)$ of the pulse envelope (simply called A from now on for clarity), the basic propagation equation that governs the evolution of a pulse inside a single-mode fibre can be written as [19]:

$$\frac{\partial A}{\partial z} = -\frac{\alpha}{2}A - \frac{i\beta_2}{2}\frac{\partial^2 A}{\partial T^2} + \frac{\beta_3}{6}\frac{\partial^3 A}{\partial T^3} + i\gamma\left|A\right|^2 A, \tag{2.1.3}$$

$\swarrow$	$\downarrow$	$\downarrow$	$\searrow$
linear attenuation	*second order dispersion*	*third order dispersion*	*Kerr effect*

where a frame of reference moving with the pulse at the group velocity ν_g is used by making the transformation

$$T = t - \frac{z}{\nu_g} \equiv t - \beta_1 z. \tag{2.1.4}$$

The reason for this transformation can be explained by noting that in the second term of Eq. (2.1.1) it is possible to observe a linear phase ramp in frequency which corresponds, through the Fourier shift theorem, to a delay of the pulse in time [21] that does not affect its shape.

The quantity α in Eq. (2.1.3) is the fibre attenuation parameter [1/km], β_2 is the second order propagation constant defined in Eq. (2.1.2c) [ps^2/km], β_3 is the third order propagation constant defined in Eq. (2.1.2d) [ps^3/km], and γ is the

Kerr nonlinear parameter $[\text{km}^{-1} \cdot \text{W}^{-1}]$ defined as

$$\gamma(\omega_0) = \frac{n_2(\omega_0) \cdot \omega_0}{c \cdot A_{eff}}, \qquad (2.1.5)$$

where n_2 is the nonlinear refractive index and A_{eff} is known as the effective mode area and depends on fibre parameters such as the core radius and the core-cladding index difference. The pulse amplitude A in Eq. (2.1.3) is assumed to be normalised such that $|A|^2$ represents the optical power, thus if n_2 is expressed in units of $[\text{m}^2/\text{W}]$ the quantity $\gamma |A|^2$ is then measured in $[\text{m}^{-1}]$.

In general, the cubic and higher order terms in the Eq. (2.1.1) are negligible in the case of quasi-monochromatic light, that is if the spectral width $\Delta\omega = (\omega - \omega_0)$ of the pulse satisfies the condition $\Delta\omega \ll \omega_0$ [1]. Therefore, as long as the carrier wavelength is not in the proximity of the zero-dispersion region, Eq. (2.1.3) can be further simplified to

$$\frac{\partial A}{\partial z} = \left[i\gamma|A|^2 - \left(\frac{i\beta_2}{2} \frac{\partial^2}{\partial T^2} + \frac{\alpha}{2} \right) \right] A = (\mathbf{N} + \mathbf{L})A, \qquad (2.1.6)$$

where $\mathbf{N}$ and $\mathbf{L}$ are respectively the nonlinear and linear operators defined as

$$\mathbf{N} = i\gamma|A|^2, \qquad (2.1.7\text{a})$$

$$\mathbf{L} = -\frac{i\beta_2}{2} \frac{\partial^2}{\partial T^2} - \frac{\alpha}{2}. \qquad (2.1.7\text{b})$$

Eq. (2.1.6) is the simplest nonlinear equation for studying third order nonlinear effects in optical fibres and when $\alpha = 0$ it is referred to as the nonlinear Schrödinger equation (NLSE). Note that in order to study systems with higher-order nonlinear effects (e.g. systems characterised by high peak powers, ultra-short optical pulses, or that take into account inelastic scattering processes, etc.) Eq. (2.1.3) needs to be modified suitably to include their contribution. However, this remains beyond the scope of this thesis and is not further discussed[2].

---

[1]Note however that when the centre wavelength of an optical signal is near the zero-dispersion wavelength, as for broad spectrum signals, then the β_3 terms should be included.

[2]The reader can refer to [19] for a detailed description on the topic.

2.1.1   Linear Distortions

In this section the main fibre linear effects such as fibre loss, GVD, PMD, and adjacent channel crosstalk are briefly discussed.

Fibre propagation losses:

If the group velocity dispersion β_2 and the Kerr nonlinear parameter γ are neglected, the NLSE (Eq. (2.1.6)) can be simply rewritten as $\partial A/\partial z = -A \cdot \alpha/2$. This means that the complex envelope of the electric field at the output of an optical fibre of length $z = L$ is given by

$$A(L) = A(0) \cdot e^{-L \cdot \alpha/2}, \tag{2.1.8}$$

where $A(0)$ denotes the electrical field at the fibre input. From Eq. (2.1.8) it is clear that the optical power $P(L) = |A(L)|^2$ decreases exponentially as $e^{-L \cdot \alpha}$ with increasing distance. The attenuation coefficient α is often expressed in dB per unit length and is related to the linear scale coefficient by the following relationship:

$$\alpha_{dB} = -\frac{10}{L} \log \left[\frac{P(L)}{P(0)} \right] = 4.343 \cdot \alpha. \tag{2.1.9}$$

The attenuation in optical fibres can be caused by intrinsic factors like scattering and material absorption, and by extrinsic factors which include stress from the
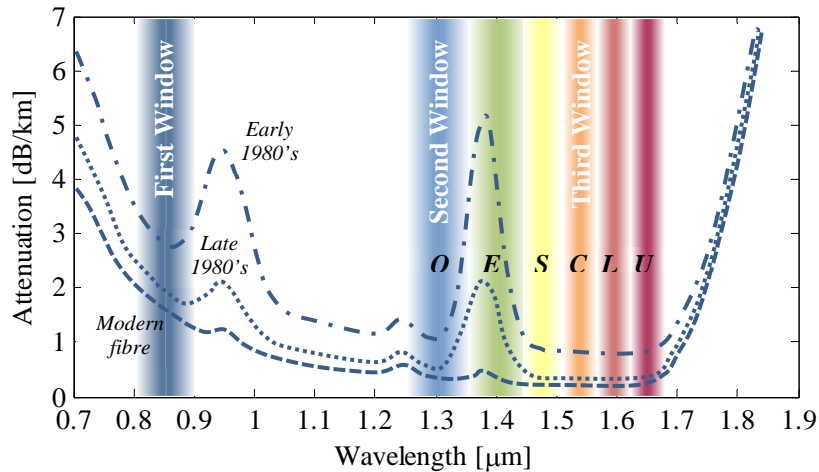

Figure 2.1: Fibre loss as a function of wavelength and operating bands.

manufacturing process, environmental and physical bending. Also, as one may expect, fibre losses depend on the wavelength: the attenuation spectrum for a few different silica single mode fibres developed over the years, along with the typical operating bands terminology, are shown in Fig. 2.1.

The wavelength range used in optical systems is defined in the ITU standard [22]: it spans from 1260nm to 1625nm and is divided into 6 bands, namely O, E, S, C, L, and U as illustrated in Fig. 2.1. Such operating bands are summarised in Table 2.1. The most of the experiments and simulations presented in this thesis employ the C-band, except for the ones presented in Chapter 3, which are performed in the O-band.

Band	Description	Range	Bandwidth
O - band	Original	1260-1360nm	100nm (17.5THz)
E - band	Extended	1360-1460nm	100nm (15.1THz)
S – band	Short wavelength	1460-1530nm	70nm (9.4THz)
C - band	Conventional	1530-1565nm	35nm (4.4THz)
L - band	Long wavelength	1565-1625nm	60nm (7.1THz)
U - band	Ultra long wavelength	1625-1675nm	50nm (5.5THz)

Table 2.1: Operating wavelength bands for single mode fibre optic communication.

Since bending losses can be minimised, the main contribution to fibre attenuation is given by material absorption and Rayleigh scattering. Material absorption consists of the intrinsic absorption of pure silica and extrinsic absorption of impurities or dopants. Pure fused silica has strong absorption in the ultraviolet (UV) and far-infrared (IR), but relatively low intrinsic absorption in the telecom windows. The absorption peaks seen near the telecom wavelengths at approximately 0.95-, 1.24-, and 1.39μm are due to the OH ion, which are present due to unavoidable water vapour in the fabrication process. Rayleigh scattering, instead, results from microscopic fluctuations in material density as a result of the rapid cooling of the glass during the final stage of the fabrication process. These structural variations manifest themselves as refractive index variations on a scale much smaller than the optical wavelength. In the region 800-1600nm, and hence in the wavelength operating bands used in conventional communication systems, Rayleigh scattering is the dominant loss factor. Despite the fact that its contribution is significantly reduced in the far-IR region beyond 2μm, silica fibres cannot be used

at these wavelengths since IR absorption related to vibrational resonances in the bonds of the silica molecules begins to dominate the fibre loss beyond 1.6μm. In spite of all these effects, a minimum loss of $\alpha_{dB} < 0.2$dB/km can be achieved for silica fibres around 1.5μm when employing appropriate manufacturing processes. Although this loss is wavelength dependent, it can be assumed to be constant within the modulation bandwidth of a single-channel for current data rates [23].

Modal dispersion:

When light travels in multimode fibres that have core diameters of about 50 to 80μm[1], each mode travels at a different speed for a given fibre length. In fact, because different modes are associated to different light paths, it is obvious that the mode following the shortest overall path near the centre of the core arrives at the end of the fibre before the mode following the longer outer path, even assuming that the speed of all the modes are constant. Since in a multimode fibre an individual optical pulse may comprise a significant number of modes, the potential for pulse broadening and hence signal degradation due to modal dispersion is considerable. In order to avoid strong signal distortion, it is usually necessary to keep the pulses long enough to maintain a reasonable temporal overlap of components from different modes, and this unavoidably sets a limit on the data rate. As a result, modal dispersion in multimode fibres limits the maximum transmission rate and the achievable reach.

However, due to the low cost and ease of connection, multimode fibres are still the choice for short reach applications. If cost is not a concern, then, a natural way of eliminating modal dispersion is to use single mode fibres. Since all the analysis and experiments presented in this thesis are performed using single mode fibre, modal dispersion is no longer taken into account or discussed (more details on the topic can be found in [20]).

Chromatic dispersion:

Single mode fibres effectively eliminate the impact of modal dispersion by limiting the number of modes to just one through a smaller diameter ($\sim$ 8-10μm). However, despite the fact that the energy of the injected pulse is transported

---

[1]Optimal performance in short-distance optical connections can be achieved using $50/125\mu$m multimode graded index optical fibres [24].

only by the fundamental mode, there can still be pulse broadening due to chromatic dispersion. Chromatic dispersion arises from the wavelength dependence of the propagation constant $\beta(\omega)$, as discussed above: this causes different spectral components to propagate along the fibre with different group velocities. In particular, if the attenuation parameter α and the Kerr nonlinear parameter γ are neglected, the NLSE (Eq. (2.1.6)) can be rewritten as

$$\frac{\partial A}{\partial z} = -\frac{i\beta_2}{2}\frac{\partial^2 A}{\partial T^2},\tag{2.1.10}$$

whose solution, shown in frequency domain for simplicity, is given by

$$\widetilde{A}(z,\omega) = \widetilde{A}(0,\omega)e^{i\frac{\beta_2}{2}\omega^2 z},\tag{2.1.11}$$

where $\widetilde{A}(z,\omega)$ is the Fourier transform of $A(z,T)$. Equation (2.1.11) shows that the group velocity dispersion parameter β_2 changes the phase of each spectral component of the pulse by an amount that depends on both the frequency and the propagated distance [19]. Therefore, β_2 is used as quantitative measure of the frequency-dependent delay accumulated over a certain fibre length by different spectral components. In optical communications the GVD parameter β_2 is usually defined as a derivative with respect to wavelength rather than angular frequency:

$$D_\lambda = \frac{\partial}{\partial\lambda}\left(\frac{1}{\nu_g}\right) = -\frac{2\pi c}{\lambda^2}\cdot GVD.\tag{2.1.12}$$

D_λ is called the dispersion parameter and is expressed in [ps/(nm $\cdot$ km)]. It is important to realise the different signs of GVD and D_λ, result from the fact that a longer wavelength corresponds to a smaller optical frequency. In order to avoid confusion, the terms normal ($\beta_2 > 0$, $D_\lambda < 0$) and anomalous ($\beta_2 < 0$, $D_\lambda > 0$) dispersion can be used instead of positive and negative dispersion. In material with positive GVD the components at longer wavelengths move faster than components at shorter wavelengths, whereas in material with the negative GVD the situation is the opposite. The larger the group velocity dispersion GVD, the larger the broadening of the temporal pulse. It is said, that the pulse is positively chirped, when the longer wavelength components lead the shorter ones, and vice versa. Hence, anomalous dispersion induces negative chirp. Note that when the signal is transmitted at a wavelength not coinciding with the zero-

dispersion wavelength, the frequency chirp is translated to amplitude distortion by phase modulation (PM)-to-amplitude modulation (AM) conversion induced by GVD [25, 26].

In general, different types of fibre have different dispersion characteristics; however, for a standard single mode fibre, the dispersion parameter D_λ can usually be extrapolated using the following expression [27]:

$$D_\lambda = \frac{S_0}{4} \left(\lambda - \frac{\lambda_0^4}{\lambda^3} \right), \tag{2.1.13}$$

where λ_0 is the zero-dispersion wavelength and S_0 the dispersion slope ($S_\lambda \equiv dD_\lambda/d\lambda$, see Eq. (2.1.16)) at the zero dispersion wavelength. For standard single mode fibre λ_0 lies around 1312nm and S_0 is approximately 0.090ps/(nm^2·km). The corresponding dispersion parameter D_λ (called D from now on for simplicity) obtained using Eq. (2.1.13) is summarised in Fig. 2.2.
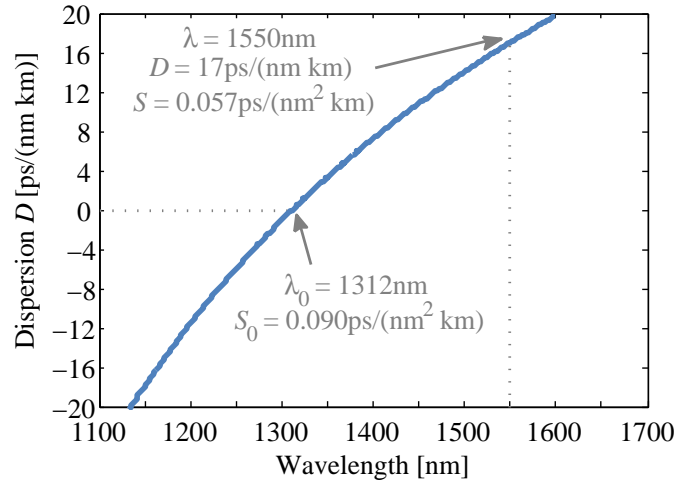

Figure 2.2: Dispersion parameter D as a function of the wavelength for standard single mode fibre.

Both material property and waveguide structure may contribute to the dispersion parameter D and they are referred to as material dispersion and waveguide dispersion, respectively. Material dispersion is caused by the dependence of the refractive index of the material used for fibre manufacturing on the optical wavelength. On a fundamental level, the origin of material dispersion is related to the characteristic resonance frequencies at which the material absorbs the electromagnetic radiation. In the wavelength region where the absorption is negligible,

the refractive index can be described using an empirical formula known as the Sellmeier equation [20]:

$$n^2(\lambda) = 1 + \sum_k \frac{A_k \cdot \lambda^2}{\lambda^2 - \lambda_k^2}, \qquad (2.1.14)$$

where λ_k is the resonance wavelength and A_k is the strength of the kth resonance. For silica, a three-term sum is normally used and the parameters λ_k and A_k are experimentally estimated by fitting the measured dispersion curve to Eq. (2.1.14). They are found to be [19] $A_1 = 0.6961663$, $A_2 = 0.4079426$, $A_3 = 0.8974794$, and $\lambda_1 = 0.0684043\mu m$, $\lambda_2 = 0.1162414\mu m$, $\lambda_3 = 9.896161\mu m$. The resulting variation of refractive index n and group index n_g with wavelength for fused silica is shown in Fig. 2.3.
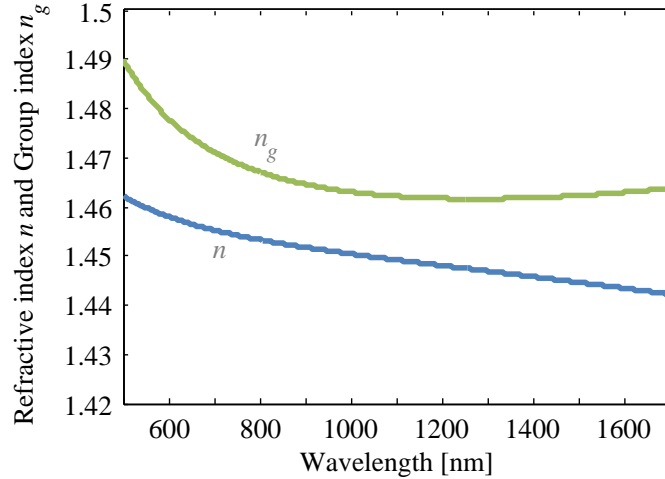

Figure 2.3: Refractive index n and group index n_g as a function of the wavelength for standard single mode fibre.

Waveguide dispersion, on the other hand, arises from the guiding properties of the fibre and is caused by the boundary conditions at the fibre surface which are influenced by geometrical parameters and chemical composition. In standard single mode fibre the optical field is not entirely confined to the core, and a percentage of the energy actually propagates through the inner layer of the cladding, where the propagation velocity is greater than that of the core due to the smaller refractive index. Consequently, waveguide dispersion can also cause pulse broadening. Note that this type of dispersion would occur even if the refractive indices of the core and cladding were independent of wavelength.

In general, if left unmanaged, pulse spreading caused by chromatic dispersion eventually results in inter-symbol interference (ISI) when adjacent pulses overlap, leading to errors in the recovery of transmitted bits, as shown in Fig. 2.4. This, unavoidably, places a limit on the maximum distance a signal can be transmitted without being regenerated or without using dispersion compensation techniques. Such distance can be determined as shown in Eq. (2.1.15).
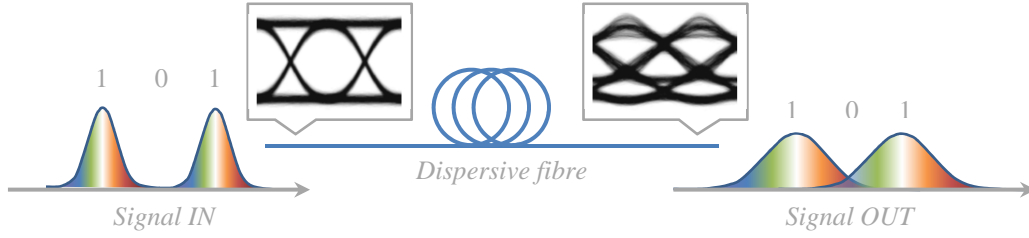

Figure 2.4: Chromatic dispersion in standard single-mode fibre: shorter wavelengths travel faster than the longer ones. The broadening of pulses due to chromatic dispersion leads to optical eye closure.

If $\Delta\lambda$ is the range of wavelengths of the optical pulse propagating through the fibre of length L, the extent of pulse broadening is given by $\Delta T = |D| \cdot L \cdot \Delta\lambda$. The effect of dispersion on the bitrate B can be estimated by using the criterion $B \cdot \Delta T < 1$ [20], that is to say the broadening is smaller than the bit period. In the specific case of a signal generated by external modulation with non-return-to-zero on-off-keying (NRZ-OOK, simply called NRZ from now on for clarity), which is the most widely used modulation format in optical access networks, the optical bandwidth in frequency units can be considered to be approximately $\Delta\omega \approx 1.2 \cdot B$ [28]. Converting to wavelength units this means that, for a 10Gb/s NRZ signal centered at $\lambda = 1550$nm, $\Delta\lambda = (1.2 \cdot B \cdot \lambda^2)/c \approx 0.1$nm. Therefore, the transmission distance L_D at which the pulse has broadened by one bit interval ($B \cdot \Delta T = 1$) can be calculated as

$$L_D = \frac{1}{B|D|\Delta\lambda} = \frac{c}{1.2B^2|D|\lambda^2}\bigg|_{\substack{D=17\text{ps/(nm} \cdot \text{km)} \\ B=10\text{Gb/s} \\ \lambda=1550\text{nm}}} \approx 61[\text{km}]. \qquad (2.1.15)$$

This estimated limit is close to the 70km observed in practice for a 1dB power-penalty [28], and therefore it can be used to calculate the maximum transmission distance at which the penalty due to dispersion can still be assumed negligible. From Eq. (2.1.15) it is clear that the amount of chromatic dispersion that a

system can tolerate is inversely proportional to the square of the bit rate because an increased data rate means not only a wider spectrum and increased spreading, but also narrower bit slots that are more sensitive to the spreading of neighbouring pulses. Also, from Eq. (2.1.15) it appears that the transmission distance L_D can be increased indefinitely by operating at the zero-dispersion wavelength where $D = 0$. However, as mentioned above, optical pulses still experience broadening because of higher order dispersive effects [20], and this is due to the fact that D cannot be made zero at all the wavelengths contained within the pulse spectrum. The higher order effects are governed by the differential-dispersion parameter S, which is expressed in [ps/(nm^2·km)] and related to the coefficient β_3 according to

$$S \equiv \frac{dD}{d\lambda} = \left(\frac{2\pi c}{\lambda^2}\right)^2 \beta_3 + \left(\frac{4\pi c}{\lambda^3}\right)\beta_2. \qquad (2.1.16)$$

Note that since the bandwidths of a 10Gb/s signal are much narrower than the bandwidth over which β_2 varies for the most common fibre types [29], the TOD coefficient β_3 represents an effective change of β_2 from channel to channel in a wavelength-division-multiplexing (WDM) system rather than having a noticeable impact within a WDM channel itself. In case of a signal operating near the zero-dispersion wavelength the effective value of dispersion can be seen as $D_{eff} = D + \Delta\lambda \cdot S \approx \Delta\lambda \cdot S$, and the limiting bit-rate distance product now can be written as $B \cdot L \cdot |S| \cdot \Delta\lambda < 1$ [20].

Polarisation mode dispersion (PMD):

PMD is a source of pulse broadening caused by fibre birefringence, which is the difference in refractive index experienced by light in different polarisation modes. In fact, despite the name, even a single mode fibre is not truly single mode because it can support two degenerate modes polarised in two orthogonal directions. In ideal optical fibres, these two modes have identical propagation properties and are indistinguishable. In reality, however, minute waveguide asymmetries, either due to intrinsic perturbations[1] or due to extrinsic perturbations[2] cause the two polarisation modes to become slightly non-degenerate. The resulting two polarisation states, propagating in the x- and y-direction respectively, are called

---

[1]Permanent features caused by manufacturing imperfections like non-circular fibre core geometry, etc.

[2]Stress imposed by mechanical vibrations, bending, temperature variations, etc.

principal states of polarisation, and they are characterised by different mode-propagation constants β_x and β_y. In other words, the PMD resulting from fibre birefringence leads to fast and slow modes of propagation and consequently to dispersion. The extent of pulse broadening can be estimated from the time delay ΔT occurring between the two polarisation components of the optical pulse. For a fibre of length L and constant birefringence, ΔT is given by [19]

$$\Delta T = \left| \frac{L}{\nu_{gx}} - \frac{L}{\nu_{gy}} \right| = L \cdot |\beta_{1x} - \beta_{1y}| = L \cdot \Delta\beta_1, \qquad (2.1.17)$$

where ν_{gx} and ν_{gy} are the group velocities in the x- and y-polarisation components of the signal, and $\Delta\beta_1$ is the group velocity mismatch. However, for standard telecommunication fibres, Eq. (2.1.17) cannot be used to estimate the PMD because of the random changes in birefringence occurring along the fibre. These changes tend to average the propagation time for the principal states of polarisation. In fact, although ΔT can have large variations, it will be close for the most of the time to some average value, and therefore PMD can be characterised by the root mean square (RMS) ΔT_{RMS} obtained averaging the random perturbations [20]:

$$\Delta T_{RMS} = D_p \cdot \sqrt{L}, \qquad (2.1.18)$$

where D_p is the PMD parameter and is expressed in [ps/$\sqrt{\text{km}}$]. Typical values for D_p are in the range of 0.1 to 1ps/$\sqrt{\text{km}}$. Because of the $\sqrt{L}$ dependence, PMD-induced pulse broadening is relatively weak compared to the broadening caused by chromatic dispersion. The maximum tolerable PMD without compensation is estimated to be around 15% of the data period [30, 31], and for a 10Gb/s NRZ signal operating at 1550nm on a fibre with $D_p \approx 1$ps/$\sqrt{\text{km}}$ this means that the maximum transmission distance limited by PMD is around 170km [31], well above the chromatic dispersion limiting distance obtained using Eq. (2.1.15) for the same signal. Note, however, that PMD can become a limiting factor at higher bit rates (i.e. $\geqslant$ 40Gb/s) or in the case of systems designed to operate over long distances near the zero-dispersion wavelength of the fibre [19].

Note that all the experimental results presented in this thesis were carried out at either bit rates or transmission distances not high enough to allow PMD to become a limiting factor in comparison to other impairments such as CD. For this reason PMD is no longer discussed and its effects are not taken into account

in the simulations presented throughout the thesis.

Other linear effects:

Two additional key impairments present in optical networks that are not an issue in point-to-point WDM systems are in-band (linear) crosstalk and signal distortion from filter concatenation [32]. Both of these impairments can arise after filtering and multiplexing/demultiplexing operations at an optical node, where optical cross-connects and optical add/drop multiplexers (OADMs) are employed to add, drop, and switch channels from one optical fiber to another (without optical-to-electrical-to-optical (OEO) regeneration). In particular, linear crosstalk is introduced by an optical filter/mux whose pass-band leaks other channels that are not spaced far apart, while filter-induced distortion can arise as a result of filter concatenation when the signal passes through a large number of optical filters (cascading of many filters may narrow bandwidth enough to produce clipping of the signal spectrum). Note that as this thesis concentrates mainly on single optical channel transmission and on access network applications where the overall number of employed filters/multiplexer is limited to a few, such impairments do not represent a major issue and for this reason they are no longer taken into account or discussed. Further details on this topic can be found in [20, 32, 33].

2.1.2 Nonlinear Effects

In optics, the terms linear and nonlinear, mean intensity-independent and intensity-dependent phenomena respectively [34]. In particular, nonlinear effects in optical fibres occur due to changes in the refractive index of the medium with optical intensity (also known as the Kerr-effect) and to inelastic scattering phenomena.

Kerr-nonlinearities:

Depending on the type of input signal, the Kerr-nonlinearity manifests itself in three different effects: self-phase modulation (SPM), cross-phase modulation (XPM or CPM) and four-wave mixing (FWM). SPM is a nonlinear phase modulation of a beam that is caused by its own intensity. This means that, due to the intensity dependent variations in the refractive index, optical power fluctuations in a light wave are converted into phase fluctuations. In this way, an initial

unchirped optical pulse acquires a chirp, i.e., a temporally varying instantaneous frequency.

XPM is a nonlinear impairment affecting WDM systems where the optical intensity of one beam influences the phase change of another co-propagating beam. XPM arises from the Kerr-effect as SPM, but the result of XPM is more relevant for multi-channel transmission while in single-channel transmission systems only SPM is significant. For this reason, in principle, XPM can potentially impose more limitations than SPM in WDM systems since a significant number of channels contribute to generate the phase shift and intensity fluctuations.

Another impairment that occurs in WDM systems is FWM. It is an inter-modulation phenomenon by which two (or more) signals at different wavelengths modulate the refractive index of the fibre. As a consequence, two (or more) modulated indices of refraction result, and the phase matching between the signals produces beating. This beating creates additional signals at new wavelengths at the expense of the power of the original signals.

Inelastic scattering phenomena:

At high power levels, the energy of an optical pulse travelling along a fibre can also be affected by stimulated scattering phenomena such as stimulated Brillouin scattering (SBS) and stimulated Raman scattering (SRS) which lead to an intensity dependent attenuation constant. In both these inelastic processes, scattering of an incident photon interacting with the dielectric medium results in a lower energy photon, while the energy difference is released in the form of phonons. The main difference between SBS and SRS scattering is that the former generates acoustic phonons that are coherent and give rise to a macroscopic acoustic wave in the fibre, while the latter generates optical phonons that are incoherent and do not result in macroscopic wave formation. In particular, SBS is a narrow band effect (the Brillouin gain has an intrinsic bandwidth of 50MHz) relative to signals operating in the terahertz range and the physical process behind it is the tendency of materials to compress in the presence of an electric field. The acoustic wave generated by the incident signal modulates the refractive index of the fibre and the resulting periodic variation causes back-reflection similar to the effect of a Bragg grating. Such a Bragg grating moves with a certain acoustic velocity depending on the material of the medium, and in silica glass fibre it causes a shift of approximately 11GHz between the original and reflected wave.

On the other hand, SRS is an interaction between the vibrations of the atoms in the fibre (associated with optical phonons) and the incident optical signal. Indeed, the light propagating through the fibre can excite the atoms to higher energy vibrational states. The energy removed from the incident signal is then scattered by such excited atoms as a new light wave. Contrary to SBS, SRS can scatter light in both directions and the Raman gain extends over a much larger frequency range (up to 40THz, with maximum at 13THz [19]).

Both the SBS and SRS phenomena have a threshold-like behaviour which means that the intensity of scattered light grows exponentially if the incident power exceeds a certain threshold value. SRS does not represent a practical issue for the systems taken into account in this thesis, as signal degradation occurs only at very high powers, typically in the hundreds of milliwatt range. However, SBS can be observed at powers as low as several milliwatt depending on the transmitter and fibre characteristics. Nevertheless, SBS can be significantly suppressed by applying a frequency dither to the laser bias, which causes a broadening of the laser optical spectrum above the Brillouin gain bandwidth. As a matter of fact, all experiments presented in this thesis were carried out applying such frequency dither to suppress SBS, which effectively had no impact on the system performance.

Impact of nonlinear effects on the systems under consideration:

As the effect of both SBS and SRS can be neglected, they have not been taken into account in any of the simulations or experiments presented here and for this reason they are not further discussed. Regarding the Kerr-nonlinearities described above, since the main focus of this thesis is to investigate single optical channel only, FWM has also been ignored.

In the burst-mode applications of interest in this work, SPM was found to have no influence on the system performance for most of the burst powers taken into account, and to be actually beneficial (resulting in lower system penalty) for the highest burst powers. In fact, it is well known [19, 20] that the interplay of SPM and GVD can be advantageous when operating in the anomalous dispersion regime. This is due to the fact that SPM-induced chirp is positive while GVD-induced chirp is negative in the anomalous dispersion regime, hence they compensate each other resulting in lower broadening than for the case of GVD alone. Therefore, for the fibre launched powers involved in this thesis work, there

was no penalty observed due to SPM, and for this reason it has been effectively ignored in all simulations and experiments presented here.

In summary, of all the various nonlinear effects discussed above, none have a significant impact on the system performance for the power levels, bit rates, and transmission distances taken into account, and as a consequence attention is focused on CD only, which is the dominant linear effect degrading the signal quality.

2.2 Loss Management: Optical Amplification

Optical amplifiers are of strategic importance for telecommunications as they compensate for fibre propagation losses in long distance links and branching losses in access networks avoiding costly optical-electrical-optical (OEO) regeneration. Indeed, before the commercialisation of optical amplifiers, it was necessary to electronically regenerate the optical signals every 80-100km in order to achieve transmission over long distances. While this can still be feasible when transmitting a single low capacity optical channel, it quickly becomes not viable when transmitting tens of high capacity WDM channels, resulting in a highly expensive, power-hungry and bulky regenerator stations. In addition, regenerators are typically channel number, bit-rate, and modulation format specific, meaning that any upgrade to the link would require an upgrade of the regenerators as well. In
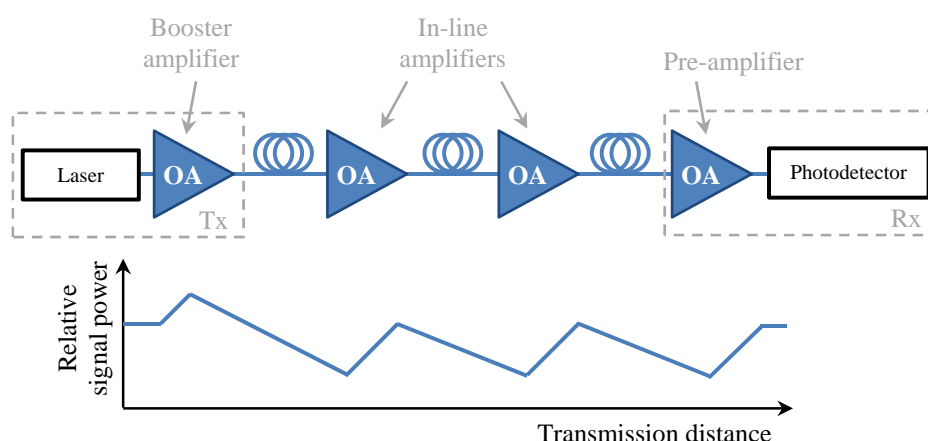

Figure 2.5: Applications of optical amplifiers as booster amplifier, in-line amplifier and pre-amplifier (OA: optical amplifier, Tx: transmitter, Rx: receiver).

contrast, an optical amplifier can handle multiple WDM channels simultaneously and is generally transparent to bit-rate and modulation format. In other words, a single optical amplifier can replace all the multiple components necessary for OEO regeneration. Note also that the transparency of optical amplifiers imply that the link can be upgraded without the need to alter or replace the amplifier itself.

The main applications of optical amplifiers in communication systems can be classified into three areas [35], as illustrated in Fig. 2.5: booster amplifiers to increase the transmitted power, in-line amplifiers to compensate the fibre and other transmission losses, and pre-amplifiers to improve receiver sensitivity. The two types of amplifiers that are of most interest for the access architecture presented in this thesis are erbium doped fibre amplifiers (EDFAs) and semiconductor optical amplifiers (SOAs). Both types are discussed more in detail in Chapter 3 with regards to their different implications when used in the burst-mode systems studied in this work, whereas in the remainder of this section their common aspects such as gain saturation and signal degradation due to amplifier noise are briefly described.

2.2.1 Gain Saturation

The gain of an optical amplifier can be dependent on the input signal level. This condition, known as gain saturation, is caused (in the semiconductor case) by a reduction in the number of electrons in the conduction band available for stimulated emission and occurs when the rate of input photons is greater than the rate at which electrons used for stimulated emission can be replaced by current injection [36]. The gain G of an optical amplifier is defined as the ratio of the output power P_{out} to the input power P_{in} of the continuous-wave signal being amplified:

$$G = \frac{P_{out}}{P_{in}}. \tag{2.2.1}$$

It can be determined by knowing the relation that describes the power evolution through the gain media:
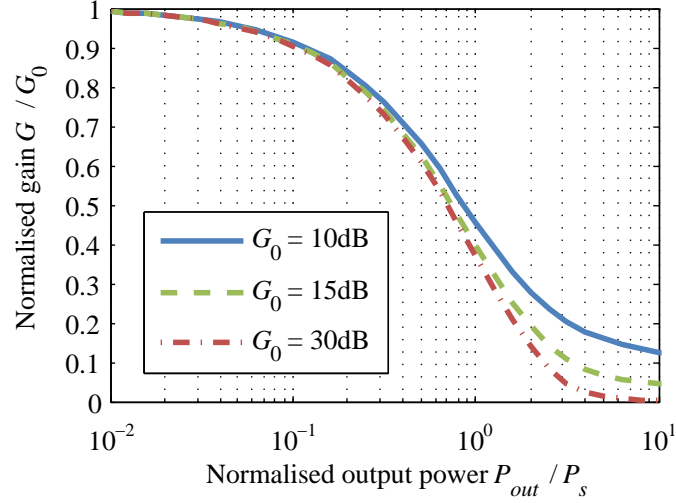
$$\frac{dP(z)}{dz} = g(\omega)P(z), \tag{2.2.2}$$

Figure 2.6: Amplifier gain G (normalised to the unsaturated gain G_0) as a function of the output power P_{out} (normalised to the saturation power P_s).

where P is the optical power at a distance z from the input end ($z = 0$), and g is the material gain that, under the assumption of incident frequency tuned to the peak gain[1], can be expressed as a function of the saturation power P_s of such a gain medium and the small-signal gain g_0 as [20]:

$$g(\omega) = \frac{g_0}{1 + P/P_s}. \tag{2.2.3}$$

By solving the differential equation obtained by combining Eq. (2.2.2) and (2.2.3) for an amplifier medium of length L with respect to the boundary conditions $P(0) = P_{in}$ and $P(L) = P_{out} = G \cdot P_{in}$, the large-signal amplifier gain can be written as

$$G = G_0 \exp\left[-\frac{G-1}{G}\frac{P_{out}}{P_s}\right], \tag{2.2.4}$$

where $G_0 = \exp[g_0 \cdot L]$ is the unsaturated gain of the amplifier (i.e. for $P \ll P_s$). Equation (2.2.4) shows that the gain G decreases from G_0 when P_{out} approaches P_s. Figure 2.6 shows the saturation characteristics for three different unsaturated gain values. Another quantity of practical interest is the output saturation power P_{out}^s defined as the output power for which the amplifier gain G is reduced by a factor of 2 (i.e. 3dB) from its unsaturated value G_0:

---

[1]i.e. the incident frequency coincides with the atomic transition frequency.

$$P_{out}^s = \frac{G_0 \cdot \ln 2}{G_0 - 2} P_s. \tag{2.2.5}$$

Effects of saturation in SOAs:

When working in the saturation regime, the SOA behaviour becomes nonlinear causing a number of effects to occur, including cross-gain modulation (XGM), cross-phase modulation (XPM), four-wave mixing (FWM), self-phase modulation (SPM), and self-gain modulation (SGM). The latter is the only effect of interest in this thesis, so the other effects are not considered further[1].

When an SOA amplifies a high intensity modulated signal, SGM can lead to a serious waveform distortion commonly referred to as patterning. In fact, under these conditions, an SOA is effectively a nonlinear element with memory [38]. The nonlinearity of the SOA is mainly due to carrier depletion induced saturation, whereas its memory is due to the finite carrier lifetime (in the order of 100–500ps). The signal-dependent instantaneous gain of the saturated SOA results in non-Gaussian statistics of the optical noise at the output, and the finite memory of the SOA leads to bit patterning effects, thus resulting in signal-dependent enhancement of the intersymbol interference (ISI), on top of the linear ISI enhancement stemming from fibre dispersion, optical and electrical filters, etc. Such a concept is illustrated in Fig. 2.7, where a typical eye diagram of a signal affected by patterning is shown.
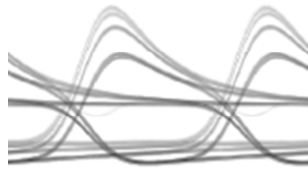

Figure 2.7: Example of a (simulated) eye diagram for a signal affected by patterning.

Therefore, if the input signal to the SOA has a bit-rate comparable (or lower) than the gain recovery time, an isolated '1' or multiple '1s' after a long sequence of '0s' will be characterised by the leading part of the pulse being amplified with unsaturated gain and the trailing part being amplified with a lower gain as the

---

[1]Note however that their consequences are conceptually the same of the respective counterpart described in Section 2.1.2 in regards to the fibre nonlinear effects; further details can also be found in [35, 37].

SOA approaches saturation. Moreover, for even higher bit-rates the amplifier gain does not return to the unsaturated value and also the leading part is amplified with a partially reduced gain.

Due to their slow relaxation response in comparison to SOAs, EDFAs do not exhibit such bit pattern dependence. On the other hand, they can still exhibit large saturation-induced gain transients (in the order of up to several milliseconds) for signal level changes occurring on microsecond or millisecond timescales. More details on this phenomenon and its implications on the burst-mode systems of interest can be found in Section 3.2.1.

2.2.2 Amplifier Noise

The main disadvantage of optical amplification is the generation of ASE (amplified spontaneous emission) noise. While the ASE generated in the wavelength region not coincident with the signal can be suppressed by using an optical (narrow-band) filter, the ASE that appears in the signal wavelength region cannot be separated and constitutes the added noise from the amplifier, which in the case of multi span systems can build up compromising the maximum achievable OSNR (optical signal-to-noise ratio). The ASE spectral density S_{ASE} [W/Hz] can be written as in [20]

$$S_{ASE} = n_{sp}(G-1)h\nu, \qquad (2.2.6)$$

where G is the amplifier gain, h is the Planck's constant, ν is the optical frequency (i.e. $h\nu$ is the energy of one photon at the signal frequency), and n_{sp} is the spontaneous-emission factor (known also as population-inversion factor). For a two level system n_{sp} is given by

$$n_{sp} = \frac{N_2}{N_2 - N_1}, \qquad (2.2.7)$$

where N_1 and N_2 are the atomic populations for the ground and excited states respectively. The ASE power P_{ASE} [W] is related to S_{ASE} as

$$P_{ASE} = 2S_{ASE}B_{ref} = 2n_{sp}(G-1)h\nu B_{ref}. \qquad (2.2.8)$$

Note that the spectral density of Eq. (2.2.6) is per spatial and polarisation mode, and as the single mode fibres (and fibre amplifiers) have two orthogonal polarisation modes (see Section 2.1.1), Eq. (2.2.8) includes a factor of 2 to get

the total ASE power.

The OSNR is defined as the average optical signal power divided by the ASE power, and is typically measured in both polarisations and with an optical reference bandwidth B_{ref} of 12.5GHz ($\sim$0.1nm). Therefore, at the output of an optical amplifier the OSNR can be written as

$$OSNR = \frac{P_{out}}{P_{ASE}} = \frac{P_{out}}{2S_{ASE}B_{ref}} = \frac{GP_{in}}{2n_{sp}(G-1)h\nu B_{ref}}, \qquad (2.2.9)$$

where P_{in} and P_{out} are the optical signal power at the input and output of the amplifier respectively.

In practice, the degradation of the signal-to-noise ratio associated to the use of an amplifier is quantified in terms of a parameter known as noise figure (NF), which can be expressed as a function of the ASE power and the optical reference bandwidth [39]:

$$NF = \frac{P_{ASE}}{h\nu B_{ref}G} + \frac{1}{G} = \frac{2S_{ASE}}{h\nu G} + \frac{1}{G} = \frac{2n_{sp}(G-1)}{G} + \frac{1}{G}\bigg|_{G\gg1} \approx 2n_{sp}. \quad (2.2.10)$$

Note from Eq. (2.2.10) that even an ideal amplifier for which $n_{sp} = 1$ would result in a noise figure NF of 2 (i.e. 3dB), meaning that in practical situations any amplifier degrades the SNR at least by a factor of 2. Combining Eqs. (2.2.9) and (2.2.10) it is possible to express the OSNR at the output of an amplifier in terms of its noise figure and input power as

$$OSNR = \frac{GP_{in}}{(NF \cdot G - 1)h\nu B_{ref}}\bigg|_{G\gg1} \approx \frac{P_{in}}{NFh\nu B_{ref}}. \qquad (2.2.11)$$

2.3   Receiver Noise Mechanisms

An optical receiver converts data from the optical domain into the electrical domain using a photodiode. It is well known that photodiodes are square law detectors whose output is not proportional to the optical electric field but rather to the square of the field. In other words, the output is linearly proportional to the power or intensity of the light, with no direct dependence on optical frequency, phase, or polarisation. The relation between the optical power and the

photocurrent is linear, i.e.

$$\langle i_{sig}(t) \rangle = R \cdot P_{in}, \qquad (2.3.1)$$

where $\langle i_{sig}(t) \rangle$ is the photo-current ($\langle \cdot \rangle$ refers to an average quantity), R is the responsivity of the photo-detector [A/W], and P_{in} is the incident optical power. The responsivity R can be written as [20]:

$$R = \frac{\eta q}{h\nu} \approx \frac{\lambda_{\mu m}}{1.24}\eta, \qquad (2.3.2)$$

where η is a fundamental quantity known as quantum efficiency and defined as the percentage of incident photons which contribute to the external photocurrent.

Note that Eq. (2.3.1) assumes that such a conversion is noise free. However, the interaction of photons with the matter in a photodetector is a statistical process. This means that even in an ideal receiver the aforesaid linear relationship is valid in an average sense only. In other words, if the behaviour of the incoming photons is studied on a microscopic level, it would be possible to observe considerable fluctuations in the photocurrent around its mean. Such fluctuations represent the receiver noise.

The receiver performance, then, can be expressed in terms of electrical signal-to-noise ratio (SNR), defined as the ratio of the electrical peak power of a 1-bit $\langle i_{sig,1}(t) \rangle^2$ to the associated noise variance σ_n^2 [40]:

$$SNR = \frac{\langle i_{sig,1}(t) \rangle^2}{\sigma_n^2}. \qquad (2.3.3)$$

For noise processes that can be approximated by Gaussian statistics, the mean is always zero and the variance is equal to the mean-square value $\sigma_n^2 = \langle i_n^2(t) \rangle$. Note that as the autocorrelation function of $\langle i_n(t) \rangle$ is related to the spectral density $S_n(f)$ by the Wiener-Khinchin theorem [20], it is possible to express the variance of the received photocurrent noise as

$$\sigma_n^2 = \langle i_n^2(t) \rangle = \int_{B_e} S_n(f)df, \qquad (2.3.4)$$

where B_e [Hz] is the effective noise electrical bandwidth of the receiver. The ultimate value of $\sigma_n^2 = \langle i_n^2(t) \rangle$ depends on the actual noise mechanism responsible for the current fluctuations. In particular, the two fundamental noise mechanisms

generated at the receiver are thermal noise and shot noise. Note that in addition to these mechanisms also the optical noise accumulated along the transmission system can be responsible for signal degradation. For instance, if optical amplifiers are used in order to compensate for the fibre losses, it is logical to expect that the system performance has a dependence on the received OSNR, as the optical noise gets converted into electrical beat-noise components. In the remaining part of this section thermal noise, shot noise, and beat noise are briefly discussed.

A final point to note here is that the SNR described by Eq. (2.3.3) only accounts for the 1-bit statistics. This implies that if the extinction ratio of the transmitted signal is not large enough (i.e. $i_{sig,0} \ll i_{sig,1}$ is not true), only crude system performance estimates can be made [40]. For more accurate analysis, then, the Q-factor should be taken into account as it includes both 0-bit and 1-bit statistics (see Section 2.4).

Thermal noise:

Thermal noise, also known as Johnson noise or Nyquist noise, is the electronic noise generated by the thermal agitation of electrons inside an electrical conductor at equilibrium, and it can be seen as a consequence of Brownian motion [41]. In optical receivers, the random thermal motion of electrons in the load resistor of the receiver front-end manifests as fluctuations to the current generated by the photodiode. As thermal noise is characterised by a random nature, it must be treated by statistical means. Indeed, even though the actual noise waveform cannot be predicted, it is possible to estimate the statistics such as the mean (average) and variance. The current fluctuation $i_{th}(t)$ induced by thermal noise can be mathematically modelled as a stationary Gaussian random process with a spectral density $S_{th}(f)$ that is nearly frequency independent (up to approximately 1THz) [20]. That is, for all bandwidths of interest, thermal noise is white. The spectral density is given by

$$S_{th}(f) = \frac{2k_B T}{R_L},$$ (2.3.5)

where k_B is the Boltzman constant, T is the absolute temperature, and R_L is the load resistor. Using Eq. (2.3.4) it is then possible to express the thermal noise variance as

$$\sigma_{th}^2 = \langle i_{th}^2(t)\rangle = \int_{B_e} S_{th}(f)df = \frac{4k_BT}{R_L}B_e. \qquad (2.3.6)$$

Note that Eq. (2.3.4) includes only the thermal noise generated by the load resistor. In practical situations, however, many other electrical components can contribute additional noise, for example electrical amplifiers. A common approach accounts for such noise by introducing the parameter F_n, known as the amplifier noise figure, to Eq. (2.3.4) which can be rewritten as follows

$$\sigma_{th}^2 = \frac{4k_BT}{R_L}F_nB_e. \qquad (2.3.7)$$

Accordingly, when thermal noise is the only mechanism of noise taken into account, the SNR can be calculated as

$$SNR = \frac{\langle i_{sig,1}(t)\rangle^2}{\sigma_{th}^2} = \frac{R^2P_{sig,1}^2R_L}{4k_BT \cdot F_n \cdot B_e}. \qquad (2.3.8)$$

From Eq. (2.3.8) it is possible to note the SNR is proportional to $P_{sig,1}^2$ when the system is thermal noise limited. Also, another important aspect is that the SNR could be improved in principle by employing a large load resistor R_L (i.e. a high impedance front end). However, increasing excessively the value of the load resistor to reduce thermal noise reduces the receiver bandwidth as well.

Shot noise:

Electrical currents do not flow uniformly and do not vary smoothly in time like the standard water flow analogy. Current flow is not continuous, but results from the motion of charged particles (i.e. electrons and holes) which are discrete and independent [42]. Indeed, at a microscopic level, currents vary in unpredictable ways. For instance, photodiodes work on the basic principle that when photons strike the surface they generate free electrons and the movement of the free electrons results in a measurable current. Shot noise in the current is due to the statistical nature of the generation of the free electrons. In any given time interval, there will be random fluctuations in the number of free electrons generated as the photons strike that surface. As a result, the noise current is a stationary random process described by Poisson statistics. However, given the large number of photons involved in the process (10^2-10^3 photons/pulse), a Gaussian distribu-

tion can be used as a valid approximation. The spectral density of the shot noise is practically constant over a very wide band (i.e. the noise can be effectively considered as white) and is given by

$$S_{shot}(f) = q\langle i_{sig,1}(t)\rangle. \tag{2.3.9}$$

Using Eq. (2.3.4) the variance of the shot noise can be written as

$$\sigma_{shot}^2 = \langle i_{shot}^2(t)\rangle = \int_{B_e} S_{shot}(f)df = 2q\langle i_{sig,1}(t)\rangle B_e, \tag{2.3.10}$$

and the SNR for a shot noise limited system becomes

$$SNR = \frac{\langle i_{sig,1}(t)\rangle^2}{\sigma_{shot}^2} = \frac{\langle i_{sig,1}(t)\rangle}{2qB_e} = \frac{\eta P_{sig,1}}{2h\nu B_e}. \tag{2.3.11}$$

Eq. (2.3.11) shows that for shot noise limited systems the SNR varies linearly with $P_{sig,1}$. Furthermore, comparing Eqs. (2.3.8) and (2.3.11) using for R_L, F_n, B_e, and η some typical values obtained from the datasheets of commercially available PIN receivers employed in a number of experiments presented in this thesis [43], it is possible to see that thermal noise effectively dominates the receiver performance for all practical cases of interest.

Beat noise from ASE:

As discussed in Section 2.2.2, in multi span systems the ASE noise from optical amplifiers can build up compromising the maximum achievable OSNR. At the receiver side, the ASE noise power is converted from an optical to an electrical level in parallel with the optical signal conversion. However, as the detector is inherently a square law device which responds to the intensity of the incoming optical field, the ASE is not simply converted to the corresponding electrical noise due to the beating process between the ASE electric field $E_{ASE}(t)$ and the signal electric field $E_{sig}(t)$. This process results in the appearance of several components that are often called the beat noise components. As a result, the total photocurrent generated at the receiver output can be written as

$$\begin{aligned} i_{rx}(t) &= R \cdot |E_{sig}(t) + E_{ASE}(t)|^2 \\ &= R \cdot |E_{sig}(t)|^2 + 2R \cdot \Re\left[E_{sig}(t) \cdot E_{ASE}^*(t)\right] + R \cdot |E_{ASE}(t)|^2, \end{aligned} \tag{2.3.12}$$

where R is the photodiode responsivity defined in Eq. (2.3.2), $\Re[\cdot]$ is the real part of a complex quantity, and $*$ represents the complex conjugate. From Eq. (2.2.8) and recalling the relation $P_{ASE} = 2S_{ASE}B_{ref} = 2|E_{ASE}|^2$ it is clear that Eq. (2.3.12) contains only half of the noise power. This is because the orthogonally polarised components cannot beat effectively as it does not coherently interfere with the signal, and only the components that have the same polarisation with the signal can contribute to the beat noise.

The first term in Eq. (2.3.12) represents the desired information; the second one is the beating of the signal with the ASE noise and it is often referred to as signal-ASE beat noise; the last term represents the instantaneous power of the noise field generated by the beating of its different components, and it is often referred to as ASE-ASE beat noise. Note that while the ASE-ASE beat noise generated in the wavelength region not coincident with the signal can be suppressed by using a narrow optical filter, the signal-ASE beat noise cannot be separated and effectively contributes to the OSNR degradation.

Under the assumption that the optical filter bandwidth of the receiver significantly exceeds both the bandwidth of the optical signal and the electrical bandwidth of the receiver[1], the beat noise variances can be expressed as [40]:

$$\sigma^2_{sig-ASE} = \langle i^2_{sig-ASE}(t) \rangle = 4R^2 S_{ASE} P_{sig,1} B_e, \qquad (2.3.13)$$

$$\sigma^2_{ASE-ASE} = \langle i^2_{ASE-ASE}(t) \rangle = 4R^2 S^2_{ASE} B_{opt} B_e, \qquad (2.3.14)$$

where $P_{sig,1}$ is the optical power of a 1-bit incident to the photodetector, B_e is the effective noise electrical bandwidth of the receiver, S_{ASE} is the ASE spectral density defined in Eq. (2.2.6), and B_{opt} is the bandwidth of the optical filter centred at the signal wavelength.

As mentioned above, since the contribution of the ASE-ASE beat noise of Eq. (2.3.14) can be suppressed by proper filtering, the sig-ASE beat noise can be considered the dominant term. Accordingly, for beat noise limited systems the SNR defined in Eq. (2.3.3) can be expressed in terms of OSNR as

$$SNR = \frac{\langle i_{sig,1}(t) \rangle^2}{\sigma^2_{sig-ASE}} = \frac{R^2 P^2_{sig,1}}{4R^2 S_{ASE} P_{sig,1} B_e} = OSNR \cdot \frac{B_{ref}}{B_e}, \qquad (2.3.15)$$

---

[1]This approximation is reasonably accurate, unless highly spectrally efficient systems are considered.

where the OSNR has been derived from Eqs. (2.2.8) and (2.2.9) as follows

$$OSNR = \frac{P_{sig,average}}{2 \cdot S_{ASE} B_{ref}} = \frac{P_{sig,1}}{4 \cdot S_{ASE} B_{ref}}.$$

(2.3.16)

Combination of multiple noise mechanisms:

Equations (2.3.8), (2.3.11), and (2.3.15) provide a convenient expression that can be used to estimate the received SNR when the system is thermal noise limited, shot noise limited, or beat noise limited respectively. In some practical cases, however, it is possible that none of the aforesaid mechanisms is dominant, and that all are actually contributing in different ways to the signal degradation. In this scenario all the noise terms must be included in the SNR calculation in order to ensure an accurate estimation of the system performance. Since all the noise sources discussed above are statistically independent and approximated as Gaussian, their sum can also be considered Gaussian and the overall noise term (simply called electronic noise) is determined by the sum of the individual noise variances. Accordingly, the overall SNR can be written as

$$SNR = \frac{\langle i_{sig,1}(t) \rangle^2}{\sigma_{total}^2} = \frac{R^2 P_{sig,1}^2}{\sigma_{sig-ASE}^2 + \sigma_{ASE-ASE}^2 + \sigma_{shot}^2 + \sigma_{th}^2}.$$

(2.3.17)

2.4 System Performance Evaluation

The SNR parameter used in the previous section is a convenient measure used in engineering to quantify how much a signal has been corrupted by noise. For digital signals, it can limit the reliability of detecting correctly, which can be quantified with a bit-error-rate (BER). Indeed, the BER is the ultimate performance measure of optical communication systems. It is statistically defined as the time-averaged ratio of bits that have errors relative to the total number of bits received in a transmission. For long averaging times, the BER can also be considered as the probability of having a detection error for an individual bit [40]. Note that the maximum capacity of a reliable data transmission system is not reached by keeping the BER at an extremely low level (nearly avoiding any bit errors), but by pushing the data rate to a level where some tolerable BER (typically between 10^{-12} and 10^{-9}) can be maintained. A virtually error-free transmission

can still be achieved by detecting and correcting most of the remaining bit errors, e.g. based on check sums.

Figure 2.8 shows the eye diagram and associated histograms of a received signal sampled at the decision instant T_d and with a threshold value I_d. Conceptually, the BER depends on the probability $P(1/0)$ of deciding a 1 when 0 is received, and on the probability $P(0/1)$ of deciding 0 when 1 is received:

$$BER = \frac{1}{2} \left[P(0/1) + P(1/0) \right], \tag{2.4.1}$$

where the factor of $\frac{1}{2}$ indicates equal probability of 0s and 1s to occur.
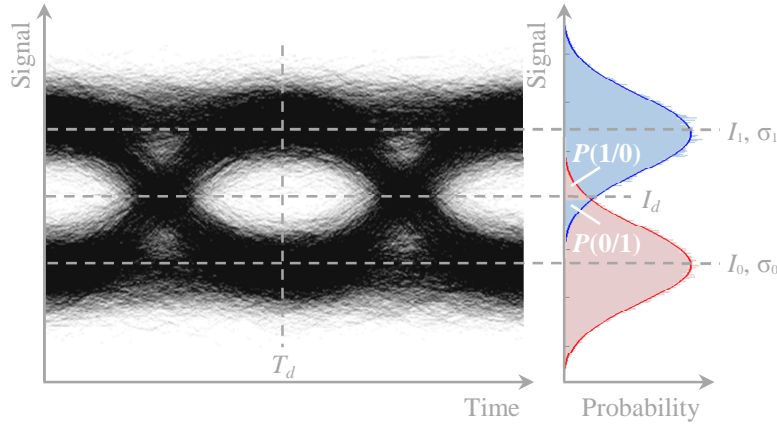
Figure 2.8: Electrical eye diagram at the receiver output and Gaussian probability densities of 1- and 0-bits. $P(0/1)$ and $P(1/0)$ represent the probability of incorrect identification when the data is sampled at a decision instant T_d with a threshold value I_d.

The BER is often expressed in terms of a more convenient parameter called Q-factor, and their relation is given by

$$BER = \frac{1}{2} \text{erfc} \left(\frac{Q}{\sqrt{2}} \right), \tag{2.4.2}$$

where $\text{erfc}\,(\cdot)$ is the complimentary error function. One of the reasons why the evaluation of the system performance through the Q-factor can sometimes be more convenient is that the BER measurement for a high performance transmission link can be extremely impractical. For example, to measure a BER of 10^{-15} with 95% confidence level by counting errors for a bit rate of 10Gb/s, approximately 3.5days are required. This value rises drastically up to over 35days for a BER of 10^{-16} at the same confidence level. On the other hand, the Q-factor is

a prediction of system performance, based on the observation of mean and standard deviation of the electrical signal at the decision circuit, rather than on error counting. Under the common approximation of Gaussian noise statistics [20, 40] and optimised decision threshold I_d, the Q-factor is defined as

$$Q = \frac{I_1 - I_0}{\sigma_1 + \sigma_0}, \tag{2.4.3}$$

where $I_{0,1}$ are the noise-free average signal currents for the 0- and 1-bits respectively, and $\sigma_{0,1}$ are the associated noise standard deviations (see Fig. 2.8).

From Eq. (2.4.3) it is possible to see that under the frequently met assumption of good signal extinction ratio ($P_{sig,1} \gg P_{sig,0}$, i.e. $I_1 \gg I_0$), for NRZ modulation format the Q-factor is directly related to the SNR as follows:

$$Q = \frac{\sqrt{SNR}}{2} \quad \text{for thermal noise limited systems,} \tag{2.4.4}$$

$$Q = \sqrt{SNR} \quad \text{for beat noise limited systems.} \tag{2.4.5}$$

By combining Eq. (2.4.2) with Eqs. (2.4.4) and (2.4.5), the BER can be expressed in terms of SNR as

$$BER = \frac{1}{2}\text{erfc}\left(\frac{1}{2}\sqrt{\frac{SNR}{2}}\right) \quad \text{for thermal noise limited systems,} \tag{2.4.6}$$

$$\begin{aligned} BER &= \frac{1}{2}\text{erfc}\left(\sqrt{\frac{SNR}{2}}\right) \\ &\approx \frac{1}{2}\text{erfc}\left(\sqrt{\frac{OSNR \cdot B_{ref}}{2 \cdot B_e}}\right) \quad \text{for beat noise limited systems.} \end{aligned} \tag{2.4.7}$$

In other words the SNR, Q-factor, and BER of a received signal are all interrelated, and each one of them can be equally used based on what is more convenient for a given application. Note, however, that the exact relationship between them depends on the detection scheme that is used and on the aforesaid assumptions of Gaussian noise, optimised decision threshold, and high extinction ratio, that if violated could lead to inaccurate system performance estimates.

Impact of intersymbol interference and pattern effects on BER:

Another important aspect that cannot be overlooked when estimating the BER through the Q-factor is the presence of inter-symbol interference (ISI) or pattern effects on the detected signal. In fact, in this case, there is typically no single value for I_0 and I_1 or for σ_0 and σ_1, as the eye diagram exhibits a number of different traces for the 1-bits and 0-bits. To illustrate this concept Fig. 2.9 shows the eye diagram and associated histograms of a sequence of bits intentionally degraded by using a low pass filter with a cut-off frequency of 2.5GHz in order to induce ISI.
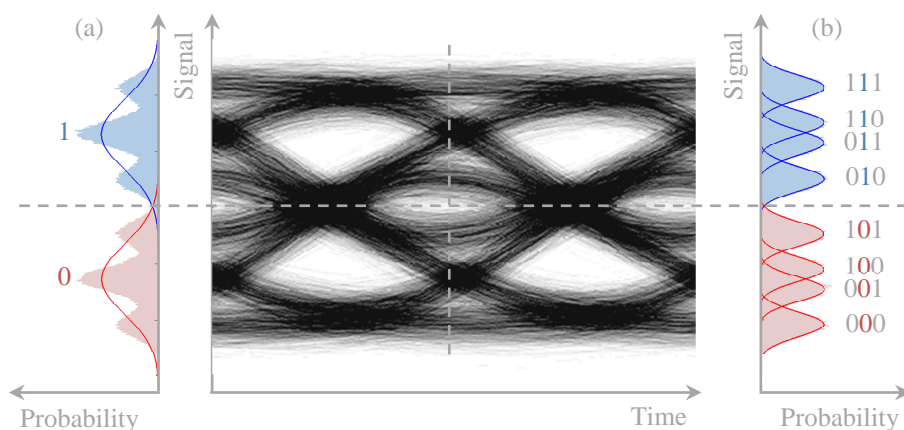
Figure 2.9: Electrical eye diagram at the receiver output and Gaussian probability densities of 1- and 0-bits with: no ISI-prebits and ISI-postbits (a); one ISI-prebit and one ISI-postbit (b).

ISI can be seen as the dependence of the signal representing the current bit on the preceding and following bits. The effect of ISI on stochastic BER estimation is to overestimate the BER (Fig. 2.9(a)). However, this overestimation can be reduced by grouping identical patterns of bits before estimating the associated probability density functions and hence their BERs (Fig. 2.9(b)). The numbers of preceding and following bits to be grouped in a pattern are often called ISI-prebits and ISI-postbits. Such a bit pattern is referred to as a meta-symbol. For example, if only one preceding and one following bit is considered, there are eight possible meta-symbols[1]: four corresponding to a logical '1' (i.e. 010, 011, 110, 111) and four meta-symbols corresponding to a logical '0' (i.e. 000, 001, 100, 101). As with the case of simple '1' and '0' symbols, the BER can be

---

[1] $2^{\text{1-pre+1-current+1-post}} = 2^3$.

calculated separately for each meta-symbol using Eqs. (2.4.2) and (2.4.3) with the respective values of average currents and standard deviations associated to such meta-symbol. The total error probability is then given by a weighted sum of all the 'partial' BERs estimated for the various meta-symbols. This is the principle behind the stochastic BER estimators used in current design automation software for photonic systems such as VPItransmissionMaker[TM]. In the experiments and simulations presented in this thesis, both conventional counting techniques and stochastic estimation techniques have been employed. Note however that all the BER values reported in the following chapters are measured by counting, while estimation techniques are used only as a further verification and to gain a deeper insight on the impairments taken into account by generating useful eye pattern histograms and statistical data not otherwise easily obtainable.

2.4.1   OSNR and Power Penalties

The transmission of a signal over the fibre can suffer from a number of different impairments, as described in the previous sections. In optically pre-amplified systems the effect of such impairments on the transmission performance can be captured by the difference between the required OSNR[1] measured with and without the respective impairment. This difference is referred to as OSNR penalty [44]. In order to measure and understand the system performance in terms of BER, then the receiver needs to be deliberately stressed to introduce the effects of the various noise mechanisms discussed above. For instance, in optically pre-amplified systems where the beat noise (signal-ASE) is typically the dominant noise mechanism, the receiver can be stressed with respect to the impairment under test by adding a controlled amount of ASE noise to the incoming signal in order to degrade the OSNR (and thus the electrical SNR, see Eqs. (2.3.15) and (2.3.16)). This concept is illustrated in Fig. 2.10(a), where the system BER is plotted as a function of the received OSNR for different values of transmitter extinction ratio[2].

Note that sweeping the extinction ratio effectively captures the difference between a 'good' and a 'poor' transmitter rather than the effect of one of the fibre impairments discussed above. The extinction ratio is used in this context

---

[1]Defined as the minimum necessary OSNR that is required to achieved a target BER.
[2]The extinction ratio is defined as the ratio between the optical power P_1 of a 1-bit and the optical power P_0 of a 0-bit.
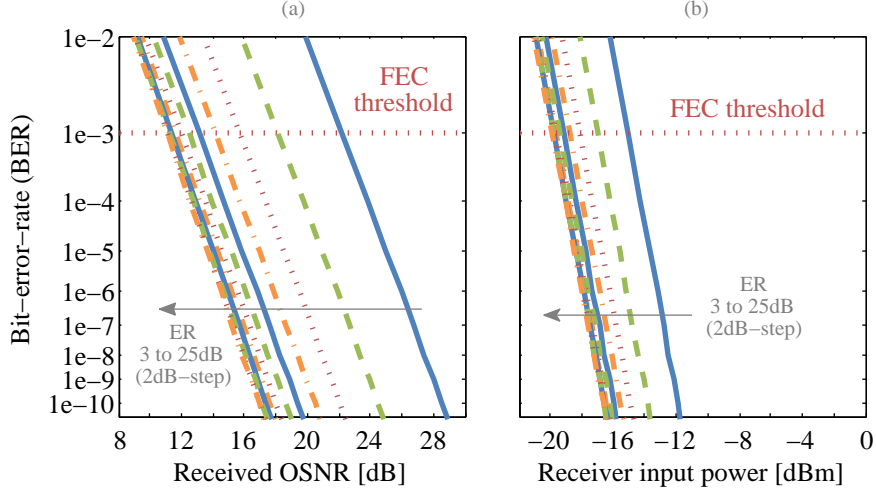
Figure 2.10: Simulated (analytical) results showing the dependence of system BER on input received OSNR (a) and power (b) for different values of transmitter extinction ratio (ER, from 3dB to 25dB in steps of 2dB).

purely for convenience to make this treatment easier to follow and to understand. In fact, the effects of extinction ratio are relatively simpler to describe analytically in comparison to the effects of other system impairments such as CD, PMD, patterning-induced distortions, etc. Conceptually, however, the same system characterisation methods can be applied also to any of the aforesaid fibre impairments with no difference whatsoever. For example, an extensive (numerical) analysis on CD will be presented in the following chapters using the system characterisation techniques discussed in this section.

If the systems of interest are not optically pre-amplified, on the other hand, they are typically thermal noise limited and the performance is therefore measured in terms of power penalty rather than OSNR penalty. In this case the receiver can be stressed with respect to the impairment under test by reducing the input power to the receiver (for the same amount of thermal noise) to degrade the electrical SNR (see Eq. (2.3.8)). This concept is illustrated in Fig. 2.10(b), where the system BER is plotted as a function of the receiver input power for different values of transmitter extinction ratio. Similarly to the beat noise limited case, the effects of the impairment of interest (i.e. extinction ratio in this case) are captured by the difference between the required input power to achieve a target BER with and without the respective impairment. This difference is referred to as power penalty. In the remainder of this thesis, the systems characterised by reducing the OSNR (Fig. 2.10(a)) are referred to as OSNR-limited systems,

whereas the systems characterised by reducing the optical input power to the receiver (Fig. 2.10(b)) are referred to as power-limited systems.
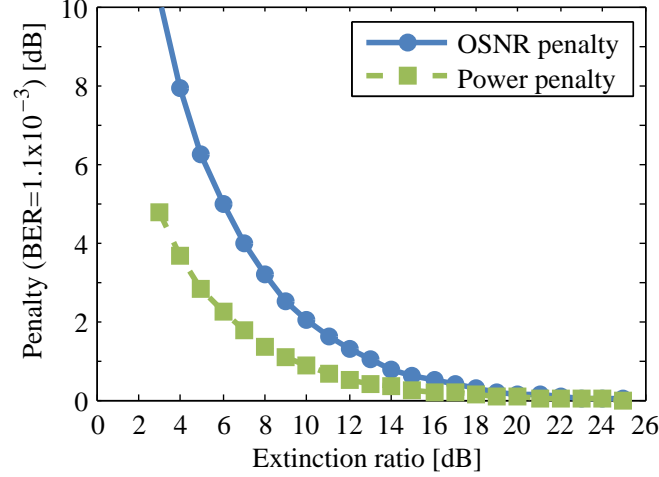

Figure 2.11: OSNR and power penalties at FEC threshold (BER=1.1×10^{-3}) as a function of the transmitter extinction ratio.

Both the x-axes of Figs. 2.10(a) and 2.10(b) are intentionally plotted using the same scale to cover for an input OSNR and power range of approximately 20dB(m). This is deliberately done in order to better emphasise the different nature of the two systems under test, whose curves clearly result in significantly different slopes and shifts. In particular, in the power-limited case the curves present a greater slope in comparison to the OSNR-limited case, as well as a reduced shift between different extinction ratio values. Another way of looking at this is to plot the respective OSNR and power penalties necessary to achieve a target BER of e.g. 1.1×10^{-3} for the different values of extinction ratio taken into account[1]. This is shown in Fig. 2.11, where the OSNR and power penalties are calculated using as reference the respective highest extinction ratio curve taken into account (25dB). From Figs. 2.10 and 2.11 it is clear that for high extinction ratio values (e.g. >15dB) both system types present similar performance with nearly negligible penalty in comparison to their respective reference curve. However, when the extinction ratio is reduced to more realistic values (<15dB, i.e. typical values achieved by the modulators employed in the experiments presented in this thesis), the two system penalties start to perform rather differently, with

---

[1]Throughout this thesis the use of Reed-Solomon (223,255) forward error correction (FEC) is assumed, as is commonly incorporated in PON standards today.

the OSNR-limited case rising much faster than the power-limited one. In order to better understand the reasons behind such a different behaviour, the OSNR-limited and power-limited cases can be compared by taking a detailed look at the analytical expressions used to model the system BERs of Fig. 2.10.

Note that Eqs. (2.4.4)-(2.4.7), which link the BER to the electrical SNR for thermal noise limited systems and beat noise limited systems, cannot be used in this context as the assumption of high extinction ratio is violated. For this reason it is necessary to rewrite the BER for the two system cases as a function of their respective Q-factor, which includes the 0-bits statistics as well.

Power-limited case:

From Eq. (2.4.3) the Q-factor for the power-limited case is given by

$$Q = \frac{I_1 - I_0}{\sigma_1 + \sigma_0} = \left. \frac{R \cdot P_{sig,1} - R \cdot P_{sig,0}}{\sigma_1 + \sigma_0} \right|_{\sigma_0 = \sigma_1 = \sigma_{th}} = \frac{R \cdot (P_{sig,1} - P_{sig,0})}{2 \cdot \sigma_{th}}, \quad (2.4.8)$$

where σ_{th} is derived from Eq. (2.3.7) and can be rewritten as

$$\sigma_{th} = \left(\frac{4k_B T}{R_L} F_n B_e \right)^{\frac{1}{2}} = NEP \cdot R \cdot \sqrt{B_e}. \quad (2.4.9)$$

The parameter k_B in Eq. (2.4.9) is the Boltzman constant, T is the absolute temperature, R_L is the load resistor, F_n is the (front-end) amplifier noise figure, and B_e is the effective noise electrical bandwidth of the receiver. The quantity

$$NEP = \left(\frac{4k_B T}{R_L \cdot R^2} F_n \right)^{\frac{1}{2}}, \quad (2.4.10)$$

is called noise-equivalent power (NEP) and is defined as the minimum optical power per unit bandwidth required to produce an SNR = 1. It is essentially a measure of the sensitivity of a photodetector and it is often used to compare different receiver noise specifications. Regarding the effective noise electrical bandwidth of the receiver B_e, note that it is different from the typically stated 3dB bandwidth (B_{3dB}). For a Bessel filter response (as is often the case for these applications [45]), for example, the two are related according to the relation $B_e = (\pi/2) \cdot B_{3dB}$. Remembering that the extinction ratio ER and the received

average optical power P_{Rx} are defined respectively as

$$ER = \frac{P_1}{P_0},\tag{2.4.11a}$$

$$P_{Rx} = \frac{P_0 + P_1}{2},\tag{2.4.11b}$$

it is possible to rewrite Eq. (2.4.8) as

$$Q = \frac{R \cdot P_{Rx}}{\sigma_{th}}\left(\frac{ER - 1}{ER + 1}\right).\tag{2.4.12}$$

Note that the curves of Fig. 2.10(b) have been generated by substituting Eq. (2.4.12) into Eq. (2.4.2), with a B_{3dB} of 12.5GHz and a NEP of 24pW/Hz$^{\frac{1}{2}}$. Both these values have been obtained from the datasheet of a conventional 10Gb/s off-the-shelf receiver.

OSNR-limited case:

Using the expressions for the signal-ASE and ASE-ASE beat noise variance in Eqs. (2.3.13)-(2.3.14) and the relation between P_{ASE} and S_{ASE} of Eq. (2.2.8), the noise variance corresponding to the 1-bits can be written as

$$\sigma_1^2 = 2R^2 P_{ASE} P_{sig,1}\frac{B_e}{B_{ref}} + R^2 P_{ASE}^2 \frac{B_e}{B_{ref}^2}B_{opt},\tag{2.4.13}$$

where B_{opt} [Hz] is the bandwidth of the optical filter used before the receiver. Expressing Eq. (2.4.13) in terms of extinction ratio ER and OSNR, the noise variance for the 1-bits becomes

$$\sigma_1^2 = R^2 P_{ASE}^2 \frac{B_e}{B_{ref}}\left(4 \cdot OSNR\frac{ER}{ER + 1} + \frac{B_{opt}}{B_{ref}}\right).\tag{2.4.14}$$

Similarly, the noise variance for the 0-bits can be derived as

$$\sigma_0^2 = R^2 P_{ASE}^2 \frac{B_e}{B_{ref}}\left(\frac{4 \cdot OSNR}{ER + 1} + \frac{B_{opt}}{B_{ref}}\right).\tag{2.4.15}$$

Using, once again, Eq. (2.4.3) the Q-factor for the OSNR-limited case can be finally written as

$$Q = \frac{I_1 - I_0}{\sigma_1 + \sigma_0} = \frac{R \cdot P_{sig,1} - R \cdot P_{sig,0}}{\sigma_1 + \sigma_0}$$

$$= \frac{2 \cdot OSNR \left(\frac{ER-1}{ER+1}\right) \cdot \sqrt{\frac{B_{ref}}{B_e}}}{\sqrt{4 \cdot OSNR \frac{ER}{ER+1} + \frac{B_{opt}}{B_{ref}}} + \sqrt{\frac{4 \cdot OSNR}{ER+1} + \frac{B_{opt}}{B_{ref}}}}. \quad (2.4.16)$$

Note that the curves of Fig. 2.10(a) have been generated by substituting Eq. (2.4.16) into Eq. (2.4.2), with $B_{ref} = 12.5$GHz, $B_{3dB} = (2/\pi) \cdot B_e = 12.5$GHz, and $B_{opt} = 50$GHz.

OSNR and power penalties different behaviour:

From Eqs. (2.4.9) and (2.4.13)-(2.4.15) it is clear that the noise variances for the power-limited and OSNR-limited systems have radically different characteristics. In fact, while the thermal noise variance is completely independent of the optical power of the signal incident on the photodetector, the beat noise variance is proportional to it, as well as to the power of the optical noise. This means that if in a power-limited system the Q-factor needs to be increased by a certain amount in order to compensate for the effect of a given impairment, it will be sufficient to increase the received input power P_{Rx} by the same amount (see Eq. (2.4.12)).

In contrast, this is not true for the case of OSNR-limited systems, as increasing the OSNR by the aforesaid amount also increases the beat noise by a proportional factor. Indeed, looking at Eq. (2.4.16), it is possible to note that both the numerator and denominator are dependent on the OSNR. However, while the numerator is characterised by a linear relation with the OSNR, the denominator is only proportional to its square root, and hence increasing the OSNR is still beneficial. This different dependence of the noise variance on P_{Rx} and on the OSNR for thermal noise limited and beat noise limited systems respectively, is fundamentally the physical reason for the different trend between the curves of Fig. 2.10(a) and Fig. 2.10(b) (or, equivalently, the reason why the OSNR penalty curve of Fig. 2.11 rises faster than the power penalty curve for the same amount of impairment). It is possible to conclude from this line of reasoning that the concept of penalty could potentially be misleading if the type of noise limited system that the penalty is associated with is not specified.

2.5 Summary

In this chapter, the fundamental impairments that affect a fibre optic system have been described. These can be categorised as linear distortions (such as fibre loss, GVD, PMD, and adjacent channel crosstalk), nonlinear effects (such as Kerr-effects and inelastic scattering phenomena), and noise. Each one of the aforesaid linear and nonlinear effects has been briefly discussed. For the power levels, bit rates, and transmission distances of interest in this work, the majority of them do not have a significant impact on the system performance, or can even be beneficial like the interplay of SPM and GVD. As a result, chromatic dispersion can be reasonably assumed to be the dominant effect degrading the signal quality, and for this reason in the remainder of the thesis attention is focused on this type of impairment only. The pulse broadening resulting from chromatic dispersion has been discussed, and the physical reason for this is the wavelength dependence of the fibre's refractive index.

The transmission distance of any fibre optic system is eventually limited by fibre losses. The use of optical amplifiers to compensate for such losses, along with the general concepts common to all optical amplifiers such as gain saturation and signal degradation due to amplifier noise, have been discussed. In particular, it has been shown that the main disadvantage of optical amplification is the generation of amplified spontaneous emission noise, which can accumulate along a transmission link eventually compromising the maximum achievable OSNR.

The dependence of optically amplified system performance on the received OSNR due to the optical noise that is converted into electrical beat noise components has been discussed. In addition to such a beat noise contribution, the other two fundamental noise mechanisms generated at the receiver, namely the thermal noise and shot noise, have also been described. For the applications of interest in this work, thermal noise and beat noise can be assumed to be the dominant mechanism of noise in a power-limited system and OSNR-limited system respectively.

Finally, it has been shown that the impact of a given impairment on the system performance can be captured in terms of bit-error-rate by deliberately stressing the receiver in order to introduce the effects of the aforesaid noise mechanisms. That is, thermal noise for power-limited systems and beat noise for OSNR-limited ones. The overall performance of these two system types in terms of power

penalty and OSNR penalty respectively can be significantly different. This has been demonstrated both qualitatively (through bit-error-rate and power/OSNR penalty curves) and analytically. The reason for such a different behaviour is due to the fact that, unlike the thermal noise of the receiver, the signal-ASE beat noise is proportional to the optical power of the signal as well as the optical noise incident on the photodetector. As a consequence of this, it should be noted that the concept of penalty alone without any information on the system that the penalty is associated with (e.g. power-limited or OSNR-limited), could potentially be misleading, as the same value of penalty in different systems can have a radically different interpretation and impact.

Chapter 3

Next Generation Optical Access

The present access network, which connects subscribers to their immediate service provider, is still mainly copper cable-based and it is currently being upgraded in order to support the growing bandwidth demand. In fact, copper cables have effectively achieved their physical limits and more advanced solutions capable of meeting the bandwidth requirements of (future) new services, such as video on demand, videoconferencing, high-definition TV (HDTV), E-learning, interactive games, voice over IP, etc., are therefore necessary. Wireless access technology, such as WiMAX, is relatively simple and cost-effective, but, although continuously improving, it will never approach the current or future speed achievable via fibre optic-based solutions. Indeed, passive optical networks (PONs) are seen by telecom operators and the research community as one of the most promising and future-proof candidates for next-generation optical access [6]. In this chapter, some of the proposed schemes for all optical access networks as well as the major challenges associated with them will be discussed.

Section 3.1 illustrates the evolution of today's access networks. Some of the technologies that are commercially available and already deployed are reviewed, and the new trends that are aiming at increasing the network efficiency and flexibility and at reducing the operating costs are also discussed.

The burst-mode nature of the upstream link in PONs represents one of the major challenges related to the use of time division multiple access protocols. This type of transmission along with some of its key enabling technologies is briefly presented in Section 3.2.

The long-reach of next-generation PONs in combination with bit-rates of at least 10Gbit/s necessitates the use of some form of chromatic dispersion compen-

sation, in particular if cost-effective transmitters are employed in the upstream direction of the network. Some of the main optical and electrical compensators are briefly presented and compared in Section 3.3. Some of the implementation options for an electronic-based compensator are also discussed.

Section 3.4 describes a novel solution that could potentially be used as an upstream reach-extender in traditional PONs. Such a reach-extender consists of a cascade of two semiconductor optical amplifiers which can be carefully optimised to provide a significant dynamic range compression and to enable the use of an ac-coupled continuous-mode receiver at the optical line terminator.

3.1 Access Network Evolution

To keep up with increasing bandwidth demands, telecoms operators are migrating from copper-based networks to fibre-based networks, which promise to deliver higher speeds. However, migration to an all-fibre network infrastructure requires major investment and takes considerable time to complete. In the short term, therefore, access to high-speed broadband services will still be provided by copper-based solutions [3]. Among these, the most widely used employ DSL (digital subscriber line) technologies and coaxial cable-based schemes. The latter reutilise the cable television (CATV) network that was originally established as a high-quality alternative to terrestrial television broadcasting. On the other hand, the DSL family includes asymmetric digital subscriber line (ADSL) and very high speed digital subscriber line (VDSL) solutions, and provide digital data over the wires of a local telephone network (the classical 'twisted pair'). A number of wireless technologies are also used to provide broadband services: these include mobile radio solutions (e.g. HSPA, LTE), fixed radio solutions (e.g. WiMAX), and satellite solutions. However, it is clear that copper-based and wireless technologies will not be able to satisfy the continuously growing demand for higher bit-rates due to physical media constraints which eventually limit the performance either in terms of bandwidth or physical reach.

This has driven operators to consider new architectures, based e.g. on optical fibre cables, that can provide a significant increase in bandwidth in comparison to the more conventional media outlined above, while reducing at the same time the cost associated with such a bandwidth provision. One of the most effective ways to reduce costs in telecommunications networks has been, historically, sharing

network capacity among multiple users. This has been a natural choice in metro and core networks, where traffic is progressively aggregated into a smaller number of higher-capacity links [46]. In the access, however, because of the need to maximally reuse the already existing infrastructures, networks have been deployed as point-to-point links connecting users directly to the local exchanges. Nevertheless, the recent deployment of fibre technology in the access has removed such capacity constraints, making sharing of access link capacity feasible and cost effective. Indeed, this idea has been exploited in current passive optical network (PON) deployments.

A PON is a point-to-multipoint fibre-to-the-X (FTTX[1]) network architecture in which optical splitters are used to enable a single optical fibre to serve multiple users. The term passive derives from the fact that in a conventional PON there are no powered components deployed in the field. A PON consists of an optical line terminal (OLT) at the local exchange (LE) and a number of optical network units (ONUs) at customer premises. It is immediately clear that a PON configuration reduces the amount of fibre and central office equipment required compared with point-to-point architectures.

DS
λ_D: 1.49μm

Passive optical splitter (1×N)

Optical line termination (OLT) at local exchange (LE)

US
λ_U: 1.31μm

Optical network units (ONUs) at customer premises
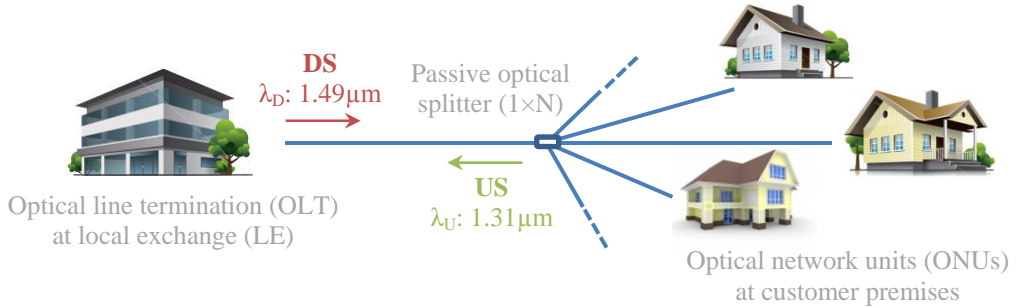
Figure 3.1: Typical configuration for E-PON, and G-PON.

It is widely accepted that PONs are the most promising, cost-effective, and high-performance access network solutions [47, 48, 49]. PON technology has been available since the mid-1990s, and significant development activities occurred during the early 2000s with the Gigabit-capable solutions [50]. The first generation of these solutions are now standardised and commercially available: the Ethernet PON (E-PON) from IEEE [7] and the Gigabit PON (G-PON) from ITU-T [8], typically offer 2.5Gb/s or 1.25Gb/s downstream and 1.25Gb/s upstream shared

---

[1]X is a generic letter indicating how close the fibre-end comes to the actual user: H for home, O for office, P for premises, C for curb/cabinet, N for neighbourhood.

between 32 customers via passive optical splitters and time division multiple access (TDMA) protocols, over a reach of up to 20km [51]. A simplified illustration of E-PON and G-PON architecture is shown in Fig. 3.1, where single-fibre operation is made possible using wavelength division multiplexing (WDM) with upstream wavelengths in the 1310nm region and downstream wavelengths in the 1490nm region [52].

PONs have been widely deployed around the world. In Europe, smaller operators have installed point-to-point Ethernet networks, but G-PON is rapidly becoming the preferred choice among major operators. G-PON is the dominant technology choice in North America. Asia saw significant E-PON deployments in Japan and South Korea. China, which is the world's largest FTTH market, recently embarked on a large-scale deployment using a mix of E-PON and G-PON [53].

3.1.1 Long-Reach PONs

One of the problems facing the telecommunications industry is that the cost of increasing network capacity to meet the inevitable demand for bandwidth driven by broadband services can far exceed the subsequent growth in revenues [6]. Conventional networks are built upon a large base of electronic equipment which only price declines in line with the usual price declines seen within the electronics industry[1]. In [5] it is also shown that if this learning curve is applied when the expected bandwidth growth is substituted for volume, the growth of the associated costs is remarkably steeper even than any overly optimistic (greater than typical sustainable rates) revenue growth. In other words, future network architectures that continue to use traditional electronic solutions will not be able to price decline sufficiently fast to be able to maintain profitability. From this perspective it is clear that with these bandwidth growth figures there will be a decline in margins unless new solutions are found, that can yield faster unit cost decline than electronic solutions have traditionally produced. Radical new architectures may be necessary to change the network structure and massively reduce the cost of bandwidth provision [54].

One potential solution to this problem is to simplify the current network ar-

---

[1]On average, electronic products have traditionally followed an 80% price learning curve [5], i.e. for every doubling of product volume the unit price dropped to 80% of the previous price.

chitecture: this could be achieved, for instance, by combining the access and metro networks into a single, integrated, all-optical system by using optical amplification, as shown in Fig. 3.2. This would allow the disposal of rather expensive electronic components and nodes within the network (such as optical/electrical/optical converters), offering much higher capacities and much smaller equipment inventory [6]. The idea of increasing the reach and/or split of PONs via intermediate equipment has been of research interest since the 1990s, and in more recent years the attention has been focused on extending the reach of G-PON and E-PON via mid-span optical amplifiers [52], a concept that has recently been standardised by ITU-T [55]. Now, this technology is known as long-reach PON[1]. The actual achievable transmission distance physically depends on factors like splitting-ratio, wavelength, laser type, etc., and for traditional systems like G-PON the protocol supports a maximum logical reach of 60km [14]. However, for more advanced network architectures this target reach can be increased significantly up to 100km or beyond (see Section 3.1.3).
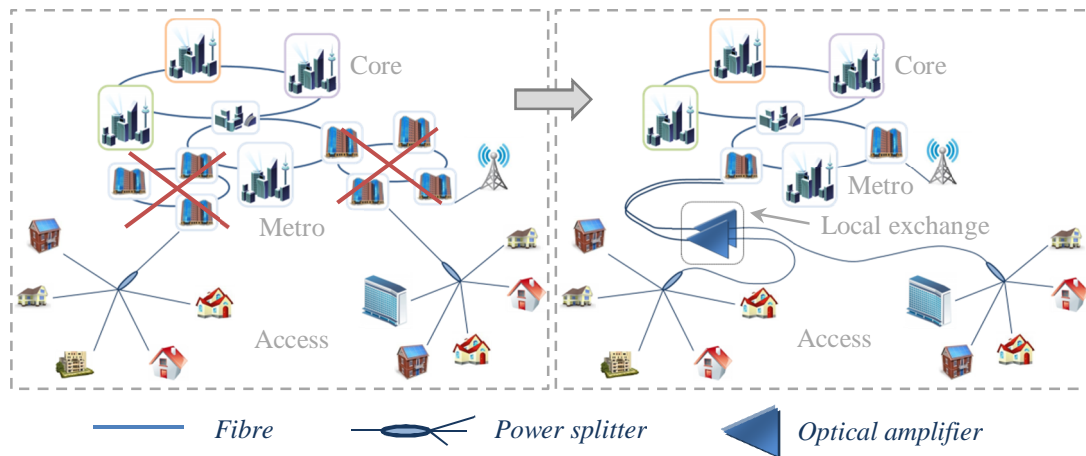
Figure 3.2: Example of network simplification and node consolidation through integration of access and metro networks into a single all-optical system by using optical amplification.

Optical amplifier technology options:

There are available several technology options to provide optical amplification employing either optical fibre or semiconductor gain media. In metro and long-

---

[1]Note that in this context the term passive does not strictly mean unpowered, but is related to the absence of active electronic routing elements in the field.

haul networks erbium-doped fibre amplifiers (EDFAs) are widely used as they provide excellent gain, power, and noise performance in the 1530–1565nm wavelength window. The range can be shifted to the longer wavelength band (e.g., 1570-1605nm) by changing the design parameters [51]. EDFAs allow amplification in the low attenuation region of the optical fibre and for this reason they rapidly became one of the most popular options for present fibre links. While the vast majority of commercial optical-fibre amplifiers deployed to date are EDFAs, alternative fibre amplifiers, which operate in other wavelength regions, are possible. Of particular interest with regard to a standard PON are praseodymium doped fibre amplifiers (PDFAs) for the upstream and thulium doped fibre amplifiers (TDFAs) for the downstream. Note, however, that these options are not taken into account in this work (the reader can refer to [56, 57, 58] for further details).

An alternative to fibre amplifiers are the semiconductor optical amplifiers (SOAs), which are based on mature III-V semiconductor technology and, as such, there are commercial devices available from many vendors in the marketplace. This should ensure that costs can be low enough for the access network, and that there is little development required to bring suitable products to volume production [58]. While SOAs do not provide as good gain and noise performance as EDFAs, they have the advantages of small size, high reliability, low power consumption, easy integration with other components on a single planar substrate, as well as the advantage of being able to operate at any wavelength of interest (800-, 1300-, and 1500nm windows) [52]. For this reason SOAs are considered attractive candidates for reach extension in conventional (e.g. G-PON and E-PON) systems.

In this thesis, both the SOA and EDFA options are explored for the LR-PON application and further details on their operation are provided in the remainder of this chapter. In particular, in Section 3.4 a comprehensive study is presented to illustrate a special case of an SOA-based reach-extender suitable for use in the current G-PON or E-PON standards. In the remaining part of the thesis, attention is moved towards more radical new architectures where the optical amplifiers have to support multiple WDM channels, and hence higher aggregate powers, operating over longer reaches compared to G-PON or E-PON. In this case, EDFAs offer significantly superior performance to SOAs and have been chosen as reach-extenders and/or preamplifier solutions.

3.1.2   Next Generation PONs (NG-PONs)

Worldwide, operators are seeking to increase revenue by developing new services: an example is represented by HDTV, which requires about 20Mb/s per channel [59]. Furthermore, in the near future, new business models such as home video editing, online gaming, interactive E-learning, remote medical services, and next-generation 3D-TV will dramatically increase bandwidth demand. As a consequence, much more is expected from PONs, including improved bandwidths and service support capabilities, as well as enhanced performance of access nodes and supportive equipment over their existing PON networks. All this implies that operators need to make a careful decision about the investment into FTTX technology. For this reason, in early 2006, IEEE began to work on an even higher-speed 10Gb/s Ethernet PON (10G-EPON) standard, that was ratified in 2009 as IEEE 802.3av [15]. Similarly, in late 2006, the full-service access network (FSAN) group and ITU-T began to work on the standard that would follow the G-PON. At first, a number of systems were proposed as possible candidates, but it proved rather difficult to perform a realistic comparison between them as many of them were radically different in architecture and service profile. As a consequence, the system proposals were divided into two groups, as shown in Fig. 3.3:
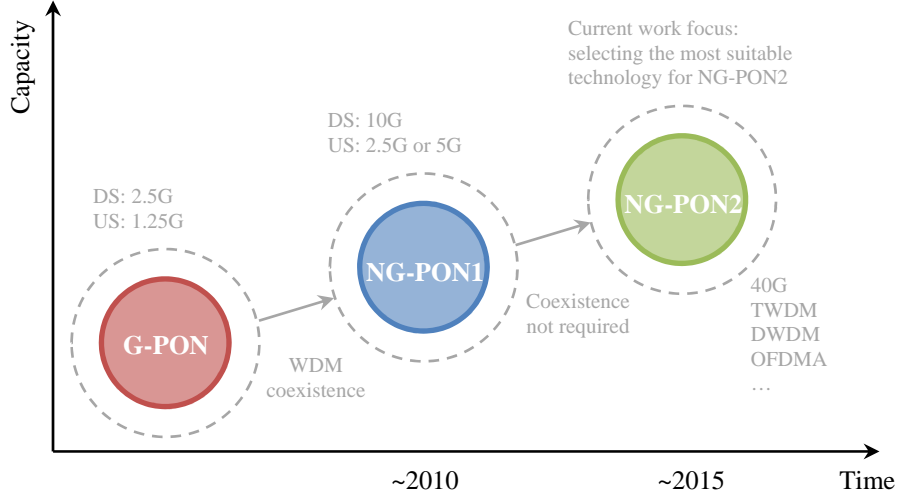
Figure 3.3: NG-PON roadmap by FSAN [59] (DS: downstream, US: upstream, TWDM: time and wavelength division multiplexing, DWDM: dense wavelength division multiplexing, OFDMA: orthogonal frequency division multiple access).

NG-PON1:

The next-generation PONs (NG-PONs) was divided into two phases namely NG-PON1 and NG-PON2, a mid-term and a long-term solution respectively. The first group included systems that could coexist with G-PON on the very same optical distribution network (ODN), while the second group included all other systems that either required a different ODN, or required technologies that were not available in the expected time horizon. This key decision on the scope of NG-PON1 enabled the comparison of a reasonable set of alternative systems (see [60] for further details), among which the 10Gb/s downstream (DS) and 2.5Gb/s upstream (US) was selected the best candidate for standardisation development as an optimum compromise between compatibility, technical risk (not too forward looking), costs, etc. [59, 61]. This system, named XG-PON and described in the ITU G.987 series [16], was standardised in 2010 and it can be effectively seen as an enhancement of G-PON in terms of channel rates.

NG-PON2: TWDM-PON:

The NG-PON2 project was initiated by FSAN in 2011 with the objective of investigating new technologies enabling a bandwidth increase beyond 10Gb/s [62]: the basic requirements were for a system with at least 40Gb/s of capacity, 40km reach, 1:64 split-ratio, and at least 1Gb/s access rate per ONU, but not necessarily backward compatible with existing ODN technology or even previous PON systems. Based on this very loose scope of requirements, many different systems were proposed, among which [12]:

- 40Gb/s TDM-PON (named XLG-PON), which increases the single carrier serial downstream bit rate for XG-PON from 10Gb/s to 40Gb/s, while the upstream supports a 10Gb/s serial TDMA bit rate;

- Time and wavelength division multiplexed PON (TWDM-PON), which stacks multiple XG-PONs using WDM;

- WDM-PON, which provide a dedicated wavelength channel at the rate of 1Gb/s (symmetrical) to each ONU;

- Orthogonal frequency division multiplexed (OFDM)-based PON, which employs quadrature amplitude modulation and fast Fourier transform to generate digital OFDM signals for transmission.

In 2012 the FSAN community selected the TWDM-PON as the primary approach for NG-PON2, which is now in the process of being standardised by ITU-T. In fact, operators consider TWDM-PON to be less risky, less disruptive and less expensive than other approaches because it reuses existing components and technologies. Fig. 3.4 shows the basic TWDM-PON architecture, where four pairs of wavelengths support aggregated rates of 40Gbps in the downstream (DS, 4×10Gb/s) and 10Gbps in the upstream (US, 4×2.5Gb/s), effectively stacking four XG-PON architectures. The proposed wavelength plan (ITU-T G.989.2 – draft in progress) defines a 100GHz DWDM (dense WDM) grid from 1596.34nm to 1603nm for the DS, and a 50GHz or 100GHz DWDM grid from 1524nm to 1544nm for the US.
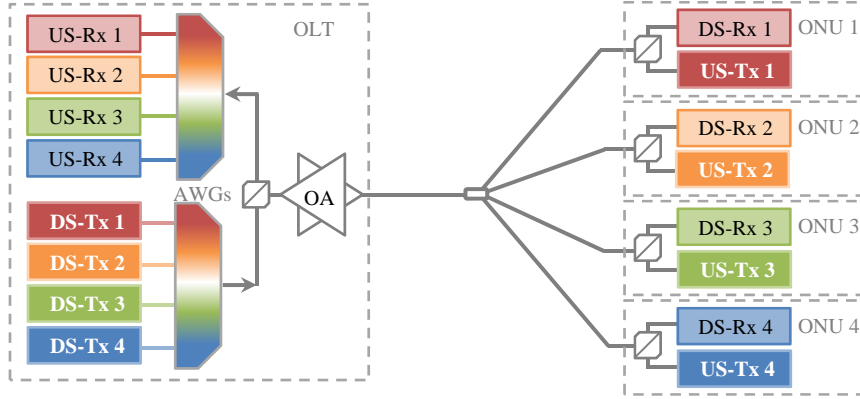
Figure 3.4: Simplified TWDM-PON system architecture (US: upstream, DS: downstream, Tx: transmitter, Rx: receiver, OA: optical amplifier, OLT: optical line terminal, ONU: optical network unit, AWG: arrayed waveguide grating).

Each ONU is equipped with a tunable transceiver, so it can selectively transmit and receive data on a pair of US/DS wavelengths. This avoids ONU inventory issues and supports load balancing within the TWDM-PON. On the other hand, the need for such tuneable optical components represents the main challenge for TWDM-PON architectures. In fact, while most of the TWDM-PON components are commercially available[1], tuneable devices (such as tunable lasers and tunable filters) based on current technologies require expensive temperature-stabilisation control circuitry and despite research activities to lower the cost of these technologies, they are not ready for mass production. This problem is still being

---

[1]Already developed for XG-PON reusing the mature technology from the optical transport network.

addressed and vendors are currently developing new technologies to help reduce the costs. The use of photonic integrated circuits (PICs), for instance, is highly attractive because the potentially low cost manufacturing process would enable mass deployment [53].

In order to achieve a power budget higher than that of XG-PON, optical amplifiers (OAs) are used at the optical line terminal (OLT) side to boost the DS signals as well as to preamplify the US ones. Note that despite the use of active elements (they are located at the OLT side), the ODN remains passive. The preliminary information on this NG-PON2 architecture indicates that, given the similarity in ODN loss budget compared to XG-PON, the reach can also be increased from 20km up to 60km by using an intermediate reach-extender.

The current situation for XG-PON and 10GE-PON is that products are available from multiple vendors, and these products are being trialled at low volume. However, while accessible for some time, these solutions have generated little traction in the market, since there is limited near or medium term demand for 10Gb/s residential service to justify investment in new technology [61]. In the meantime, emerging technologies such as the TDWM-PON described above are also offering capabilities beyond higher speeds, and as a consequence the market focus is certainly moving towards NG-PON2. What is likely to happen, therefore, is that there will be a minor amount of XG-PON deployment, followed on by more extended deployments of NG-PON2. Nevertheless, this should not to be seen as NG-PON2 taking over the market from XG-PON as the majority of work that went into XG-PON is effectively being reused [61].

3.1.3   Long Term PON Developments

While the TWDM-PON architecture discussed above undeniably offers a significant improvement with respect to E-PON/G-PON and 10G-EPON/XG-PON, it does not introduce a radical innovation, but rather an incremental one. For this reason, researchers have always shown interest in more radical improvements to the PON architectures in comparison to NG-PON2, which would allow an even greater exploitation of the opportunities that are enabled by the introduction of optical fibre into the access network. A number of research projects ([9, 10, 11] among others), showed how employing hybrid DWDM-TDM approaches it is possible to achieve features totally beyond the capability of today's PONs: for

instance, using 32 wavelengths each carrying 10Gb/s shared by up to 512 ONUs, it is possible to achieve a network capacity of 320Gb/s with up to 16,384 users and over reaches of 100km [10]. Although the aforesaid projects have been very successful in demonstrating the potential of LR-PON and node consolidation concepts, they were not conceived with the objective of carrying out an exhaustive investigation of all the new key enabling technologies. For example, such systems were implemented using a static WDM approach, whereas the trend for future solutions is to avoid the lack of flexibility associated with these methods and to implement dynamic wavelength and time slot allocation, addressing one of the key limitations of today's existing access infrastructure. As a consequence, in 2012 the European FP7 Integrated Project DISCUS (DIStributed Core for unlimited bandwidth supply for all Users and Services) [46] was founded with the objective of filling the gaps of previous projects and of continuing the development of the missing enabling technologies.
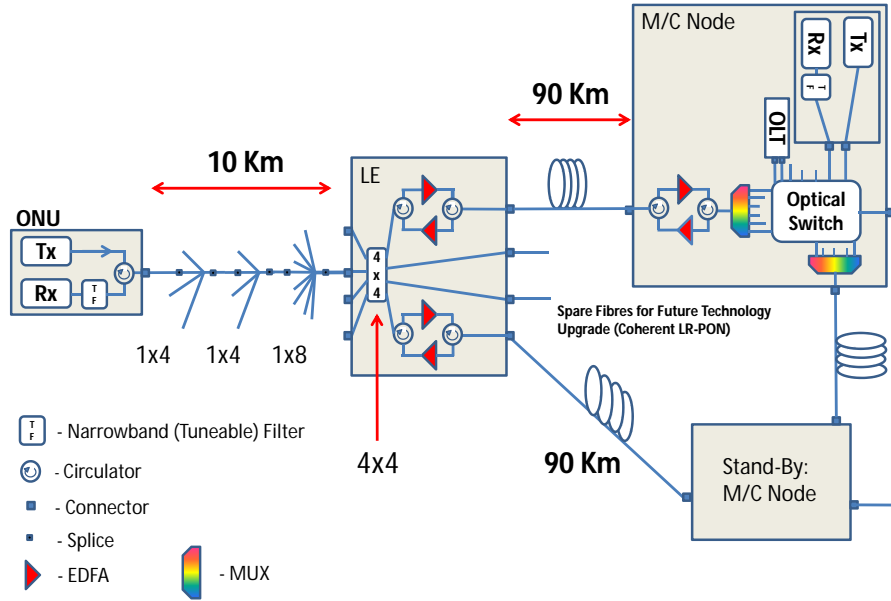
Figure 3.5: DISCUS initial (simplified) architecture (ONU: optical network unit, Tx: transmitter, Rx: receiver, ODN: optical distribution network, LE: local-exchange, M/C node: metro/core node, OLT: optical line terminal, EDFA: erbium-doped fibre amplifier, MUX: multiplexer).

The overall goal of the DISCUS project is to design a network architecture that can deliver ubiquitous high speed broadband access to all users independent of their geographical location. Figure 3.5 shows a simplified block diagram of one of

the basic (single fibre working in the ODN and two fibres working in the backhaul) DISCUS architectures which is currently under study. From this diagram it is clear that by introducing a longer fibre reach (>100km) from the user to the network node and a larger split in the ODN, a much larger number of customers (≥512) can be served by the same infrastructure. The longer optical reach allows fibre terminations from many PONs to be concentrated into a smaller number of nodes, each covering large areas. Thus, a substantial number of nodes deployed in current telecoms networks, which carry out electronic packet switching and processing, can be consolidated as long-reach access systems that can bypass local exchanges and terminate directly on a core node.

Recent studies have shown that the proposed DISCUS architecture would reduce the number of nodes carrying out electronic packet processing by almost two orders of magnitude [46, 63]. For instance, in a test scenario carried out for the U.K. network, the number of nodes with electronic processing equipment can technically be reduced from about 5600 down to around 75 [46, 64]. Similarly, the number of nodes of the Irish network could be reduced from 1100 to approximately 18 [64, 65], as illustrated in Fig. 3.6.

<table>
<tr><td>(a)</td><td>(b)</td></tr>
</table>
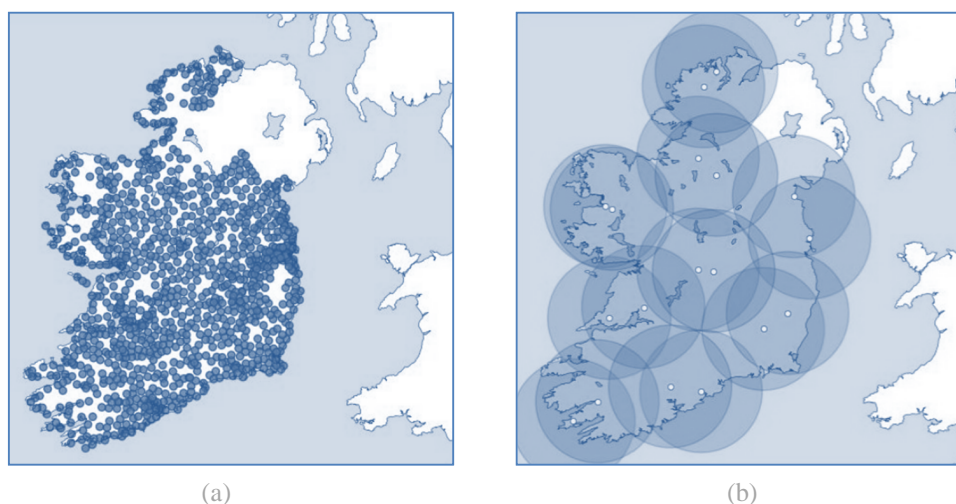
Figure 3.6: Ireland with all 1100 exchange buildings (a), and with 18 nodes (b).

The other main areas of interest within DISCUS include low cost tunable transceivers (with tunable optical filters), burst-mode electronic dispersion compensation (BM-EDC), burst-mode forward error correction (BM-FEC), dynamic bandwidth assignment (DBA), dynamic wavelength assignment (DWA), and higher rate multipoint and point-to-point wavelength services over PON infrastructure.

Among the above, the subject of particular interest in this thesis is the development of a BM-EDC: a number of simulations and experiments will be presented throughout the next chapters to demonstrate the feasibility of this technology as well as the requirements to operate in the network topologies presented in this section. The other key enabling technologies will not be discussed here and for a more complete description about the objectives and impact of the DISCUS project the reader can refer to [46, 65, 66, 67].

3.2 Burst-Mode Nature of Upstream Link

In a TDM PON system, all the users share the same wavelength and fiber infrastructure. In the downstream (DS) direction, data packets are broadcast to all ONUs and hence OLT transmitters and ONU receivers operate in continuous-mode (CM). Synchronisation is maintained at all times since, even if there is no data to send, the ONUs can still retrieve the clock continuously from the downstream signal as the OLT keeps transmitting idle bit patterns. In the upstream (US) direction, however, to avoid packet collision only one packet from a single ONU can be sent to the OLT at any given time[1]. Figure 3.7 illustrates such a concept, and this type of communication is known as burst-mode (BM) transmission.
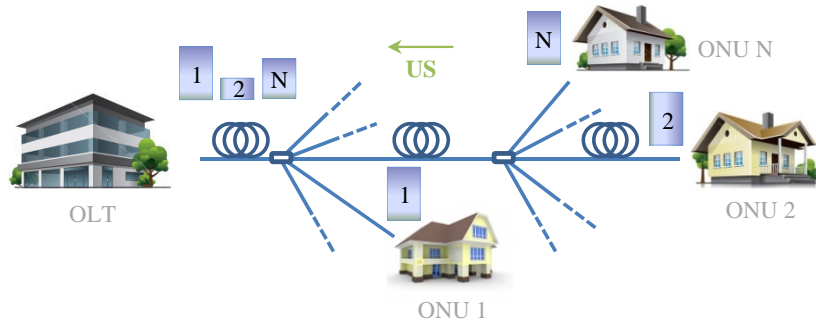
Figure 3.7: Example of a burst-mode upstream (US) link. The three optical network units (ONUs) operate in time division multiple access (TDMA) protocol and communicates with the optical line terminal (OLT) in their given time slot.

---

[1]The OLT coordinates all the upstream transmissions scheduling the time-slot associated to each user.

3.2.1 Key Enabling Technologies

While the state-of-the-art data rate for CM optical links is already over 40Gb/s, the BM components at Gb/s data rates still remain very challenging. In this section some of the key aspects associated with BM transmission are briefly discussed.

Burst-mode transmitters and receivers:

The fundamental difference of BM transmission from the conventional CM one is that even if all packets are launched from each ONU at the same average optical power, every one of them will undergo a different amount of fibre and number of splitters and arrive at the OLT with varying power levels depending on the individual path loss. Throughout this thesis, the burst arriving at the OLT with the highest power is referred to as loud packet (LP) and the one arriving with the lowest power as soft packet (SP). In Fig. 3.7, for instance, they correspond to packet 1 and 2 respectively. The power difference between bursts is often referred to as dynamic range and for the network topologies taken into account in this thesis it can be greater than 20dB ($\times 100$) [15, 16].

Furthermore, each burst arrives at the OLT with different (unknown) bit phase, as the propagation delay of the fibres will have a large variation compared to the bit period. This means that the OLT receiver should be able to adjust to different power levels as well as synchronise the phase on a burst-by-burst basis in a short period of time (e.g. tens of nanoseconds): that is, a BM transimpedance amplifier (BM-TIA) and a BM clock and data recovery (BM-CDR) need to be employed respectively. Similarly, at the ONU side each transmitter has to work in burst mode and this implies that it must be enabled/disabled in a brief period of time (from tens to hundreds of nanoseconds). In addition to such short turn-on/-off performance, the ONUs have also to guarantee substantial optical power suppression during the idle state, as the maximum limit on the aggregate off-state power is given by the sum of all off-state powers of inactive users. Therefore, another critical requirement in high-split networks is to minimise this sum sufficiently to prevent penalties arising from in-band crosstalk [68, 69].

As a result receivers and transmitters for PONs are quite different from their counterparts in point-to-point CM optical communication links and their design represents one of the major challenges posed by these transmission schemes.

Optical amplifiers in burst-mode:

In order to achieve long-reaches, it is necessary to employ optical amplification at the local exchange as well as pre-amplification in the metro/core node (see, e.g., Fig. 3.5). As mentioned in Section 3.1, EDFAs remain the preferred option due to their excellent performance in DWDM applications (high gain and output power, low noise etc.). Nevertheless, there is a major issue associated with the use of EDFAs in a PON and this is related to the BM nature of the upstream data. EDFAs operating with high output powers exhibit gain saturation effects, in which their gain is reduced. While this does not represent a problem for long-haul CM applications as the gain is not affected by any variation in the data stream, in the upstream link of a PON input power fluctuations can occur in a timescale of (fractions of) microseconds. Since EDFAs exhibit a slow relaxation response to variations in input signal level, this results in output signal distortion. In other words, if a LP enters the EDFA after a SP, the corresponding amplified signal would exhibit a large saturation-induced gain transient. As a BM receiver sets its gain and extracts a decision threshold from a short (tens of nanoseconds) preamble, any long transient (∼microseconds) will result in significant performance degradation and/or sync loss, or even damage to the receiver. Accordingly, suitable mitigation strategies must be employed.

The requirement to support channel add/drop in reconfigurable WDM networks, has recently driven developments in EDFA transient control circuitry [70] that may also provide a solution for supporting BM traffic. A number of gain stabilisation techniques have been reported for BM operation of EDFAs by using, for example electro-optical feedback [71, 72]. The details of these techniques are outside the scope of this thesis, but, in order to avoid the aforesaid issues, all experiments presented in Chapter 6 employ commercially available gain transient-suppressed EDFAs, which will be referred to as BM-EDFAs.

On the other hand SOAs do not introduce envelope transients in the packets because of their fast relaxation response. Hence, SOAs are able to operate in BM without need for additional control circuitry or out-of-band optical stabilising signals [52]. For this reason, they are often used not only as amplifiers, but also as gate switching devices [73]. A disadvantage of the SOA's fast relaxation response or gain recovery time (typically 100-500ps) is that when intense signals at a bit rate comparable to (or faster than) the gain recovery time are input to an SOA, the signal waveform can be distorted due to gain saturation. This effect

is also known as patterning (see Section 2.2.1 for further details). This means that a LP entering the SOA after a SP may not be affected by envelope transient distortion. However, it is very likely to be affected by patterning if extra measures are not adopted in order to avoid it. Indeed, if the dynamic-range between the two packets is high (for a 10G-EPON class PR20 the dynamic-range can be as high as 20dB [15]) the LP will certainly drive the SOA into (deep) saturation, resulting in a loss of performance. Further details on this matter will be given in Section 3.4.

This effect of distortion due to gain saturation not only results in patterning effects in single channel systems, but also in channel cross-talk in WDM systems. This is another reason why EDFAs are in general preferred for WDM amplification. However, SOAs are potentially low cost compared to EDFAs and, although they can effectively be used only for single-channel operation, they are suitable for the 'pay as you grow' business model often adopted in current PONs deployments [74].

3.3 Equalisation in Modern Optical Systems

As discussed in the previous sections, hybrid DWDM and TDMA PONs, which integrate fibre-to-the-home with metro networks, have been the subject of intensive research in recent years. The trend outlined in Section 3.1.3 indicates that such systems will have reaches greater than 100km and bit rates of at least 10Gb/s per wavelength in the downstream and upstream directions. It is clear that with increasing bit rates and increasing complexity of the optical layer, signal distortions are increasing as well, while the components and system tolerances are typically decreasing. Both linear and nonlinear distortions (in the optical domain) can limit the system performance. However, as outlined in Chapter 2, for the applications of interest in this work CD is assumed to be the dominant impairment, and for this reason in the remainder of this thesis attention will be focused mainly on this type of distortion.

Multiple techniques have been proposed and implemented in order to compensate/mitigate the physical impairments which arise in fibre optic systems. These techniques can be classified as purely optical or optoelectronic-based solutions. In the first case, compensators try to mimic the inverse transfer function of the linear physical impairment in the optical regime. For instance, the chromatic

dispersion accumulated over a given length of standard single mode fibre can be cancelled by sending the signal through a spool of fibre with the same magnitude but opposite sign of dispersion. On the other hand, optoelectronic compensators do not directly try to undo a specific physical effect but rather attempt to simultaneously address signal distortions of various physical origins by minimising the inter-symbol interference at the decision time point of each bit [13, 75, 76]. This minimisation concept will be discussed in greater detail in Section 4.4. In the following section, a brief review is presented in order to highlight the main advantages/disadvantages of both techniques.

3.3.1 Optical vs Electrical Equalisation

In direct-detection systems, the advantages of optical compensators/equalisers compared to electronic ones are manifold. To name a few, they operate prior to square-law photodetection, and can therefore make use of the full optical field information (amplitude and phase) rather than the optical intensity only, resulting in better performance of the equaliser. In addition, when used in WDM systems, optical equalisers can be placed in front of the WDM demultiplexer and operate simultaneously on multiple channels that are affected by similar impairments [77]. In contrast, electronic equalisers always act on the optical intensities of an individual channels after square-law photodetection, and are therefore inherently per-channel devices. On the other hand, compensation carried out in the analog optical domain employing, for instance, dispersion compensating fiber (DCF) or dispersion compensating gratings (DCGs) can present multiple disadvantages. DCF is bulky, costly, has large insertion loss, and is characterised by strong optical non-linear effects due to its small mode size. DCGs, as compared to DCF, present smaller form factor, lower cost, insertion loss, and optical non-linear effects. However, these methods have drawbacks such as sophisticated structures and complex control systems, limited tuneability, and undulatory behaviour of the dispersion (also known as group-delay ripple) that can lead to performance penalties [78]. Moreover, even though DCGs are optically transparent and can operate over a broad range of wavelengths, they typically suffer from the drawback that they do not achieve precise dispersion compensation across all channels.

In addition to all this, looking at the evolution of optical access networks, it is clear that the objective of future PONs is to provide enhanced agile architec-

tures combining TDM and WDM to increase user-density and resource-sharing, particularly allowing smooth upgrade to reconfigurable optical networks capable of dynamic bandwidth and wavelength allocation. In this scenario, optical compensators such as DCF or DCG present a another significant disadvantage, as the amount of dispersion compensation required in the upstream link of a TDMA-PON can vary from user-to-user and hence needs to be tuned on a case-by-case by the operator. In fact, DCF/DCG compensate well for CD as long as the differential reach (difference between maximum and minimum fiber length of all ONUs) is sufficiently small compared to the total network reach. If this is not the case, then a shared DCF/DCG module is no longer viable. This issue could be overcome using, e.g., an optical switch in order to interchange different DCF/DCG modules on a burst-by-burst basis: note, however, that this solution would exacerbate the disadvantages of cost, physical volume and optical insertion loss even further.

Consequently, electronic compensation techniques provide a superior solution in many respects, as they have no inherent insertion loss, negligible physical volume, and reduced CAPEX and inventory cost compared to DCF/DCG. Additionally, if electronic equalisation can be made adaptive from one TDMA burst to the next, high differential reach can also be supported. In direct-detection systems, it is reasonable to expect a lower CD tolerance of electronic compensators in comparison to optical ones, as the former does not retain the full optical field information. Nevertheless, it has been shown that the required reach (>100km) for the applications of interest in this thesis, can be achieved using 10Gb/s electronic equalisation with direct-detection [79]. Note that, in principle, EDC based on co-herent detection could also be implemented and has already been demonstrated [80, 81]. Such schemes can access both the intensity and the phase of the optical field, thus allowing full CD compensation. However, they require additional tight-specification optical components, and signal polarization and phase tracking or recovery, as well as power-hungry digital signal processing (DSP) circuitry which add additional hardware complexity and hence cost.

As a result, electronic compensation based on direct detection represents the preferable solution for the access applications of interest, and for this reason the remainder of this thesis will focus on such techniques. Table 3.1 summarises the advantages and disadvantages of both optical and electrical techniques, making a high-level comparison between them when employed to compensate for CD.

Feature	Optical	Electrical
Cost	✖	✔
Volume (space)	✖	✔
Bandwidth	✔ (multiple channel)	✖ (per-channel)
Bit-rate/format	✔ (possibly independent)	✖ (dependent)
CD tolerance	✔✔ (full optical field info)	✔ (lower benefit due to direct-detection)
Adaptive (burst-to-burst)	✖	✔

Table 3.1: High-level comparison between optical and electrical compensation.

EDC implementation options:

Electronic compensation circuits can improve system performance at a small cost premium once they have entered large volumes and development cost is negligible. Indeed, transponder vendors start to utilise these circuits to increase transmission distance, improve margins, or allow less expensive optical components. Today, there are two main electronic dispersion compensation (EDC) implementations: firstly, an analog or mixed-signal M-tap (fractionally or symbol-spaced) feedforward equaliser (FFE) combined with an N-tap decision feedback equaliser (DFE), and secondly a DSP based equalisers which first digitise the signal from the photodiode(s) using an analog-to-digital converter (ADC) and then use DSP to recover the data. Analog or mixed-signal fractionally-spaced FFE/DFE have found wide application in optical receivers, where deep submicron CMOS technologies are used to achieve high speed operation with relatively low power consumption ($\sim$1W). The ultimate performance is achieved with DSP based equaliser chips, as these allow implementation of maximum likelihood sequence estimation (MLSE) which has significantly better equalisation performance than FFE/DFE structures [76, 82, 83]. However, this is at the cost of complex (i.e. costly) and power

hungry ADC+DSP electronics. For access applications, cost and power consumption are major concerns, and for this reason the FFE/DFE based EDC has been selected as optimum trade-off between performance and implementation complexity. This architecture is discussed in more detail in the following chapters. A high-level comparison of the three electronic dispersion compensation techniques discussed above is shown in Table 3.2.

Feature	FFE	FFE/DFE	MLSE
Complexity	✓✓	✓	✗
CD tolerance	✗	✓	✓✓
Cost	✓✓	✓	✗
Power consumption	✓	✓	✗

Table 3.2: High-level comparison between electronic dispersion compensation technologies for access applications.

3.4 Reach-Extender Based on SOA Cascade

As mentioned in the previous sections, recently there has been significant interest in developing mid-span reach-extenders (REs) in order to increase the PON optical budget and support the additional insertion loss of the trunk fibres. SOAs have been shown to be good candidates for REs in conventional G-PONs [84] and several authors have considered their use in 10Gb/s PONs [85, 86, 87]. A solution explored in [85, 86, 87] is to also use the SOA to compress the input dynamic-range of the upstream channel, thus reducing the required dynamic-range for the BM receiver located in the OLT.

In [85], it is proposed to boost the signal and compress the input dynamic-range by operating the SOAs in deep saturation for strong input signals. However, as discussed in the previous section, operation in deep saturation of conventional SOAs leads to large overshoots on rising edges in the input signal and eye closure due to gain compression and recovery effects. The authors in [85] therefore propose to use an SOA with an increased gain recovery time (in the order of a nanosecond or more) and show theoretically that this reduces the signal quality

degradation. However, standard SOAs do not exhibit such long gain recovery times, making this option rather impractical.

Another solution uses a narrow optical filter at the receiver side to reduce the signal distortion by suppressing the broadening caused by the chirped components of the signal in the frequency domain [86]. However, this introduces loss and would require the use of tightly wavelength-specified, temperature-controlled lasers in the ONU, which are expensive. In contrast, recent 10Gb/s PON standards specify a wide 20nm wavelength band for the upstream channel to allow the use of uncooled lasers at the ONU.

In [87], it is proposed to switch the SOA bias current based on the magnitude of the incoming packets. While this allows significant compression of the input dynamic-range and avoids saturation of the SOA, it requires a monitoring photodiode and high-speed electronics to adjust the bias current on a per packet basis. This section demonstrates the feasibility of an upstream RE based on an optimised cascade of two SOAs that overcomes the disadvantages of the above methods. The scheme gives sufficient dynamic-range compression without any dynamic control to enable the use of an ac-coupled, CM receiver at the optical line termination.
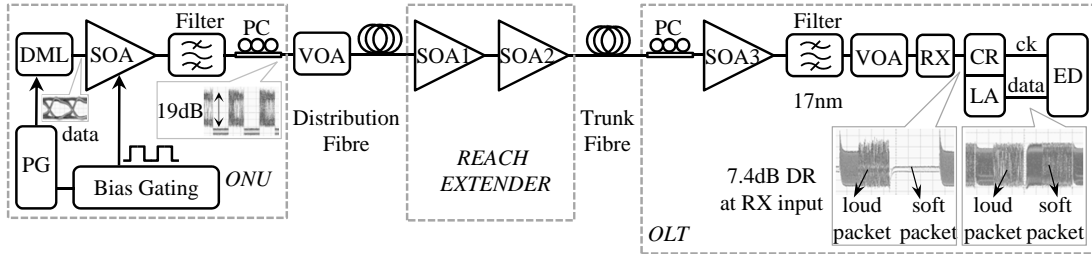
Figure 3.8: Experimental setup (DML: directly modulated laser, PG: pattern generator, PC: polarisation controller, VOA: variable optical attenuator, RX: receiver, CR: clock recovery, LA: limiting amplifier, ED: error detector, DR: dynamic range).

Figure 3.8 shows the experimental setup. The ONU employs a 1310nm DFB laser (as a 1270nm laser was not available for this experiment) which is directly modulated at a bit-rate of 10.3125Gb/s (NRZ, $2^{31} - 1$ PRBS, 6.5dB extinction ratio, close to the worst-case 10G-EPON specification). An SOA whose bias current is modulated on a per packet basis is used to emulate an alternating sequence of LPs (corresponding to the maximum expected input power to the RE) and SPs (corresponding to the minimum expected input power to the RE)

thus emulating two ONUs with different path losses to the OLT. For correct emulation, a 1nm wide optical filter is used to suppress the ASE noise from this gated SOA. A variable optical attenuator is used to emulate splitting loss in the PON distribution network. The RE is located between the distribution network (split: 32, reach: 10km) and a 60km trunk fibre. Due to differential access loss, the power of packets at the input of the RE is assumed to range from -25dBm (SP) to -6dBm (LP) according to the IEEE 802.3av standard, class PR20 [15].

The RE consists of a cascade of two SOAs where the first SOA provides low-noise amplification and the second SOA provides additional compression of the input dynamic range and boosts the signal launched into the trunk fibre. A mid-stage optical filter, which is typically used to remove out-of-band ASE noise from the first SOA, was intentionally omitted here. Note that in order to satisfy the specifications in [15] for a 10G-EPON system (which defines the upstream wavelength window from 1260 to 1280nm), the bandwidth of any mid-stage filter needs to be at least 20nm wide.

The OLT comprises an SOA preamplifier, a 17nm band-pass filter for out-of-band amplified spontaneous emission (ASE) suppression and a conventional CM PIN receiver with a reduced 56ns ac-coupling time constant (560pF coupling capacitor) to make it suitable for BM operation with less than 800ns preamble (10G-EPON standard). The 20nm filter specified in [15] was not available at the time, however this does not alter the outcomes of this experiment. A variable optical attenuator is added in front of the PIN receiver to measure power penalties. The SOAs used in the experiments has +21dB small signal gain, -3dB gain saturation output power of +11dBm, 1dB polarisation dependent gain (PDG) and a 7dB noise figure at 1310nm wavelength and 250mA bias. The polarisation controllers are for experimental characterisation purposes only and would not be required in a real deployed system, where the reach-extender would need to provide sufficient system margin for all input polarisation states, including the worst-case state.

ASE as 'holding' beam to speed-up SOA gain recovery:

The reach-extender was first characterised in continuous-mode and in a back-to-back (B2B) configuration without the fibres and the OLT preamplifier SOA. Figure 3.9 shows the eye diagrams measured at the output of the reach-extender for the SP case (bias current of the 2nd stage SOA: 250mA) with and without

the mid-stage filter. It is evident that a significant reduction of the eye-closure induced by patterning can be achieved by omitting such a filter. As mentioned in the previous sections, patterning occurs when the input signals at a bit rate comparable to the gain recovery time are sufficiently strong to saturate the SOA, leading to carrier depletion in the gain medium and consequently reducing the optical gain. The signal-dependent gain of the saturated SOA leads to distortions at the bit level, which results in a signal-dependent extinction ratio degradation and intersymbol interference (ISI) [38, 73]. The observed reduction in patterning can be explained by noting that for SPs the input to the 2nd stage SOA mainly consists of ASE noise (-4.5dBm signal power, +2.7dBm ASE power). The total power is sufficiently high to saturate the 2nd stage SOA. The ASE noise acts as a 'holding' beam, which is known to speed-up the gain recovery in the SOA and reduce the patterning. In general, the term holding beam refers to a saturating continuous-wave (CW) beam at a wavelength other than that of the signal to be amplified that is incident on the SOA and increases its effective carrier recovery rate [88]. The effect of such a holding beam is to clamp the carrier concentration depressing the SOA gain, and this leads to faster recovery times for the gain and phase (hence the patterning reduction).
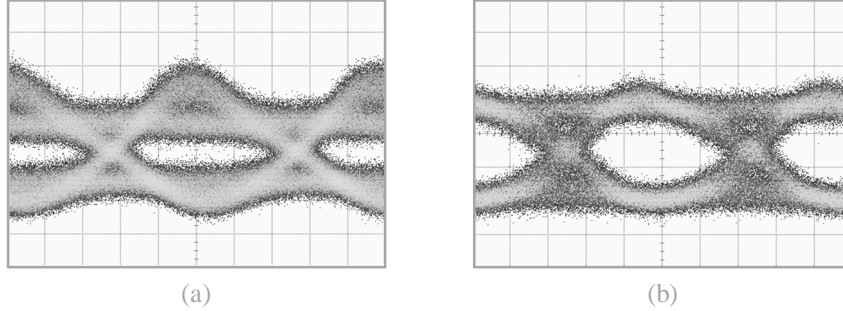
Figure 3.9: Soft packet eye diagrams (time scale: 20ps/division) at the RE output in back-to-back when using a 17nm band-pass filter (a), and without any optical filter (b).

No similar improvement can be observed for LPs, which is consistent with the above explanation as the input to the 2nd stage SOA is then dominated by the signal rather than the ASE from the first SOA. Hence, a mid-stage filter is unnecessary for LPs and its omission is shown to enhance the performance in the SPs case, besides being a more cost-effective solution.

Dynamic-range compression and patterning mitigation:

In principle, SOA gain saturation can be used to reduce the dynamic-range that must be supported by the OLT receiver if the concomitant patterning effect can be ameliorated. In this section it is demonstrated that this can be achieved by reducing the bias current of the 2nd stage SOA. This allows significant reduction of patterning induced penalties stemming from deep saturation of the 2nd stage SOA, while at the same time maintaining essentially the same amount of input dynamic-range compression. An explanation for this is provided hereafter. The large-signal gain of an SOA can be written according to Eq. (2.2.4) as [20]:

$$G = G_0 \exp\left[-(G-1)\frac{P_{in}}{P_s}\right], \tag{3.4.1}$$

where G represents the amplifier gain, G_0 its unsaturated value, P_{in} the input power of the signal being amplified, and P_s the saturation power which depends on the gain-medium properties. The input saturation power P_{in}^s of an amplifier can be defined as the input power for which the gain G is reduced by half (or by 3dB) from its unsaturated value G_0, and can be derived from Eq. (3.4.1) by using $G = G_0/2$:

$$P_{in}^s = \frac{2\ln(2)}{[G_0(I_{bias}) - 2]} P_s(I_{bias}), \tag{3.4.2}$$
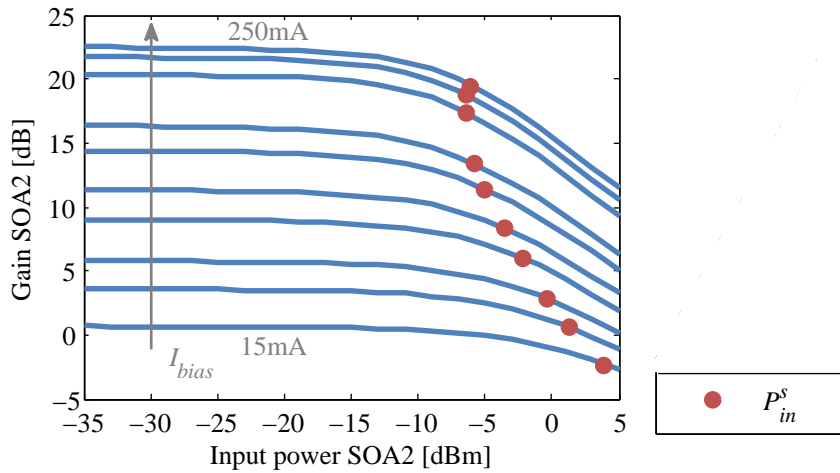
Figure 3.10: 2nd stage SOA gain as a function of the input power (solid lines) and P_{in}^s for different bias currents (dots).

where it is indicated explicitly that G_0 and P_s are both dependant on the amplifier bias settings I_{bias}. Both Eqs. (3.4.1) and (3.4.2) agree with the experimental data shown respectively in Figs. 3.10 and 3.11, where G_0 and P_s are measured for different values of the 2nd stage SOA bias current (15, 17.5, 20, 25, 30, 40, 50, 100, 150, 250mA). Figure 3.10 shows the well-known relation between the gain of the amplifier and its input power. The input saturation powers P_{in}^s are emphasised with a circular marker for each bias current. From this set of curves one can see that P_{in}^s rapidly decreases with increasing SOA bias current. This is especially clear when re-plotting P_{in}^s as a function of bias current as shown in Fig. 3.11.
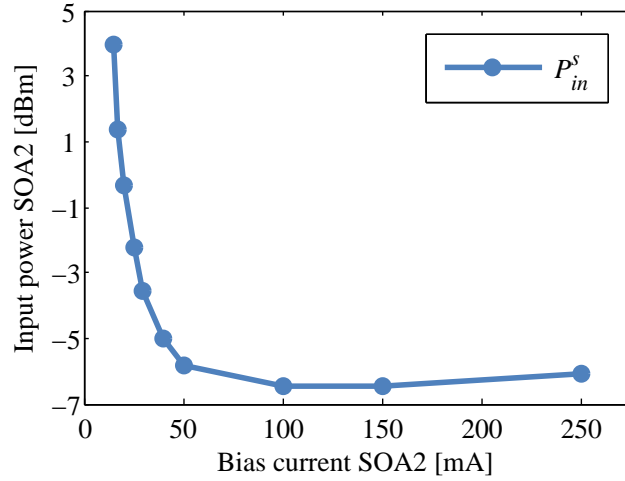
Figure 3.11: Input saturation power of the 2nd stage SOA as a function of the SOA bias current.

For the maximum bias current of 250mA P_{in}^s is -6dBm, while for a bias current of 15mA P_{in}^s increases up to +4dBm. In other words, if the bias current is reduced from 250 to 15mA, the 2nd stage SOA is able to tolerate a 10dB stronger input signal before entering the saturation regime.

Reducing the bias current of the 2nd stage SOA may degrade the overall noise figure, however here such degradation is negligible. Indeed the noise figure NF_{tot} of the cascaded SOA equals to [89]:

$$NF_{tot} = NF_1 + \frac{(NF_2 - 1)}{G_1} \approx NF_1, \tag{3.4.3}$$

where NF_1 and G_1 are respectively the noise figure and the gain of the first

SOA, and NF_2 the noise figure of the second SOA. The approximation holds when the gain of the first SOA is sufficiently large and the noise figure of the 2nd SOA reasonably small (which is the case here as the gain of the 1st SOA is greater than 20dB, and the noise figure of the 2nd SOA equals 7dB). In the worst-case a negligible 0.25dB degradation of the overall noise figure is measured for a reduction of the bias current from 250mA to 15mA.
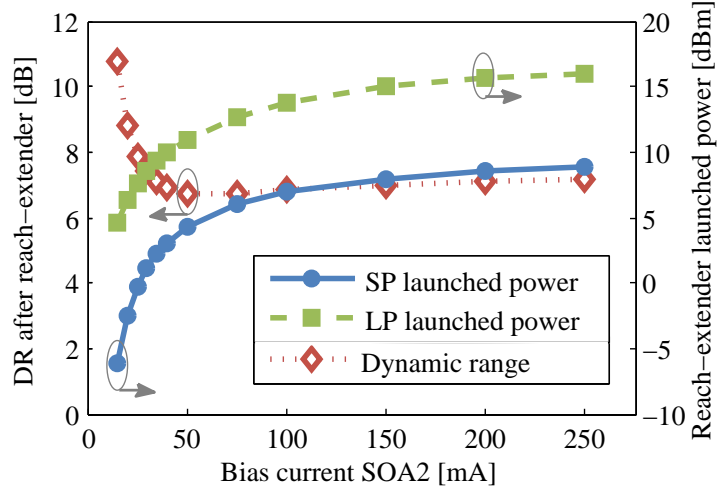
Figure 3.12: Dynamic range after the reach-extender and launched power for SP and LP as a function of the SOA bias current (B2B).

Note that reduction of the bias current reduces the power launched into the trunk fibre, but this is acceptable as long as the input power to the OLT receiver remains higher than its sensitivity. Obviously, this requirement is most stringent for the SP. With the setup shown in Fig. 3.8, in order to support 60km trunk fibre for the SP, it is found that a launched power at the output of the cascade of at least 0dBm is sufficient. Figure 3.12 shows the output power of the reach-extender for both LP and SP. For the LP sufficient launch power is always available, however for the SP the bias current of the 2nd stage SOA needs to be at least 30mA. Figure 3.12 also shows the RE output dynamic range for a 19dB input dynamic-range. It can be seen how larger dynamic-range compression is achieved for higher bias currents. For bias currents higher than 30mA an almost constant output dynamic-range of 7dB can be observed.

Next, the power penalty induced by patterning is obtained by measuring the power on the PIN photodiode (without SOA3) required to achieve a bit-error-rate (BER) of 1.1×10^{-3} (FEC threshold for RS(255,223) encoding, as specified in

10G-EPON), and comparing it to the receiver sensitivity. The results, which are taken in CM and B2B for both SP and LP power levels, are shown in Fig. 3.13 plotted as a function of the 2nd stage SOA bias current. Up to 5dB reduction in patterning-penalty can be obtained for the LP by reducing the 2nd stage SOA bias current from 250 to 30mA. Note that although the LP power penalty is only reduced and not entirely removed, these residual penalty values do not represent a practical issue as the LPs are characterised by large received powers.
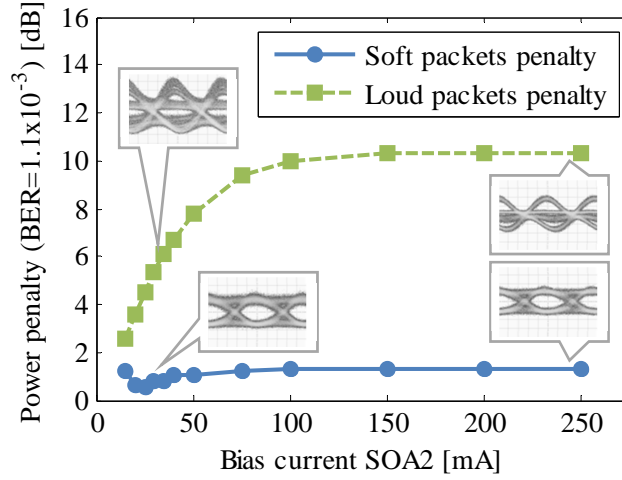
Figure 3.13: SP and LP power penalty at FEC threshold (BER=1.1×10^{-3}) as a function of the SOA bias current (B2B).

From Fig. 3.12, one can see that this results in a negligible 0.3dB reduction in output dynamic-range compression. The SP output power is reduced to +1dBm at 30mA bias, which results in an OLT input power of -20dBm if a 60km trunk fibre with 21dB (0.35dB/km) insertion loss is used. To avoid additional bit errors due to thermal noise of the receiver electronics, this requires the use of an avalanche photodiode (APD) receiver to ensure operation sufficiently above the receiver sensitivity. As a suitable ac-coupled APD receiver was not available for this experiment, an SOA preamplifier (SOA3) was used instead.

Receiver recovery time and system performance:

The optimised cascade has then been used in a BM transmission experiment, designed to emulate a 10G-EPON system. Sufficient reduction in dynamic-range is obtained to enable the use of a conventional ac-coupled continuous-mode PIN receiver (albeit with a reduced 56ns ac-coupling constant) followed by a conven-

tional 10Gb/s limiting amplifier which equalises the different amplitudes of the packets after detection. When operating ac-coupled receivers in burst-mode, the ac-coupling time constant sets the required time needed to discharge the coupling capacitor after the end of a burst, and charge the coupling capacitor for a new burst. The worst-case situation occurs when a SP occurs immediately after a LP. It can be shown that the recovery time for a given power penalty α_R (expressed as a linear value) is then given by [90]:

$$t_{Rx} = \tau \ln \left(\frac{1 + ER}{1 - ER} \cdot (DR_{lin} - 1) \cdot \frac{\alpha_R}{\alpha_R - 1} \right), \qquad (3.4.4)$$

where τ is the RC time constant of the ac-coupling network, ER is the extinction ratio (defined as the power in a 1 to the power in a 0) and DR_{lin} is the is the loud/soft ratio (i.e. the dynamic-range expressed as a linear value). For a negligible power penalty of 0.5dB, an extinction ratio of 6.5dB, a dynamic-range of 7.4dB at the input of the receiver and the mentioned 56ns ac-coupling constant, the recovery time is calculated to be 292ns which is well in line with the 10G-EPON standard preamble time of 800ns. It should be noted that if the ac-coupled receiver is required to handle the entire dynamic-range of 19dB, the recovery time would be 452ns, hence the achieved dynamic-range compression allows a significant reduction in the required receiver recovery time. It is known that a smaller ac-coupling capacitor increases the baseline wander, which introduces a power penalty. This power penalty α_P can be calculated as [90]:

$$\alpha_P = \exp \left[CBD_{AV} \cdot \left(\frac{T_b}{\tau} \right) \right], \qquad (3.4.5)$$

where CBD_{AV} is the averaged cumulative bit difference in the received bit sequence (difference between number of transmitted 1s and number of transmitted 0s) [91] and T_b the bit period. For the 64B/66B scrambling specified in the 10G-EPON standard, CBD_{AV} is 8, resulting in a negligible 0.1dB penalty due to baseline wander.

Figure 3.14 shows the structure of the packet signal used to evaluate the performance of the network at a bit rate of 10.3125Gb/s. Each packet (2040ns) consists of a preamble (800ns, alternating '1010' pattern) followed by the BM synchronisation pattern, a burst delimiter and a data payload. The data payload (1240ns) consists of $2^{31} - 1$ pseudo-random bit sequence (PRBS) sequences,

additionally stressed with 66 consecutive 1s and 66 consecutive 0s. The pattern terminates with an end burst delimiter. The guard time between successive bursts is 25.6ns. The synchronisation pattern, burst delimiter, and end burst delimiter structures have been adopted from the IEEE Standard 802.3av, and they are all considered as part of the payload in measuring the burst BER.
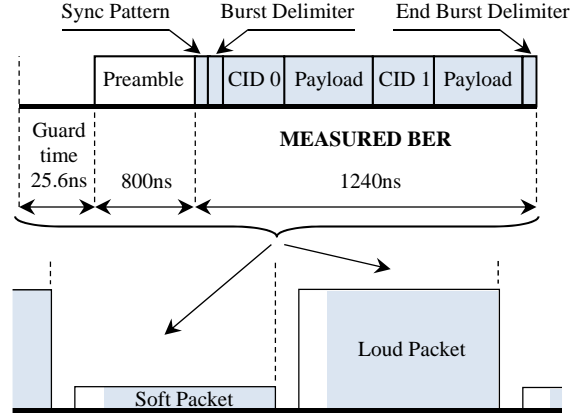
Figure 3.14: Pattern structure of packets used to evaluate the performance.

The BER is measured in a given packet, always preceded by the worst-case packet that maximally stressed the packet under consideration. For SP, the worst-case preceding packet is the LP and similarly, for the LP, the worst-case preceding packet is the SP. The measured BER as a function of the power input at the reach-extender is shown in Fig. 3.15 for the best-case and worst-case polarisations. For best-case polarisation, over 19dB dynamic range (assuming a BER less than 1.1×10^{-3}) corresponding to the 10G-EPON power levels is easily achievable. For practical reasons the maximum packet power level is limited to -6dBm for the measurements presented here. However, the trend of the best polarisation curve suggests that this dynamic-range could be further improved, since for the LP there is still a significant margin before the FEC threshold is reached. If the attention is focused on the worst-case polarisation it is possible to see that the dynamic-range supported by the RE before achieving the FEC threshold is reduced to approximately 14dB. This is attributed to the relatively large combined PDG of the three SOAs used in the system. In principle, this can be improved by using lower PDG SOAs in the RE along with an APD receiver at the OLT (which avoids PDG of the third SOA).

The curves in Fig. 3.15 confirm that the RE structure under consideration
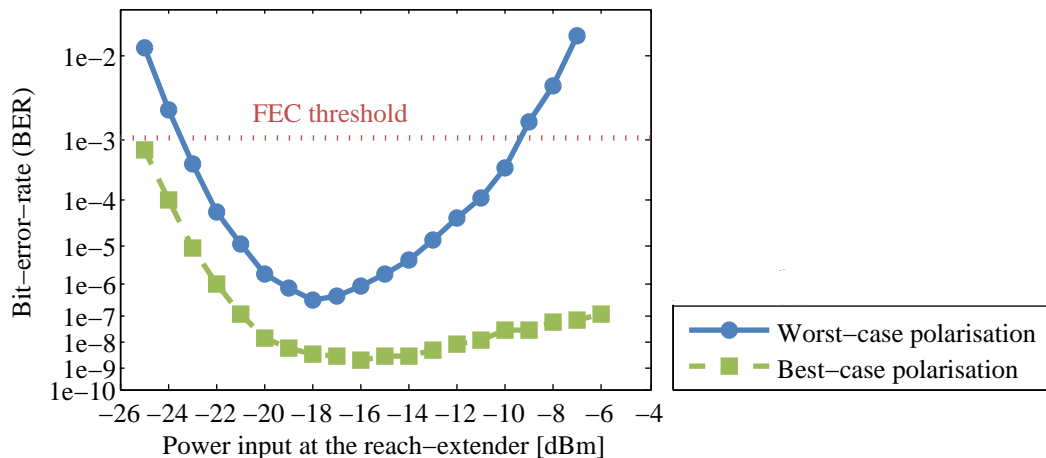
Figure 3.15: BER as a function of the input power to the reach-extender.

gives sufficient dynamic-range compression without any dynamic control to support 70km reach for a 32-split 10Gb/s PON. Note that although the aforesaid technique enables the use of a conventional ac-coupled CM receiver, this has not to be interpreted as a solution for replacing the BM receiver with a less complex CM one, but rather for reducing the BM receiver specifications. If such a BM receiver is linear, then, electronic equalisation could also be employed to further improve the system performance and reduce the penalty induced by patterning. This point will be briefly discussed in Section 5.3.

3.5   Summary

This chapter reviews the state-of-the-art technologies in optical access, focusing on the PON architectures that are believed to be the most promising candidates for the mass market. The evolution from current E-PON and G-PON architectures to more advanced (short term) 10G-EPON and XG-PON schemes as well as the migration scenarios towards next-generation PONs is briefly described. The attention is focussed on the hybrid TDWM approach which has been selected as primary solution to NG-PON2, and on long-reach architectures which can offer higher capacities and much lower bandwidth costs than any electronic-intensive-based solution. Such long-reach TWDM PONs, along with a number of more radical future-looking schemes, are currently being investigated under the European FP7 Integrated Project DISCUS, which was founded with the objective

of filling the gaps of previous projects and of developing the missing enabling technologies. Among all these key technologies, burst-mode electronic dispersion compensation represents the main subject of interest in this thesis, and an exhaustive analysis will be presented throughout the next chapters to demonstrate the feasibility of this technology as well as its requirements to operate in the network topologies discussed in this chapter.

In order to achieve long-reaches, optical amplification must be employed at the local exchange as well as pre-amplification in the metro/core node. Several technology options employing either optical fiber or semiconductor gain media are currently available and, among these, EDFA- and SOA-based reach-extender solutions are considered. EDFAs seem to be the best choice of amplifiers for next generation access networks and for this reason they have been employed as reach-extenders and/or preamplifiers in the majority of the experiments presented in this thesis. On the other hand, SOAs are certainly suitable for the 'pay as you grow' business model often adopted in current PON deployments.

Some of the main optical and electrical compensators necessary to mitigate dispersion in long-reach PONs enabling the use of cost-effective transmitters are briefly presented. A high-level comparison between optical and electrical techniques is illustrated and the reason for choosing an electronic-based solution for access applications is also discussed.

Finally, a potential solution for an SOA-based reach-extender is presented and analysed experimentally in detail. Up to 12dB compression of a 19dB input dynamic-range is achieved without any dynamic control. A reduction in patterning induced penalties for SPs can also be achieved by using the broadband ASE from the 1st stage SOA to clamp the gain of the 2nd stage SOA. For LPs, it is shown that significant reduction in patterning induced penalties can be achieved through careful optimisation of the bias current of the 2nd stage SOA. The reach-extender is shown to be able to support 70km reach for a 32-split 10Gb/s PON.

Chapter 4

Design of an Electronic Dispersion Compensator for Long-Reach PONs

Over the past few decades, several equalisation techniques have been proposed in order to combat frequency selective and dispersive transmission channels, which introduce intersymbol interference (ISI) in digital communication systems. It is known [92] that the optimum receiver in terms of BER is the maximum likelihood sequence estimation (MLSE) detector, but its associated computational cost grows exponentially with the channel memory [93] and this makes it unattractive for many applications. Linear feedforward equalisers (FFE) followed by a symbol-by-symbol detector are attractive in terms of complexity, although they might introduce excessive noise enhancement if the channel frequency response presents deep nulls [94]. Decision feedback equalisers (DFE), on the other hand, provide post-cursor ISI cancellation with reduced noise enhancement and are widely recognised to offer better steady-state performance than pure FFEs.

In this chapter, a characterisation of the FFE and DFE (simulated) performance is presented in order to understand how such electronic equalisation techniques can be used to mitigate the ISI due to chromatic dispersion (CD) in long-reach passive optical networks (LR-PONs). Since CD is the dominant impairment taken into account in this thesis, the FFE/DFE structures here analysed will be also referred to as electronic dispersion compensators (EDCs). Note that all the analyses presented throughout this chapter (and Chapter 5) are con-

ducted using continuous-mode packets in order to focus on the ability of the EDC in mitigating the impairment under study, rather than the adaptation speed of the EDC itself (for a detailed analysis on the latter, see Chapter 6).

Section 4.1 illustrates the simulation setup employed to simulate the EDC dispersion tolerance, and describes in detail each key device/component.

In Section 4.2 the principle of operation of a linear transversal filter is discussed and the ability of a symbol-spaced equaliser (SSE) and fractionally-spaced equaliser (FSE) to mitigate CD in a power-limited system is compared in order to highlight the advantages offered by the latter. An optimisation of the FSE in terms of tap-spacing and number of taps is also performed.

The basic concepts behind decision feedback equalisation (DFE) are covered in Section 4.3, where it is shown that the addition of a feedback section to the conventional FFE can significantly improve the equaliser performance. As for the linear equaliser case, the optimum number of FFE/DFE taps is also discussed.

Section 4.4 deals with the basic concepts behind the adaptation process of an equaliser of the type FFE/DFE. The steepest descent method is recalled from theory and its instantaneous approximation that leads to the well-known least mean square (LMS) algorithm is described. Some practical considerations on the convergence of the LMS algorithm along with its adaptation speed are also emphasised: in particular it is shown how a careful choice of the step-size parameter in the LMS update equation can guarantee a good trade-off between adaptation speed (essential for the burst-mode applications that this thesis is focusing on) and low steady-state error.

Finally, a brief summary about the main results and inferences obtained from these analyses and characterisations is presented in Section 4.5.

4.1   Simulation Testbed

In Chapter 2 it is explained that if the systems of interest are not optically pre-amplified they are typically thermal noise limited and the performance is normally measured in terms of power penalty. On the other hand, in optically pre-amplified systems where the beat noise (signal-ASE) is typically the dominant noise mechanisms, the performance is normally measured in terms of OSNR penalty. In Chapter 2 it is also shown that these two noise mechanisms have significantly different nature which can lead to radically different system performance in terms

of power penalty and OSNR penalty respectively. Even though the ASE beat noise is often approximated as Gaussian (under the assumption of systems with Gaussian filters and Gaussian optical pulses [40]) after square-law detection it can actually contain a signal dependent non-symmetric Gaussian term having a variance determined by the signals level of bits (0 and 1), and a nonzero-mean non-central χ^2 term [95]. Thermal noise, in contrast, is well described by Gaussian statistics [20, 96].

Taking this into account, one may wonder whether these two noise mechanisms have a different impact on the performance of a given electronic equaliser. In particular, as will be discussed in greater detail later in this chapter, attention is focused on adaptive equalisers based on the standard least mean square (LMS) algorithm. The reason for this choice is that the use of LMS is highly desirable in access networks due to its simplicity, robustness, and low computational cost. However, it is well known [95] that the LMS algorithm is optimum for Gaussian noise, but not necessarily for noise with other probability density functions. Therefore, the study of the LMS based electronic equaliser is divided into two phases. Firstly, in Chapter 4, power-limited systems are taken into account to evaluate a possible best-case scenario where the presence of thermal noise guarantees the equaliser-under-test to perform to its full potential. Once this is done, it is then reasonable to quantify the potential loss in performance (if there is any) when ASE beat noise is dominant and the LMS algorithm might prove to be a sub-optimal choice (a detailed analysis on this matter is presented in Section 5.1, where the system taken into account is OSNR-limited rather than power-limited).

In order to compare the performance of different LMS based equaliser structures in the context of optical access networks, the setup in Fig. 4.1 has been implemented using the numerical computing environment Matlab®. Such a setup will be used throughout Chapter 4 and Chapter 5 to study the effect of different network impairments (and mechanisms of noise) on the system performance, and to quantify the benefits introduced by an electronic equaliser under these circumstances. Table 4.1 summarises the network impairments taken into account, along with the noise mechanisms used to stress the system.

The setup emulates a simplified 10Gb/s LR-PON upstream link and it consists of three main blocks: the transmitter (Tx), the optical channel, and the receiver (Rx).
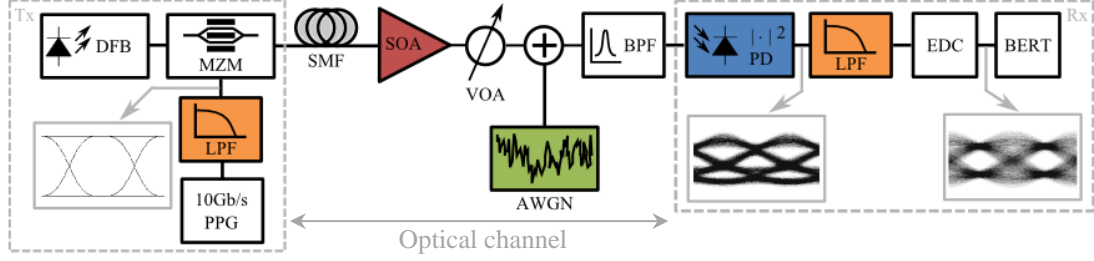
Figure 4.1: System setup of a simplified LR-PON upstream link implemented in Matlab® or VPItransmissionMaker™(Tx: transmitter, DFB: distributed feedback laser, MZM: Mach-Zehnder modulator, PPG: pulse pattern generator, LPF: low-pass filter, SMF: single mode fibre, SOA: semiconductor optical amplifier, VOA: variable optical attenuator, AWGN: additive white Gaussian noise, BPF: band-pass filter, PD: photodetector, EDC: electronic dispersion compensation, BERT: bit error rate tester, Rx: receiver).

Network impairment	Nature	Solution
Chromatic dispersion (Chapters 4 and 5)	deterministic	Electronic equalisation
Rx thermal noise (Chapter 4 and Section 5.1)	stochastic	FEC
Unwanted Tx/Rx (electrical) filtering effects (Section 5.1)	deterministic	Electronic equalisation
ASE beat noise (Section 5.2 and 5.3)	stochastic	FEC
SOA patterning (Section 5.3)	deterministic	Electronic equalisation

Table 4.1: Summary of network impairments studied in Chapter 4 and Chapter 5.

Transmitter:

The transmitter employs a distributed feedback laser (DFB) operating at a wavelength of 1550nm, followed by a Mach-Zehender modulator (MZM) driven in continuous-mode at 10Gb/s with a 2^7-1 PRBS (pseudo random bit sequence) non-return-to-zero pattern. Since the aim of this analysis is to quantify the impact of the equalisers-under-test on the channel impairments (for example chromatic dispersion), the transmitter has been implemented using quasi-ideal components, ensuring that the measured penalty at the receiver side is effectively given by the impairment under consideration, rather than a poor choice/design of components. In the latter case, indeed, it would be quite challenging to distinguish

among the different sources of penalty and to establish which one is eventually limiting the equaliser. Therefore, the DFB has been implemented as an ideal zero-noise monochromatic source (linewidth $\to 0$) with infinite side-mode suppression ratio (SMSR), and the MZM as an ideal push-pull driven (zero-chirp), lossless external-modulator, based on e.g. LiNbO$_3$ (lithium niobate) technology. Under these assumptions, the input-output relation for the MZM electric field E can be written as

$$E_{out} = E_{in} \cos\left[\frac{\pi}{2}\frac{\Delta v(t)}{V_\pi}\right], \qquad (4.1.1)$$

where $\Delta v(t)$ is the differential RF voltage between the two arms of the modulator, and V_π the voltage required to change the optical power transfer function from the minimum to the maximum [27] [1]. The MZM generates an optical signal whose extinction-ratio (ER) is set to 10dB, and is driven by a pulse pattern generator (PPG) with an inbuilt rise-time Gaussian filter that transforms the ideal rectangular electrical pulses into smoother ones with a rise-time (10%-90% of the pulse height) of approximately $1/4^{th}$ of the bit-period. This limits the bandwidth of the modulated optical signal in order to avoid numerical errors during computation. Since one of the objectives of this analysis is also to study the effect of the Tx bandwidth on the equaliser performance (see Section 5.1), an additional 4th order Bessel low-pass filter (LPF) is added after the PPG: unless specified otherwise, its cut-off frequency (-3dB) is set 12.5GHz. The resulting electrical drive-signal is shown in the Tx-inset of Fig. 4.1.

Optical channel:

The modulated optical signal at the output of the MZM is then launched into a spool of standard single mode fibre (SMF) with variable length. As discussed in Section 2.1, the dependence of the fibre's refractive index on frequency causes the signal's spectral components to travel at different velocities along the fibre, so that this chromatic dispersion (CD) spreads the optical pulse in time, leading to ISI. This is one of the most important limiting factors in optical communication systems and, for this reason, the remainder of the thesis will focus attention mainly on this fibre impairment, showing how efficiently different equaliser struc-

---

[1]Note that since $P_{out} = |E_{out}|^2$ and $P_{in} = |E_{in}|^2$ respectively, the MZM power transfer function can be easily derived from Eq. (4.1.1).

tures can compensate for it. Before discussing how the SMF dispersive nature has been emulated in the setup above, a number of assumptions have to be made. For instance, since the focus of this thesis is on single optical channels only, FWM and XPM are not taken into account in the model. Furthermore, if the peak power of the optical pulse is lower than the respective nonlinear thresholds of the transmission fibre, then also the other nonlinear effects of the fibre like SPM and inelastic scattering effects (SBS, SRS) can be ignored (approximately -5 to 0dBm for SPM, up to +7dBm or higher for SBS/SRS). Lastly, PMD can be neglected as well, since the bit-rate and transmission distances considered in this thesis are not high enough for it to become a limiting factor with modern fibre (see Section 2.1.1 for further details). Under these assumptions it is possible to isolate the effect of CD and to obtain an equivalent baseband linear-time-invariant model for the optical fibre. Indeed, the SMF is modelled as a band-pass filter with flat amplitude response and linear group delay within the data bandwidth [97, 98]. These are valid assumptions, since the transmission system considered has a narrow bandwidth with respect to the absolute value of the optical frequency [97]. The fibre can therefore be expressed in terms of its frequency response as

$$H(\omega) = \exp\left[-i\left(\frac{1}{2}\beta_2\omega^2 + \frac{1}{6}\beta_3\omega^3\right)\cdot L_{fibre}\right], \qquad (4.1.2)$$

where β_2 and β_3 are defined in Eqs. (2.1.2c) and (2.1.2d) respectively, and are obtained under the assumption of quasi-monochromatic light[1]. The propagation constant $\beta(\omega)$ can then be expanded in a Taylor series around the carrier frequency according to Eq. (2.1.1). In this way the CD-impaired optical signal at the fibre-end can be easily computed by multiplying the fibre transfer function of Eq. (4.1.2) with the Fourier-transform (FT) of the signal launched into the channel (i.e. the FT of Eq. (4.1.1)). Note that the attenuation of the fibre has not been taken into account at this stage, in order to isolate and highlight the effects of dispersion. However, attenuation will be included in later chapters. Figure 4.2 depicts the phase of $H(\omega)$ for an SMF at 1550nm (193.41THz) and three transmission lengths L: 10, 50, and 100km. Note that the phase of $H(\omega)$ is wrapped for clarity in the interval $[-\pi, \pi]$ and the discontinuities visible for transmission lengths of 50km and 100km are only an artefact of the representa-

---

[1]i.e. pulses characterised by a spectral width $\Delta\omega = (\omega - \omega_0)$ much smaller than the carrier frequency ω_0.
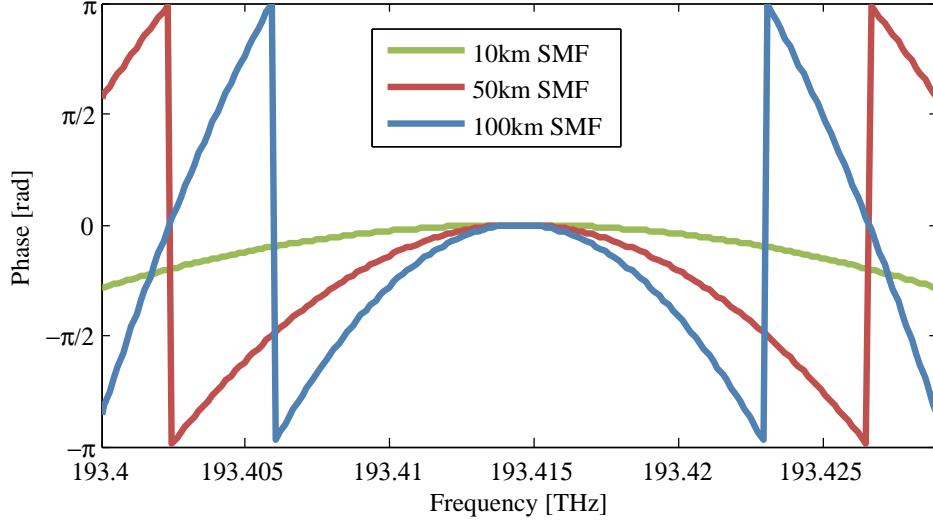
Figure 4.2: Wrapped phases in the interval $[-\pi, \pi]$ of SMF as a function of the optical frequency for a transmission distance of 10, 50, and 100km.

tion that reflect the actual periodicity of the phase response. The phase of $H(\omega)$ varies parabolically and periodically with a maximum value at 193.41THz[1] and the phase reduces for frequencies at either side of the maximum because of the ω^2 term in Eq. (4.1.2) (the term ω^3 is nearly negligible). One may wonder why the phase of $H(\omega)$ is now taken into account as, eventually, any phase information is lost after detection: note, however, that when the signal is transmitted at a wavelength not coinciding with the zero-dispersion wavelength, the frequency chirp is translated to amplitude distortion by phase modulation-to-amplitude modulation conversion induced by GVD [25], as explained in Chapter 2.

The optical channel also includes a semiconductor optical amplifier (SOA) which is used in the next chapter (Section 5.3) in order to study how efficient an electronic equaliser is in mitigating its saturation effects. An additive white Gaussian noise generator is used then to emulate the ASE arising from the amplifier and to stress the system limiting the achieved OSNR at the receiver side. Finally, before detection, the signal is optically filtered to remove out-of-band noise, or to perform wavelength division demultiplexing: such a filter emulates an optical band-pass filter (BPF) with a 1st order Gaussian transfer function and a bandwidth of 40GHz ($\sim$0.3nm). Note that since the main objective in Chapter

---

[1]This is equivalent to a wavelength of 1550nm, corresponding to the carrier frequency around which the propagation constant is expanded in Taylor series.

4 is to study thermal noise limited systems, the SOA can be ignored at this stage, or equivalently it can be thought as an ideal unitary-gain, noise-free amplifier for modelling purposes (the AWGN generator is effectively switched off).

Receiver:

At the receiver side of Fig. 4.1, the optical signal is incident on a photodiode for optical-to-electrical conversion. The detector block emulates a positive-intrinsic-negative (PIN) junction photodiode, which produces an electrical current proportional to the incident optical power. Inside the detector, a transimpedance amplifier (TIA) converts the photodetector current into a sufficiently large voltage suitable for further signal processing. The photodiode can be viewed as a band-limited square-law device that produces the following output current

$$i_{Rx}(t) = R \cdot |E_{Rx}(t)|^2 + N_{th}(t), \tag{4.1.3}$$

where R [A/W] is the responsivity of the detector (typically between 0.6A/W and 0.85A/W for InGaAs-based PIN receivers), $E_{Rx}(t)$ is the received electric field at the fibre output, and $N_{th}(t)$ is the input-referred additive Gaussian noise introduced by the receiver electronics. From Eq. (4.1.3) it is clear that the use of a square-law device makes, by definition, the system nonlinear. This is a characteristic that distinguishes all direct-detection systems, and one of the fundamental reasons why the conventional linear (or quasi-linear) equalisers present a loss in performance when used in an optical system rather than for example an electrical communication link or an optical system employing a coherent receiver. Indeed, a key issue in the effectiveness of ISI compensation using electronic equalisation techniques is the linearity of the ISI itself. As explained in Chapter 2, CD is a linear phenomenon, but linear in the field not in the intensity. In principle, the simulation setup under consideration (or in general any direct-detection optical
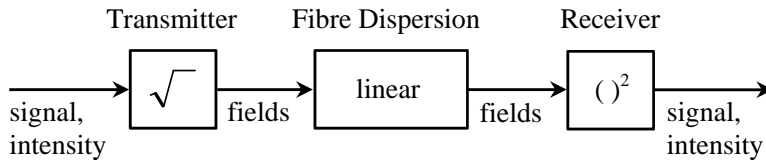
Figure 4.3: Block diagram of a direct-detection optical system.

system) can be represented as the block diagram shown in Fig. 4.3.

An electrical signal is converted into light which is carried by an electromagnetic field proportional to the square-root of its intensity. This field disperses linearly in the fibre and at the receiver side it is reconverted into an electrical signal proportional to the square of the field. This is clearly a nonlinear system; note that the nonlinearity being discussed is due to the square-law relating the intensity and the field, and has nothing to do with the fibre nonlinear effects discussed in Section 2.1.2. Therefore, the result of direct square-law detection on a linear optical impairment such as CD is to make it nonlinear in the electrical domain. This unavoidably limits a linear equaliser performance [83] that cannot offer the same benefits introduced by more advanced nonlinear electronic equalisers or by optical equalisers. Indeed, the former can include a more effective nonlinear combination of the input samples taken at different time instances [99] in comparison to the much simpler linear combination carried out by conventional equalisers (see Sections 4.2 and 4.3), while the latter act before square-law detection and have effectively access also to the phase information. At this stage, one may wonder why the study of linear/quasi-linear equalisers in the context of optical access networks should be of any interest, since it is clear that they can only represent a sub-optimal solution. The answer is that, due to their inherent simplicity and reduced implementation complexity, linear/quasi-linear equalisers can improve system performance at a small cost premium and, once they have entered large volume production, this cost would become insignificant. Therefore, the advantages offered by these techniques justify the loss in performance. For this reason they can be seen as a promising and cost-effective method to extend the reach of current access networks.

After detection, the resulting electrical signal is sent through a 4th order Bessel low-pass filter (LPF) that, unless specified otherwise, has a 3dB cut-off frequency of 7.5GHz. This operation is performed in order to reduce the out-of-band noise arising from the receiver electronics.

Finally, the signal is processed by the equaliser under test. Bit-error estimation or error counting is done by a bit-error-rate tester (BERT, see Section 2.4). Note that at this stage no further details on the equaliser block are provided, as the aim of this analysis is to compare the performance of different equaliser structures which will be discussed in detail one by one in the following sections.

4.2 Linear Transversal Equaliser

As discussed in Section 3.4, in principle the ISI introduced by a linear channel can be removed using a linear equaliser that inverts the channel frequency response maximising the probability of correct decisions at the receiver. Such an equaliser can be implemented as a transversal filter (called feedforward equaliser (FFE) and also known as tapped-delay-line) with adjustable coefficients as shown in Fig. 4.4 [92, 100].
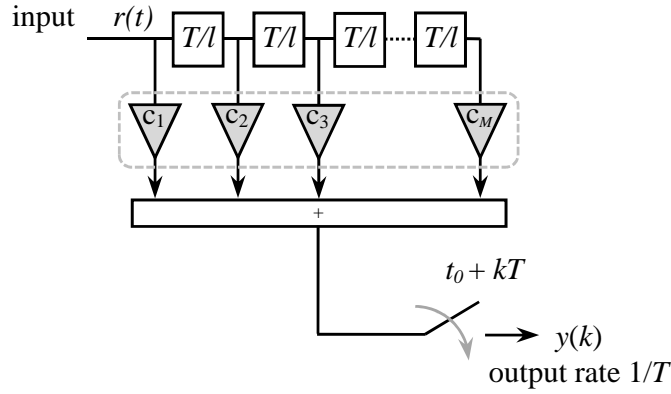
Figure 4.4: Schematic diagram of a linear transversal equaliser.

The number of delay elements M determines the duration of the filter impulse response and is called the filter order. When the delay $\tau = T/l$ between consecutive taps is equal to the symbol interval T (i.e. $l = 1$) the filter is known as symbol-spaced equaliser (SSE), whereas for delays smaller than T (i.e. $l > 1$) the filter is known as fractionally-spaced equaliser (FSE). After the delay-line, the current and past values of the received signal are linearly weighted by appropriate tap coefficients c_m, $m = 1, 2, \ldots, M$, and summed once per symbol to produce the filter output $y(t_0 + kT)$, called $y(k)$ for simplicity, according to

$$y(k) = \sum_{m=1}^{M} c_m r(t_0 + kT - m\tau), \qquad (4.2.1)$$

where $r(t_0 + kT - m\tau)$ is the received signal sampled at the instant $t_0 + kT - m\tau$. These M coefficients may be chosen to force the samples of the combined channel and equaliser impulse response to zero at all except one of the M symbol-spaced instants in the span of the equaliser [92, 94]. Such an equaliser is known as a zero-forcing (ZF) equaliser and, in the ideal case of an infinite tapped-delay-line (i.e.

$M \to \infty$) and noise-free conditions, it would guarantee the ISI to be zero at its output. If implemented as a SSE , its frequency response $H_{eq}(f)$ is periodic with a period equal to the symbol rate $1/T$, and the combined response of the channel with the equaliser must satisfy Nyquist's first criterion of zero ISI condition

$$H_{ch}(f) \cdot H_{eq}(f) = 1, \qquad |f| < \frac{1}{2T}, \qquad (4.2.2)$$

where $H_{ch}(f)$ is the folded, i.e. aliased or overlapped, channel spectral response after symbol-rate sampling[1]. In other words, this means that an infinite length ZF equaliser is simply an inverse filter which inverts the folded frequency response of the channel. However, the above equaliser structure is unfeasible since an infinite length transversal filter cannot be realised, and in practical cases the inverse channel response is approximated using a finite-impulse response (FIR) filter instead. In fact, the ISI caused by channel distortion is usually limited to a finite number of symbols on either side of the desired one, and therefore a finite-length ZF equaliser can be used to compensate for the aliased channel-distorted signal. One of the disadvantages of such a ZF equaliser is that it neglects the effect of noise altogether and the resulting inverse filter may excessively amplify the noise at frequencies where the folded channel spectrum presents spectral nulls or, more generally, high attenuation. For this reason, in practice, other criteria are used to determine the coefficients of the equaliser. An example is the minimum mean squared error (MMSE) method, which relaxes the zero ISI condition and selects the channel equaliser characteristic such that the combined signal power in the residual ISI and the additive noise at the output of the equaliser is minimised[2]. This is discussed more in detail in Section 4.4 in the context of adaptive equalisers.

4.2.1 Symbol-Spaced vs Fractionally-Spaced Equaliser

A significant drawback of a SSE is that it cannot perform matched filtering, and therefore it cannot realise, by itself, the optimal linear receiving filter. Matched filters are used to maximise the peak signal to noise ratio (SNR) in the presence of additive stochastic noise in all applications where SNR is of critical importance. The principle of operation of a matched filter is illustrated in Fig. 4.5.

---

[1]Note that in this context $H_{ch}(f)$ should be interpreted as the combined impulse response of the transmitter, the channel itself and the RF section of the receiver.

[2]i.e. it maximises the signal to noise-plus-distortion ratio.
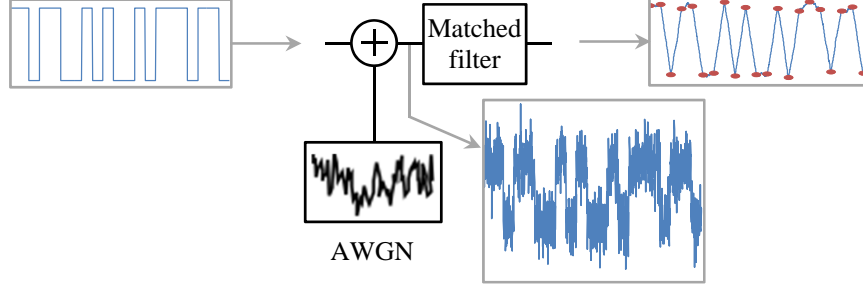
Figure 4.5: SNR improvement after matched filtering.

Matched filtering:

In signal processing, matched filtering is obtained by correlating a known signal, or template, with an unknown signal to detect the presence of the template in it. For instance, in the example of Fig. 4.5, the received signal is convolved with a filter matched to an NRZ pulse[1] resulting in the 'clean' signal shown on the top-right inset. Note that to fully exploit the benefits introduced by the matched filter, the resulting signal still needs to be sampled at the correct sampling instants, as shown by the red dots in Fig. 4.5.
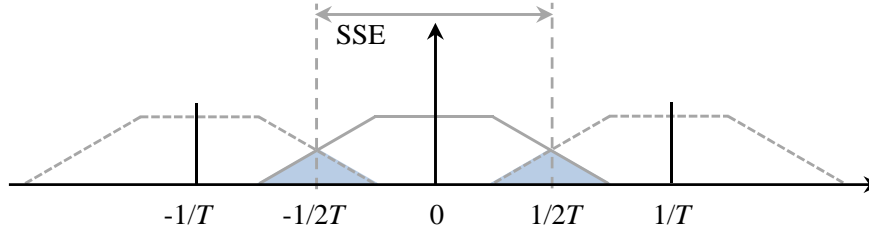
Figure 4.6: Spectral overlap (aliasing) caused by symbol-rate sampling at the SSE input.

Based on the aforesaid concepts, it is clear that matched filtering cannot be achieved by a SSE alone, since folding around $1/2T$ takes place before equalisation leading to aliasing at the transition band as shown in Fig. 4.6 (the SNR is no longer optimum). Indeed, it is well known [94, 101] that the optimum receive filter in a linear system is represented by the cascade of a filter matched to the actual channel-distorted transmitted pulse with a transversal SSE. In other words, a separate matched filter must be employed prior to equalising with a SSE. In most applications, however, the channel pulse response may not be accurately

---

[1]i.e. the matched filter impulse response is a (time-reversed complex conjugate) rectangular function.

known at the receiver, and hence the design of a matched filter becomes a rather challenging task[1].

Tolerance to sampling phase:

Even if a suitable matched filter could be easily realised, the SSE would still need to sample the received signal at its maximum strength (i.e. best eye opening) as shown in Fig. 4.5 (red dots in top-right inset), and this implies that the optimum sampling phase must be precisely known. This is often not the case, in particular for the applications that this thesis is focusing on, and therefore the use of an SSE can represent a major limitation. Indeed, as introduced in Chapter 3, the receiver in the upstream link of a time-division multiple access (TDMA) system does not see a continuous stream of data symbols. In such a burst-mode link specific time slots are assigned to each customer, whose data is allocated into fixed-length packets that can arrive at the receiver with unknown random bit phase. As a consequence, a SSE becomes impractical in this context and for this reason the remainder of this thesis will focus on fractionally-spaced solutions.
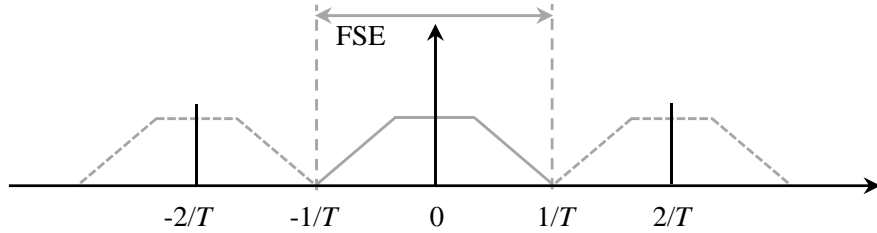
Figure 4.7: An FSE with tap spacing $\tau > 2|f|$ satisfies the sampling theorem.

As a matter of fact, an FSE with tap spacing τ selected such that the bandwidth occupied by the signal at the equaliser input is $|f| < 1/2\tau$ (i.e. τ-sampling satisfies the sampling theorem, as shown in Fig. 4.7) can effectively compensate for more severe delay distortion than an SSE, and exhibit a significant improvement in sensitivity to sampling-phase errors [94, 101]. If the tap spacing τ satisfies the aforesaid condition, an FSE with an adequate number of taps can synthesise and combine the characteristics of an adaptive matched filter and an SSE, eliminating the need for an actual analog matched filter[2]. This improvement in the FSE per-

---

[1]Note that this is true even when the transmission is performed using a 'static' channel, since the channel itself slowly changes in time due to e.g. temperature variations.

[2]Note, however, that an anti-aliasing filter is still necessary in order to avoid spectral overlap at the input of the FSE.

formance in comparison to a conventional SSE can be explained as follows: when a signal is sampled after an anti-aliasing filter at least at the Nyquist rate, then information about the entire signal waveform is retained. In other words, the FSE can synthesise, via its transfer characteristic, a phase adjustment (conceptually interpolating to the correct phase) so as to correct the timing offset in the sampling device [102]. The symbol-spaced equaliser, on the other hand, cannot interpolate to the correct phase because no interpolation is correctly performed at the symbol rate.

Noise enhancement:

Besides a better tolerance to sampling-phase errors, an FSE can also mitigate amplitude distortion with less noise enhancement than an SSE, since the occurrence of spectral nulls due to cancellation by aliasing is no longer an issue [94]. Indeed, as shown in Figs. 4.6 and 4.7, a FSE equalises before it aliases[1], whereas a SSE aliases before it equalises and as a consequence it has to compensate for the aliased version of the channel rather than the actual channel[2]. When implemented as an FIR filter, the major drawback of a T/l FSE over a SSE is that to span the same interval in time it requires a factor l more coefficients, leading to an increase in memory by a factor l. The FSE outputs may also appear to be computed l times more often, however, since the signal at the input of the decision device has to be at symbol-rate, only $(1/l)^{\text{th}}$ of the output samples need be actually computed. In other words, computation of an FSE is approximately l times that of an SSE, due to the l additional coefficients necessary to span the same time interval.

System simulations on SSE and FSE tolerance to sampling phase:

In order to summarise the aforesaid concepts and illustrate the advantages offered by an FSE over an SSE, a number of simulations have been run for different equaliser configurations using the setup presented in Section 4.1. As outlined above, an SSE should be preceded by a matched filter in order to obtain optimum performance. However, in most applications it is impractical to design

---

[1]Aliasing does occur at the output of the equaliser where symbol-rate sampling is performed, see block diagram of Fig. 4.4.

[2]This can possibly lead to noise enhancement if nulls are created due to aliasing with destructive interference between overlapping components.
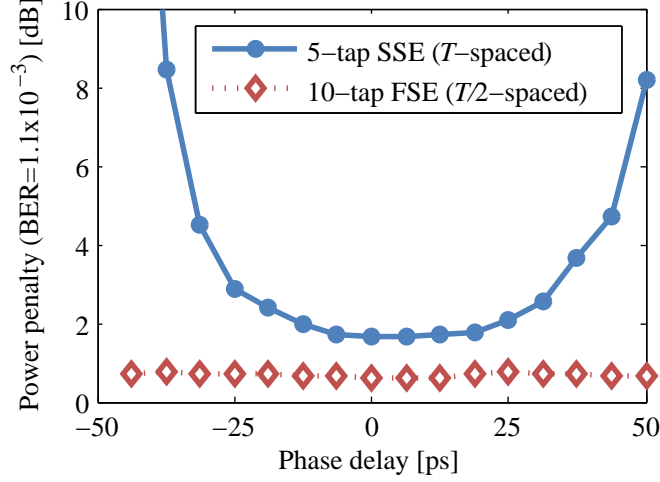
Figure 4.8: SSE and FSE performance comparison: power penalty at FEC threshold (BER=1.1×10⁻³) as a function of the sampling phase delay after 100km of SMF.

in advance a filter which is reasonably matched to the variety of received signal spectra resulting from transmissions over different channels or a time-varying channel, thus, very often, a fixed-filter is used instead. The fixed-filter response is either matched to the transmitted signal shape or is designed as a best-effort equaliser which attempts to equalise the average of the class of line characteristics expected for the application [94]. In this specific analysis, a standard 4th order Bessel LPF with a cut-off of 7.5GHz (see setup of Fig. 4.1) is employed in order to replace the matched-filter. Note that the same filter is used also for the FSE case, where it acts as anti-aliasing filter. The performance is shown in terms of received power penalty to achieve a BER of 1.1×10⁻³, and the curves are normalised to the back-to-back (B2B) case without equalisation. Figure 4.8 compares a standard 5-tap SSE with a 10-tap $T/2$-FSE[1] as a function of different sampling phase delays and for a transmission length of 100km. For simplicity, the optimum sampling phase corresponding to the best eye opening is normalised to 0ps. Note that, at this stage, the number of taps is simply chosen to span an arbitrary time interval equivalent to 5bits (i.e. equal to $5 \times T = 10 \times T/2 = 500$ps, with $T = 100$ps) larger than the channel memory for the transmission lengths taken into account in this analysis (<300ps), but it is not necessarily the optimal one. This matter is discussed in more detail in the remainder of this

---

[1]As explained above, the FSE requires double the number of taps compared to the SSE in order to cover the same time window.

section, where a proper analysis is carried out in order to determine the optimum number of taps for a linear equaliser. From the curves in Fig. 4.8 it is apparent that the performance of the SSE is closely dependent on the sampling phase which, if not within $\pm 20\%$ of the bit period from the optimum phase (i.e. ± 20ps at 10Gb/s), causes the penalty to rise very quickly losing all the benefits introduced by the equaliser. On the contrary, the performance of the FSE is virtually independent of the sampling phase and shows a nearly flat response across the complete range of sampling values that span over an entire bit period (± 50ps). This shows that the sampling device at the FSE output needs only to be locked to the symbol rate, but can otherwise provide any sampling delay, since the phase is effectively corrected to the optimum value inside the linear filter implementing the FSE [102]. In addition, the curves in Fig. 4.8 also show that, for the same optimum sampling delay (0ps), the performance of an FSE is superior by about 1dB to that of an SSE. Note that although this is generally true since an FSE does not have to compensate for an aliased signal like an SSE (with possible noise enhancement), in this specific case a fraction of that penalty could be actually due to the non-optimal choice of a 7.5GHz LPF as matched filter for the SSE.

Optimum tap-spacing for a FSE:

The next aspect to be investigated is the optimum tap-spacing for the linear equaliser. In this analysis, as in the previous case, the overall time window covered by the equaliser is set to 500ps (5bits memory). Figure 4.9 compares the case where no equalisation is used with three equaliser structures: a 5-tap SSE, a 10-tap $T/2$-FSE, and a 20-tap $T/4$-FSE. These curves are plotted as a function of the transmission length and confirm that, in general, an FSE performs better than an SSE (at optimum sampling phase). In fact, looking at the transmission lengths that result in 1dB penalty, it can be seen that a SSE only increases the distance from ~ 73km (no equalisation) to ~ 81km providing a gain of about 1.1, while a FSE extends it up to ~ 110km providing a gain of about 1.5. The other interesting aspect is that no significant improvement is measured when reducing the tap-spacing from $T/2$ to $T/4$. Moreover, in order to cover for the same time window with a reduced tap-spacing it is necessary to increase the number of taps, which increases the implementation complexity. Therefore, the optimum trade-off between performance and complexity is represented by the 10-tap $T/2$-FSE. Consequently, the remainder of this thesis will focus on FSE structures of the

$T/2$-type. Another interesting aspect that is evident from Fig. 4.9 is that even in B2B both FSE structures improve the receiver sensitivity by approximately 0.5dB in comparison to case without equalisation. This is probably due to the fact that the 4th order Bessel 7.5GHz LPF used after the receiver is not an optimum filter for this system, and the equaliser compensates for this by effectively acting as matched filter. This is indirectly confirmed by the SSE curve, which does not show the aforesaid improvement since an SSE cannot perform matched filtering for the reason outlined above.
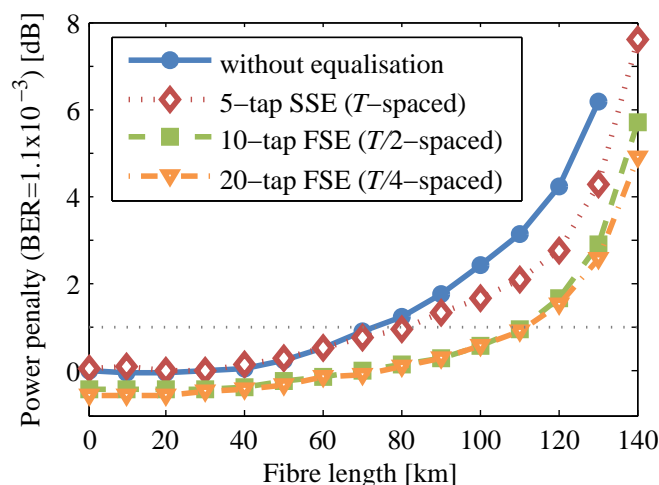
Figure 4.9: SSE and FSE performance comparison: power penalty at FEC threshold (BER=1.1×10^{-3}) as a function of the transmission length for different tap-spacings.

Optimum number of taps for a $T/2$-spaced FSE:

The remaining question to be addressed in this study on linear equalisers, is to determine the minimum number of taps that guarantee optimum equaliser performance. If the system was linear, in principle, a relatively simple way to do so would be to quantify the memory of the channel[1] and, indirectly, estimate the number of taps necessary to construct an equaliser with at least the same memory. However, since the result of direct-detection is to make the ISI nonlinear in the electrical domain, even an accurate estimation of the channel memory would not guarantee such an equaliser to be the best choice. Nevertheless, due to its simplicity, this method could still be used as a rule of thumb to extract an

---

[1]i.e. the number symbols on either side of the desired one that are responsible for most of the ISI.

approximate number of taps which can then be rounded up to the next integer to account for possible errors introduced by the linear assumption[1]. This is shown in the following example, where Eq. (2.1.15) has been rewritten to express the pulse broadening (and hence the channel memory) as a function of a specific fibre length according to:

$$N_{bit-broadening} = L_{fibre}B|D|\Delta\lambda = \frac{L_{fibre}1.2B^2|D|\lambda^2}{c}, \qquad (4.2.3)$$

where L_{fibre} is the transmission distance under consideration, $B = 10$Gb/s is the bit-rate, $\lambda = 1550$nm is the wavelength, and $D = 17$ps/(nm·km) is the dispersion parameter at that wavelength. For instance, when the fibre length is 120km, the overall amount of spreading is $N_{bit-broadening} = 1.96 \approx 2$bits. This means that, assuming symmetrical broadening, most of the ISI is caused by one bit on either side of the desired one, making the overall channel memory equal to 3bits. Accordingly, an FSE of the $T/2$-type should have at least 6 taps to compensate for that channel. In order to reduce any possible error associated with the linear approximation and to have a safety margin (ensure more, not less than the minimum), this number can be increased by adding an extra tap on both sides, bringing the overall number to 8 taps[2]. Note, however, that adding extra taps does increase the complexity and does not necessarily guarantee that the equaliser will have improved performance due to the nonlinear nature of the ISI. Therefore, it requires prudent engineering analysis to determine the number of taps in the different applications.

To confirm this finding, in the absence of a more accurate analytical model that could be used in this nonlinear system, a series of numerical simulations have been carried out using the setup of Fig. 4.1. The performance of a $T/2$-FSE has been measured as a function of the transmission distance and for different equaliser lengths ranging from 3 taps to 12 taps. The corresponding results are shown in Fig. 4.10 in terms of received power penalty to achieve a BER of 1.1×10^{-3} (normalised to the B2B case without equalisation). From these curves it is clear that for small lengths, e.g. 3 taps, the equaliser does not introduce any advantage in comparison to the case without equalisation. To see a visible improvement a minimum number of 4 taps is required: comparing the transmission

---

[1]A recommended value is about 25-50% more than is required to cover the delay spread [103].

[2]i.e. 4bits memory, approximately 33% more than required to cover for the delay spread.

lengths at which the power penalty is equal to 1dB, it is possible to observe a gain of about 1.2 (from 73.1km to 90.7km). If the equaliser length is increased up to 6-taps the gain is approximately 1.4 (from 73.1km to 102.3km), and for an 8-tap FSE it becomes 1.45 (from 73.1km to 106km). It is clear that a further increase in length beyond 8 taps does not bring any major benefit (apart from offering more tolerance to the sampling phase) since the gain offered by a 10-tap and a 12-tap FSE only moves to 1.5 and 1.53 respectively and this does not justify the additional implementation complexity.
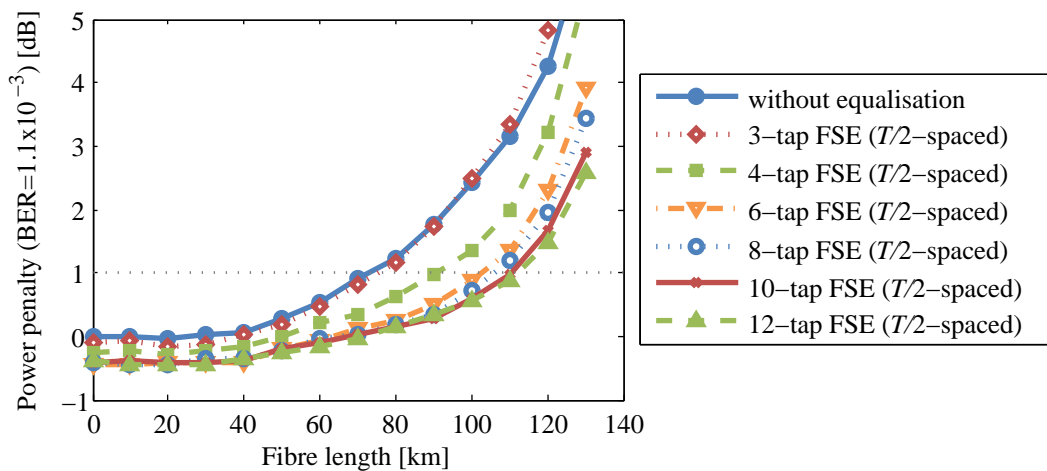
Figure 4.10: Power penalty at FEC threshold (BER=1.1×10^{-3}) as a function of the transmission length and for different equaliser lengths.

It is only for reaches greater than 120km that an appreciable improvement in performance is seen when using a 12-tap FSE in comparison to an 8-tap FSE, but it is obvious that at those transmission distances the equaliser starts to lose its effectiveness due to the highly nonlinear ISI. In fact, beyond 120km the power penalty rises extremely quickly demonstrating that a linear equaliser cannot provide significant dispersion compensation at long distance even when the number of taps is very large. The results show that the best trade-off between performance and complexity when working with transmission distances of up to 120km is offered by the 8-tap $T/2$-FSE. This confirms the rule of thumb discussed above which, although only approximate, can still provide good guidance on the best choice of equaliser when a proper analytical model or a numerical simulation environment are not available. Note that these findings will also be verified experimentally in Chapter 6.

SSE vs FSE summary:

To conclude this section, Table 4.2 is used to summarise the main results obtained comparing a SSE with a FSE.

Feature	SSE (T-spaced)	FSE ($T/2$-spaced)
Simple to implement	✔✔	✔
Can perform matched filtering	✘	✔
Mitigates noise enhancement	✘	✔
Retains info of entire signal before equalising (satisfies sampling theorem)	✘	✔
Tolerant to sampling phase (can perform as CDR)	✘	✔

Table 4.2: SSE vs FSE summary.

Note that for all the cases taken into account in this section the optimum tap weights that guarantee the best performance of the equalisers-under-test are assumed to be known. In practice, however, they are estimated during an adaptation process which is described in detail in Section 4.4.

4.3 Decision Feedback Equaliser

A common technique that may provide significantly better performance than a linear equaliser in the presence of severe amplitude distortion is represented by the decision feedback equaliser (DFE). The idea behind a DFE is that if decisions on past symbols have been made and are assumed to be correct, the ISI from these past symbols on the current symbol can be reconstructed and subtracted with appropriate weighting from the equaliser output before a new decision is made [94, 103]. The structure of a DFE is shown in Fig. 4.11. It consists of a linear feedforward equaliser (FFE) of the types illustrated in Section 4.2 (very often an FSE structure is used, with $\tau = T/2$), followed by a linear causal feedback filter which accepts as input the decision from the previous symbol (thus, the name 'decision feedback'). Note that in literature the term DFE often refers to the combination of the feedforward and feedback sections. However, for the remainder of this thesis
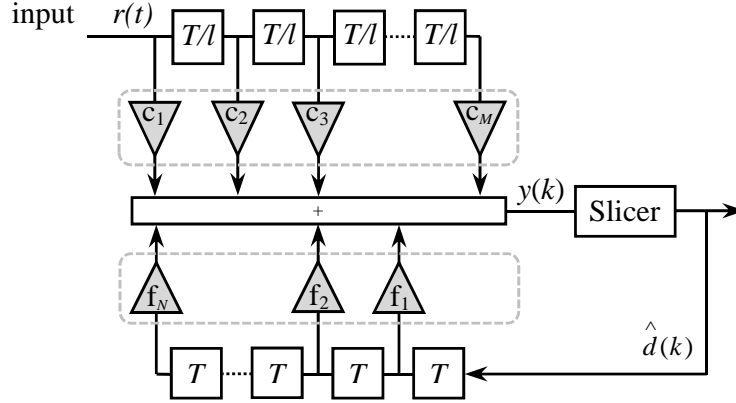
Figure 4.11: Schematic diagram of a decision feedback equaliser.

DFE indicates only the feedback part, while the structure in Fig. 4.11 is referred to as FFE/DFE for clarity. The feedback section is normally implemented as a FIR symbol-spaced filter that, combined with the feedforward section, forms a filter with infinite impulse response (IIR). The equalized signal prior to the decision is given by the sum of the feedforward and feedback filter outputs to produce $y(t_0 + kT)$, called $y(k)$ for simplicity, according to:

$$y(k) = \sum_{m=1}^{M} c_m r(t_0 + kT - m\tau) + \sum_{n=1}^{N} f_n \hat{d}(k - n), \qquad (4.3.1)$$

where c_m and f_n are the forward and feedback tap coefficients respectively (with $m = 1, 2,\ldots, M$, and $n = 1, 2,\ldots, N$), $r(t_0 + kT - m\tau)$ is the received signal sampled at the instant $t_0 + kT - m\tau$, and $\hat{d}(k - n)$ are the previously detected symbols after the decision device. The M-tap feedforward section is used to shape the channel output signal so that it is causal and with minimum ISI induced by 'future' symbols (often known as pre-cursor ISI), while the N-tap feedback section subtracts any trailing ISI (post-cursor ISI) before the decision is made. Note that since the output of the feedback section is a weighted sum of noise-free past decisions, the feedback coefficients play no part in determining the noise power at the equaliser output [94]. The forward and feedback tap coefficients may be adjusted simultaneously, and this can be done either with a zero-forcing or an MMSE approach, as for the linear equaliser discussed above. In this thesis only the latter case is taken into account (see Section 4.4 for further details). Note

99

that, because of the presence of a slicer (i.e. the decision device), the FFE/DFE is inherently a nonlinear device; however, it can be analysed using linear techniques, if one assumes all previous decisions are correct [102]. For this reason, the FFE/DFE is sometimes referred to as a 'quasi-linear' equaliser. In practice, the assumption of correct decisions may not be true, and this can be a significant weakness of a FFE/DFE that cannot be overlooked, since the analysis becomes intractable if it includes errors in the feedback section. One of the most efficient ways to specify the effect of those errors has often been via measurement [102], however, this goes beyond the scope of this work and, hence, it is not further discussed. At this stage the slicer is assumed to be ideal (i.e. with optimised threshold), while in Section 5.2 a more comprehensive analysis on the impact of non-optimum threshold is presented.

Optimum number of FFE/DFE taps:

A performance analysis of the FFE/DFE is carried out using the setup shown in Fig. 4.1, and the relative results are shown in Fig. 4.12. Note that the feedforward section is implemented as a FSE with $\tau = T/2$. Firstly, the power penalty is measured as a function of the number of taps that compose the equaliser, using as reference the B2B case without equalisation; the number of FFE-taps is swept from 3 to 12, while the number of DFE-taps from 0 to 3. The curve representing the 0-tap DFE (i.e. FFE only) is essentially a subset of the results shown in Fig. 4.10, and it is used here in order to better emphasise the benefits introduced by using a feedback section. These benefits can clearly be seen in the results, which show that when 1 or more DFE taps are used, the performance is greatly improved. Importantly, a FFE/DFE can provide the same amount of ISI mitigation as a linear FFE using a much smaller total number of filter coefficients. For instance, a 3-tap FFE + 1-tap DFE performs similarly to a 12-tap FFE, resulting in a power penalty of about 1.3dB and 1.5dB respectively. Moreover, if the comparison is done using the same total number of taps, it is possible to see that a 3-tap FFE + 1-tap DFE results in a power penalty that is about 2dB lower than a 4-tap FFE, further emphasising the superior performance offered by a FFE/DFE. The reason for this difference in performance between the two types of equalisers is explained in the final part of this section.

Another interesting characteristic that can be inferred from the curves in Fig. 4.12 is that, for the 120km transmission length considered, increasing the number
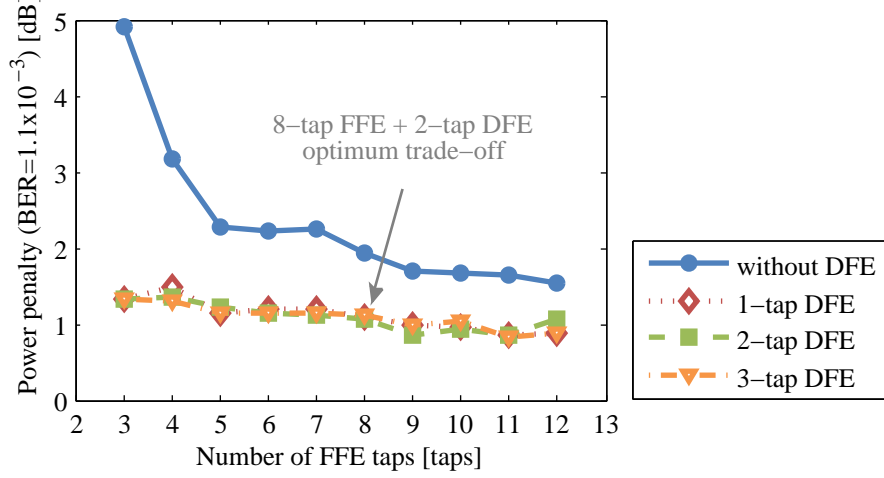
Figure 4.12: Power penalty at FEC threshold (BER=1.1×10^{-3}) as a function of the number of FFE/DFE taps after 120km of SMF.

of taps in the feedback section above 1-tap does not introduce any significant benefit. In fact, the three curves corresponding to the 1-,2-, and 3-tap DFE cases are basically overlying each other, and for all three of them the change in power penalty is only related to the increasing number of taps in the feedforward section. The need for a single feedback tap indirectly confirms the results reported in Section 4.2.1 where, assuming a symmetrical broadening, the amount of pulse spreading is estimated to be about 2bits (one bit on either side of the desired one). In other words, a feedback section characterised by one symbol-spaced tap is enough to cover for most of the post-cursor ISI accumulated over 120km, while compensating the pre-cursor ISI is done by the feedforward section. However, as for the linear equaliser case reported in the previous section, a conservative and recommended approach [103] is to increase the required number of taps by about 25-50% (rounding to the next integer value): for this reason, the overall number of taps for the feedback section is fixed to 2-taps.

Regarding the number of feedforward taps, the results in Fig. 4.12 show that when a feedback section is used the FFE can be reduced down to 3- or 4-taps with only negligible loss in performance compared to a 12-tap FFE. While choosing a 4-tap FFE + 2-tap DFE would significantly simplify the hardware complexity, however, it does not represent an optimum choice due to the fact that a reduced FFE length corresponds to a reduced tolerance to sampling phase[1]. This is a

---

[1]A longer FFE has better resilience against sampling phase drift.

crucial aspect that cannot be overlooked in particular in the context of burst-mode links where each packet can arrive at the receiver with unknown random bit phase. Furthermore, an adequate tolerance to sampling phase can also relax the design specifications of an actual training sequence generator, which as will be explained in Section 4.4 is needed to adapt the coefficients of the equaliser. Without this tolerance, the training sequence would need to be synchronised with great accuracy to the incoming (unknown) signal phase. Once again, this confirms that prudent engineering analysis is required to determine the optimum number of taps which can be different from application to application even when the required level of impairment compensation is the same.

Therefore, in this work the number of FFE taps is set to 8 taps, as concluded in the previous section for the linear equaliser case: this is not only the recommended 25-50% more than is required to cover for the delay spread over the transmission lengths taken into account, but also offers much greater tolerance to the sampling phase. This brings the overall number of taps up to 10-taps (8-tap FFE + 2-tap DFE), which can be considered a reasonable and practical trade-off between optimal performance and hardware complexity, being on the same order of the total number of taps in commercially available equalisers currently used for similar applications (for instance the 'Vitesse' VSC824X clock and data recovery with integrated adaptive continuous-mode EDC, designed for use in 10Gb/s Ethernet applications compliant with IEEE 802.3ae and IEEE 802.3aq, consists of 9-tap FFE + 4-tap DFE).

Tolerance of an 8-tap FFE + 2-tap DFE against CD (power-limited case):

In Fig. 4.13, the performance of the 8-tap FFE + 2-tap DFE is shown as a function of the transmission distance and compared with the case of the 8-tap FFE discussed in the previous section. The case without equalisation is also shown to better illustrate the benefits introduced by equalisation, and the B2B performance is used as reference for the power penalty calculation. It is possible to see that for short distances the FFE can perform the same as the FFE/DFE, however, after about 80km the power penalty of the FFE starts to increase rapidly whereas the penalty for the FFE/DFE remains smaller than 2dB up to almost 150km. This result indirectly suggests that the ISI can be approximated as linear up to about 80km, and only for longer distances its nonlinear nature starts to dominate making a linear equaliser only a suboptimal solution [83].

The FFE/DFE can clearly outperform the FFE in presence of nonlinear ISI however it is not able to completely compensate for it, confirming the limits of this quasi-linear equaliser architecture. To further improve the performance, more advanced equalisers such as the nonlinear FFE/DFE or MLSE/Viterbi equaliser [76, 104] must be employed. However, the latter possibility is not considered in this work since Fig. 4.13 clearly shows that a FFE/DFE can compensate for a significant portion of the dispersion accumulated over distances comparable to, or greater than, those targeted for LR-PONs, with the advantage of much lower complexity compared to more advanced equaliser designs. In fact, the 8-tap FFE + 2-tap DFE can achieve transmission distances of nearly 120km at 1dB penalty, compared to just 73km obtained for the case without equalisation, providing a gain greater than 1.6 times.
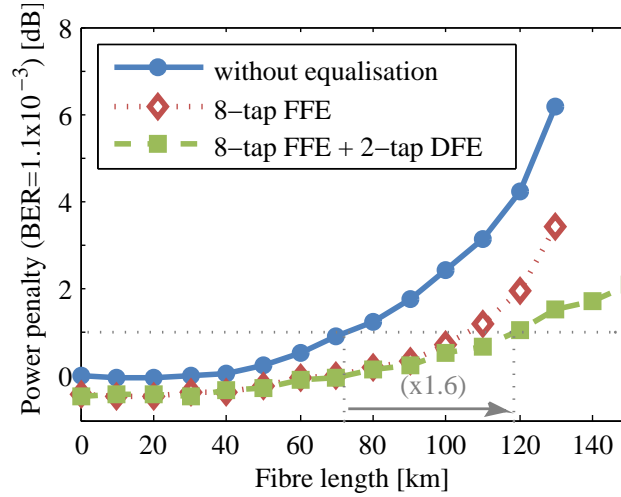
Figure 4.13: Power penalty at FEC threshold (BER=1.1×10^{-3}) as a function of the transmission length for different equaliser structures.

Strengths and weaknesses of a FFE/DFE over a linear equaliser:

An intuitive explanation for the advantages offered by the FFE/DFE over a linear equaliser is the following [94]. The coefficients of a FFE are selected to force the combined channel and equaliser impulse response to approximate a unit pulse. In a FFE/DFE, the ability of the feedback section to cancel the post-cursor ISI imposes fewer constraints in the choice of the coefficients of the feedforward section which now only has to suppress the pre-cursor ISI. The combined impulse response of the channel and FFE section may have non-zero samples following the

main pulse, meaning that the feedforward section does not need to approximate the inverse of the channel characteristics and therefore avoids excessive noise enhancement showing also less sensitivity to the sampling phase [94] in comparison to a linear equaliser. In fact, the post–cursor ISI cancelled by the feedback filter causes no additional noise enhancement at all since the slicer eliminates the noise before feedback.

As mentioned earlier, one disadvantage of the FFE/DFE architecture is that incorrect decisions result in error propagation. Fortunately, for bit error rates below 10^{-2} [105], this error propagation is usually not catastrophic but causes some performance degradation compared to error free feedback.

Table 4.3 summarises the main results discussed throughout this section regarding the advantages introduced by a FFE/DFE over a FFE-only structure.

Advantages ✔	Disadvantages ✖
Total number of FFE/DFE coefficients is smaller than for a FFE providing the same amount of ISI mitigation.	Additional implementation complexity.
For the same number of taps, a FFE/DFE has superior performance to a FFE.	
The DFE allows more freedom in the choice of the FFE coefficients.	Error propagation.
No noise enhancement for post-curst ISI cancellation.	

Table 4.3: Summary of advantages/disadvantages of a FFE/DFE.

4.4 Adaptive Equalisers

In recent decades a large amount of research has been conducted on adaptive equalisation schemes [94, 100, 105]. Traditionally, adaptive filters are required to compensate for the distortion effects of changing channel conditions: in fact, in practical situations the channel parameters are not known in advance and moreover they may vary significantly with time. Adaptive filters, therefore, can be defined as computational devices that attempt to model the relationship between

two signals (the received one and the desired one) in real time and in an iterative manner [96], providing the means of tracking the channel characteristics. In the context of the burst-mode applications discussed in this thesis, adaptation can represent a rather challenging task since it has been shown [79, 106, 107] that it must be performed on a packet-by-packet basis, in particular when the differential reach of the PON is a significant fraction of the total reach (effectively, it is as if each packet went through a different channel). Note that, in such burst-mode systems, the main reason for adaptation is to initialise the filter coefficients for each new incoming packet rather than tracking of the channel characteristics, as the channel time variation is slower than the duration of the bursts. In general, since the channel response is unknown, the adaptive algorithm that determines the updating of the filter coefficients requires extra information, and this is usually given in the form of a reference (known) signal called the desired signal or training sequence which is embedded at the beginning of each burst.
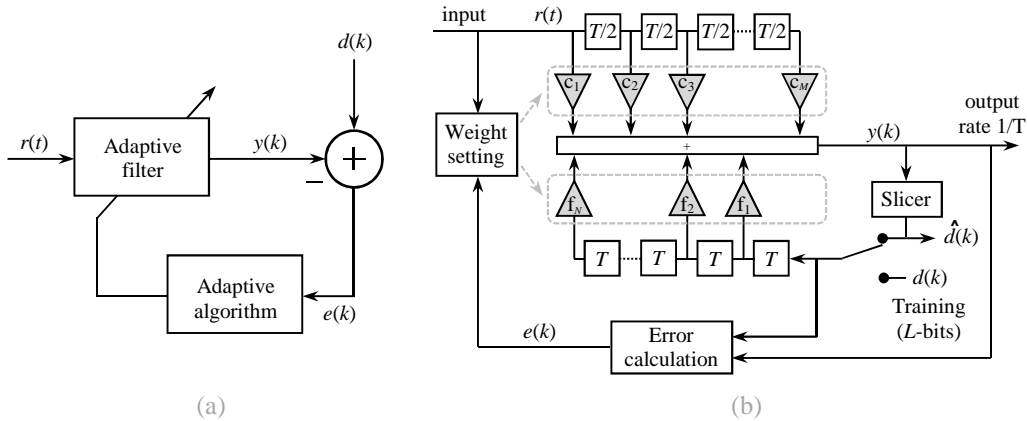
Figure 4.14: Generic adaptive filter structure (a) and corresponding adaptive FFE/DFE (b).

The generic structure of a channel equalisation system is shown in Fig. 4.14(a) where $r(t)$ and $y(k)$ are respectively the received signal and the signal at the output of the equaliser sampled at the instant k, while the block diagram corresponding to an adaptive equaliser of the type FFE/DFE described in the previous section is shown in Fig. 4.14(b). In the literature, adaptation is performed in two steps, namely first training, followed by decision-directed (or tracking) mode. In training mode, a synchronised version $d(k)$ of the desired signal is generated at the receiver in order to acquire information about the channel characteristics.

105

Then, a sequence of error samples defined as

$$e(k) = d(k) - y(k), \tag{4.4.1}$$

is computed at the equaliser output and used to form a performance function (often known as the cost function) that is required by the adaptation algorithm in order to determine the appropriate updating of the filter coefficients. In principle, the minimisation of this cost function implies that the signal at the equaliser output is matching the desired signal (at the sampling point). Once the training sequence is terminated and the coefficients are near optimal, the equaliser can be switched to decision-directed mode, where the output signal after the decision device is used to compute the error instead of the training sequence (Eq. (4.4.1) becomes: $e(k) = \hat{d}(k) - y(k)$). In this way, the equaliser tracks the changing channel and continuously updates its coefficients accordingly over time.
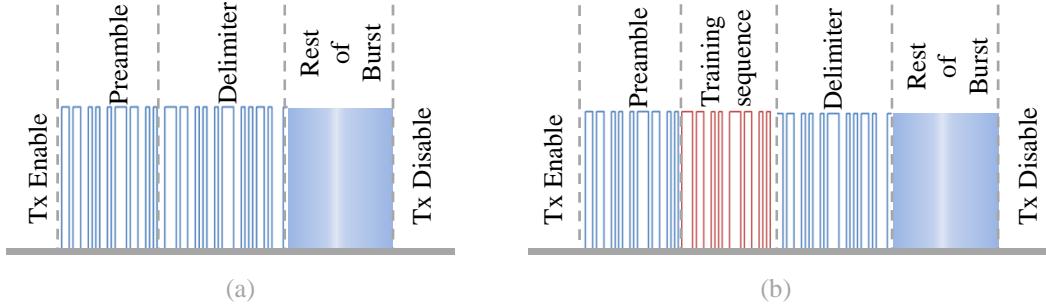
Figure 4.15: Example of burst-mode required overhead for a conventional non-equalised system (a) and for a system that employs electronic adaptive equalisation in trained mode (b).

The training sequence:

Note that the inclusion of the training sequence with the transmitted information adds an overhead and thus reduces the traffic efficiency of the system[1]. This is illustrated in Fig. 4.15, where it is shown that the required burst overhead in a conventional non-equalised system (Fig. 4.15(a)) needs to be further extended to accommodate the training sequence necessary in systems which employ an electronic adaptive equaliser (Fig. 4.15(b)). For this reason, in some applications, adaptation schemes that do not require the aid of a training sequence $d(k)$

---

[1]The traffic efficiency is defined as the ratio of transmitted data bits to the total number of transmitted bits.

are preferred, and the resulting equalisers are known as blind or self-recovering equalisers. In such cases, one can use additional information about the characteristics of a 'hypothetical' $d(k)$ (such as its predicted statistical behaviour or amplitude characteristics) to form suitable estimates of $d(k)$ from the signals available to the adaptive filter [96]. Based on these definitions, for example, an intuitive way of performing blind equalisation could be skipping the training mode mentioned above and running straight in decision-directed mode from the beginning of the adaptation process. Note that blind equalisers present a number of disadvantages when compared with the traditional trained equalisers. In particular, the undesired local minima and the slower convergence rate can be considered main drawbacks of these self-learning structures [108, 109]. The presence of such local minima can eventually lead to instability and possibly divergence. For this reason, blind equalisation is beyond the scope of this work and is not discussed further in detail.

At this stage one may wonder what type of sequence should be used for training. In general, it may consist of periodic isolated pulses or a continuous sequence with a broad uniform spectrum such as a pseudo-noise (PN) sequence [94]: the latter has the advantage of much greater average power, hence a larger SNR for the same peak transmitted power. The best known example of such PN waveform is a maximal length pseudorandom binary sequence (m-sequences or PRBS), which is essentially a two-valued PN-signal. The reason why PRBS are often used as a general-purpose test pattern in NRZ applications is that they can provide some of the statistical properties of random signals (average, power, spectrum, etc.) but with predictable values. The PRBS is typically denoted as a $2^X - 1$ PRBS, where the power X indicates the shift register length used to create the pattern. Each $2^X - 1$ PRBS contains every possible combination of X bits (except one). It is clear that not any value of X is suitable for the applications of interest in this thesis: in fact, as will be explained throughout the next few chapters, if training has to be concluded within a limited number of bits (e.g. in the order of few hundred bits), X must be smaller than 8. As a matter of fact, a short PRBS such as the $2^7 - 1$ PRBS (127 bits), is often used in Ethernet, Fibre Channel, and high-speed video test-applications, because it provides a good approximation to an 8b10b-encoded NRZ data stream [110], and for this reason it is employed in all the experiments presented throughout the thesis as training sequence.

As mentioned above, in order to iteratively update the equaliser coefficients, an adaptive algorithm driven by the error computed during the training process is needed. Although different methods are available, this thesis focuses on the least mean square (LMS) scheme, as it is has good performance, is easy to implement, and is very robust [100, 111]. These characteristics enable a trade-off between performance and computational complexity (thus cost), making it an excellent candidate as an adaptation algorithm for cost-effective equalisers in access networks. The main concepts behind the LMS algorithm and its properties are explained in Section 4.4.1 below.

4.4.1 MSE Criterion and LMS Algorithm

In the context of equalisation, the idea behind a generic LMS-based algorithm is to find the optimal filter weights which minimise a particular cost function using the steepest descent (or gradient descent) method [112]. As the name implies, the method relies on the slope at any point on the surface of the cost function to provide the best direction in which to move[1]. With the knowledge of this direction it is then possible to move to a lower point on the surface and hence find the bottom of the surface (i.e. the optimum value for the weights) in an iterative manner.

Steepest descent method:

For a FFE/DFE the cost function can be defined according to the mean-squared-error (MSE) criterion as:

$$J(k) = E\left[e^2(k)\right] = E\left[(d(k) - y(k))^2\right] = E\left[(d(k) - \boldsymbol{W}(k) \cdot \boldsymbol{X}^T(k))^2\right], \quad (4.4.2)$$

where $e(k)$ is the error computed according to Eq. (4.4.1), $E[\cdot]$ is the shorthand for the expected value, $\boldsymbol{X}(k) = [r(t_0 + kT - \tau) \ldots r(t_0 + kT - M\tau) \, d(k-1) \ldots d(k-N)]$ is the vector of input signal samples in the feedforward and feedback section of the equaliser, $[\cdot]^T$ is the transpose of a matrix, $d(k)$ is the training signal[2], and $\boldsymbol{W}(k) = [c_1(k) \ldots c_M(k) \, f_1(k) \ldots f_N(k)]$ is the vector containing the coefficients of the feedforward and feedback sections at the sampled instant

---

[1]The steepest descent direction gives the greatest change in elevation of such a surface.

[2]Note that if the equaliser is operated in decision directed mode instead of training mode, $d(k)$ in Eq. (4.4.2) must be replaced by the equaliser output signal after the decision device , see Fig. 4.14(b).

k. Note that the choice of a cost function is not limited to the MSE criterion, and any arbitrary function of the error $\Phi(e(k))$ that has the following characteristics can, in principle, be employed:

- $\Phi(e(k))$ is an even function of the estimation error signal, i.e. $\Phi(e(k))$ is equal to $\Phi(-e(k))$;

- $\Phi(e(k))$ is monotonically increasing in the argument $|e(k)|$: given two errors e_1 and e_2, with $|e_1| < |e2|$, $\Phi(e_1) < \Phi(e_2)$ must hold.

A complete derivation of the steepest descent method is beyond the scope of this thesis. However, the reader may refer to [96, 100, 112, 113] for a complete treatment of the topic, where the authors present a general approach for the coefficient optimisation in the case of adaptive FIR filters. The authors show that for these filter structures the error $e(k)$ is a linear function of the weights and $E[e^2(k)]$ represents a quadratic error surface that has a single global minimum point at which gradient algorithms can successfully converge. In contrast, for IIR filters the analysis becomes somewhat complicated due to the fact that the output signal is a nonlinear function of the weights (the current output itself depends on previous weights) and the MSE is no longer a quadratic function of the feedback coefficients, although it is for the feedforward equalisers. This means that the error surface may not be unimodal [114] and, therefore, gradient algorithms may converge to undesired local minima where the estimates can be only sub-optimal.

Nevertheless, if adaptation is performed using an 'ideal' training sequence to compute the error according to Eq. (4.4.1), then, it is still possible to obtain a cost function with a unique, global minimum. In fact, since the training signal $d(k)$ is independent of the equaliser output, one can conceptually think of the feedforward and feedback sections of an IIR filter as of two independent FIR filters whose sum $y(k)$ produces an error (calculated using Eq. (4.4.1)) that is a linear function of the weights [115, 116]. Therefore, under the aforesaid conditions, the same procedure used for adaptive FIR filters can be directly applied to adaptive IIR filters as well [96], and the resulting weights update equation is given by:

$$\begin{aligned}
\boldsymbol{W}(k+1) &= \boldsymbol{W}(k) - \frac{1}{2}\mu\nabla_{\boldsymbol{W}(k)}J(k) \\
&= \boldsymbol{W}(k) + \mu E\left[e(k)\boldsymbol{X}(k)\right],
\end{aligned} \tag{4.4.3}$$

where $\nabla_{\boldsymbol{W}(k)}J(k) = \partial J(k)/\partial \boldsymbol{W}(k) = -2E[e(k)\boldsymbol{X}(k)]$ denotes the gradient of $J(k)$ with respect to $\boldsymbol{W}$, and μ is the adaptation gain often called step-size, which is a real-valued positive constant.

Instantaneous gradient approximation:

From Eqs. (4.4.2) and (4.4.3), it is clear that this method uses the statistics of the input and desired signals and not the actual measured signal. In practice, the input signal statistics are not known a priori and, moreover, if they were known it could be possible to find the optimum solution directly in one step [112]. Accordingly, the method of steepest descent described above cannot be used as estimation procedure on its own in most practical situations, and a simple approximation that yields an efficient variation of the steepest descent algorithm is used instead. Instead of using the MSE cost function defined in Eq. (4.4.2), an instantaneous squared error function given by

$$J(k) = e^2(k), \tag{4.4.4}$$

is used. In other words, the gradient vector $-2E[e(k)\boldsymbol{X}(k)]$ is replaced with the quantity $-2e(k)\boldsymbol{X}(k)$: this approximation is known as the instantaneous gradient of the mean-squared error surface, and the adaptive filters that are based on it are often called stochastic gradient adaptive filters. Accordingly, Eq. (4.4.3) can be rewritten as

$$\boldsymbol{W}(k+1) = \boldsymbol{W}(k) + \mu e(k)\boldsymbol{X}(k). \tag{4.4.5}$$

Note that the only difference between the procedure given by Eq. (4.4.5) and the steepest descent method of Eq. (4.4.3) is the removal of the expectation operator $E[\cdot]$ from the gradient estimate. This is a crude approximation of the gradient of the MSE surface, however, the quantity points in the same direction as the true gradient on average. Since the step-size μ is normally chosen to be a moderate value in order to ensure a low steady-state MSE, any errors introduced by this instantaneous gradient approximation are averaged over several iterations, and hence the performance loss is relatively small [112]. The algorithm described by Eq. (4.4.5) has become known as the Least-Mean-Square (LMS) adaptive filter, a name coined by its originators (Widrow and Hoff, 1960 [117]), and because of its simplicity and properties it is the most widely used adaptive filter today.

4.4.2 Considerations on Convergence with LMS algorithm

As the LMS algorithm does not use the operator $E[\cdot]$ in the gradient estimate, the weights may never reach their optimal value in the absolute sense, but a convergence is possible on average [112]. This means that even though the weights may keep changing slightly, they change around their optimal value. However, if the variance with which the weights change is large, convergence in the mean would be misleading: this problem may occur, if the value of step-size is not chosen properly. In fact, from Eq. (4.4.5) it is clear that the step-size μ plays a critical role in determining the convergence behaviour of the LMS adaptive filter (or whether it converges at all!).

An upper bound for the step-size:

Once again, a complete derivation of the conditions for which μ guarantees the convergence of the coefficient's mean values is beyond the scope of this work. However, the reader can find an exhaustive analysis on the topic in [96, 100, 112, 113], where stringent bounds on the step-size values are derived for both FIR and IIR adaptive filters in order to guarantee their convergence. The final well-known expression for the FIR case is reported below:

$$0 < \mu < \frac{2}{M\sigma_r^2}, \tag{4.4.6}$$

where M is the number of coefficients in the filter, and σ_r^2 represents the mean-squared value of the input signal (i.e. its power). For the IIR case, instead, μ can be chosen to be

$$0 < \mu < \frac{1}{M\sigma_r^2 + N\sigma_d^2}, \tag{4.4.7}$$

where the first term in the denominator is defined above, N is the number of feedback coefficients, and σ_d^2 represents the power of the input signal of the feedback section. From Eqs. (4.4.6) and (4.4.7) it is clear that the step-size must be positive[1] and at the same time smaller than a quantity that is inversely proportional to the power of the signals entering the respective sections.

It is possible to see an immediate practical difficulty with the LMS algorithm in some real applications: namely that some knowledge of the input signal statis-

---

[1] A negative value would cause the coefficients to move 'up' the MSE surface.

tics is required in order to choose a reasonable step-size value, and this knowledge might not be available. In this case, however, one can always select a conservative μ value so that the LMS algorithm converges for the ranges of input statistics expected for a given application. In fact, the equations above do not offer a specific value for the step-size, and it is up to the designer of the system to provide the best trade-off for each particular application. Regarding the experimental results presented in this thesis, the knowledge of the signal powers does not represent a problem at all, since even the lab-data is always processed offline and hence the required information can be easily estimated.

Note that, although this could seem an unrealistic approach at first sight, it is actually very close to the 'real-world' application that the experiments presented in this thesis are trying to address. As is explained in more detail in Section 6.1, the input signal of the feedforward section of a potential 'real-world' BM-EDC is coming directly from the linear burst-mode receiver (LBMRx), whose output signal is characterised by a peak-to-peak amplitude that is decided by the designer (and it is constant for optical input signals with a dynamic-range of less than 15dB). Similarly, the training sequence entering the feedback section (or the slicer output if the equaliser is operated in decision-directed mode) is characterized by a well-known amplitude. Therefore, an accurate upper bound for the step-size can be easily estimated a priori as effectively done with simulations/offline processing. Note, however, that in practice the value of μ should not be chosen close to the upper bounds specified in Eqs. (4.4.6) and (4.4.7), since they are somewhat optimistic due to approximations and assumptions made in the derivation of the bound.

Trade-off between adaptation speed and steady-state error:

A more precise value of μ that guarantees a reasonable trade-off between performance and adaptation speed can be derived as follows. As mentioned above, in the context of burst-mode application, reducing the overhead introduced by the use of a training sequence is a crucial aspect that needs to be addressed in order to improve traffic efficiency. The idea in this work, is to attempt to limit the length of the training period to be at most of the same order as the burst overhead in current standards, but with the objective of reducing it even further. For instance, in current 10Gb/s PON standards like the ITU-T Recommendation

G.987.2 (2010) or the IEEE 802.3av (2009) [118, 119], the burst overhead[1] is of the order of hundreds of nanoseconds, or equivalently thousands of bits. Therefore, in order to determine an optimal μ value, one approach is to measure the performance of a FFE/DFE in terms of power penalty as a function of different step-size values for a target training length of, e.g., 1000bits (100ns, assuming one iteration per bit).

The setup used for this experiment is, once again, the one shown in Fig. 4.1, where the transmission distance is set to 120km and the equaliser-under-test employs an 8-tap FFE + 2-tap DFE as determined in the previous section. In order to extract a more generic behaviour which is not necessarily related to the specific power levels considered in the simulation, a normalisation of the step-size in terms of the upper bound has been adopted. That is, μ can be expressed in terms of a variable which is a fraction of the upper bound. In the remaining part of this section, such a variable is called the step-size scaling factor (SF). Note that instead of using Eq. (4.4.7) for the upper bound estimation as is often done for IIR filters [96], a slightly different approach has been used. In principle, it is possible that the input power in the feedforward section is significantly different from the power in the feedback one, and therefore updating all the weights using as step-size a fraction of the same upper bound may not be an optimal choice (though it is more conservative). In fact, since during the training process one can conceptually think of the feedforward and feedback sections of an IIR filter as two independent FIR filters [115], the weights from the two sections can be updated separately using different values of step-size. Therefore, in this work, instead of using the generic LMS update equation given by Eq. (4.4.5), two separate update equations are used for the feedforward and feedback section respectively:

$$\boldsymbol{c}(k+1) = \boldsymbol{c}(k) + \mu_{FFE} \cdot e(k) \cdot \boldsymbol{r}(k), \tag{4.4.8}$$

$$\boldsymbol{f}(k+1) = \boldsymbol{f}(k) + \mu_{DFE} \cdot e(k) \cdot \boldsymbol{d}(k), \tag{4.4.9}$$

where μ_{FFE} and μ_{DFE} are calculated separately using the upper bound of Eq. (4.4.6) as

$$\mu_{FFE} = SF \frac{2}{M\sigma_r^2}, \tag{4.4.10a}$$

---

[1]The burst overhead is necessary in order to accommodate several physical processes like laser on/off time, timing drift tolerance, level recovery, receiver settling, clock recovery, and start of burst delimitation.

$$\mu_{DFE} = SF \frac{2}{N\sigma_d^2}. \tag{4.4.10b}$$

Figure 4.16 shows the power penalty required to achieve a BER of 1.1×10^{-3} relative to the B2B case without equalisation, obtained using this approach. The results are presented in as a function of the step-size scaling factor SF (log-scale). The penalty curve resembles a 'U' shape, which is a characteristic behaviour of the system. The increase in power penalty for small scaling factors (i.e. $SF < 1/100$) is due to the fact that adaptation is performed 'too slowly', whereas when the scaling factors approaches unity (i.e. for step-size values that approach the upper bound) the adaptation is performed 'too fast' and the equaliser becomes unstable. To clarify this concept, the evolution of the weights as a function of the iteration number (up to a thousand bits, i.e. a thousand iterations) is shown in the insets of Fig. 4.16 for a few different values of SF.
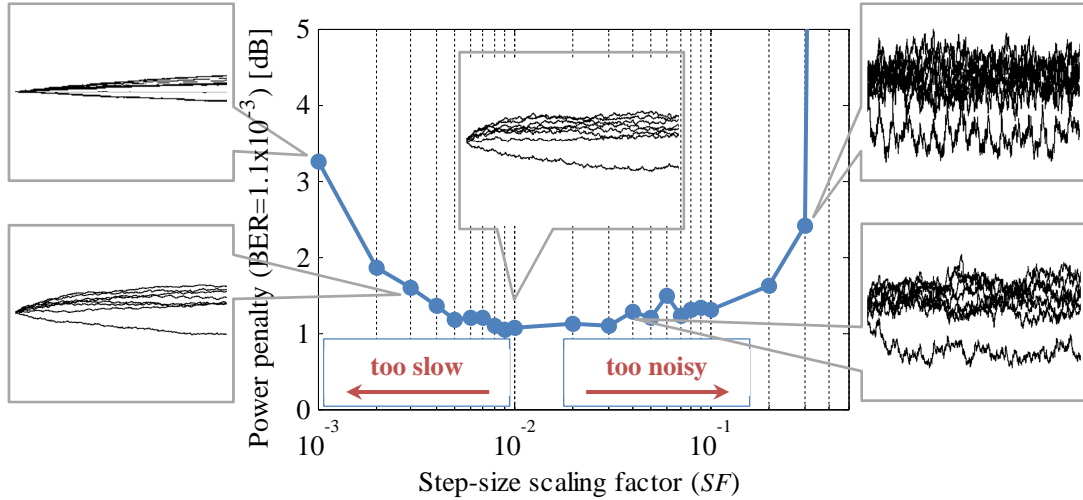
Figure 4.16: Power penalty at FEC threshold (BER=1.1×10^{-3}) as a function of the step-size scaling factor (SF) after 120km of SMF when using an equaliser with 8-tap FFE + 2-tap DFE trained for 1000bits. The insets show the evolution of the FFE weights as a function of the iteration number (up to 1000bits) for few different SF values.

For simplicity only the 8-FFE coefficients are reported and, to better illustrate the concept, all insets are shown using the same scale. Looking at the inset on the bottom-left side, which corresponds to a SF of 1/200, it is clear that the choice of a small step-size leads to a slow adaptation. However, it also results in a low fluctuation of the filter coefficients in the steady-state from their optimum values. Note that if the step-size is too small, however, these optimum values

may not be achieved within the desired number of iterations due to the fact that adaptation is excessively slow, and this can result in additional penalty. This is the case illustrated by the upper-left inset, where SF is chosen to be 1/1000. Conversely, looking at the inset on the bottom-right side, which corresponds to a SF of 1/20, one can see that choosing a large step-size leads to a much faster adaptation at the expense of a large deviation in the filter coefficients from their optimum steady-state value. In the extreme case of very large step-sizes, e.g. the case corresponding to the upper-right inset where SF is about 1/3, the noise due to these fluctuations becomes so high that a significant penalty is measured in comparison to previous cases. At this stage it is obvious that a compromise is necessary in order to achieve the best performance in terms of adaptation speed and low steady-state noise. This is well illustrated, for example, by the case shown in the inset at the centre of Fig. 4.16, which corresponds to a SF of 1/100. Indeed, all the step-sizes in the vicinity of this value could represent an optimal trade-off for the application being studied. Therefore, for the remainder of this thesis, the scaling factor used to compute μ_{FFE} and μ_{DFE} according to Eqs. (4.4.10a) and (4.4.10b) is fixed to $SF = 1/50$, unless specified otherwise.

4.5 Summary

This chapter presented a review of linear and quasi-linear electronic equalisers. For the first time to the best of our knowledge, the analysis was extended specifically to consider the optimisation of equalisers for applications in long reach PONs. The attention was focused on the design and comparison of SSE, FSE, and FFE/DFE structures employed to compensate mainly for the CD accumulated over >100km of SMF. In particular, it has been shown that an FSE with tap spacing τ selected such that τ-sampling satisfies the sampling theorem can effectively compensate for more severe distortion than an SSE, and exhibit a significant improvement in sensitivity to sampling-phase errors. Such a FSE can synthesise and combine the characteristics of an adaptive matched filter and a SSE, eliminating the need for an actual analog matched filter. In addition to improved tolerance to sampling-phase errors, a FSE can also mitigate amplitude distortion with less noise enhancement than a SSE, since spectral nulls arising from cancellation by aliasing are eliminated.

A rule of thumb is presented to estimate the optimum number of taps for a

linear equaliser (SSE or FSE) used to compensate for CD over up to 120km of SMF, and the corresponding results are validated through numerical simulations. It is found that a further increase in length beyond 8-tap does not bring any major benefit (the slight improvement does not justify the additional implementation complexity).

A DFE provides significantly better performance than a linear equaliser in the presence of severe amplitude distortion by reconstructing and subtracting (with appropriate weighting) the past-symbol-induced ISI from the equaliser output before a new decision is made. A detailed study on the optimum number of FFE/DFE taps was carried out and it was shown that, for the applications of interest, a reasonable and practical trade-off between optimal performance and hardware complexity is given by the 8-tap FFE + 2-tap DFE structure. Such an equaliser can achieve transmission distances of about 120km at 1dB power penalty against the just 73km obtained for the case without equalisation, providing a gain greater than 1.6 times.

Finally, a number of considerations on the LMS adaptation speed and its convergence were discussed: in particular, it was shown that a careful choice of the step-size parameter in the LMS update equation can ensure convergence in timescales compatible with the burst-mode overhead in current PON standards (while providing low steady-state noise). This is achieved by using a scaling factor of 1/50 in Eqs. (4.4.10a) and (4.4.10b).

Chapter 5

Impact of Multiple Impairments
on EDC Performance

In the previous chapter, a detailed study and optimisation of a modelled electronic dispersion compensator (EDC) to be used in access applications was carried out under the assumption that chromatic dispersion (CD) along with the thermal noise from the receiver are the only effects impairing the desired signal. In practical situations this may not be the case, and other impairments or noise mechanisms could contribute to the signal degradation as mentioned in Section 2.1. In this chapter, the performance of adaptive equalisers (with adaptation based upon the LMS algorithm) used to compensate for CD is discussed when other degrading effects are also involved, and a detailed numerical analysis is carried out in order to determine whether the same equaliser can also mitigate for such effects without losing its effectiveness in compensating CD.

In Section 5.1, the attention is focused on how non-optimal transmitter and receiver bandwidths impact the system performance and how an 8-tap FFE + 2-tap DFE of the type described in Chapter 4 can be used to compensate for such bandwidth restrictions.

Section 5.2 repeats the analysis presented in Section 4.3, where CD is the dominant impairment taken into account: here, however, the system is stressed from noise arising from optical amplifiers to reduce the optical signal-to-noise ratio (OSNR), rather than the thermal noise from the receiver. This study investigates whether the FFE/DFE exhibits a loss in performance in comparison to the previous case, and evaluates the impact of such different noise mechanisms on the equaliser design, with focus on the optimisation of the DFE slicing-threshold.

The emphasis of Section 5.3 is on the performance degradation occurring in the presence of patterning introduced by a semiconductor optical amplifier (SOA) which is employed as a reach-extender or preamplifier. The benefits introduced by an FFE/DFE in mitigating patterning are discussed, as well as the equaliser limits with such impairments.

Finally, a brief summary of the main results obtained in this chapter is presented in Section 5.4.

5.1   Non-Optimal Tx and Rx Bandwidths

This section first studies the performance of a power-limited system in order to determine the optimum receiver (Rx) electrical filter bandwidth and analyses the impact of bandwidth variations[1] on receiver sensitivity for the case without equalisation. Subsequently, the investigation is repeated with the equaliser in order to understand the effects of the same bandwidth variations on equalised systems.

To make this study even more complete, the same analysis is then extended to the electrical filter bandwidth of the transmitter (Tx), both with and without equalisation. The setup employed for these simulations is again the one reported in Fig. 4.1 and discussed in detail in Section 4.1[2]. Then, in order to emulate different Tx and Rx bandwidths, the (-3dB) cut-off frequency of the two Bessel filters is swept respectively between 1.5- and 15GHz for the Tx filter, and between 1.5- and 10.5GHz for the Rx filter (note that the filter order is maintained constant and equal to four throughout the sweeps).

5.1.1   Rx-Bandwidth

Over the past several years a number of studies have been carried out in order to determine the optimum bandwidth for a generic transimpedance front end and subsequent filter employed in a fiber optic receiver modules [45, 120, 121, 122]. For NRZ transmission, the best receiver performance relies on a balance between the noise admitted by filters with bandwidths higher than required, and the ISI

---

[1]This may occur due to for example temperature drift and fabrication tolerances in the optical receiver integrated circuit.

[2]Once again, the SOA is assumed ideal and the AWGN generator is disabled, meaning that thermal noise is the main noise mechanism limiting system performance

generated by excessive filtering [123]. This concept is illustrated in Fig. 5.1, which shows the general trend of BER as a function of the Rx filter bandwidth for a fixed input power to the receiver and fixed bit rate of 10Gb/s. The eye diagrams and histograms at the sampling instant (red dashed line) relative to the 3-, 6-, and 15GHz cases are also shown in the insets.
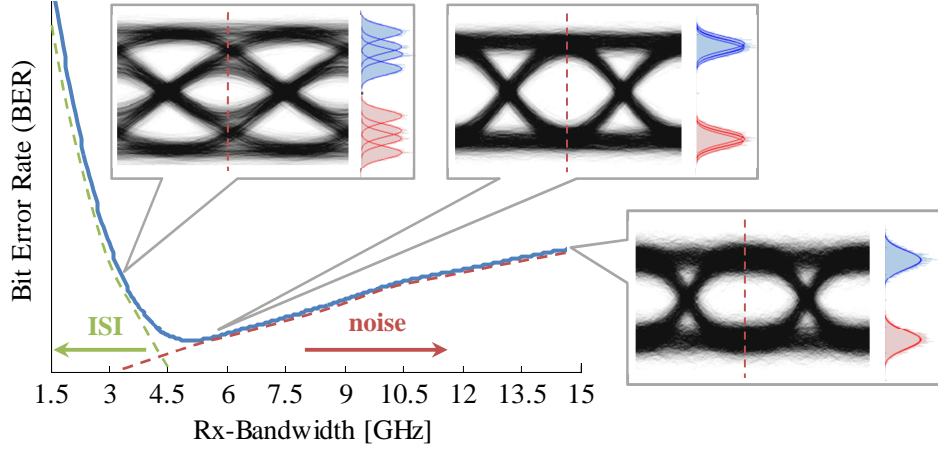
Figure 5.1: BER trend as a function of the receiver filter bandwidth for a fixed power input to the receiver. The insets show the relative eye diagrams and histograms (B2B).

ISI vs noise:

If the receiver bandwidth is too wide, the receiver preserves the signal waveform without distortions, but at the same time it is affected by a considerable amount of noise, which induces bit errors and hence translates into low receiver sensitivity (e.g. 15GHz case, right-side inset). On the other, if the receiver bandwidth is too narrow, the noise is reduced and thus the sensitivity is improved, but extra penalty is introduced due to intersymbol interference (ISI). ISI also reduces the sensitivity because the output signal swing is reduced for certain bit sequences (for example, the signal swing for a '01010101...' sequence will be lower than that for a '00110011...' sequence), and hence the eye at the receiver output closes. In order to make this effect more evident the histograms of Fig. 5.1 (one per meta-symbol) are created using a BER estimator with 1pre-bit and 1post-bit (see Section 2.3). In other words, the meta-symbols taken in account are 2^3 (i.e. 000, 001, 010, 011, 100, 101, 110, 111) and each one of them is represented by a different noise distribution. This is very clear from the histograms relative to the 3GHz case (left-side inset). Note that the BER estimator is used here only

to generate the histograms for a qualitative analysis, but all the BER results presented in this thesis are obtained using counting techniques.

It is possible to conclude from this line of reasoning that there must be an optimum receiver bandwidth for which the sensitivity is best. As a rule of thumb for NRZ receivers, it is often assumed that the optimum bandwidth is approximately a value close to three quarters of the bitrate (e.g. a number between 0.7 and 0.75 times the bitrate). However, in reality, the optimum bandwidth depends on the roll-off rate and phase response (group delay) of the receiver. In fact, it can be shown that the faster the roll-off rate, the lower the bandwidth required, and the greater the achieved sensitivity due to the narrower bandwidth over which broadband noise is amplified [124]. In other words, different receiver designs will have different sensitivities.

B2B (non-optimal Rx bandwidth only):

To better study this behaviour for the applications of interest, the performance is measured in terms of power penalty required to achieve a BER of 1.1×10^{-3} as a function of the Rx bandwidth, using as reference the 7.5GHz Rx filter case. The results (with respect to the 7.5GHz case) are presented in Fig. 5.2.

The curves are shown for the B2B case (solid symbols) and for a target transmission length of 120km (open symbols), with and without an 8-tap FFE + 2-tap DFE LMS-equaliser (dashed lines and solid lines respectively). Note that the Tx filter bandwidth is fixed to 12GHz while the Rx filter bandwidth is swept. From Fig. 5.2 it is possible to see that in the B2B case without equalisation the optimum filter bandwidth is around 4.5- to 6GHz, proving that the assumption of optimum filter bandwidth for a cut-off frequency corresponding to three quarters of the bitrate is not necessary accurate and cannot be generalised.

This curve suggests that for cut-off frequencies in the range from 10GHz (hence equal to the bit rate) down to 4.5GHz, the benefits introduced by filtering the thermal noise are greater than the ISI penalty associated with the filtering itself. However, for filter bandwidths smaller than about 4GHz, the power penalty increases extremely fast up to the point that it is no longer possible to achieve a BER of 1.1×10^{-3} because of error flooring associated with ISI (the penalty is greater than 10dB at about 2GHz). This means that, in general, broader than optimum filtering (>6GHz) is to be preferred to too narrow filtering (<3.5GHz), since the degrading effect of increasing noise power is less severe than spectrally

120
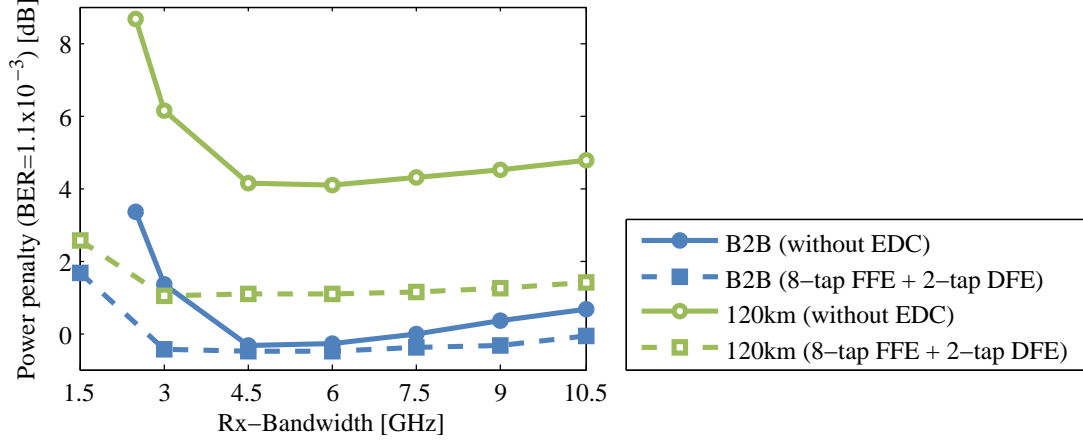
Figure 5.2: Power penalty at FEC threshold (BER=1.1×10^{-3}) as a function of the receiver filter bandwidth in B2B and after 120km of SMF, with and without equalisation.

truncating the signal [45]. The FFE/DFE (trained for an ideal length of 10000bits using the LMS algorithm) is able to compensate for the bandwidth reduction due to low pass filtering down to frequencies of 1.5GHz with less than 2dB penalty overall, proving that this type of equaliser can be very efficient when compensating for linear ISI (it can completely correct ISI down to 3GHz with no penalty).

Transmission over 120km of SMF (non-optimal Rx bandwidth + CD):

The curves for the 120km transmission case show the same trend as the B2B results, except they are shifted by the expected penalty due to chromatic dispersion (CD) of about 1.5dB and 4.5dB for the cases with and without equalisation, respectively (see Fig. 4.13 at 120km). The fact that the two curves corresponding to the equalised cases (B2B and 120km) show approximately the penalty difference for the entire range of bandwidths (except for the lowest values), indicates that the equaliser is able to simultaneously mitigate the ISI introduced by a non-optimal Rx filter bandwidth and the ISI due to CD with no extra penalty due to their combination; the effectiveness of the equaliser in compensating CD is not compromised whatsoever.

5.1.2 Tx-Bandwidth

The attention is now focused on the transmitter, whose bandwidth is swept from 1.5- to 15GHz while the receiver bandwidth is kept fixed to 7.5GHz. Intuitively, one should expect a slightly different general trend for the BER curve in comparison to the receiver case presented above. In fact, the way that ISI and thermal noise affect the performance in this case is conceptually different from the previous one: while the Tx filter bandwidth is swept, the Rx one is kept fixed, meaning that the amount of thermal noise is now constant throughout all the cut-off values considered and, therefore, is independent of the Tx bandwidth. This is illustrated in Fig. 5.3, where the general trend of the BER is plotted as a function of the Tx filter bandwidth for a fixed input power to the receiver. The eye diagrams and histograms at the sampling instant (red dashed line) relative to the 3-, 4.5-, and 15GHz cases are also shown in the insets. As for the previous case, the histograms are created using a BER estimator with 1pre-bit and 1post-bit in order to better see the effects of ISI on different meta-symbols.
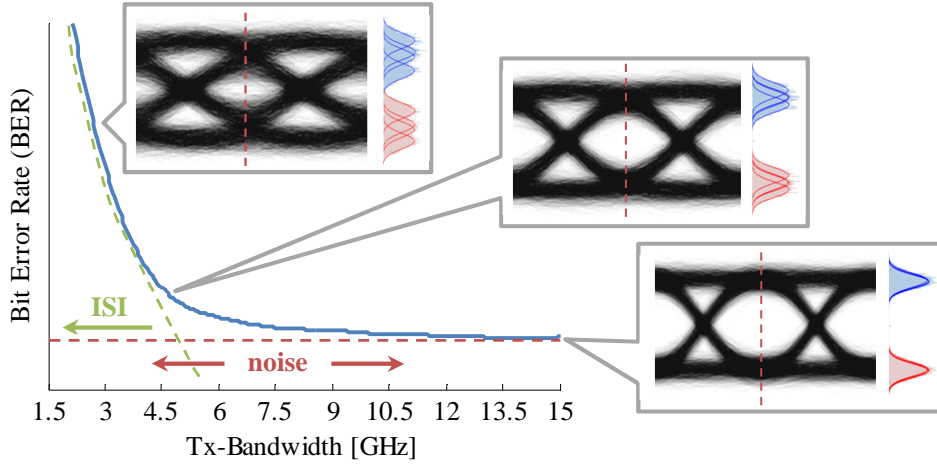
Figure 5.3: BER trend as a function of the transmitter filter bandwidth for a fixed power input to the receiver (the Rx bandwidth is fixed to 7.5GHz). The insets show the relative eye diagrams and histograms (B2B).

The penalty does not increase for cut-off frequencies greater than the bitrate, as there is not additional thermal noise to degrade the performance. Moreover, there is no advantage in reducing the filter bandwidth below the bitrate as this only increases ISI without reducing noise, as was the case with the Rx filter. To analyse the impact of this behaviour in the applications of interest, the perfor-
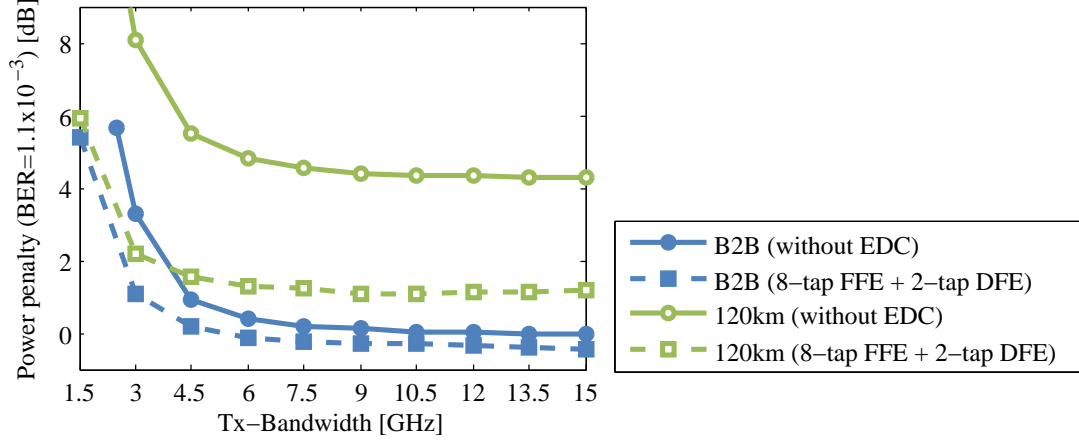
Figure 5.4: Power penalty at FEC threshold (BER=1.1×10^{-3}) as a function of the transmitter filter bandwidth in B2B and after 120km of SMF, with and without equalisation.

mance of the system in Fig. 4.1 is measured in terms of power penalty required to achieve a BER of 1.1×10^{-3} as a function of the Tx bandwidth. The relative results are presented in Fig. 5.4 using the 15GHz Tx filter case as reference. The curves are shown for the B2B case (solid symbols) and for a target transmission length of 120km (open symbols), with and without an 8-tap FFE + 2-tap DFE LMS-equaliser (dashed lines and solid lines respectively). As mentioned above, note that when the Tx filter bandwidth is swept the Rx filter bandwidth is maintained at 7.5GHz. Once again, the main finding of this analysis is that, when an equaliser is used the shift between the B2B and the transmission curve (120km) is approximately constant at around 1.5dB for all the modelled filter bandwidths, except for the lower frequency values where the signal is more tolerant to dispersion. This indicates that the equaliser can mitigate the ISI introduced by a non-optimal Tx filter bandwidth and the ISI due to CD simultaneously, as if they were acting independently and with no extra penalty due to their combination. Note also that for low cut-offs the penalty rises much faster than for the Rx case of Section 5.1.1, indicating that excessive Tx-side filtering should be avoided whenever possible.

Equalisation for enabling lower data-rate Rxs and Txs:

In summary, from these results it is clear that when using an LMS-equaliser of the

FFE/DFE type presented in Section 4.3 to compensate for CD it is also possible to compensate for the ISI due to non-optimal bandwidths of both Tx and Rx 'at no extra cost'. Or, in other words, when an equaliser is used with the main objective of mitigating the effect of dispersion and increasing the system reach, a further important advantage can be obtained, namely the possibility to relax the specifications of the Tx and Rx photonics (modulator or laser diode, transimpedance amplifier and photodetector). This relaxation can be very significant up to the point that Tx and Rx designed for 2.5Gb/s systems could be employed in a 10Gb/s system with minimal penalty. For example, after 120km of fibre, the penalty measured for both Rx and Tx cases is nearly flat (around 2dB power penalty) in the range 3- to 15GHz, proving that in principle lower specification, and hence lower cost, photonics could be used with minimal loss in performance (this would not be true without an equaliser).

Note, finally, that the results presented in this section are obtained for a power-limited system and the absolute values of optimum Tx/Rx bandwidths may not necessarily be the same for OSNR-limited systems (though the principle of compensating also for the ISI introduced by non-optimal filters still holds).

5.2 Dispersion in OSNR-Limited Systems

In this thesis, under the assumptions discussed in Chapter 2, CD is considered as the major impairment limiting the transmission distance, and it represents the main reason for this work's interest in electronic equalisation. In Sections 4.2-4.4, different equaliser designs have been analysed in detail to determine the optimum structure that can be used to compensate for such impairment in power-limited systems, where the thermal noise from the receiver is the dominating noise mechanism. When optical amplifiers are used in the network, however, the accumulated ASE noise may become significant and the system performance could be no longer limited by the signal optical power that reaches the receiver, but instead by the optical signal-to-noise ratio (OSNR), as explained in Section 2.3. In fact, with the use of optical amplifiers, the level of optical power at the receiver can usually be high enough that the thermal noise can be neglected in comparison with signal-ASE beat noise [27].

In order to understand whether a different mechanism of noise can influence the design and/or the performance of the LMS-equaliser employed to compen-

sate for CD, the setup of Fig. 4.1 has been re-implemented using the numerical computing environment VPItransmissionMaker^{TM}: this time, in contrast to all cases presented so far, the additive white Gaussian noise (AWGN) source before the receiver is enabled in order to emulate the ASE-noise introduced by optical amplifiers (the SOA, however, is still assumed ideal at this stage), and the power input to the receiver is maintained at high enough levels to ensure negligible penalty from thermal noise.

Optimum number of FFE/DFE taps:

A completely equivalent analysis to the one presented in Section 4.3 is repeated in order to characterise the equaliser under test in terms of the optimum number of taps and impairment tolerance (i.e. system penalty reduction, or transmission-reach extension) when CD is the main impairment in the OSNR-limited system. The relative results are shown in Fig. 5.5, where the OSNR penalty is measured as a function of the number of equaliser taps, for a target fiber length of 120km and using the B2B case without equalisation as reference.

These curves have exactly the same trend as the ones presented in Section 4.3. Note, however, that the OSNR penalty is more prominent compared to the power penalty, lying in the range from about 3 to 10dB instead of 1 to 5dB as in the power limited case. The reason for this discrepancy lies in the different nature of the two noise mechanisms used to limit the performance and in their different impact on BER (or equivalently on the Q-factor, see Eqs. (2.4.12) and (2.4.16)) for a given amount of CD. In fact, as anticipated in Section 2.4.1, it is not entirely correct to compare the two types of penalty using the same scale, and in principle it would be misleading to state that a given LMS-equaliser structure in an OSNR limited system has poorer performance than the same structure in a power limited case, since it can still guarantee the same impairment tolerance (this is demonstrated in the remaining part of this section).

Therefore, despite the fact that the two mechanisms of noise result in different system penalties, all the conclusions drawn from the analysis presented in Section 4.3 are still valid. As a matter of fact, the 8-tap FFE + 2-tap DFE can be considered once again the optimum trade-off between performance and implementation complexity (increasing the number of taps beyond these values does not lead to any observable performance improvement whatsoever). Due to the substantial similarities with the power limited case, Fig. 5.5 is not discussed further and the
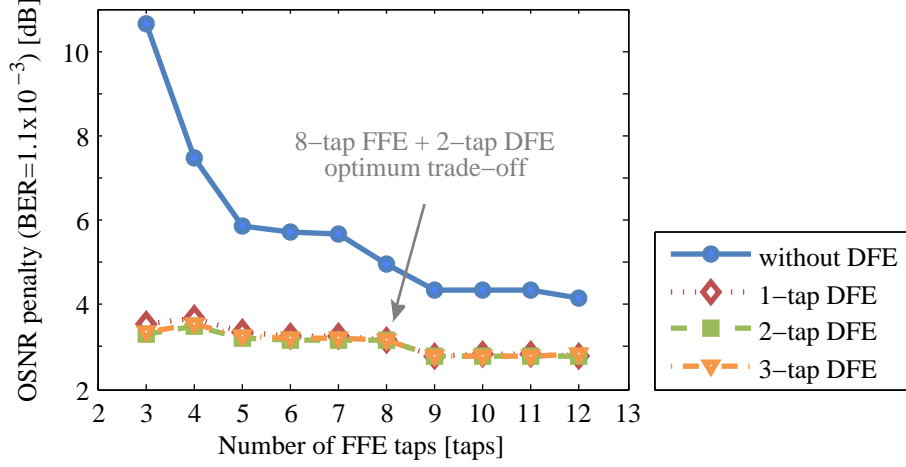
Figure 5.5: OSNR penalty at FEC threshold (BER=1.1×10^{-3}) as a function of the number of FFE/DFE taps after 120km of SMF.

reader is referred instead to Section 4.3 for a more comprehensive description of the observed behaviour.

FFE/DFE performance against CD (OSNR-limited system):

Comparing the trends of the curves in Fig. 4.13 and Fig. 5.5, it is clear that the optimum number of taps is determined solely by the amount of ISI introduced by CD and is not dependent at all on the noise mechanism limiting the system. Hence, for these tap numbers, the LMS-equaliser performs identically for both noise mechanisms considered here. This is confirmed by the curves shown in Fig. 5.6, where the performance of the 8-tap FFE + 2-tap DFE is measured as a function of the transmission distance and compared with the case of an 8-tap FFE (both trained for an ideal length of 10000bits using the LMS algorithm). The curve corresponding to the case without equalisation, whose B2B point is used as reference for the OSNR penalty calculation, is also shown for clarity.

The 8-tap FFE + 2-tap DFE can still provide the same improvement seen in the power limited case for a given target reach: for instance, a transmission distance of about 120km can be achieved at the same OSNR penalty necessary for an unequalised system to achieve just 72km (i.e. 3dB). This corresponds to a length increase of about 1.6 times, which is the same as the result obtained for power limited systems with the same reach in Section 4.3 (see Fig. 4.13). This confirms that the proposed 8-tap FFE + 2-tap DFE structure performs equally

well for both noise mechanisms. Similar conclusions can be drawn for the 8-tap FFE structure which, at an OSNR penalty of 3dB, can increase the transmission distance by a factor of about 1.5 (from 72km to 108km) as seen in Section 4.3 (Fig. 4.13, 8-tap FFE case). Note, however, that the FFE becomes suboptimal for reaches greater than 80/100km, if compared with an FFE/DFE structure, as also found in Section 4.3.
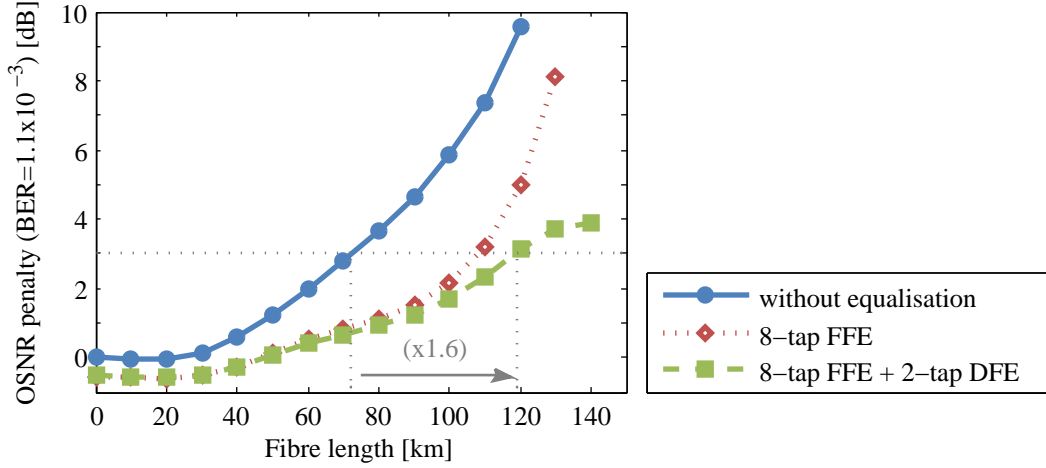
Figure 5.6: OSNR penalty at FEC threshold (BER=1.1×10^{-3}) as a function of the transmission length for different equaliser structures.

5.2.1 Impact of Noise on EDC Design

All the analyses presented so far are based on the assumption that the slicer in the feedback loop is an ideal decision device with an optimised threshold that guarantees the minimum achievable BER. In reality, however, this might be not the case: in order to meet the aforesaid condition, an automatic threshold control algorithm should be designed to track the incoming signal profile and automatically adjust the threshold accordingly based on the signal distribution [95]. In the burst-mode applications studied in this thesis, consecutive bursts could have significantly different noise statistics, and hence different optimum slicing thresholds. For instance, it is well known that thermal noise is well described by Gaussian statistics [20, 96], whereas ASE noise, which can be still be modelled as AWGN in the optical field, becomes non-Gaussian and signal-dependent after square-law detection and is often better described by a non-central chi-squared

(χ^2) probability density function [95, 125, 126]. Hence, even in continuous-mode applications, the optimum DFE slicing-threshold value for an equaliser used in a power limited system could be sub-optimal if the same equaliser is used in an OSNR limited one, or vice versa. Therefore, even if consecutive packets are degraded by similar level of impairments, it cannot be assumed that the same FFE/DFE structure with non-optimal fixed threshold can perform equally well in systems limited by different noise mechanisms.

Qualitative analysis through eye diagrams and histograms:

In this section, in order to make a more complete analysis of the optimum FFE/DFE design for systems where chromatic dispersion is the dominant impairment, a detailed investigation on the impact of non-ideal DFE slicing-threshold values on the equaliser performance is carried out. Figure 5.7 shows the eye diagrams (with relative '0' and '1' level histograms at the optimum sampling instant) after square-law detection using a photodiode in the case of a power limited system (a, b, c) and an OSNR limited system (d, e, f), for transmission distances of 0-, 80-, and 120km (a&d, b&e, c&f respectively). Figure 5.8 shows the corresponding eye diagrams after an 8-tap FFE + 2-tap DFE with DFE slicing-threshold set to the midpoint between '0' and '1' levels (note that the eyes after equalisation are 'reconstructed' from a signal characterised by one sample per bit and therefore they are only accurate at the sampling instant where the histograms are also measured). For clarity, all signals are ac-coupled and their peak voltage levels are all normalised to ± 1V, with the expected mean at 50% of the eye amplitude (i.e. 0V, represented by the red dashed-lines in both Figs. 5.7 and 5.8). Furthermore, note that all eye diagrams and histograms are measured at similar BER levels (even after equalisation) in order to facilitate the visual comparison between all the cases taken into account and to simplify this qualitative analysis.

Looking at the B2B case without equalisation in Fig. 5.7a&d it is clear that power-limited and OSNR-limited systems exhibit very different '0' and '1' distributions: the power-limited case is characterised by symmetric probability density functions (PDF) of '0' and '1' bits centred with respect to the 0V midpoint, while the OSNR-limited case is characterised by a broader '1' PDF and much narrower '0' PDF non-centred around the midpoint. The reason for this difference can be explained as follows. In a power-limited system, thermal noise is added to the
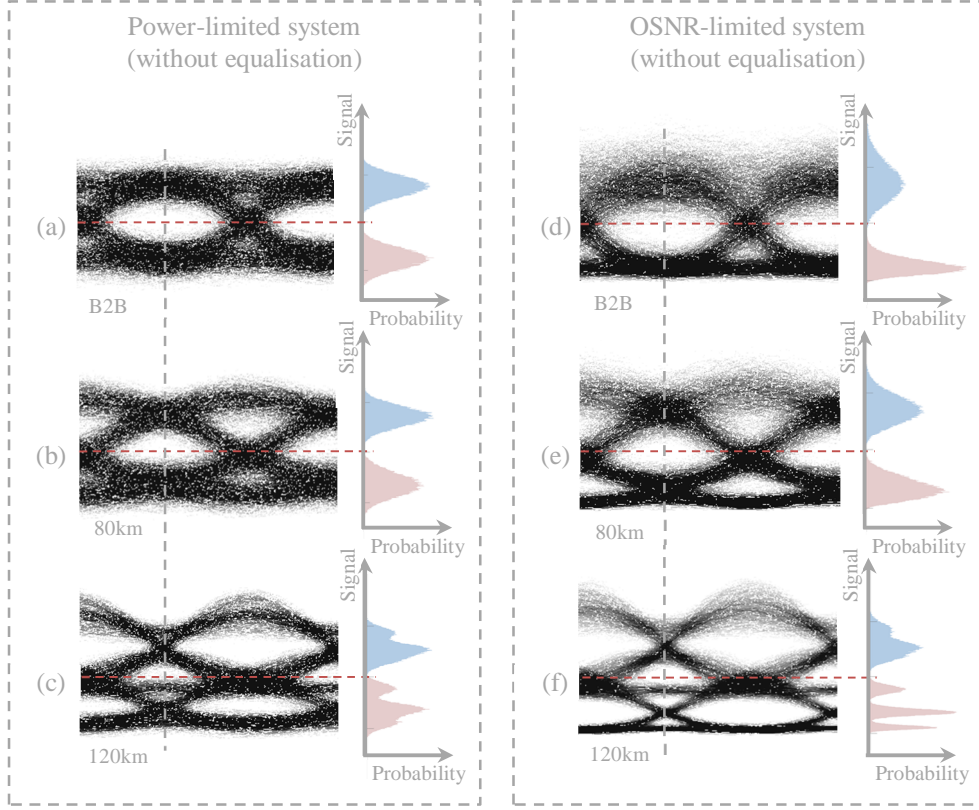
Figure 5.7: Eye diagrams and relative 0-1 level histograms for transmission lengths of 0-, 80-, 120km (a&d, b&e, and c&f respectively) for power limited systems (a, b, c) and OSNR limited ones (d, e, f) without equalisation.

electrical signal after detection and is independent from the signal levels (hence the noisy signal looks symmetric). On the other hand, in OSNR-limited systems the ASE noise is added in the optical domain and, as a result, after square-law detection the noisy signal contains a signal dependent non-symmetric term having a variance that depends on the signal levels, and a nonzero-mean non-central χ^2 term [95]. This suggests that, in contrast to a power-limited case, the optimum DFE slicing-threshold for an OSNR-limited system in B2B is not necessarily around 50%, and better performance would be achieved by reducing the slicer level down to 35-40% (measured from simulations and confirmed by the histograms of Figs. 5.7d and 5.8j). When the signal is transmitted through 80km and 120km of SMF with no equalisation (Fig. 5.7b&e,c&f), because of ISI due to CD, the energy associated with some of the '1' symbols is transferred to adjacent '0' symbols and this inevitably affects both PDFs which start to 'split'
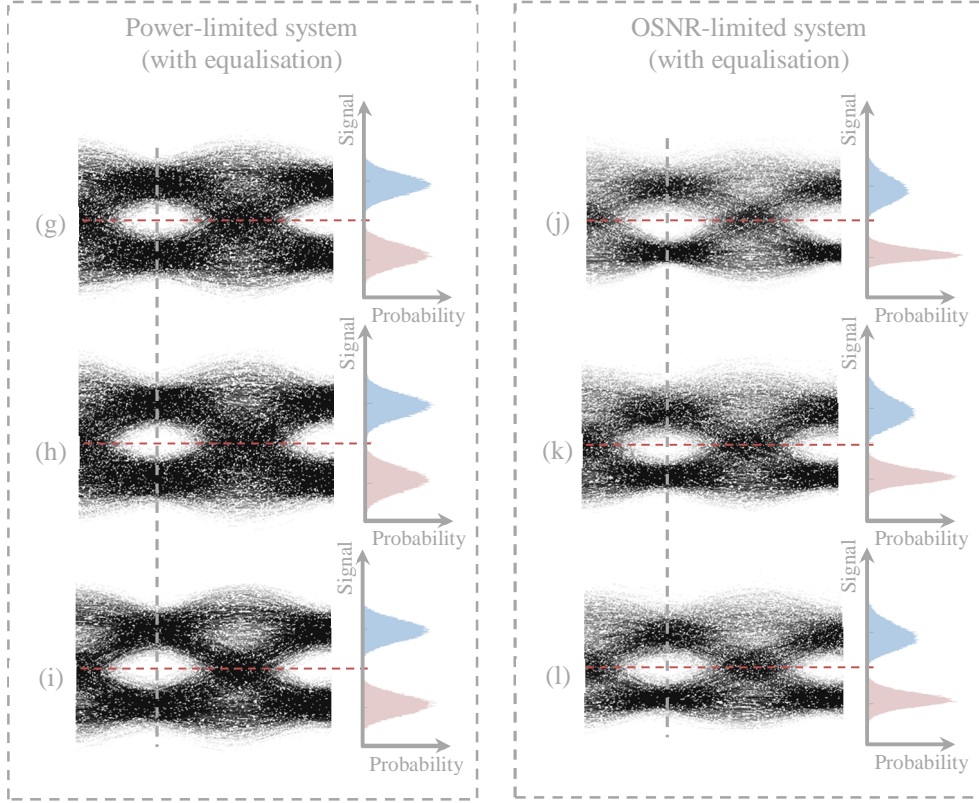
Figure 5.8: Eye diagrams and relative 0-1 level histograms for transmission lengths of 0-, 80-, 120km (g&j, h&k, and i&l respectively) for power limited systems (g, h, i) and OSNR limited ones (j, k, l) with a 8-tap FFE + 2-tap DFE equaliser.

into multiple PDFs associated with the different meta-symbols[1]. As a result, the mean values of the '0' and '1' levels start shifting towards the midpoint causing eye closure: since this shift is more pronounced for the '0' family, the optimum slicing-threshold without equalisation also changes with respect to the value seen in B2B and drifts above the midpoint for both the mechanisms of noise.

Fig. 5.8h&k,i&l then shows how this drift affects the optimum slicing-threshold when an equaliser is employed: the equaliser tries to mitigate the effects of ISI shifting back the '0' and '1' mean levels to the original values seen in B2B (Fig. 5.8g&j), which would result in an optimum DFE slicing-threshold around 50% for the power-limited case and 35-40% for the OSNR-limited one. However, since the equaliser cannot completely compensate for the ISI due to CD, the optimum DFE slicing-threshold after transmission through the fibre stays approximately

---

[1]An isolated '1' between two '0s', i.e. '010', behaves differently than a '1' between two '1s', i.e. '111'.

at 50% (slightly above) for the power-limited case, while it drifts to about 40-45% for the OSNR-limited case.

This means that the 8-tap FFE + 2-tap DFE with threshold set to 50% used in all previous analyses can provide near optimal performance for transmission over up to 120km of SMF in a power-limited system, but can be only sub-optimal for the same case in an OSNR-limited system.

Numerical analysis:

In order to confirm the inferences made from the previous qualitative analysis and quantify the penalty associated with a non-optimal DFE slicing-threshold, the performance of the 8-tap FFE + 2-tap DFE architecture (trained for an ideal length of 10000bits using the LMS algorithm) is evaluated through numerical simulations for both a power-limited and an OSNR limited system. In particular, the BER is measured at the output of the DFE slicer comparing the logical signal after hard-decision ($\hat{d}(k)$ in Fig. 4.14(b)) with the original transmitted sequence. Firstly, Fig. 5.9 illustrates the power-limited case whose results are obtained using the setup of Fig. 4.1 (with the AWGN generator switched off and with an ideal SOA): the curves show the power penalty required to achieve a BER of 1.1×10^{-3} as a function of the DFE slicing-threshold level for the B2B case and for transmission over 120km of SMF (using as reference the B2B case without equalisation). Both curves confirm the intuitive results obtained from the eye dia-
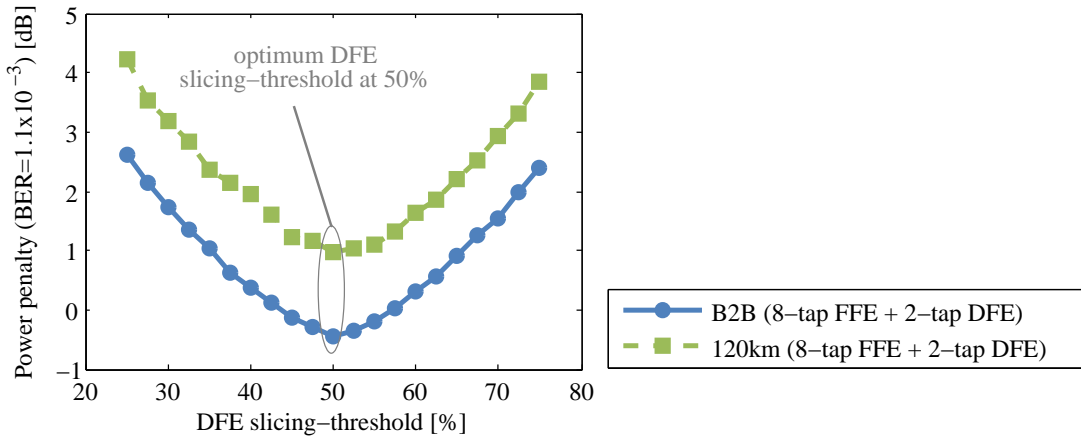
Figure 5.9: Power penalty at FEC threshold (BER=1.1×10^{-3}) as a function of the DFE slicing-threshold level for a 8-tap FFE + 2-tap DFE in B2B and after 120km of SMF for a power-limited system.

grams and histograms analysis, showing that the optimum DFE slicing-threshold in a power-limited system stays around 50% for all the transmission distances of interest.

Secondly, the same experiment is then repeated using the setup of Fig. 4.1 with the AWGN generator enabled (the SOA is still modelled as ideal, i.e, gain saturation and noise are not taken into account) in order to emulate an OSNR-limited system. The corresponding curves are shown in Fig. 5.10. Once again, the curves confirm the trend expected from the qualitative analysis of eye diagrams and relative histograms, showing that for an OSNR-limited system the optimum DFE slicing-threshold can vary as a function of the amount of CD that the signal has experienced from about 40% in B2B, up to about 45% for transmission over 120km of SMF.
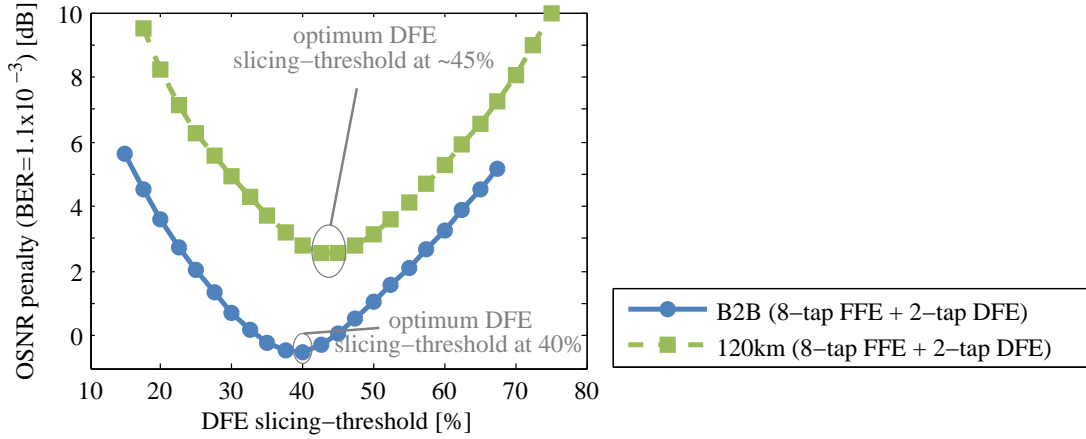
Figure 5.10: OSNR penalty at FEC threshold (BER=1.1×10^{-3}) as a function of the DFE slicing-threshold level for a 8-tap FFE + 2-tap DFE in B2B and after 120km of SMF for an OSNR-limited system.

From the results presented in Figs. 5.9 and 5.10 it is clear that in order to achieve the ultimate system performance the equaliser should employ an automatic threshold control algorithm that tracks the signal profile and adjust the DFE slicing-threshold accordingly. However, this solution would result in additional hardware complexity and thus costs: nevertheless, a reasonable trade-off can be achieved by fixing the DFE slicing-threshold to a mid-value between the 50% optimum level of power-limited systems and the 40% level of OSNR-limited systems at low transmission distances. Fixing the DFE slicing-threshold to about 45%, for example, would avoid the issues associated with the design and imple-

mentation of extra components, ensuring at the same time a minimal loss in performance of less than 0.3dB for power-limited systems (both in B2B or after transmission), and of less than 0.6dB for OSNR-limited systems in B2B. Note also that since the system is in general designed to guarantee a certain margin even in the worst-case scenario (after transmission), the already small B2B penalty of 0.6dB does not represent a practical issue as this penalty will be significantly smaller than the system margin at such distances.

In other words, for the systems taken into account in this thesis where CD is the dominant impairment, a careful optimisation of the DFE slicing-threshold to a fixed 45% level can considerably simplify the equaliser design at the expense of only a negligible increase in penalty.

5.3 Patterning from SOAs

In Sections 3.2 and 3.4 the possibility of increasing the conventional PON optical budget using mid-span reach-extenders that employ semiconductor optical amplifiers (SOAs) is discussed. The use of SOAs as preamplifiers at the receiver end of the system is also very attractive since the SOA can boost the signal to a high level such that the receiver performance is no longer limited by thermal noise, thereby increasing the receiver sensitivity. In principle, the SOA can be monolithically integrated with the photodiode to enable compact receivers to be realised [20]. One of the drawbacks of using SOAs in these configurations, however, is represented by the so-called patterning effect. This phenomenon, which is discussed in detail in Section 3.4, is a form of self-gain modulation (SGM) that depends on the data pattern of the high power intensity modulated signal that the SOA is amplifying. Indeed, patterning occurs when the input signals at a bit rate comparable to the gain recovery time are sufficiently strong to saturate the SOA, leading to carrier depletion in the gain medium and consequent reduction of the optical gain. The signal-dependent gain of the saturated SOA leads to distortions at the bit level, which results in a signal-dependent extinction ratio degradation and intersymbol interference (ISI).

An obvious solution in order to avoid patterning is to limit the optical power of the input signal to the SOA to levels below the input saturation power[1] P_{in}^s.

---

[1] P_{in}^s is defined as the input power for which the gain is reduced by half from its unsaturated value, not to be confused with the output saturation power.

However, in the burst-mode applications discussed in this thesis this is not always possible, particularly if the dynamic-range between packets is high. Since the minimum input power of a soft-packet (SP) to the SOA is dictated by the minimum required OSNR for a given network architecture, it is rather challenging to ensure that a loud-packet (LP), whose power can be e.g. 20dB higher than the SP, meets the aforesaid condition. For instance, in [127] it is shown that, due to the differential access loss, the input power to the reach-extender of a 10GEPON class PR20 can range from -25dBm (SP) up to -6dBm (LP). Note that the latter value of input power corresponding to LPs is significantly greater than the typical P_{in}^s of medium to high gain SOAs. For example, the value for P_{in}^s in the simulations presented in this section is of approximately -12dBm.

Patterning mitigation using electronic equalisation:

It is clear that not all SOAs can operate in their linear regime for such a wide range of input powers, and very likely the LPs will cause the SOA to saturate. While this could be convenient in terms of dynamic-range compression (the output dynamic-range will be smaller than the input dynamic-range, see [127]) and could relax the burst-mode receiver specifications, it is definitely undesirable because of the loss in performance due to patterning-induced distortions. The main objective of this section is to understand whether an equaliser of the FFE/DFE type discussed earlier can be used also to mitigate patterning (along with chromatic dispersion). In order to do that, the setup in Fig. 4.1 has been implemented using the numerical computing environment VPItransmissionMaker™: in this case, however, the SOA is no longer assumed ideal and it is modelled in Matlab® (in co-simulation) to emulate a commercially available device (SOA-S-OEC-1550) manufactured by CIP Technologies (now Huawei). A detailed list of the parameters used in the SOA model calculations can be found in [128].

Figure 5.11 shows the gain curve of such an SOA as a function of its input power. The eye diagrams relative to input powers of -25, -19, -15, -9, and -5dBm are also shown in the insets. From Fig. 5.11 it is clear that as soon as the input power to the SOA exceeds P_{in}^s ($\sim$ -12dBm), the eyes are heavily impaired by patterning. In order to quantify to what extent it can be corrected using an 8-tap FFE + 2-tap DFE, the performance is measured in terms of OSNR penalty required to achieve a BER of 1.1×10^{-3} as a function of the input power to the SOA. The corresponding results are shown in Fig. 5.12 for the B2B case
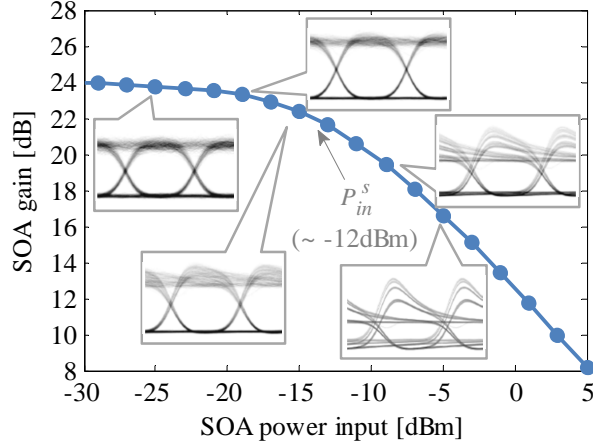
Figure 5.11: Gain as a function of the input power of a modelled SOA and relative eye diagrams showing the patterning effect due to saturation.

(solid symbols) and for transmission over 120km of SMF (open symbols), with and without equalisation (dashed and solid lines respectively). The equaliser is trained for an ideal length of 10000bits using the LMS algorithm.

B2B (patterning only):

From the B2B curve without equalisation one can see that as soon as the input power to the SOA approaches P_{in}^s, the OSNR penalty starts rising very quickly, as expected from the eye diagrams. If the SOA were to be used as a reach-extender in the 10GEPON system mentioned earlier, this means that it would not be able to deal with the required dynamic ranges (up to 19dB) without degrading the packets that have input powers greater than -12dBm. For even greater dynamic ranges, e.g. 25dB (i.e. input powers from -25dBm to 0dBm), the performance would be even worse, with nearly 9dB OSNR penalty for the LP (0dBm input power to the SOA).

The curve corresponding to the B2B case with an 8-tap FFE + 2-tap DFE shows that the type of equalisers taken into account can mitigate for the patterning-induced distortions, but cannot completely correct for it. In fact, the improvement in performance is not outstanding, but is still significant. For example, for an OSNR penalty of 3dB and assuming the minimum SP power of -25dBm, an unequalised system can deal with a maximum DR of about 16dB, while with the FFE/DFE it can be extended up to 21dB, resulting in 5dB improvement. Note
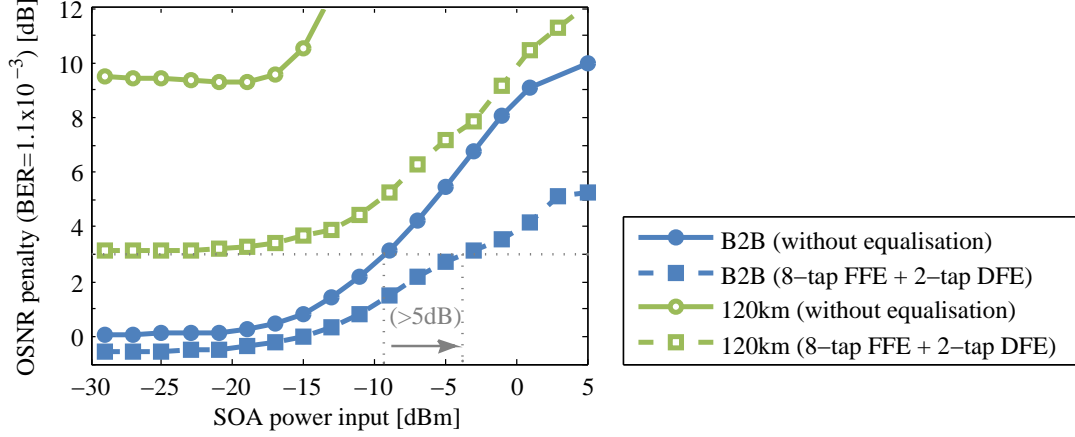
Figure 5.12: OSNR penalty at FEC threshold (BER=$1.1{\times}10^{-3}$) as a function of the input power to the SOA in B2B and after transmission over 120km of SMF, without equalisation and with an 8-tap FFE + 2-tap DFE.

that the SOA also introduces some other advantages such as DR compression at the SOA output, but this aspect is not discussed further in this context. For higher OSNR penalties, the DR improvement is even more appreciable, reaching 8dB for an OSNR penalty of 5dB, for example. Another way of reading these curves is that for very high input DRs, for instance 25dB (i.e. input powers from -25dBm to 0dBm), the unequalised system results in nearly 9dB OSNR penalty for the loud packet, whereas with an FFE/DFE this penalty is reduce down to less than 4dB.

Transmission over 120km of SMF (patterning + CD):

Figure 5.12 also shows the curves after transmission over 120km of SMF (open symbols) when the system is unequalised (solid line) and with the 8-tap FFE + 2-tap DFE (dashed line). Without equalisation the performance of the system is rather poor even for low input powers to the SOA (no-patterning), resulting in nearly 10dB OSNR penalty due CD, as expected from Fig. 5.6 for such a transmission distance. For higher input powers, the patterning induced distortions also contribute to the loss in performance, causing the OSNR penalty to increase even further up to impractical values. This curve shows that even if the system was designed to account for an OSNR penalty of e.g. 10dB, after 120km of SMF an unequalised system could only deal with less than 10dB DR at the input of the SOA (assuming once again the minimum SP power equal to

-25dBm). The performance is visibly improved using an FFE/DFE: when the SOA operates at low input powers, only about 3dB OSNR penalty due to CD is measured, as expected from Fig. 5.6. The penalty is maintained below 5dB for input powers up to -10dBm, which results in a DR of 15dB at the SOA input. Once again, if the system was designed to account for an OSNR penalty of 10dB as in the previous case, the input DR to the SOA could be increased up to 25dB when using equalisation, resulting in an improvement of 15dB in comparison to the unequalised system (plus the advantages of a greater DR compression).

Another interesting aspect that can be seen from Fig. 5.12 is that the shift between the two curves corresponding to the equalised case in B2B and after 120km stay approximately constant (the curves stay at the same distance from each other) for all the input powers up to almost -5dBm: this indicates that the equaliser can still guarantee the same performance with respect to each one of the two impairments taken into account as if they were acting separately. In other words, the equaliser's ability to compensate CD is not affected by the presence of a second impairment of radically different nature. Thus, the FFE/DFE is able to simultaneously mitigate the effects of CD and the effects of patterning with no extra penalty due to their combination for input powers up to -5dBm, which would cover more than the entire DR expected for a potential reach-extender used in a 10GEPON class PR20. For higher input powers, however, this is not guaranteed and an additional loss in performance could be encountered because of the combination of the two impairment types.

Non-linear nature of patterning:

The reason why the equaliser is not able to entirely correct patterning is due, once again, to the non-linear nature of the impairment itself (in both the optical and electrical domain). If the bitrate of the signal is comparable with the timescale of the gain transient, the gain seen by the '1' bits is dependent on the sequence of previous bits (for instance an isolated '1' will see higher gain than a '1' preceded by a long sequence of '1s'). Similarly, the gain seen by the '0' bits is also depending on the previous bits, however the transients are less pronounced than in the '1' bits case since the average '0s' power is much lower than the average '1s' power. In other words, the effect due to patterning could be conceptually compared to the one produced by a non-linear high-pass filter which affects mainly the '1' bits and only partially the '0' bits, resulting in non-symmetric '0-1' distributions.
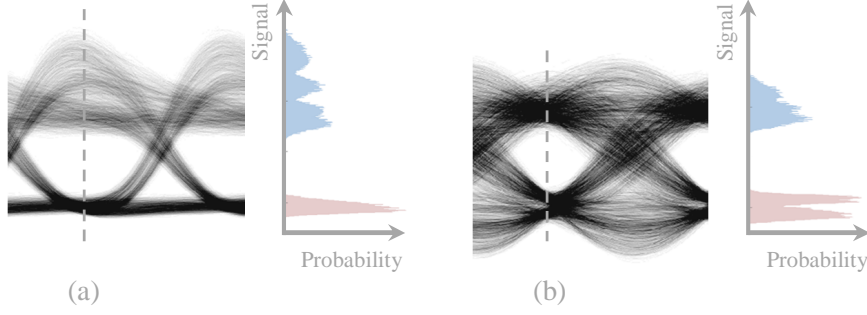
Figure 5.13: B2B eye diagrams and relative 0-1 level histograms of the modelled SOA for an input power of -10dBm: (a) without equalisation, and (b) with an 8-tap FFE + 2-tap DFE.

Figure 5.13 illustrates this concept showing the B2B eye diagrams with relative '0' and '1' level histograms at the optimum sampling instant for an input power to the SOA equal to -10dBm, when the system is unequalised (a) and when a 8-tap FFE + 2-tap DFE is used (b). To make this qualitative analysis easier, the eyes/histograms are measured at relatively high OSNR (>20dB) in order to ensure that the noise does not 'hide' the features of the histograms. From Fig. 5.13(a), as anticipated, it is clear that the patterning induced distortions are mainly affecting the '1' bits, whose PDF is significantly broader then the '0s' and can be thought of as the sum of all the meta-symbol PDFs of the '1' bit family. The equaliser, then, tries to increase the eye opening at the sampling point effectively reducing the spread of all the aforesaid meta-symbol PDFs as shown in Fig. 5.13(b) (ideally these should all be superimposed as for small input powers). However, note that in improving this aspect, the equaliser causes a separation of the '0' bits sub-symbol PDFs that were originally all overlying.

In other words, in order to improve the '1' bits distribution the equaliser compromises the distribution of the '0' bits. An intuitive explanation for this behaviour can be obtained by examining the way in which the LMS algorithm is implemented: in fact, the objective of the algorithm is to minimise the error used in the update Eqs. (4.4.8) and (4.4.9) on average. Such error, however, is much higher for the '1' bits than the '0' bits (in the latter case the error is nearly negligible), but since the algorithm does not distinguish between the errors associated with '1' bits or '0' bits and only minimises the average value, it ends-up compromising the error for the '0' bits.

The significant asymmetry between the '0' and '1' distributions due to the non-

linear nature of patterning is the fundamental reason why this type of distortion cannot be completely corrected using the equaliser structure considered here.

5.4   Summary

In this chapter it has been shown that the electronic dispersion compensator of the type 8-tap FFE + 2-tap DFE presented in Chapter 4 can be used to mitigate for other impairments (of radically different nature) without compromising its performance in terms of CD tolerance. Particular attention has been focused on the impact of non-optimal Tx and Rx bandwidths on the system performance: this can represent a recurring issue in the access applications of interest due to, for example, to the cost-effective nature of the components themselves that cannot be optimised on a case-by-case basis. The results confirm that the equaliser can mitigate simultaneously the ISI introduced by a non-optimal Tx or Rx bandwidth and the ISI due to CD as if they were acting independently and with no extra penalty due to their combination. In other words, if an equaliser is used with the main objective of mitigating the effects of CD, this could be also used advantageously in order to relax significantly the specifications of Tx and Rx (i.e. modulator, laser diode, photodetector, and transimpedance amplifier), up to the point that devices designed for 2.5Gb/s systems could be employed with minimal penalty.

A similar analysis to the one presented in Chapter 4 has been carried out in order to understand whether a different mechanism of noise can influence the design of the aforesaid FFE/DFE structure when it used to mitigate the ISI due to CD in OSNR-limited systems (instead of a power-limited system as in for the previous case). As expected, it is confirmed that the optimum number of taps is only dictated by the amount of ISI introduced by CD and is not dependent at all on the mechanism of noise limiting the system: in fact, under this condition the equaliser can still provide the same gain ($\sim$1.6) in terms of reach extension, as for the power limited case. Nevertheless, it is shown that the two mechanisms of noise taken into account can impact on the design of the equaliser in terms of optimum DFE slicing-threshold. Through numerical simulations it is demonstrated that the optimum slicing-threshold value for power-limited systems lies around 50%, whereas for OSNR-limited systems it varies from 40% up to 50% depending on the target transmission distance. It is shown that fixing the threshold to about 45%

can guarantee near optimum performance with only negligible loss for all practical cases of interest. This would also avoid the use of an automatic threshold control algorithm, otherwise necessary in order to track the incoming signal profile and automatically adjust the threshold accordingly based on the signal distribution.

Finally, the results indicate that the same 8-tap FFE + 2-tap DFE used to compensate for CD can also be employed to reduce the effects of patterning introduced by an SOA-based reach extender operating with high input dynamic ranges. The influence of this further impairment does not result in any loss in FFE/DFE performance with respect to CD compensation. In fact, it is shown that the equaliser is able to simultaneously mitigate the effects of CD and the effects of patterning with no extra penalty due to their combination for a range of input powers that would cover more than the entire dynamic range expected by a 10GEPON system, class PR20. However, despite offering a substantial improvement in performance, the FFE/DFE is not able to entirely correct patterning due to the non-linear nature of the impairment.

Chapter 6

Demonstration of 10Gb/s Burst-Mode Equalisation

As evident from recent updates to the ITU-T GPON and XGPON standards, which now support a 40km differential reach rather than the conventional 20km [14], there is a great interest in supporting larger differential reaches in access networks. This means that the use of dispersion compensating fibre (DCF, often placed at the head-end of the PON [9, 10]) is then no longer a viable solution for mitigating the effects of CD as successive bursts may have undergone different amounts of dispersion. Electronic dispersion compensation (EDC) can provide a superior solution: EDC has no insertion loss, negligible physical volume (a small chip, which would replace the BM-CDR in today's OLTs), negligible additional power consumption[1], and reduced CAPEX and inventory costs. BM-EDC can also be used to correct distortion introduced by the ONU transmitter and to mitigate the effect of patterning, as demonstrated in Chapter 4 and in [106]. Therefore, if EDC can be made adaptive from one burst to the next, high differential reach can be supported [79, 106]. To realise BM-EDC, several challenges need to be overcome. Firstly when combined with a direct detection receiver optical phase and polarisation information is lost, which limits the dispersion tolerance compared to a DCF solution. However, in Chapter 4 it is demonstrated through simulations that the dispersion tolerance for the required reach ($\sim$100km) is achievable at 10Gb/s using direct detection. Secondly, BM-EDC requires a training sequence embedded in the preamble of each burst [79]. The

---

[1]Expected to be no more than 1.5W, compared to the overall 10W per port on a typical OLT line-card [129].

number of training symbols then needs to be small in order not to reduce traffic efficiency. Finally, BM-EDC requires a linear burst-mode receiver (LBMRx), unlike today's amplitude limiting burst-mode receivers. Our group at Tyndall National Institute has demonstrated the first such LBMRx [18]. All the aforesaid challenges are discussed in more detail in the remainder of this chapter.

Section 6.1 presents the 10Gb/s burst-mode receiver (BMRx) designed at Tyndall to have high linearity (less than 5% total harmonic distortion at 250MHz) over more than 20dB (optical input power) dynamic range. The processes followed in order to assemble and package the prototype device are also illustrated.

Section 6.2 proves through transmission experiments and offline processing that EDC in 10Gb/s burst-mode links must be adapted burst-to-burst, even for bursts with the same impairment. In this analysis the average powers of consecutive bursts is kept identical to ensure that any loss in performance at the receiver arises purely from signal impairment rather than burst-mode penalties related to different burst powers.

Finally, Section 6.3 demonstrates the feasibility of 10Gb/s burst-mode transmission of high dynamic range packets (15dB) over >100km of fibre using a LBMRx and a BM-EDC emulated using off-line processing. It is shown that tap adaptation can be achieved within timescales that are compatible with the packet structure in current standards [118, 119] even using the simple LMS algorithm, allowing short preambles and thus opening the possibility of low overheads.

6.1   Burst-Mode Receiver (BMRx) Subsystem

Optical receivers (Rxs) can be classified into continuous-mode or burst-mode receivers (BMRxs). Continuous-mode Rxs are used when the input consists of bits whose amplitude varies slowly (e.g. due to temperature drift or ageing of the laser diode) with a time constant many orders of magnitude larger than the bit period. Automatic gain control (AGC) and dc-offset control loops have time constants in the microsecond to millisecond range. BMRxs are required when the input consists of bursts separated by a guard time of a few tens of nanoseconds, as discussed in Section 3.2 and shown in Fig. 6.1. For optical access, the optical power of successive bursts may vary by over 20dB ($\times 100$) [15, 16]. A BMRx thus has to adjust its gain and dc-offsets during a preamble (a few tens of nanoseconds) at the start of each burst. Continuous-mode Rxs and

BMRxs can be further classified as limiting or linear Rxs. A limiting Rx makes a hard decision whether its input represents a 0 or a 1 through comparison against a threshold, and its output takes on two levels representing a 0 or a 1. A linear Rx linearly amplifies its input such that the average or peak amplitude equals a reference. These are needed for electronic dispersion compensation (EDC) which requires preservation of the signal shape or to support advanced modulation formats such as multilevel pulse amplitude modulation and orthogonal frequency division multiplexing (OFDM) techniques. Today, continuous-mode limiting and linear Rxs with bandwidths up to at least 40Gb/s are widely available, however commercial BMRxs are only available in limiting form with speeds up to 10Gb/s [130, 131, 132]. Other techniques such as edge detecting [133] also are highly non-linear and not suitable for use with EDC.
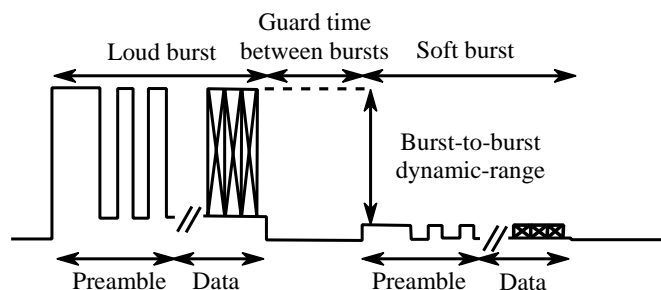
Figure 6.1: Optical signal at the input of a BMRx.

In 2011-2012, our group developed and reported for the first time upon an integrated circuit implementation of a linear BMRx (LBMRx) with fast gain adaptation [18, 134, 135, 136]. Such a LBMRx can be used in long-reach passive optical networks (LR-PONs) where dispersion compensation is needed due to the long reach and high bitrates [10]. The LMBRx must be highly linear, as characterised for example using the concept of total harmonic distortion (THD) for optical receivers, which must be sufficiently low across the entire input dynamic range. It is also important that the burst-to-burst amplitude variation at the output of the LBMRx is kept as small as possible, to enable interfacing with subsequent EDC, clock and data recovery chips or A/D converters. This requires the ability to adjust the LBMRx gain over a continuous range of values across the input dynamic range according to the strength of the incoming burst, unlike switching between a few discrete gain settings as for example in [130, 131, 132]. The objective of this section is to briefly illustrate the LBMRx top-level architecture,

describe the main steps in the realisation of the LBMRx subsystem, and present characterisation results obtained from device prototypes.

6.1.1   LBMRx Architecture

Figure 6.2 shows a block diagram of the LBMRx. In essence, its operation can be described as follows: using a measurement of the peak amplitude of the incoming burst, the gain is quickly adjusted such that the bursts at the output of the LBMRx all have the same amplitude. However, this is challenging to achieve with conventional receiver designs since the high-speed low-noise transimpedance amplifier (TIA) saturates for strong input signals. Hence, fast measurement of the peak amplitude of strong bursts is not possible. Here this is solved by adding a second measurement path as explained hereafter. The anode of a 10GHz PIN photodiode is connected to a high-speed (3dB bandwidth: 8.5GHz) TIA A_1 whose gain can be continuously adjusted from 50Ω to $1.8k\Omega$ (Fig. 6.2). The cathode of the photodiode is connected to a second, low-speed (3dB bandwidth: 75MHz) TIA A_2, which has a linear gain of 500Ω over the entire input dynamic-range (-25dBm to 0dBm, corresponding to a peak input current ranging from $5.2\mu A$ to 1.6mA at 10dB extinction ratio and a photodiode responsivity of 0.9A/W), hence its averaged output swing is proportional to the optical input power. By separating the high-speed signal path and the amplitude measurement block in this way, it is possible to individually optimise of the functions of each path. Specifically, the high-speed TIA is optimised for low-noise operation and high gain, whereas the amplitude measurement block is designed to remain linear
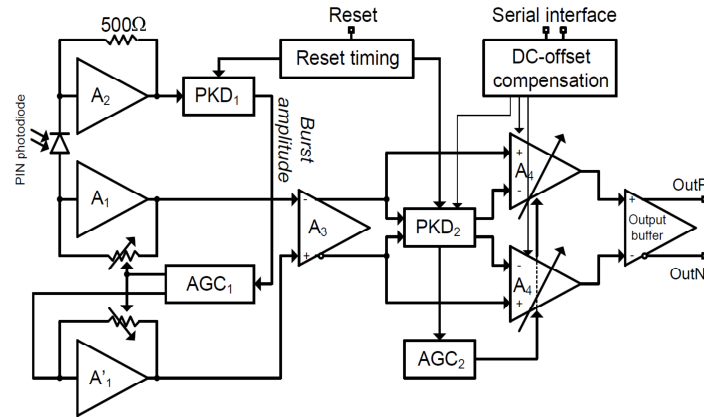
Figure 6.2: Top-level architecture of the LBMRx.

across the entire input dynamic-range.

Next, the peak detector PKD_1 measures the amplitude of each burst. This peak amplitude is provided to the gain adaptation block AGC_1 which quickly (within 25ns) adjusts the gain of A_1 such that its output swing equals a given reference. The gain adaptation block AGC_1 also provides half the peak current to a replica A_1' of the transimpedance amplifier A_1, thus creating a reference for the subsequent single-ended to differential conversion using amplifier A_3 (gain: 6dB). Additional gain is provided by post-amplifiers A_4, whose gain can be continuously adjusted from 4dB to 21dB. Using measurements of the amplitude of the burst with the peak detecting block PKD_2, the gain of the post-amplifiers A_4 is quickly (within 25ns) adjusted such that its output swing equals a given reference. Each incoming burst undergo an overall gain which is given by the combination of the TIA A_1 and the post-amplifiers A_4 gains, and the corresponding output amplitude swing is guaranteed to exceed the sensitivity of a potential EDC chip that follows the LBMRx. In fact, with input sensitivities of commercially available EDC chips as low as 20mV, even for a minimal input power of -25dBm the output swing of the LBMRx is sufficiently large[1]. The LBMRx is designed to have minimum total harmonic distortion (THD) across the input dynamic range of -25dBm to 0dBm. For the chip presented in [18], a THD smaller than 5% is observed both from simulations and experimental results: this complies with industry-agreed specifications for linear optical receivers and measured results of continuous-mode linear optical receivers [137, 138].

Between consecutive bursts, an external reset pulse (width: 10ns) is required to reset the peak detectors thus preparing the LBMRx for a new burst. The unavoidable dc-offsets stemming from mismatch between transistors and resistors are eliminated in a calibration step when the LBMRx is first put into use with the 'DC-offset compensation' block.

6.1.2 LBMRx Assembly and Packaging

IC assembly is the first processing step after wafer fabrication and dicing that enables ICs to be packaged for systems use. This process was performed in collaboration with the Photonics Packaging Group at Tyndall and consists of

---

[1] Further details on the gain ranges and outputs swing targets for the LBMRx can be found in [18].

electrically connecting I/O bond pads on the IC to the corresponding bond pads on the package. Figure 6.3 illustrates the main steps of such an assembly process. Firstly, the die ($2.1 \times 2.1\text{mm}^2$, see Fig. 6.3(a)) is flip-chipped onto an AlN ceramic substrate (Fig. 6.3(b)) with tracks and coplanar waveguides (CPWs) for DC and RF electrical connections respectively. The AlN ceramic provides very high thermal conductivity and has very low RF losses. The chip is flipped over so that its top side faces down, and aligned so that its pads align with matching tracks/CPWs. Coining of the stud bumps (Fig. 6.3(a) top-inset) is performed to provide a plane surface across all the bumps. The imprints produced on the tracks/CPWs by this process are then used to verify the alignment (Fig. 6.3(b) left-inset). Once this is completed, the die is flip-chip bonded onto the ceramic substrate using thermo-compression bonding which involves the simultaneous application of high force and heat (up to 320 °C) to create an Au-Au diffusion bond, which avoids the need to use solder. This provides good mechanical strength as well as high electrical conductance.

(a) (b) (c) (d)
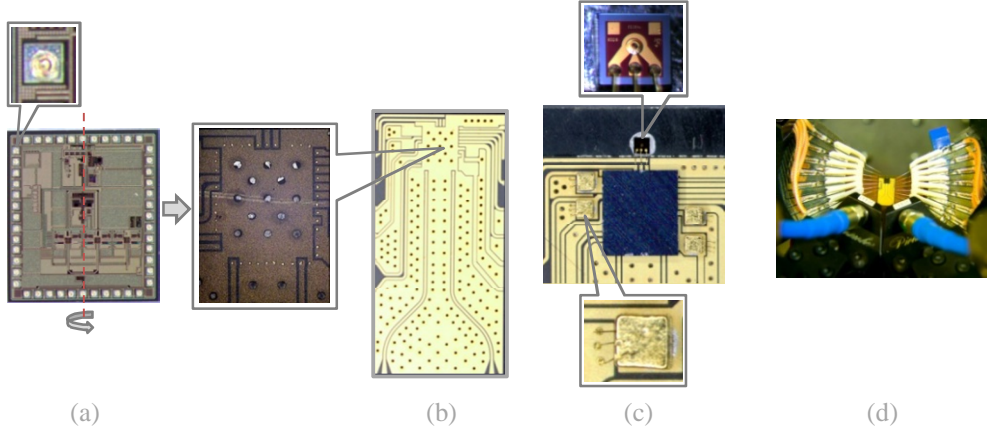
Figure 6.3: LBMRx assembly process: die micrograph (a), AlN ceramic substrate (b), flip-chipped die onto substrate with wire bonded photodiode and decoupling capacitors (c), and LBMRx assembly on probe-setup (d).

A 10Gb/s InGaAs/InP PIN photodiode along with four decoupling capacitors (1nF, one for each supply line) are attached to the substrate using silver epoxy. The photodiode and decoupling capacitors are then wire bonded to respective track lines using 18μm diameter gold wire (Fig. 6.3(c) insets). The connections between the substrate and the chip are tested simply by measuring the resistance between each pin and ground. This is done by probing the DC tracks of the sub-

assembly with multi-contact wedge probes and the two RF outputs using high performance microwave probes as shown in Fig. 6.3(d). The two RF outputs of the LBMRx are ac-coupled using 560pF capacitors.

Unpackaged LBMRx characterisation:

Once all the connection tests are passed successfully, the LBMRx is optically tested and its performance is determined by measuring the bit-error-rate (BER) at the RF-outputs when the input consists of 10Gb/s loud and soft bursts with up to ~23dB dynamic-range. The setup used to generate packets with different power levels is shown in Fig. 6.4. The outputs of two 1550nm wavelength, DFB lasers are non-return to zero (NRZ) modulated with 10Gb/s data using electro-absorption modulators (EAMs). The EAM bias voltages are both set in order to maximise the extinction-ratio in back-to-back (B2B) conditions: the extinction-ratio on the soft channel is ~10dB, whereas on the loud channel it is ~7.5dB. Next, the stream of alternating loud and soft bursts is generated using variable optical attenuators (VOAs) and two semiconductor optical amplifiers (SOAs), whose bias currents are switched on or off in alternating fashion forcing the SOAs to operate either as boosters or shutters (see Fig. 6.4, top inset). Each packet is 3.27μs long and consists of a 150ns preamble (60 '1s', 60 '0s', five times 16 '1s' and 16 '0s' for gain settling, the remaining part consists of pseudo random bit sequence (PRBS) data for settling of the transient across the cou-
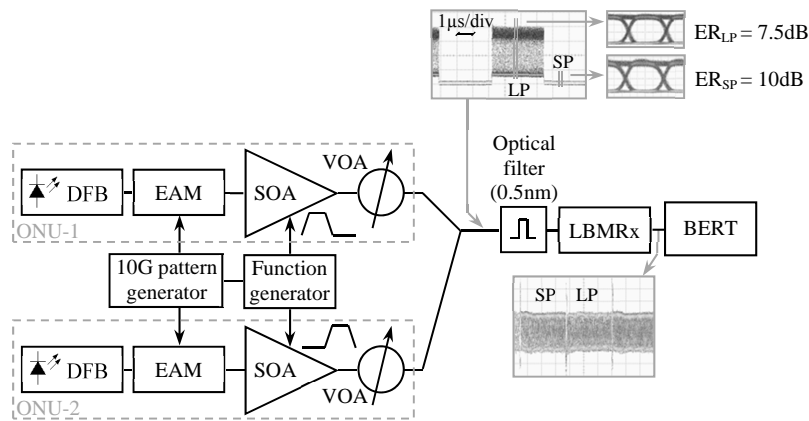
Figure 6.4: Experimental setup used to characterise the LBMRx. (ONU: optical network unit, DFB: distributed feedback laser, EAM: electroabsorption modulator, SOA: semiconductor optical amplifier, VOA: variable optical attenuator, LBMRx: linear burst-mode receiver, BERT: bit error rate tester).

pling capacitors) followed by a payload consisting of $2^7 - 1$ PRBS data on which BER is measured. Note that this overall settling time of 150ns is necessary to accommodate the transient from the ac-coupling capacitors when the LBMRx is operated with the largest dynamic-range (approximately 23dB), but it has been shown [18] that in general a much lower settling time of order 50ns is required when the dynamic-range is set to more practical and realistic values of around 15dB. The packets are separated with 25.6ns guard bands. An optical filter with a 3dB bandwidth of 0.5nm is then used to remove the out-of-band ASE noise generated by the two SOAs.
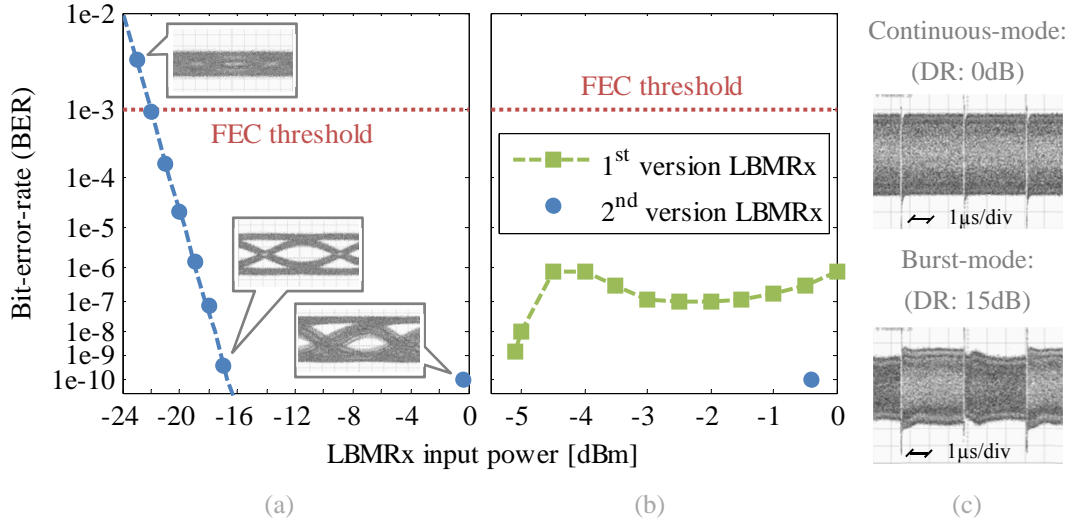
Figure 6.5: LBMRx assembly (unpackaged) performance: BER as a function of input power (a), performance comparison between first and second LBMRx version at high input powers (b), and continuous-mode (dynamic-range (DR): 0dB) versus burst-mode (dynamic-range: 15dB) envelope comparison (c).

The sensitivity and overload of the LBMRx are evaluated by measuring the BER on the PRBS portion of the SP and LP bursts respectively, as a function of the optical power: the corresponding results are shown in Fig. 6.5(a). A sensitivity lower than -22dBm is measured at a BER of 1.1×10^{-3} when the LBMRx is operated in burst-mode: the BER for powers below -16dBm is measured on the SP maintaining the LP power fixed to -2dBm (Fig. 6.5(b)), while the single point on the right is measured on the LP ($P_{in} = -0.5$dBm) with a SP power of -23dBm (the power coupled onto the photodiode is limited to 0dBm due to setup restrictions). The burst-mode curve measured at low powers presents less

than 0.5dB power penalty (at FEC threshold) in comparison to the continuous-mode case (not shown in Fig. 6.5(a) for clarity): this penalty is attributed to the transient from the ac-coupling capacitors [18].

The insets of Fig. 6.5(a) also show the eye diagrams for various input powers to the LBMRx. For very low powers, close to the receiver sensitivity, the combination of TIA and post-amplifier gain is not able to guarantee the full output swing which is achieved for powers greater than -19dBm [18], and the performance is limited by thermal noise. For higher powers, open eyes can be observed up to the point where, for LP powers greater than -2dBm, the BER starts rising again and the eyes show some features attributed to a reduction of the PIN photodiode bandwidth. Note however that this behaviour, which was reported first in [18, 135] and is due to a residual drop in the PIN photodiode bias voltage at these powers, has been considerably reduced in comparison to the first version of the chip, as shown in Fig. 6.5(b). Note that the LBMRx top-level architecture is exactly the same for first and second version, but an additional circuit has been added to the second version in order to reduce the aforesaid drop of the bias voltage. Finally, Fig. 6.5(c) shows the output envelope comparison when the LBMRx is operated in continuous-mode (dynamic-range: 0dB) and burst-mode (dynamic-range: 15dB). It is possible to see that the envelope presents an undesired distortion at the start and at the end of each packet when running in burst-mode. This problem, which is due to an insufficient decoupling capacitance on the assembly combined with the large inductance of the DC probes, has not been further investigated as it is related to a limitation in the setup rather than in the actual device.

Packaging and fibre-chip coupling:

Next, the LBMRx sub-assembly is packaged into a customised 14-pin butterfly (BTF) extended module with GPPO connections (Fig. 6.6(a)). Firstly, a Kovar heat-sink is attached into the BTF package using silver epoxy and, similarly, the assembly is attached onto the Kovar heat-sink. The ceramic is placed flush with the butterfly wall, and aligned with the GPPO connector feedthroughs. Each track line is then wire bonded to the pins of the BTF package. In this process, a $50{\times}12\mu$m ribbon bond (Fig. 6.6(a), left inset) is used instead of the standard gold bond-wire used for the photodiode and decoupling capacitors, as it consists of a rectangular-cross-section with reduced inductance rather than a circular cross-

section. Due to the absence of a Peltier TEC (thermoelectric cooler) underneath the assembly, the CPW RF-outputs are found to be not aligned to the GPPO outputs of the BTF package. To overcome this issue, a connection made of silver epoxy is built up to the GPPO level (Fig. 6.6(a), right inset). Afterwards, a metalized lensed fibre with a bevel angle of 45º is used to couple the light into the high speed photodetector (Fig. 6.6(b)). In order to optimise the coupling efficiency, an active optical alignment is performed using micro-positioning units to maximise the average photocurrent for a given optical power. Once the best alignment is found, the fibre is held in place using a nickel clip which is then welded to the fibre metal ferrule and to the Kovar heat-sink. To complete the packaging process, the fibre pigtail along with a strain relief boot is secured to the cylindrical window of the packaging using epoxy adhesive.

(a)

(b)
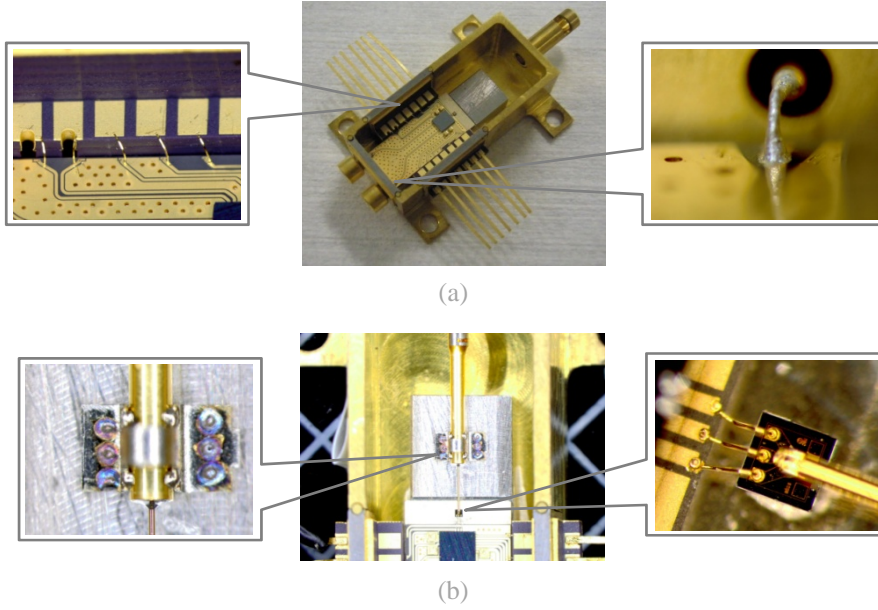
Figure 6.6: LBMRx packaging process: ribbon bonded package and GPPO connection to CPWs (a), and fibre alignment and welding (b).

LBMRx subsystem characterisation:

Finally, the packaged LBMRx is mounted on a printed circuit board (PCB) designed to simplify the interface with the rest of the setup and to avoid non-optimal connections. The PCB design was carried out at Tyndall using Cadence OrCAD PCB Designer and PCB Editor. The packaged LBMRx is soldered on the PCB and its RF outputs are connected using semi-rigid cable assemblies (GPPO to

2.4mm), as shown in Fig. 6.7(a). The LBMRx and the LV 24-33 microcontroller board used to communicate with it are then mounted together on an aluminium optical breadboard. A small PCB with a series of different ac-coupling capacitor values is also added: these capacitors are used to compensate for the residual dc-offset between consecutive packets, as mentioned above. Figure 6.7(b) shows the final LBMRx subsystem with microcontroller board.

(a)   (b)
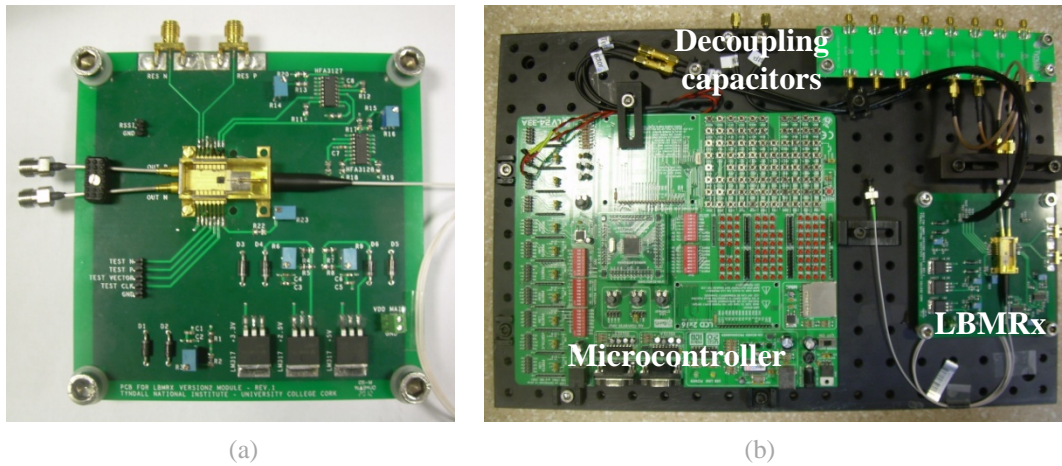
Figure 6.7: LBMRx modules: packaged LBMRx mounted on PCB (a), and LBMRx subsystem with microcontroller board (b).

At this stage all the tests performed before packaging are repeated in order to verify that the LBMRx is working properly and has not been damaged during the packaging process. The setup used for this characterisation is the same as is shown in Fig. 6.4. The BER is measured on the SP maintaining the LP power fixed to -2.6dBm and compared with the unpackaged LBMRx case: the relative results (for the worst case polarisation) are reported in Fig. 6.8(a). The curves show a power penalty at FEC threshold of nearly 2dB for the packaged device due to a non-ideal alignment/coupling. It is found that the photodiode is not high enough in comparison to the heat-sink level: the heat-sink is therefore blocking the fibre and preventing it from being further lowered. In other words, the fibre is welded at a non-optimum distance from the photodiode, resulting in a coupling loss of ∼2dB. Nevertheless, this issue can be easily addressed in future generations of the LBMRx and, due to its deterministic nature, can be accounted for in system experiments simply by increasing the input power to the receiver by approximately 2dB. To make sure that the fibre is not damaged or deformed
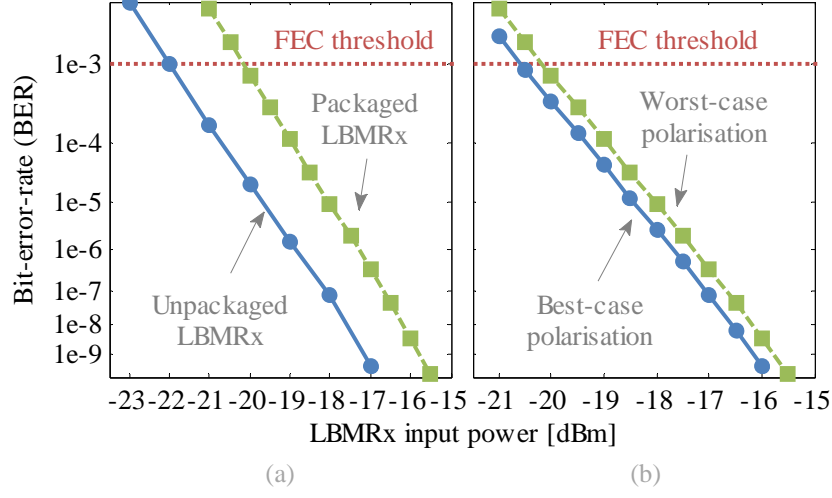
Figure 6.8: LBMRx (packaged) performance: BER as a function of input power and comparison with unpackaged LBMRx (a); BER as a function of input power for different polarisations (b).

during the packaging process resulting in an extra penalty due to possible bire-fringence, the BER was also measured as a function of the polarisation by adding a polarisation controller before the LBMRx. The relative curves are shown in Fig. 6.8(b): the penalty is found to be nearly negligible (around 0.4dB). Finally, the envelope characterisation is repeated and compared to the unpackaged LBMRx case. The results are shown in Fig. 6.9 and they indicate that the distortion is significantly improved, confirming that this issue was related to a limitation in the probe setup of Fig. 6.3(d) rather than the actual device itself.
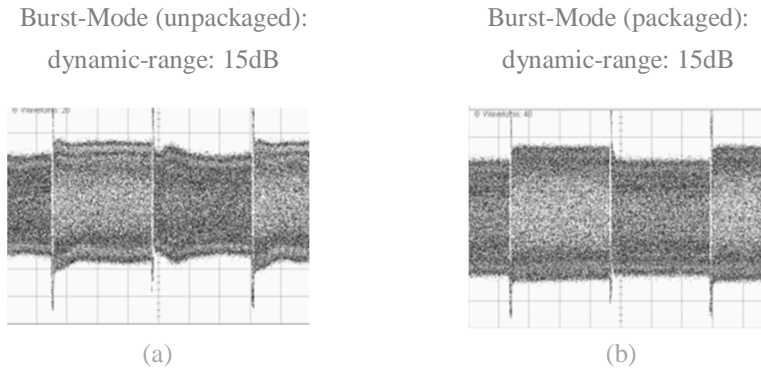
Figure 6.9: LBMRx envelope distortion comparison: unpackaged (a) and packaged (b) device operating with an input dynamic-range of 15dB (time scale: 1μs/division).

6.2 EDC Requirements in BM-Systems

In Chapters 4 and 5, a detailed analysis was carried out in order to determine the optimum electronic equaliser design for next-generation long-reach passive optical networks (LR-PONs) in terms of taps spacing, minimum number of taps required, best step-size, etc. This study included a number of simulations that were completed for power-limited as well as OSNR-limited systems under the assumption that CD is the dominant impairment. Other impairments such as non-optimal transmitter/receiver bandwidth or patterning from SOAs were also simulated, and it was shown that the equaliser is able to simultaneously mitigate them with no extra penalty due to their combination. These simulations were a necessary and valuable intermediate step in order to provide insights that might be harder to obtain from more complicated and less controllable real-world environment. However, the simulations results were generated using simplified models for the system under test, and therefore need to be experimentally validated. For instance, all the simulation results presented in Chapter 4 were obtained without including fibre nonlinearities into the model, under the assumption of an ideal zero-noise monochromatic DFB (linewidth $\rightarrow 0$) with infinite side-mode suppression ratio (SMSR), and an ideal zero-chirp lossless modulator. Furthermore, focusing attention on the equaliser, a derivation of the step-size parameter was obtained in order to guarantee an optimal trade-off between convergence speed and steady-state error. However, all simulations were run in continuous-mode and the speed of convergence has never been tested appropriately in a burst-mode environment.

Therefore, in this section transmission experiments and offline processing are combined to validate previous findings and to identify the requirements for an equaliser circuit suitable for use in burst-mode access links. Since the main impairment taken into account in the following lab-experiment is once again CD, the equaliser will often be referred to as electronic dispersion compensator (EDC) for the remaining part of this chapter.

6.2.1 Need for BM-EDC: Proof of Concept

In order to prove the need for an EDC capable of adapting on a burst-by-burst basis (instead of a conventional 'static' EDC) and investigate its requirements in a burst-mode link, two different cases are taken into account. In the first one, the

only difference between consecutive bursts is a pure phase delay (with respect to a continuously running bit-rate clock). This corresponds to the scenario where similar ONUs are located at approximately the same distance from the central office. Bursts from such ONUs will have undergone practically the same amount of dispersion, but will arrive at the central office with an unknown bit phase, as the propagation delay of the fibres will have a large variation compared to the bit period. In the second case, both bursts have significantly different levels of impairment, which corresponds to the situation where ONUs are at different distances from the central office or have different transmission characteristics.
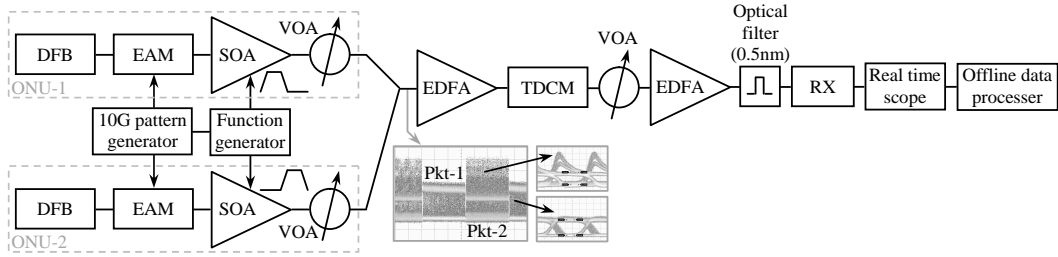
Figure 6.10: Experimental setup (ONU: optical network unit, DFB: distributed feedback laser, EAM: electroabsorption modulator, SOA: semiconductor optical amplifier, VOA: variable optical attenuator, EDFA: erbium doped fibre amplifier, TDCM: tunable dispersion compensation module, RX: receiver. The pattern and eye diagrams in the insets correspond to the case of bursts with different level of impairments).

The experimental setup is shown in Fig. 6.10 and it is essentially an extension of the one illustrated in Fig. 6.4 (with minor changes). The outputs of two DFB lasers operating at 1540nm are modulated with 10Gb/s non-return to zero pattern ($2^7 - 1$ PRBS data) using EAMs, with bias optimised for B2B and 1400ps/nm dispersion, for bursts 1 and 2 respectively. The bursts (separated by a 25.6ns guard time and with a total length of 32768 bits) are carved using SOAs whose bias currents are switched on a burst basis. VOAs are then used to adjust each burst power. Burst-2 is impaired by deliberately driving its SOA into saturation giving rise to large overshoot on the rising edges as shown in the insets. This is done in the second case only in order to emulate transmitters with different amounts of distortion and could correspond to an ONU with a degraded SOA (in the first case burst-2 is not impaired by patterning). At this stage, the average powers of both bursts are kept identical to ensure that any impairment at the receiver arises purely from signal impairment rather than potential burst-mode

penalties related to different burst powers. In Section 6.3, then, an appropriate burst-mode analysis with more realistic dynamic-range values will be presented in a concluding system demonstration of BM-transmission with an LBMRx and BM-EDC. Chromatic dispersion is added using a tuneable dispersion compensation module (up to 1400ps/nm, corresponding to ∼80km of standard single-mode fibre) to stress the EDC. Lastly, using an erbium doped fibre amplifier (EDFA) and a VOA, the OSNR is adjusted to induce a controlled amount of random bit errors. An optical filter (3dB width: 0.5nm) is used to remove out of band noise. The output of the optical receiver is sampled using a real-time sampling scope with an analog bandwidth of 12.5GHz and a sampling rate of 50GS/s.

The off-line equaliser structure used to process the sampled data is identical to the one presented in Fig. 4.14(b): it consists of an M-tap fractionally-spaced feed-forward equaliser (FFE, tap spacing: 50ps) and an N-tap decision feedback equaliser (DFE, tap spacing: 100ps). A training sequence of variable length L is embedded at the start of each burst. The taps of the equaliser are adjusted using the least mean squares (LMS) adaptation algorithm whose step-size is set according to the criterion discussed in Section 4.4.2. In the following, 'static EDC' indicates that the taps are trained on a given burst and then kept fixed for all subsequent bursts, whereas 'adaptive EDC' indicates that the taps are trained using the training sequence at the start of each burst.

Due to the large amount of lab-data necessary to 'count' the BER with a reasonable level of confidence below the forward error correction (FEC) threshold (down to approximately 10^{-4}), the number of FFE and DFE taps is not swept with as fine a granularity as in Sections 4.3 and 5.2, and only a few combinations have been taken into account. Instead of using the optimum 8-tap FFE + 2-tap DFE determined from the previous analyses in Chapter 4, at this stage a slightly more conservative 9-tap FFE + 3-tap DFE is used in order have more, not less.

Time delay difference between consecutive bursts:

First, the performance of the 9-tap FFE + 3-tap DFE is analysed when handling bursts with different phase delays, but with the same amount of dispersion and distortion (burst-2 is not impaired by patterning). Figure 6.11(a) shows the required OSNR to achieve a BER of 1.1×10^{-3} for the 1400ps/nm dispersion case as a function of the phase delay between both packets (note that the sampling clock frequency and phase are kept fixed for all bursts). Note how in the static
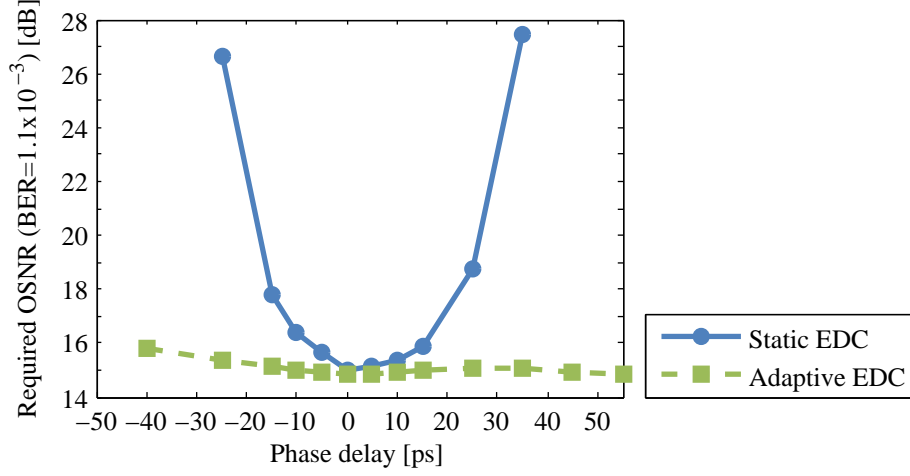
Figure 6.11: Required OSNR as a function of the phase delay for static and adaptive EDC.

case (EDC taps fixed at trained values for 0ps phase delay) the required OSNR rises quickly beyond a phase delay of ±15ps. Intuitively, this is because the taps of the EDC are adjusted such that the eye opening at the sampling times is maximised. Hence when a new burst has undergone a phase shift with respect to the burst on which the taps were trained, the taps need to be re-adjusted (performed here using the LMS algorithm and 1024 training bits). From these results it is possible to infer two very significant conclusions. Firstly, static EDC is problematical for burst mode PON systems because the TDMA protocols that control upstream transmissions do not allow packet delays to be controlled on the timescales of a bit period, so unless other measures are taken unacceptably high error rates will occur for some packets. Secondly, conversely when the taps are adjusted adaptively burst by burst this problem can be alleviated, and in this case the EDC essentially operates as a full burst-mode clock and data recovery (BM-CDR) circuit effectively incorporating clock phase alignment, data recovery and retiming functions all in one circuit. This feature of BM-CDR, which is a key aspect of a BM-EDC module, will be discussed in more detail in Section 6.3.

Different impairments between consecutive bursts:

Next, the performance of the 9-tap FFE + 3-tap DFE is analysed using successive bursts with different levels of transmitter distortion. First, the required OSNR is measured for both bursts without EDC as a reference (Fig. 6.12, solid lines + solid symbols). For burst-1, 10dB penalty is incurred for a CD of 1400ps/nm

compared to the B2B case (CD: 0ps/nm). The required OSNR for burst-2 remains relatively constant but is 3.7dB higher than for burst-1, indicating that the penalty is dominated by the pattering from the SOA saturation rather than CD (the EAM bias is optimised for 1400ps/nm dispersion). Performance is greatly improved with adaptive EDC (Fig. 6.12 solid lines + open symbols). In this case, the EDC taps are adjusted for each new burst using the LMS algorithm with 1024 training bits.
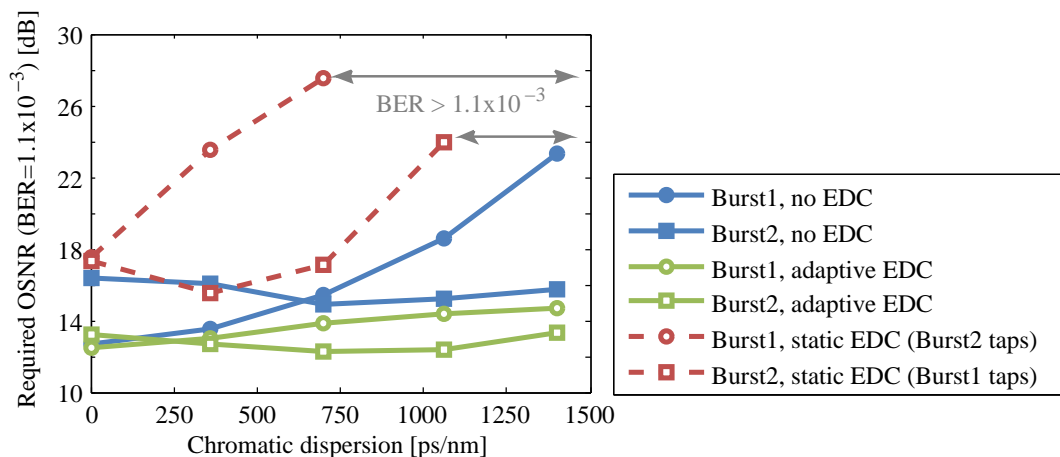
Figure 6.12: Required OSNR as a function of chromatic dispersion.

Significant improvements of up to 8dB can be observed for burst-1 at the maximum CD value. However, if the taps are adjusted using the LMS algorithm for burst-1 and then applied to burst-2 without adjustment, then a 4.9dB OSNR penalty is incurred in the B2B case (no CD) for burst-2, which is due to the different distortion of the two transmitters. This penalty increases rapidly with increasing dispersion up to the point where a BER smaller than 1.1×10^{-3} can no longer be achieved (Fig. 6.12 dashed line plus open symbols). Similar behaviour can be observed for the required OSNR of burst-1, if equalised using the taps obtained from training at the start of burst-2.

Previous demonstrators have shown how a conventional static EDC with taps fixed for successive packets can be employed (in combination with 40km of dispersion compensating fibre) to mitigate the residual CD accumulated over 150km of SMF [9]. Note, however, that this technique is effective only if consecutive packets do not show any phase delay difference with respect to the same clock (which is very unlikely in practical situations), and only under the assumption that the amount of CD to compensate is similar for all incoming packets. Indeed,

the curves presented in Figs. 6.11 and 6.12 prove that for optimum system performance the EDC taps must be trained for each new burst even if these bursts have undergone the same amount of dispersion due to unavoidable (small) phase shifts between bursts.

6.2.2   EDC Adaptation Speed

The previous results clearly demonstrate that when EDC is used in burst-mode links the filter taps must be adjusted for each new burst. The next important aspect to address is to understand how long the training sequence at the start of each packet needs to be to in order to adapt the taps to this new incoming burst. To illustrate this, Fig. 6.13 shows the evolution of the mean squared error (MSE) calculated as the expected value $E[e^2(k)]$ of the squared error $e(k) = d(k) - y(k)$ as in Eq. (4.4.2), where $d(k)$ is the kth training bit (i.e. the kth transmitted bit) and $y(k)$ the signal before the DFE slicer at the kth sampling moment. In this analysis, instead of using the instantaneous gradient approximation introduced in Section 4.4.1, the actual MSE is calculated. Note that this approach can be used only because the data are processed offline and the full knowledge of the entire sequence is available at any instant, but this would not be feasible in practical situations where the instantaneous gradient approximation must be adopted. Therefore, at this stage the actual MSE is estimated using Eq. (4.4.2) in order to measure the performance of different equalisers in terms of adaptation speed (or equivalently the number of iterations) necessary to minimise the 'true' cost function, while subsequently in Section 6.3 a similar experiment is run using the instantaneous gradient approach to confirm that no significant loss in performance is encountered because of such an approximation.

For this experiment, the MSE of burst-1 (which corresponds to the worst case penalty without EDC) is monitored when the CD is set to 1400ps/nm and the LMS algorithm is used to adjust the taps for three different EDC lengths (3-tap FFE + 1-tap DFE, 5-tap FFE + 2-tap DFE, and 9-tap FFE + 3-tap DFE). Note that even though in this analysis the MSE cost function is minimised using the steepest descent method for the gradient estimate, the adaptation algorithm is referred to as LMS for simplicity. The corresponding Q-factor for burst-1 is also shown in Fig. 6.13. Clearly, the taps adapt fastest for the 3-tap FFE + 1-tap DFE, with the trade-off of a reduced Q (8.2dB, which is smaller than the
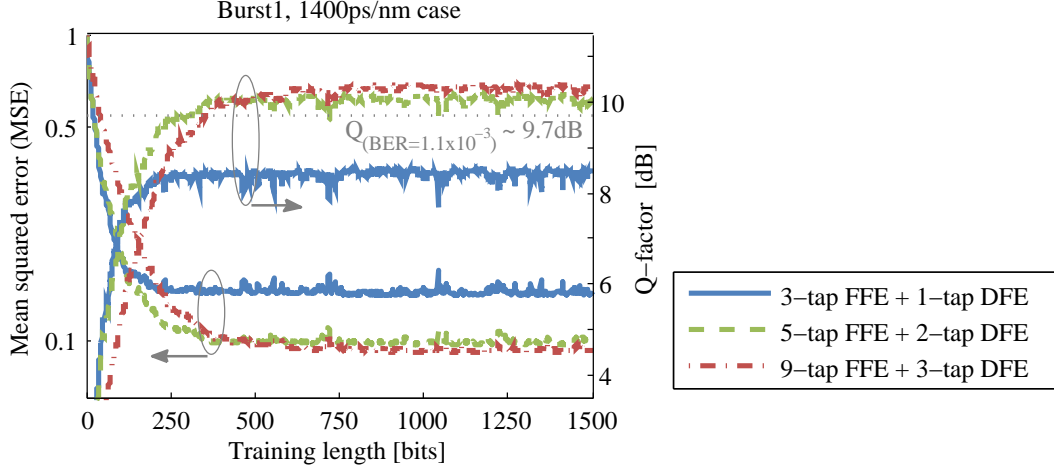
Figure 6.13: Burst-1 MSE and Q-factor as a function of the training length for different EDC lengths when dispersion is set to 1400ps/nm.

required value to ensure a BER $< 1.1 \times 10^{-3}$). The taps for the 5-tap FFE + 2-tap DFE adapt faster than the 9-tap FFE + 3-tap DFE for the burst and CD taken into account here, while both achieve practically the same Q (greater than 10dB), making the 5-tap FFE + 2-tap DFE the optimum choice due to reduced implementation complexity. This indirectly confirms the results presented in Section 4.3, where it was found that for the amount of CD taken into account (up to 120km) a 5-tap FFE + 2-tap DFE has the same performance as a 9-tap FFE + 3-tap DFE. Note however that the former would not provide the same tolerance to the sampling phase offered by the latter, and this is exactly the reason why in Chapter 4 the 8-tap FFE + 2-tap DFE is considered the optimum trade-off between performance and hardware complexity. Table 6.1 summarises the achieved MSE (along with its variation) for burst-1 after a training period of 1024bits and for the three EDC cases considered.

Note that tap adaptation is achieved in approximately 500 training bits, which is compatible with most burst-mode applications provided the training algorithm is implemented with low additional overhead. In fact, in current 10Gb/s PON standards like the ITU-T Rec. G.987.2 (2010) or the IEEE 802.3av (2009) [118, 119] the burst overhead, which is necessary in order to accommodate several physical processes, is in the order of hundreds of nanoseconds (or equivalently thousands of bits). In all the analyses presented so far, adaptation is performed using as step-size the value obtained in Section 4.4.2 (corresponding to a scaling factor SF of 1/50): Fig. 6.13 confirms that such a value is indeed a good trade-

off between adaptation speed and low steady-state noise for the application of interest. For convenience, the curves in Fig. 6.13 only show the MSE for burst-1: however, similar trends and approximately the same results in terms of adaptation speed are obtained with burst-2. The final MSE values of burst-2 are also listed in Table 6.1: the fact that no MSE improvement is registered for burst-2 when the number of taps is increased suggests that most of the (pre-cursor) ISI introduced by patterning is limited to a small number of symbols. This can be explained by noting that, as mentioned in Section 2.2.1 and Section 3.4, the memory of a saturated SOA is due to the finite carrier lifetime which occurs in timescales comparable to the bit period [38]. Hence a limited number of taps is sufficient to account for the most of the ISI introduced by patterning.

Number of taps (FFE + DFE)	Burst-1 MSE	Burst-2 MSE
9-tap FFE + 3-tap DFE	0.09 ± 7%	0.14 ± 7%
5-tap FFE + 2-tap DFE	0.10 ± 10%	0.14 ± 13%
3-tap FFE + 1-tap DFE	0.14 ± 12%	0.14 ± 18%

Table 6.1: MSE value and corresponding variation (3-sigma confidence interval) for different EDC lengths.

Adaptation using the RLS algorithm:

For burst-mode applications where traffic efficiency (defined as the ratio of the number of transmitted data bits to the total number of transmitted bits) is critical, faster tap adaptation algorithms may be considered. One example is the recursive least squares (RLS) algorithm. The RLS is an algorithm which recursively finds the filter coefficients that minimise a weighted linear least squares cost function relating to the input signals. This is in contrast to other algorithms such as the LMS that aim to reduce the mean square error. An important feature of the RLS algorithm is that it utilises information contained in the input data, extending back to the instant of time when the algorithm is initiated [100]. The resulting convergence speed is therefore typically much faster than the simple LMS algorithm.

Figure 6.14 compares the rate of convergence ($1/t$, where t is the number of training bits required for the MSE to decrease to 10% of the initial MSE value) of the RLS algorithm to that of the LMS algorithm for burst-1 at 1400ps/nm chromatic dispersion. The rate of convergence of the RLS algorithm is approximately a factor of 5 faster than the LMS algorithm, suggesting that tap adaptation can be achieved using just 100 training bits. This improvement in performance, however, is achieved at the expense of a large increase in computational complexity. In particular, it can be seen [96] that the LMS algorithm is characterised by a $O(M)$ computational complexity, whereas the RLS is computational intensive and requires $O(M^2)$. The notation $O(M)$ is used here to indicate that each iteration requires of the order of M floating point operations (additions and multiplications), where M is the filter order (number of taps). Note that the RLS algorithm remains beyond the scope of this thesis and is mentioned only to show that for applications where adaptation speed is critical, and complexity and cost are not limiting factors, there are algorithms that can perform significantly better than the standard LMS. The RLS is not further discussed and the reader can refer to [96, 100, 111, 113] for additional details and for a complete derivation of the algorithm.
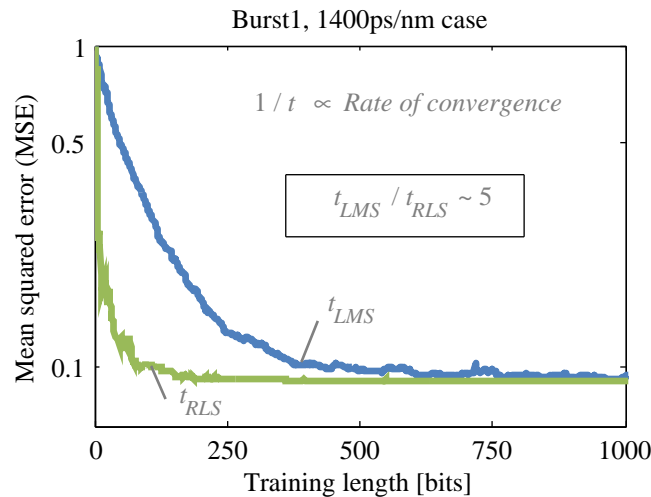
Figure 6.14: Burst-1 MSE as a function of the training length for a 9-tap FFE + 3-tap DFE adapted using different algorithms (LMS vs RLS).

6.3 10Gb/s BM-transmission using a LBMRx and BM-EDC

In the previous section it is demonstrated how BM-EDC can support optical links which carry packets with different amounts of impairments from burst to burst. This can occur in LR-PONs due to different chirp characteristics in the ONUs or due to sufficiently large differential reach[1] beyond the chromatic dispersion tolerance of the receiver. In the previous analysis attention was focused upon the performance of the BM-EDC itself as a function of the preamble length, transmission distance, etc., while assuming all bursts arrive at the BM-EDC with the same amplitude. However, in a real burst-mode link it is well known that successive bursts can exhibit large burst-to-burst amplitude variations. Typically, the hardware implementation of an EDC chip requires that the amplitude of the incoming signal remains constant with time and also that the pulse shapes are preserved, which in a continuous mode link is achieved using a linear variable gain amplifier [17]. In a burst-mode link, the LBMRx discussed in Section 6.1 is then required in order to linearly amplify the incoming packets such that they all have the same amplitude. Therefore, in this section, it is demonstrated how BM-EDC combined with an LBMRx can receive packets that have both large burst-to-burst amplitude differences while at the same time enabling burst-to-burst EDC tap adaptation. This demonstration is the first of its kind in the context of burst-mode access application, and the corresponding results were first reported in [107]. The experimental setup used in this analysis (Fig. 6.15) is a further extension of the one shown in Fig. 6.10. Only the major differences and additional features are highlighted and discussed below, while the reader can refer to Section 6.2.1 for the general description of the setup. Each DFB laser is operated at 1550nm and modulated at 10Gb/s with a $2^7 - 1$ PRBS non-return to zero pattern using EAMs whose biases are optimised for back-to-back transmission with an extinction ratio of 10dB for the soft packets (SP) and 7.5dB for the loud packets (LP). Even though the EAM bias voltage can be tuned to optimise the transmission performance this would need to be done on a device-by-device basis, which would impact the cost of the ONU. Hence, maintaining the same EAM bias voltage for all fabricated ONUs is the preferred option for cost sensitive access

---

[1]The differential reach is defined as the difference between the maximum and minimum fibre length of the ONUs to the central office.
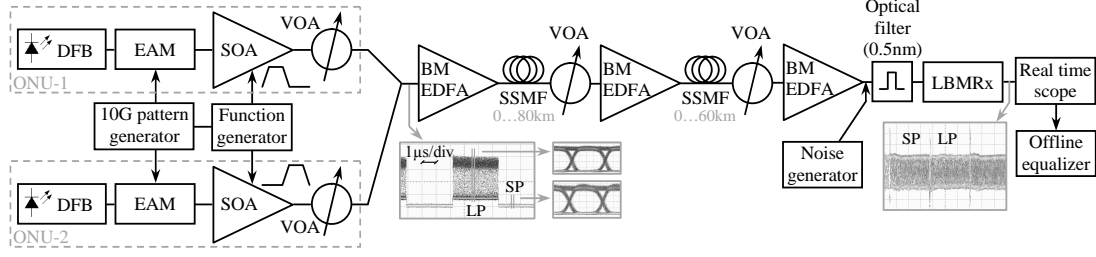
Figure 6.15: Experimental setup (ONU: optical network unit, DFB: distributed feedback laser, EAM: electroabsorption modulator, SOA: semiconductor optical amplifier, VOA: variable optical attenuator, BM-EDFA: burst-mode erbium doped fibre amplifier, SSMF: standard single mode fibre, LBMRx: linear burst-mode receiver, LP: loud packet, SP: soft packet).

applications. The optical power of each set of bursts is adjusted separately to the desired level using two VOAs in order to emulate ONUs with different path losses to the central office. The dynamic range (defined as loud/soft power ratio) is fixed to 15dB, exceeding the dynamic range for a 512-split TDM (time division multiplexed) PON that was previously reported in [10]. Each packet is separated by ∼25.6ns guard time and has a length of 32768 bits. The preamble consists of two parts: the first one is 150ns long and is needed for LBMRx settling as well as the settling of a transient due to the 560pF ac-coupling capacitors at the output of the LBMRx. The second part contains an L-bits long training sequence for adjusting the BM-EDC tap weights for each new burst: its length is discussed in the remainder of this section. Standard single mode fibre (SSMF) with a length of up to 140km is used to study the dispersion tolerance of the system. Three EDFAs (erbium doped fibre amplifiers, gain ∼20dB) are used to compensate for the fibre losses and ensure an input power to the LBMRx for the LP (SP) case of 0dBm (-15dBm). In contrast to the setup of Fig. 6.10, the EDFAs used here are commercially available gain transient suppressed devices, designed to prevent degradation of transmission quality for OADM (optical add/drop multiplexer) applications. The chromatic dispersion tolerance of the LBMRx + BMEDC under different OSNR conditions is evaluated by deliberately introducing amplified spontaneous emission (ASE) noise at the receiver using a noise generator (an EDFA). An optical filter with a 3dB width of 0.5nm is used to remove the out-of-band noise. The output of the LBMRx is sampled at 50GSamples/s using a real-time scope with an analog bandwidth of 12.5GHz. The LBMRx, which has a 3dB bandwidth of around 8GHz, acts also as an anti-aliasing filter. The

acquired data are processed using an offline equaliser implemented in Matlab®
of the FFE/DFE type illustrated in Fig. 4.14(b). The LMS adaptive algorithm
(with instantaneous gradient approximation) is used to set the tap weights at the
start of each burst.

BM-EDC enabled receiver (and BM-CDR):

The operation of the combined LBMRx and BM-EDC is summarised in Fig. 6.16.
After transmission through the fibre, the bursty signal with a loud/soft ratio of
15dB is detected by the LBMRx which performs a power-level equalisation be-
tween packets, as shown in the inset at the centre of Fig. 6.16, where the training
sequence of length L is also highlighted at the start of each burst. From the
eye diagrams it is clear that soft and loud packets present significantly different
characteristics indicating that they are affected by different levels of impairment.
Hence, the BM-EDC (here an 8-tap FFE + 2-tap DFE) potentially needs dif-
ferent values of tap weights for each incoming packet, which are decided on a
burst-by-burst basis during the training process at the beginning of each burst.

The insets on the right illustrate the evolution of the weights[1] along with the
final values at which they are frozen at the end of the respective training process.
From the frozen values it is possible to see that the optimum coefficients are
slightly different from SP to LP. Note also that both the cursors (the taps with
highest weights) are aligned to the same tap (the fifth), and this is due to the
fact that both packets were intentionally kept aligned in phase with respect to
the same clock in order to simplify the experiment. In principle, however, the
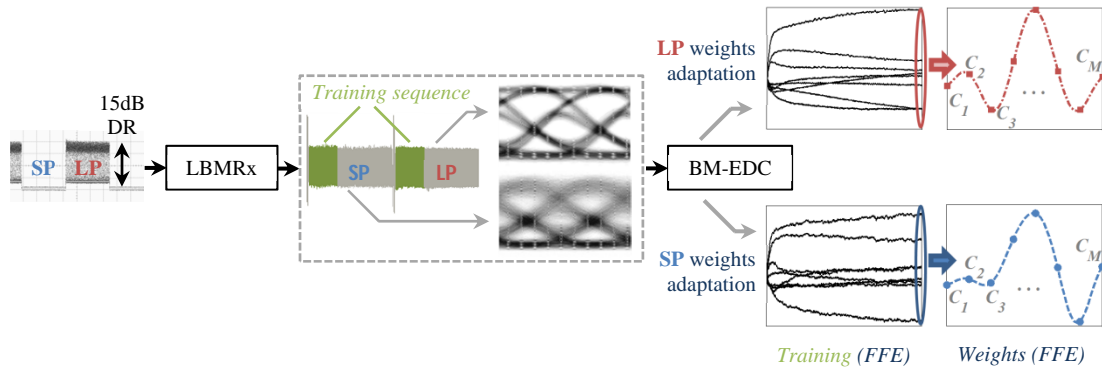
Figure 6.16: Principle of operation of the combined LBMRx and BM-EDC blocks.

---

[1]For simplicity only the FFE coefficients are shown.

164

two main cursors could lie anywhere within the feedforward section. In fact, as discussed in the previous section, the FFE effectively provides the function of the BM-CDR by adapting its delay burst-by-burst and thus shifting the incoming data such that it lines up with the OLT clock.
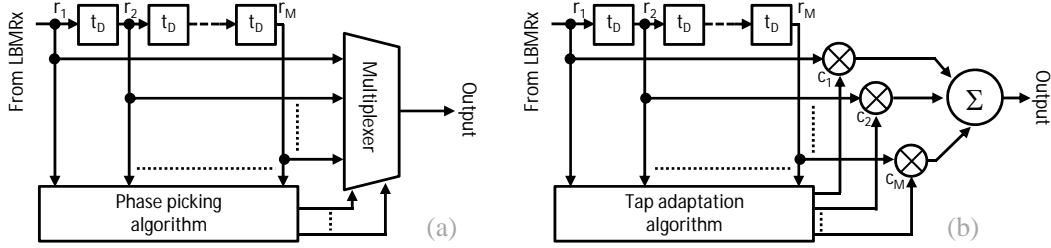
Figure 6.17: Oversampling BM-CDR (a) and feedforward equaliser (FFE)(b).

To emphasise this FFE property, Figs. 6.17(a) and 6.17(b) show an oversampling BM-CDR [139] and FFE respectively. In the BM-CDR, a delay line (unit delay t_D, a fraction of the bit period) is used to oversample the bits. The phase picking algorithm calculates which sample corresponds to the middle of the eye: this information is fed to the multiplexer which picks the corresponding sample as the output. Comparing the FFE with the BM-CDR, note that the BM-CDR is a special case of an FFE, whereby the tap coefficients c_1, c_2, ..., c_M are all zero, except for a single tap coefficient which is equal to 1 (corresponding to the optimum sampling phase). Conversely, the FFE is a generalisation of the BM-CDR, whereby the FFE output is a linear combination of samples (obtained by oversampling the incoming data, e.g. by a factor of 2 in a $T/2$ fractionally spaced FFE).

BM-EDC transmission performance:

The performance of the LBMRx + BM-EDC is studied by measuring the required OSNR of the SPs (whose signal power is kept at -15dBm) to achieve a BER of 1.1×10^{-3} for different fibre lengths, while the LPs are only used to stress the LBMRx. The taps, however, are adjusted for each burst. Figure 6.18 shows the OSNR penalty (relative to the required OSNR ($\sim$11.8dB) for the B2B case and using no EDC) and required OSNR with an 8-tap FFE and 2-tap DFE and without EDC. In the latter case the OSNR penalty increases rapidly up to almost 10dB at 110km because of poor tolerance to CD of the SP transmitter under the

aforesaid bias conditions. The performance is strongly improved when BM-EDC is used, with less than 2dB penalty compared to the B2B case without EDC measured at 110km. In this case the required OSNR is now nearly 8dB lower than with no EDC.
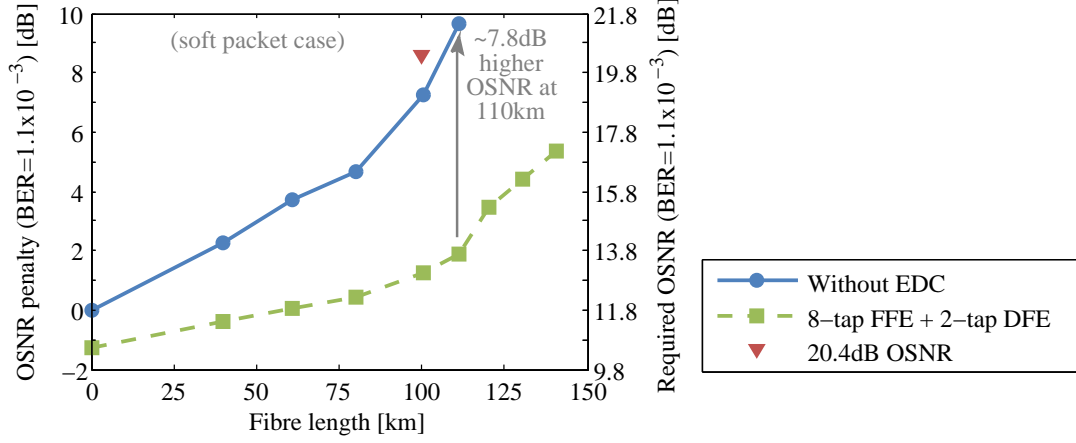
Figure 6.18: Soft packets OSNR penalty and required OSNR as a function of the fibre length without EDC (solid line) and with an 8-tap FFE + 2-tap DFE (dashed line).

Figure 6.18 also shows the worst-case achieved (measured) OSNR of 20.4dB at the input of the BMRx in the central office of a 512-split, 100km reach, 2×32 wavelength, hybrid DWDM-TDM PON (hybrid dense wavelength division multiplexed, time division multiplexed passive optical network) [10]. While only ~1.3dB system margin (defined as the achieved OSNR minus the required OSNR) is left when no EDC is used, over 7dB OSNR margin is achieved when using BM-EDC. This margin can be used to further increase the split, or absorb any additional system penalties due to e.g. transmitter ageing effects etc.

BM-EDC adaptation speed and optimum number of taps:

As done in the previous section, it is important to study the impact of the training sequence length on the BM-EDC performance. For the case above, the BM-EDC is trained for $L = 10000$bits to ensure that no extra penalty is incurred because of an insufficiently long training sequence. However, as the training sequence is part of the preamble, shorter training sequences are desired to improve traffic efficiency. In order to identify how many training bits the BM-EDC needs to adapt for each new incoming burst, the OSNR penalty is measured for different values of L ranging from 250bits up to 10000bits and also for a different number

of FFE/DFE taps in order to confirm the previous findings. The relative curves are shown in Fig. 6.19 and refer to a practical target reach of 100km. In Section 6.2.1 it is shown that short EDC lengths (e.g. 3-tap FFE + 1-tap DFE) are not sufficient, thus in this experiment the minimum EDC length considered is 5-tap FFE + 1-tap DFE. Slightly worse performance (∼0.5dB additional OSNR penalty compared to the other cases at 10000 training bits) can be observed for the 5-tap FFE + 1-tap DFE case, as well as slightly faster tap adaptation. Also, note how increasing the number of taps beyond 7 for the FFE and 1 for the DFE does not improve the transmission performance after sufficient training. Adding extra taps, however, does increase the BM-EDC circuit design complexity, therefore a 7- tap FFE + 1-tap DFE or 8-tap FFE + 2-tap DFE can be considered an optimum trade-off between transmission performance and hardware complexity.

This confirms, once again, the inferences and results presented previously in Chapter 4 and in Section 6.2. From Fig. 6.19, it is clear that the curves take about 2000 iterations in order to achieve a penalty within 0.5dB of the steady-state value, and no significant improvement in required OSNR is obtained after ∼2000 training bits, which is about four times greater than the adaptation time achieved in the analysis presented in Section 6.2.2. The reason for this modest adaptation speed increase could be due to the combination of different levels of impairments to compensate for, along with the fact that the LMS algorithm is now performed using the instantaneous gradient approximation rather than the true gradient. Recalling from Chapter 4 that the instantaneous approach
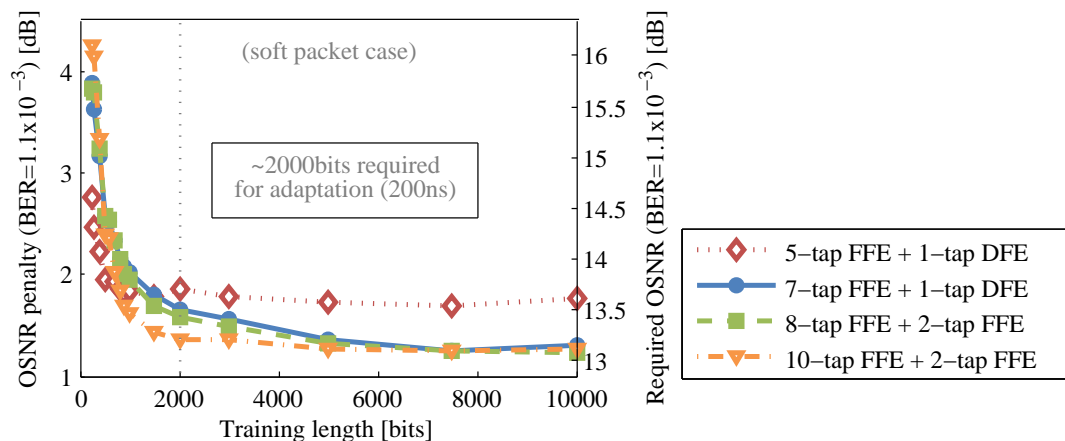
Figure 6.19: OSNR penalty and required OSNR as a function of the number of training bits for different EDC lengths and for a target transmission distance of 100km.

167

gives a crude approximation of the gradient of the MSE surface (which, how-
ever, points in the same direction as the true gradient on average), this means
that the consequent errors are only averaged over several iterations, and hence
a small loss in performance is expected [112]. Note, however, that this training
time value ($\sim$200ns) is still on the same order of the burst overhead in current
standards [118, 119] and thus only a small additional overhead would be required.

Gear shifted LMS adaptation:

As these training times might be too long for some applications, alternative tap
adaptation algorithms have also been explored. In the previous section it is
shown that, using the RLS algorithm, significantly faster tap adaptation can be
achieved. Unfortunately, due to its large number of floating point operations
(additions and multiplications), the RLS algorithm is very complex to implement
in hardware. A better alternative is the so-called gear shifted LMS algorithm
[96, 100]. In this algorithm, the step-size μ of the LMS update Equations (4.4.8)
and (4.4.9) is changed during adaptation. At the start of each burst, the step
size is set to a large value (ten times greater than the one used in all previous
analyses, where the scaling factor SF in Eqs. (4.4.10a) and (4.4.10b) is set to 1/5)
to ensure fast convergence. After a sufficient amount of training symbols (e.g.
$L/4$ or $L/2$, with L ranging from 150bits to 10000bits) it is reduced by a factor
of 10 to a sufficiently small value which ensures stability of the EDC algorithm
and low steady-state error ($SF = 1/50$ in Eqs. (4.4.10a) and (4.4.10b)). Figure
6.20 illustrates and compares the weights evolution (for simplicity only the FFE
coefficients are shown) for the standard LMS (fixed step-size) and for the gear
shifted LMS with gear shifting after $L/4$ and $L/2$. Figure 6.21 then demonstrates
how such gear shifting helps to greatly increase the tap adaptation speed (100km
case): for example, for a total of 500 training bits, gear shifting after both 250
($L/2$ case) and 125 ($L/4$ case) training bits achieves $\sim$1.5dB OSNR penalty, which
is about 1.1dB better than the standard LMS with no gear shifting. This dif-
ference is even more pronounced for shorter training sequences, e.g. at a total of
250 training bits, gear shifting after 62 ($L/4$ case) or 125 ($L/2$ case) training bits
achieves a 1.9dB or 2.3dB reduction in OSNR penalty compared to the standard
LMS (no gear shifting). In other words, if the tap adaptation were to stop after
these 250bits, a negligible 0.4dB additional OSNR penalty ($L/2$ case) would be
incurred compared to the ideal taps obtained after 10000 training bits (note that
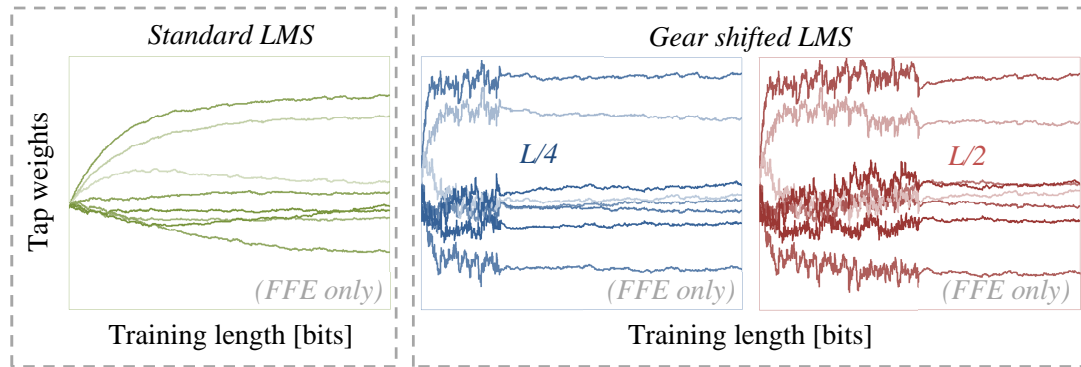
Figure 6.20: Weights evolution (FFE only) as a function of the iteration number for the standard LMS with fixed step-size, and for a gear shifted LMS with gear shifting at $L/4$ and $L/2$.

in reality the tap adaptation can be switched to a data decision directed mode, during which this small remaining penalty can be further reduced; however, this case is not taken into account here).

The analysis presented in this section summarises the principle of operation of a BM-EDC enabled receiver obtained by combining the already existent LBMRx described in Section 6.1 with a simulated 'offline' BM-EDC implemented in Matlab®. All the results and conclusions that arise from this preliminary study are being used in the design of an actual BM-EDC chip that is under development within our group at Tyndall. The device, along with a new associated (25Gb/s)
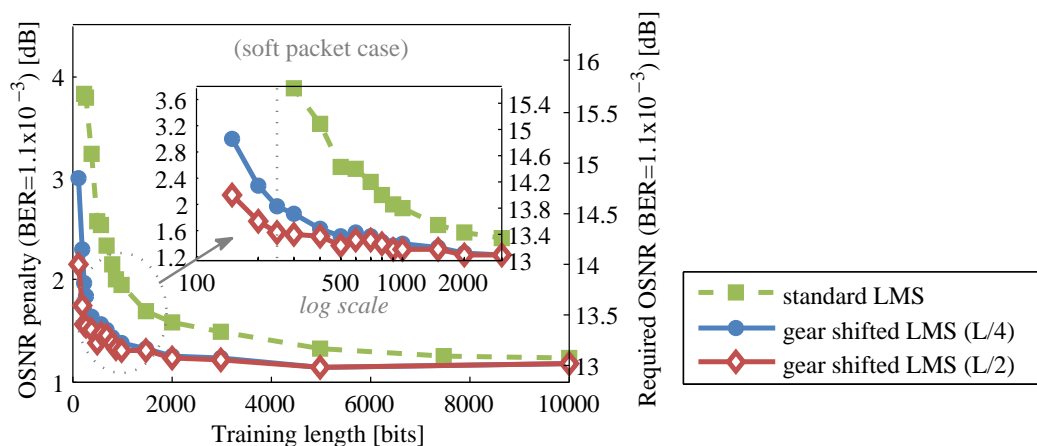
Figure 6.21: OSNR penalty and required OSNR as a function of the iteration number for the standard LMS with fixed step-size and for a gear shifted LMS with gear shifting at $L/4$ and $L/2$ at a target transmission distance of 100km.

169

LBMRx, are being developed using a 65nm CMOS and 0.13μm SiGe BiCMOS technology respectively.

6.4 Summary

In the first part of this chapter the operation of a novel 10Gb/s linear burst-mode receiver in a 0.25μm SiGe:C BiCMOS technology has been presented. The chip was designed, assembled, packaged, and characterised at the Tyndall National Institute. Measurement results confirm excellent performance such as stability of bandwidth across a large gain range and excellent linearity. Work is on-going towards a second version with significantly reduced power consumption and die area.

In the second part of the chapter, the requirements for use of EDC in optical burst-mode links with 0dB loud/soft ratio between packets (i.e. bursts that have the same average optical power) have been studied. For optimum system performance it is found that the EDC taps must be trained for each new burst even if these bursts have undergone the same amount of dispersion due to unavoidable (small) phase shifts between bursts. Such a burst-mode EDC also inherently performs the role of burst-mode data recovery. When the taps are adjusted using the gradient descent method it is found that adaptation can be achieved in a timeframe compatible with the packet structure in current PONs standards (less than 500 training bits).

Finally, for the first time to the extent of our knowledge, it is experimentally demonstrated how a linear burst-mode receiver and burst-mode electronic dispersion compensation can support transmission of 10Gb/s packets with a loud/soft ratio of 15dB over a reach of $>$100km with less than 2dB OSNR penalty compared to the B2B case. Using a gear shifted LMS algorithm, tap adaptation can be achieved with less than 250 training bits, opening the possibility of low overhead, adaptive EDC-enabled burst mode systems. This receiver is a promising technology for use in future long-reach, hybrid DWDM-TDMA PONs.

Chapter 7

Conclusions

PONs are currently one of the most attractive optical access network architectures. They are highly cost-effective solutions as the network infrastructure is shared by many customers and has no active components, such as electronic switches or routers, in the path between the central office and the customer premises. Even though conventional PONs offer significant bandwidth increases compared to copper-based approaches, they may not provide the best ultimate solution for whole network optimisation and cost reduction. As a result research attention has moved towards LR-PON architectures, which represent a more radical and future-proof network solution. The main idea behind LR-PONs is to simplify the current network structure, for example, by combining the access and metro networks into a single, integrated, all-optical system using optical amplification. Such systems target reaches greater than 100km, bit rates of at least 10Gb/s per wavelength in the downstream and upstream directions and large (>256) splitting factors.

As the low cost transmitter targeted for use in the ONUs of such LR-PONs might not have a chirp characteristic that is optimised for such reaches at 10Gb/s, dispersion compensation is required. A high-level comparison between potential optical and electrical compensation techniques used to mitigate dispersion has been briefly presented. Due to the low insertion loss, negligible physical volume, negligible additional power consumption, reduced CAPEX and inventory cost in comparison to optical-based solutions, EDCs based on direct detection represent the preferable solution for the access applications taken into account here. Among the different electronic equaliser options, an analog or mixed FFE/DFE implementation has been selected as optimum trade-off between performance and

171

implementation complexity (costs). In order to use such FFE/DFE based EDCs in LR-PON architectures, a number of challenges associated with the burst-mode nature of the upstream link need to be overcome. In particular, the EDC must be made adaptive from one burst to the next (BM-EDC) on time scales of the order of tens or hundreds of nanoseconds. The main objective of this thesis was to demonstrate the feasibility of such a concept and to prove that the aforesaid BM-EDC can be used to significantly improve the system performance. The major technical findings obtained during the course of the research are summarised below.

7.1 Overview of this Thesis Contribution

In order to achieve the aforesaid long-reaches, optical amplification must be employed at the local exchange as well as pre-amplification in the metro/core node. Even though EDFAs remain the preferred option for next generation access networks due to their excellent performance in DWDM applications, SOAs are certainly suitable for the 'pay as you grow' business model often adopted in current PONs deployments which target reaches of up to 60km. A novel solution for an SOA-based reach-extender based on an optimised SOA cascade has been presented and analysed experimentally in detail. Up to 12dB compression of a 19dB input dynamic-range is achieved without any dynamic control. A reduction in patterning induced penalties for soft packets can also be achieved by using the broadband ASE from the 1st stage SOA to clamp the gain of the 2nd stage SOA. For the loud packets, it is shown that significant reduction in patterning induced penalties can be achieved through careful optimisation of the bias current of the 2nd stage SOA. The reach-extender is shown to be able to support 70km reach for a 32-split 10Gb/s PON enabling the use of an ac-coupled, continuous mode receiver with a reduced 56ns ac-coupling constant (see List of Publications: [J3, C1]).

Focusing attention on the electronic equalisation aspect of this thesis, a detailed review of linear and quasi-linear equalisers to be used as CD compensators has been presented. For the first time to the best of our knowledge, the analysis was extended specifically to consider the optimisation of equalisers for applications in long reach PONs. A detailed numerical analysis has been carried out in order to derive the optimum EDC design parameters such as number of taps, tap

delay, step-size, and training length. For the applications of interest, a reasonable and practical trade-off between optimal performance and hardware complexity is given by combining an 8-tap fractionally spaced FFE (with a tap spacing of half the bit period) with a 2-tap symbol spaced DFE.

Such a FFE/DFE structure can also mitigate for other impairments, such as non-optimal transmitter and receiver bandwidths or patterning introduced by a saturated SOA, without losing its effectiveness in compensating CD for all practical cases of interest. A comprehensive investigation has been performed in order to determine the impact of different noise mechanisms, such as thermal noise and ASE beat noise, on the equaliser design, with focus on the optimisation of the DFE slicing-threshold. It has been shown that the optimum slicing-threshold for power-limited systems lies around 50%, whereas for OSNR-limited systems it can vary from 40% up to 50% depending on the target transmission distance. Nevertheless, fixing the threshold to about 45% can guarantee near optimum performance for both systems with only negligible penalties. This also avoids the use of an automatic threshold control algorithm, which is otherwise necessary in order to track the incoming signal profile and automatically adjust the threshold accordingly based on the signal distribution.

All the findings obtained through the aforesaid numerical analysis have been verified via transmission experiments and offline processing on an actual lab-based (emulated) burst mode link. First, the requirements for use of EDC in such a link with 0dB loud/soft ratio between packets (i.e. bursts that have the same average optical power) have been studied. For optimum system performance it is found that the EDC taps must be trained for each new burst even if these bursts have undergone the same amount of dispersion. This is due to (small) bit phase shifts between bursts that arise due to unavoidable propagation delay variations introduced by the fibre paths in the system and the limited precision of the PON time-sharing protocols. It has been shown that such a burst-mode EDC also inherently performs the role of burst-mode data recovery. When the taps are adjusted using the gradient descent method it is found that adaptation can be achieved in a timescale compatible with the packet structure in current PONs standards (less than 500 training bits) (see List of Publications: [C7, C9]). A similar analysis was then repeated when the loud/soft ratio between packets was set to 15dB. This was achieved by using a LBMRx with high linearity capable of providing a constant output amplitude swing across the entire input

dynamic range. This receiver was the first of its kind reported in literature (see List of Publications: [C2, J2]). The chip, which was designed in a 0.25μm SiGe:C BiCMOS technology, was assembled, packaged, and characterised at the Tyndall National Institute. For the first time to the extent of our knowledge, it was experimentally demonstrated how the combination of such a LBMRx with a BM-EDC (emulated using offline processing) can support transmission of 10Gb/s packets with high loud/soft ratios over a reach greater than 100km with less than 2dB OSNR penalty compared to the B2B case. Using a gear shifted LMS algorithm, tap adaptation can be achieved with less than 250 training bits, opening the possibility of low overhead, adaptive EDC-enabled burst mode systems (see List of Publications: [C8, J7]). This receiver is a promising technology for use in future long-reach, hybrid DWDM-TDMA PONs.

7.2 Future Work

The BM-EDC structure studied in this thesis was implemented offline using the numerical computing environment Matlab®. This was the first of a number of steps necessary to develop an actual BM-EDC chip. The results and inferences obtained through the simulations and the offline processing analyses presented in this thesis are currently being used for the ASIC design of such a BM-EDC chip. The device, along with a new associated (25Gb/s) LBMRx, are being developed in our group at Tyndall using a 65nm CMOS and 130nm SiGe BiCMOS technology respectively. The LBMRx chip will be then packaged according to the procedure illustrated in Section 6.1, whereas the BM-EDC chip will follow a more standard packaging approach, such as a QFN (quad-flat no-leads) package or a ball grid array (BGA) package. Finally, the packaging activity will be combined with and followed by a number of tests on each individual chip to verify their correct operation. If successfully realised, these devices will then be incorporated into the final LR-PON system demonstration under the FP7 DISCUS project, which will be built and tested by our group at Tyndall.

The analyses carried out in this thesis focused on 10Gb/s non-return-to-zero on-off-keying (NRZ-OOK) modulation. It is very likely that this modulation format will be employed for next generation optical access networks such as NG-PON1 and possibly even for some implementations of NG-PON2 (see Chapter 3). Note however that NRZ might not be the best candidate for more future

looking applications which require advanced modulation formats to increase the spectral efficiency and to improve the system performance in comparison to conventional OOK formats. This is even more true for very high (e.g. 40Gb/s) bit rates, where the signal quality is further deteriorated by the influence of dispersion (CD, PMD) and nonlinear optical effects. For this reason, optical phase shift keying methods are often applied. Among such methods, optical duobinary, or ODB, is gaining particular relevance for access applications as it combines large CD tolerance with moderate implementation complexity. Note also that if electronic equalisation techniques are used along with such advanced modulation format, the overall performance could be even further enhanced. However, it is well known that the FFE/DFE architectures presented in this thesis can only provide negligible improvement for ODB, which requires more advanced equalisation schemes based e.g. on nonlinear Volterra equalisers or MLSE equalisers. Similarly to the approach used in this work, an important aspect that could be investigated is to determine the requirements and hence the design parameters for such equalisers to be used in burst-mode access applications.

List of Abbreviations and Acronyms

ADC	analog-to-digital converter
ADSL	asymmetric digital subscriber line
APD	avalanche photodiode
ASE	amplified spontaneous emission
AWGN	additive white Gaussian noise
BER	bit error rate
BERT	bit error rate tester
BM	burst-mode
BM-CDR	burst-mode clock and data recovery
BM-EDC	burst-mode electronic dispersion compensation
BM-EDFA	burst-mode erbium doped fibre amplifier
BM-FEC	burst-mode forward error correction
BM-TIA	burst-mode transimpedance amplifier
BPF	band-pass filter
CAPEX	capital expenditure
CATV	cable television
CD	chromatic dispersion
CM	continuous-mode
CMOS	complimentary metal-oxide-semiconductor
CPW	coplanar waveguide
CW	continuous wave
DBA	dynamic bandwidth assignment
DCF	dispersion compensating fibre
DFB	distributed feedback
DFE	decision feedback equaliser
DGC	dispersion compensating grating
DISCUS	DIStributed Core for unlimited bandwidth supply for all Users and Services
DS	downstream

DSL	digital subscriber line
DSP	digital signal processing
DWA	dynamic wavelength assignment
DWDM	dense wavelength division multiplexing
EDC	electronic dispersion compensation
EDFA	erbium doped fibre amplifier
EPON	ethernet passive optical network
ER	extinction ratio
FEC	forward error correction
FFE	feedforward equaliser
FTTH	fibre to the home
FSAN	full service access network
FSE	fractionally spaced equaliser
FWM	four wave mixing
GPON	gigabit passive optical network
GVD	group velocity dispersion
HDTV	high definition television
HSPA	high speed packet access
IC	integrated circuit
IEEE	institute of electrical and electronics engineers
IR	infrared
ISI	intersymbol interference
LE	local exchange
LMS	least mean squares
LP	loud packet
LPF	low pass filter
LTE	long term evolution
MLSE	maximum likelihood sequence estimation
MZM	Mach-Zehnder modulator,
NEP	noise equivalent power
NGPON	next generation passive optical network
NLSE	nonlinear Schrödinger equation
NRZ	non return to zero
OADM	optical add/drop multiplexer
OEO	optical-electrical-optical
ODN	optical distribution network
OFDM	orthogonal frequency division multiplexing
OLT	optical line terminal
ONU	optical network unit
OSNR	optical signal-to-noise ratio
PCB	printed circuit board
PD	photodetector

PIC	photonic integrated circuit
PIN	positive-intrinsic-negative
PMD	polarisation mode dispersion
PDFA	praseodymium doped fibre amplifier
PDG	polarisation dependent gain
PON	passive optical network
PPG	pulse pattern generator
PRBS	pseudo random bit sequence
RE	reach extender
RF	radio frequency
RLS	recursive least squares
RMS	root mean square
SBS	stimulated Brillouin scattering
SMF	single mode fibre
SNR	signal-to-noise ratio
SOA	semiconductor optical amplifier
SP	soft packet
SPM	self phase modulation
SRS	stimulated Raman scattering
TDFA	thulium doped fibre amplifier
TDM	time division multiplexing
TDMA	time division multiple access
TOD	third order dispersion
TWDM	time and wavelength division multiplexing
US	upstream
UV	ultraviolet
VDSL	very high bit rate digital subscriber line
VOA	variable optical attenuator
WDM	wavelength division multiplexing
WiMAX	worldwide interoperability for microwave access
XPM	cross-phase modulation

List of Publications

<u>*Journal Publications:*</u>

[J1] A. Naughton, C. Antony, P. Ossieur, **S. Porto,** G. Talli, and P. D. Townsend, "Optimisation of SOA-REAMs for Hybrid DWDM-TDMA PON Applications," *Optics Express,* vol. 19, pp. B722-B727, 2011.

[J2] P. Ossieur, N. A. Quadir, **S. Porto,** M. Rensing, C. Antony, W. Han, P. O'Brien, Y. Chang, and P. D. Townsend, "A 10G linear burst-mode receiver supporting electronic dispersion compensation for extended-reach optical links," *Optics Express,*vol. 19, no. 26, pp. B604-B610, 2011.

[J3] **S. Porto,** C. Antony, P. Ossieur, and P. D. Townsend, "An upstream reach extender for 10Gb/s PON applications based on an optimized semiconductor amplifier cascade," *Optics Express,*vol. 20, no. 1, pp. 186-191, 2012.

[J4] P. Ossieur, N. A. Quadir, **S. Porto,** C. Antony, W. Han, M. Rensing, P. O'Brien, and P. D. Townsend, "A 10 Gb/s linear burst-mode receiver in 0.25 μm SiGe:C BiCMOS," *Solid-State Circuits, IEEE Journal of,* vol. 48, no. 2, pp. 381-390, 2013.

[J5] G. Talli, A. Naughton, **S. Porto,** C. Antony, P. Ossieur, and P. D. Townsend, "Advantageous Effects of Gain Saturation in Semiconductor Optical Amplifier-Based Integrated Reflective Modulators," *Lightwave Technology, Journal of,* vol. 32, pp. 392-401, 2014.

[J6] A. Naughton, G. Talli, **S. Porto,** C. Antony, P. Ossieur, and P. D. Townsend, "Design Optimization of R-EAM-SOA for Long-Reach Carrier-Distributed Passive Optical Networks," *Lightwave Technology, Journal of,* vol. PP, pp. 1-7, 2014.

[J7] **S. Porto,** C. Antony, A. Jain, D. Kelly, D. Carey, G. Talli, P. Ossieur, and P. D. Townsend, "Demonstration of 10 Gb/s Burst-Mode Transmission Using a Linear Burst-Mode Receiver and Burst-Mode Electronic Equalization [Invited]," *Journal of Optical Communications and Networking* vol. 7, pp. A118-A125, 2015.

Conference Publications:

[C1] **S. Porto,** C. Antony, P. Ossieur, and P. D. Townsend, "An upstream reach-extender for 10Gb/s PON applications based on an optimised semiconductor amplifier cascade," *in Optical Communication (ECOC), 2011, 37th European Conference and Exhibition on,* 2011, pp. 1-3.

[C2] P. Ossieur, N. A. Quadir, **S. Porto,** M. Rensing, C. Antony, W. Han, et al., "A 10G linear burst-mode receiver supporting electronic dispersion compensation for extended-reach optical links," *in Optical Communication (ECOC), 2011, 37th European Conference and Exhibition on,* 2011, pp. 1-3.

[C3] A. Naughton, C. Antony, P. Ossieur, **S. Porto,** G. Talli, and P. D. Townsend, "Optimisation of SOA-REAMs for hybrid DWDM-TDMA PON applications," *in Optical Communication (ECOC), 2011, 37th European Conference and Exhibition on,* 2011, pp. 1-3.

[C4] P. Ossieur, C. Antony, A. Naughton, **S. Porto,** N. A. Quadir, A. M. Clarke, et al., "Hybrid DWDM-TDMA PONs for next generation access," *in Optical Fiber Communication Conference and Exposition (OFC/NFOEC), 2012 and the National Fiber Optic Engineers Conference,* 2012, pp. 1-3.

[C5]   P. Ossieur, N. A. Quadir, **S. Porto,** M. Rensing, C. Antony, W. Han, et al., "A 10G linear burst-mode receiver," *IET Irish Signals and Systems Conference (ISSC), NUI Maynooth, Ireland,* June 2012.

[C6]   I. Cano, **S. Porto,** A. Naughton, P. Ossieur, P. D. Townsend, J. A. Lazaro, et al., "Upstream performance improvement of low cost 10Gb/s ONUs with centralized OLT equalizer and FEC," *in Transparent Optical Networks (ICTON), 2012 14th International Conference on,* 2012, pp. 1-3.

[C7]   **S. Porto,** C. Antony, G. Talli, P. Ossieur, and P. D. Townsend, "Requirements for adaptive electronic dispersion compensation in burst-mode systems," *in Optical Fiber Communication Conference and Exposition and the National Fiber Optic Engineers Conference (OFC/NFOEC), 2013,* 2013, pp. 1-3.

[C8]   **S. Porto,** C. Antony, G. Talli, D. Carey, P. Ossieur, and P. D. Townsend, "Demonstration of 10Gb/s burst-mode transmission using a linear burst-mode receiver and burst-mode electronic equalization," *in Optical Fiber Communication Conference,* San Francisco, California, 2014, p. M3I.5.

[C9]   P. Ossieur, **S. Porto,** C. Antony, A. Jain, D. Kelly, N. Quadir, et al., "Burst-mode Electronic Dispersion Compensation," *in Optical Fiber Communication Conference,* San Francisco, California, 2014, p. M3I.4.

Posters:

[P1]   **S. Porto,** C. Antony, P. Ossieur, and P. D. Townsend, "An upstream reach-extender for 10Gb/s PON applications based on an optimised semiconductor amplifier cascade," *Photonics Ireland, Dublin, Ireland,* 2011, pp. 1-3.

[P2]   **S. Porto,** C. Antony, G. Talli, P. Ossieur, and P. D. Townsend, "Requirements for adaptive electronic dispersion compensation in burst-mode systems," *Photonics Ireland, Belfast,* 2013, pp. 1-3.

List of Figures

187

List of Tables

References

[1] CorningIncorporated, "http://www.corning.com."

[2] OECD, "http://www.oecd.org/sti/broadband/oecdbroadbandportal.htm."

[3] FTTH-CouncilEurope-Deployment&OperationsCommittee, "Broadband Access Technologies," *White paper of the Deployment & Operations Committee of the FTTH Council Europe*, 25/02/2014.

[4] K. Tanaka, A. Agata, and Y. Horiuchi, "IEEE 802.3av 10G-EPON Standardization and Its Research and Development Status," *Lightwave Technology, Journal of*, vol. 28, no. 4, pp. 651–661, 2010.

[5] D. Payne and R. Davey, "Long reach access networks-avoiding the bandwidth-price dilemma," *in Proc. Broadband Europe*, Dec. 2004.

[6] D. B. Payne and R. P. Davey, "The future of fibre access systems?," *BT Technology Journal*, vol. 20, no. 4, October 2002.

[7] *IEEE Std 802.3ah*, 2004.

[8] ITU-T, "Gigabit-capable passive optical networks," *Recommendation ITU-T G.984.x.*

[9] P. Ossieur, C. Antony, A. M. Clarke, A. Naughton, H.-G. Krimmel, Y. Chang, C. Ford, A. Borghesani, D. G. Moodie, A. Poustie, R. Wyatt, B. Harmon, I. Lealman, G. Maxwell, D. Rogers, D. W. Smith, D. Nesset, R. P. Davey, and P. D. Townsend, "A 135-km 8192-Split Carrier Distributed DWDM-TDMA PON With 2 x 32 x 10 Gb/s Capacity," *Journal of Lightwave Technology*, vol. 29, no. 4, pp. 463–474, 2011.

References

[10] P. Ossieur, C. Antony, A. Naughton, A. M. Clarke, H. G. Krimmel, Y. Xin, Q. Xing-Zhi, C. Ford, A. Borghesani, D. Moodie, A. Poustie, R. Wyatt, B. Harmon, I. Lealman, G. Maxwell, D. Rogers, D. W. Smith, S. Smolorz, H. Rohde, D. Nesset, R. P. Davey, and P. D. Townsend, "Demonstration of a 32 x 512 Split, 100 km Reach, 2 x 32 x 10 Gb/s Hybrid DWDM-TDMA PON Using Tunable External Cavity Lasers in the ONUs," *Lightwave Technology, Journal of*, vol. 29, no. 24, pp. 3705–3718, 2011.

[11] G. Talli and P. D. Townsend, "Hybrid DWDM-TDM Long-Reach PON for Next-Generation Optical Access," *Journal of Lightwave Technology*, vol. 24, no. 7, p. 2827, 2006.

[12] L. Yuanqiu, Z. Xiaoping, F. Effenberger, Y. Xuejin, P. Guikai, Q. Yinbo, and M. Yiran, "Time- and Wavelength-Division Multiplexed Passive Optical Network (TWDM-PON) for Next-Generation PON Stage 2 (NG-PON2)," *Lightwave Technology, Journal of*, vol. 31, no. 4, pp. 587–593, 2013.

[13] T. Nielsen and S. Chandrasekhar, "OFC 2004 workshop on optical and electronic mitigation of impairments," *Lightwave Technology, Journal of*, vol. 23, no. 1, pp. 131–142, 2005.

[14] ITU-T, "Gigabit-capable passive optical networks (GPON): Long reach," *Recommendation ITU-T G.984.7*, July 2010.

[15] IEEE, "10Gb/s Ethernet Passive Optical Networks," *IEEE P802.3av*, Sept. 2009.

[16] ITU-T, "Ten gigabit-capable passive optical networks," *ITU-T G.987.x*, Jan. 2010.

[17] K. Azadet, E. F. Haratsch, H. Kim, F. Saibi, J. H. Saunders, M. Shaffer, S. Leilei, and Y. Meng-Lin, "Equalization and FEC techniques for optical transceivers," *Solid-State Circuits, IEEE Journal of*, vol. 37, no. 3, pp. 317–327, 2002.

[18] P. Ossieur, N. A. Quadir, S. Porto, C. Antony, W. Han, M. Rensing, P. O'Brien, and P. D. Townsend, "A 10 Gb/s Linear Burst-Mode Receiver in

0.25 um SiGe:C BiCMOS," *Solid-State Circuits, IEEE Journal of*, vol. 48, no. 2, pp. 381–390, 2013.

[19] G. Agrawal, *Nonlinear Fiber Optics.* Elsevier Science, 2001.

[20] G. P. Agrawal, *Fiber-optic communication systems.* Wiley series in microwave and optical engineering, New York: Wiley-Interscience, 3rd ed. ed., 2002.

[21] R. Thomson, C. Leburn, and D. Reid, *Ultrafast Nonlinear Optics.* Springer, 2013.

[22] ITU-T, "Optical system design and engineering considerations," *G-series Recommendations – Supplement 39*, 2006.

[23] M. Seimetz, *High-Order Modulation for Optical Fiber Transmission.* Springer, 2009.

[24] ITU-T, "Characteristics of a 50/125 μm multimode graded index optical fibre cable for the optical access network," *ITU-T Recommendation G.651.1*, July 2007.

[25] A. R. Chraplyvy, R. W. Tkach, L. L. Buhl, and R. C. Alferness, "Phase Modulation to Amplitude-Modulation Conversion of Cw Laser-Light in Optical Fibers," *Electronics Letters*, vol. 22, no. 8, pp. 409–411, 1986.

[26] J. Wang and K. Petermann, "Small signal analysis for dispersive optical fiber communication systems," *Lightwave Technology, Journal of*, vol. 10, no. 1, pp. 96–100, 1992.

[27] R. Hui and M. O'Sullivan, *Fiber Optic Measurement Techniques.* Elsevier.

[28] B. Jopson and A. Gnauck, "Dispersion compensation for optical fiber systems," *Communications Magazine, IEEE*, vol. 33, no. 6, pp. 96–102, 1995.

[29] P. J. Winzer and R. Essiambre, "Advanced Optical Modulation Formats," *Proceedings of the IEEE*, vol. 94, no. 5, pp. 952–985, 2006.

[30] F. Buchali and H. Bulow, "Adaptive PMD compensation by electrical and optical techniques," *Lightwave Technology, Journal of*, vol. 22, no. 4, pp. 1116–1126, 2004.

References

[31] F. F. Dai, "Electronic equalizations for optical fiber dispersion compensation," *Optical Engineering*, vol. 46, no. 3, pp. 035006–035006–12, 2007. 10.1117/1.2715955.

[32] J. D. Downie and A. B. Ruffin, "Analysis of signal distortion and crosstalk penalties induced by optical filters in optical networks," *Lightwave Technology, Journal of*, vol. 21, no. 9, pp. 1876–1886, 2003.

[33] H. Keang-Po and J. M. Kahn, "Methods for crosstalk measurement and reduction in dense WDM systems," *Lightwave Technology, Journal of*, vol. 14, no. 6, pp. 1127–1135, 1996.

[34] S. P. Singh, R. Gangwar, and N. Singh, "Nonlinear scattering effects in optical fibers," *Progress In Electromagnetics Research*, vol. Vol. 74, pp. 379–405, 2007.

[35] M. Connelly, *Semiconductor Optical Amplifiers*. Springer, 2002.

[36] J. Mark, M. L. Nielsen, and T. W. Berg, "The Dynamics of Semiconductor Optical Amplifiers: Modeling and Applications," *Optics and Photonics News*, vol. 14, no. 7, pp. 42–48, 2003.

[37] N. K. Dutta and Q. Wang, *Semiconductor optical amplifiers*. World Scientific Pub., 2006.

[38] A. Ghazisaeidi, F. Vacondio, A. Bononi, and L. A. Rusch, "Bit Patterning in SOAs: Statistical Characterization Through Multicanonical Monte Carlo Simulations," *Quantum Electronics, IEEE Journal of*, vol. 46, no. 4, pp. 570–578, 2010.

[39] P. Becker, A. Olsson, and J. Simpson, *Erbium-Doped Fiber Amplifiers: Fundamentals and Technology*. Elsevier Science, 1999.

[40] R.-J. Essiambre, P. J. Winzer, and D. F. Grosz, "Impact of DCF properties on system design," *Journal of Optical and Fiber Communications Reports*, vol. 3, no. 4, pp. 221–291, 2006.

[41] H. Nyquist, "Thermal Agitation of Electric Charge in Conductors," *Physical Review*, vol. 32, no. 1, pp. 110–113, 1928. PR.

[42] "Shot Noise, Lecture notes, University of California, http://123.physics.ucdavis.edu/shot_files/ShotNoise.pdf,"

[43] Newport, "http://search.newport.com/?x1=sku&q1=1544-b."

[44] I. Kaminow, T. Li, and A. Willner, *Optical Fiber Telecommunications VB: Systems and Networks.* Elsevier Science, 2010.

[45] P. J. Winzer, M. Pfennigbauer, M. M. Strasser, and W. R. Leeb, "Optimum filter bandwidths for optically preamplified NRZ receivers (vol 19, pg 1263, 2001)," *Journal of Lightwave Technology*, vol. 19, no. 11, pp. 1794–1794, 2001. Winzer, PJ Pfennigbauer, M Strasser, MM Leeb, WR.

[46] M. Ruffini, L. Wosinska, M. Achouche, C. Jiajia, N. Doran, F. Farjady, J. Montalvo, P. Ossieur, B. O'Sullivan, N. Parsons, T. Pfeiffer, Q. Xing-Zhi, C. Raack, H. Rohde, M. Schiano, P. Townsend, R. Wessaly, Y. Xin, and D. B. Payne, "DISCUS: an end-to-end solution for ubiquitous broadband optical access," *Communications Magazine, IEEE*, vol. 52, no. 2, pp. S24–S32, 2014.

[47] F. Effenberger, H. Mukai, J. i. Kani, and M. Rasztovits-Wiech, "Next-generation PON-part III: System specifications for XP-PON," *Communications Magazine, IEEE*, vol. 47, no. 11, pp. 58–64, 2009.

[48] F. J. Effenberger, H. Mukai, P. Soojin, and T. Pfeiffer, "Next-generation PON-part II: Candidate systems for next-generation PON," *Communications Magazine, IEEE*, vol. 47, no. 11, pp. 50–57, 2009.

[49] J. Kani, F. Bourgart, A. Cui, A. Rafel, M. Campbell, R. Davey, and S. Rodrigues, "Next-generation PON-part I: Technology roadmap and general requirements," *Communications Magazine, IEEE*, vol. 47, no. 11, pp. 43–49, 2009.

[50] CommScope, "GPON - EPON Comparison," *White Paper, CommScope Solutions Marketing*, October 2013.

[51] R. Davey, J. Kani, F. Bourgart, and K. McCammon, "Options for future optical access networks," *Communications Magazine, IEEE*, vol. 44, no. 10, pp. 50–56, 2006.

[52] R. P. Davey, D. B. Grossman, M. Rasztovits-Wiech, D. Payne, D. Nesset, A. E. Kelly, A. Rafel, S. Appathurai, and Y. Sheng-Hui, "Long-Reach Passive Optical Networks," *Lightwave Technology, Journal of*, vol. 27, no. 3, pp. 273–291, 2009.

[53] FTTH-CouncilEurope-Deployment&OperationsCommittee, "New ftth-based technologies and applications," *White paper of the Deployment & Operations Committee of the FTTH Council Europe*, 2014-02-03.

[54] R. P. Davey, D. B. Payne, D. Nesset, P. Tomlinson, T. Gilfedder, P. Chidgey, and A. Rafel, "Long-reach Access and Future Broadband Network economics," in *Optical Communication (ECOC), 2007 33rd European Conference and Ehxibition of*, pp. 1–4.

[55] ITU-T, "Gigabit-capable passive optical networks (GPON): Reach extension," *ITU-T Recommendation G.984.6*, 2008.

[56] S. Aozasa, H. Masuda, H. Ono, T. Sakamoto, T. Kanamori, Y. Ohishi, and M. Shimizu, "1480-1510 nm-band Tm doped fiber amplifier (TDFA) with a high power conversion efficiency of 42," in *Optical Fiber Communication Conference and Exhibit, 2001. OFC 2001*, vol. 4, pp. PD1–PD1.

[57] Y. Nishida, M. Yamada, T. Kanamori, K. Kobayashi, J. Temmyo, S. Sudo, and Y. Ohishi, "Development of an efficient praseodymium-doped fiber amplifier," *Quantum Electronics, IEEE Journal of*, vol. 34, no. 8, pp. 1332–1339, 1998.

[58] K.-I. Suzuki, Y. Fukada, D. Nesset, and R. Davey, "Amplified gigabit PON systems [Invited]," *Journal of Optical Networking*, vol. 6, no. 5, pp. 422–433, 2007.

[59] Huawei, "Next-Generation PON Evolution," 2010.

[60] F. J. Effenberger, "The XG-PON System: Cost Effective 10 Gb/s Access," *Lightwave Technology, Journal of*, vol. 29, no. 4, pp. 403–409, 2011.

[61] F. Effenberger, "XG-PON1 versus NG-PON2: Which one will win?," in *Optical Communications (ECOC), 2012 38th European Conference and Exhibition on*, pp. 1–3.

[62] F. E. Yuanqiu Luo, "TWDM-PON: The solution of choice for NG-PON2," *Huawei COMMUNICATE Magazine*, no. 68, JAN 2013.

[63] M. Ruffini, D. Payne, and L. Doyle, "Protection strategies for long-reach PON," in *Optical Communication (ECOC), 2010 36th European Conference and Exhibition on*, pp. 1–3.

[64] M. Schiano and F. J. Arribas, "Optical Transport Networks: Operator's requirements and ICT DISCUS concepts," *TI-transport-networks-trend-july-2013 (TELECOM ITALIA GROUP, Telefonica)*, July, 2013.

[65] M. Ruffini, D. Mehta, B. O'Sullivan, L. Quesada, L. Doyle, and D. Payne, "Deployment Strategies for Protected Long-Reach PON," *Optical Communications and Networking, IEEE/OSA Journal of*, vol. 4, no. 2, pp. 118–129, 2012.

[66] "The DISCUS Project,http://www.discus-fp7.eu."

[67] M. Ruffini, N. Doran, M. Achouche, N. Parsons, T. Pfeiffer, Y. Xin, H. Rohde, M. Schiano, P. Ossieur, B. O'Sullivan, R. Wessaly, L. Wosinska, J. Montalvo, and D. B. Payne, "DISCUS: End-to-end network design for ubiquitous high speed broadband services," in *Transparent Optical Networks (ICTON), 2013 15th International Conference on*, pp. 1–5.

[68] B. Baekelandt, C. Melange, J. Bauwelinck, P. Ossieur, T. De Ridder, Q. Xing-Zhi, and J. Vandewege, "OSNR Penalty Imposed by Linear In-Band Crosstalk Caused by Interburst Residual Power in Multipoint-To-Point Networks," *Photonics Technology Letters, IEEE*, vol. 20, no. 8, pp. 587–589, 2008.

[69] C. Antony, G. Talli, P. D. Townsend, J. Bauwelinck, D. W. Smith, and I. Lealman, "High extinction switching of SOAs for in-band crosstalk reduction in PON," *Electronics Letters*, vol. 44, no. 14, pp. 872–873, 2008.

[70] A. Kaszubowska-Anandarajah, R. Oberland, E. Bravi, A. Surpin, O. Aharoni, U. Ghera, R. Giller, E. Connolly, E. K. MacHale, M. Todd, G. Talli, and D. McDonald, "EDFA transient suppression in optical burst switching systems," in *Transparent Optical Networks (ICTON), 2012 14th International Conference on*, pp. 1–4.

[71] M. Fukutoku and M. Jinno, "Pump power reduction of optical feedback controlled EDFA using electrical feedforward control," in *Optical Amplifiers and Their Applications* (D. E. K. Baney and J. Wiesenfeld, eds.), vol. 25 of *OSA Trends in Optics and Photonics Series*, p. AA6, Optical Society of America.

[72] J. C. R. F. Oliveira, S. M. Rossi, R. F. Silva, J. B. Rosolem, and A. C. Bordonalli, "An EDFA hybrid gain control technique for extended input power and dynamic gain ranges with suppressed transients," in *Microwave and Optoelectronics Conference, 2007. IMOC 2007. SBMO/IEEE MTT-S International*, pp. 683–687.

[73] K. Inoue, "Waveform distortion in a gain-saturated semiconductor optical amplifier for NRZ and Manchester formats," *Optoelectronics, IEE Proceedings -*, vol. 144, no. 6, pp. 433–437, 1997.

[74] S. Huan, K. Byoung-Whi, and B. Mukherjee, "Long-reach optical access networks: A survey of research challenges, demonstrations, and bandwidth assignment mechanisms," *Communications Surveys & Tutorials, IEEE*, vol. 12, no. 1, pp. 112–123, 2010.

[75] Y. Qian, "On the Decision-Feedback Equalizer in Optically Amplified Direct-Detection Systems," *Lightwave Technology, Journal of*, vol. 25, no. 8, pp. 2090–2097, 2007.

[76] W. Rosenkranz and C. Xia, "Electrical equalization for advanced optical communication systems," *AEU - International Journal of Electronics and Communications*, vol. 61, no. 3, pp. 153–157, 2007.

[77] A. J. Weiss, "On the performance of electrical equalization in optical fiber transmission systems," *Photonics Technology Letters, IEEE*, vol. 15, no. 9, pp. 1225–1227, 2003.

[78] K. Grobe and M. Eiselt, *Wavelength Division Multiplexing: A Practical Engineering Guide*. Wiley, 2013.

[79] P. Ossieur, C. Melange, T. De Ridder, J. Bauwelinck, B. Baekelandt, Q. Xing-Zhi, and J. Vandewege, "Burst-Mode Electronic Equalization for

10-Gb/s Passive Optical Networks," *Photonics Technology Letters, IEEE*, vol. 20, no. 20, pp. 1706–1708, 2008.

[80] M. E. McCarthy, Z. Jian, A. D. Ellis, and P. Gunning, "Full-Field Electronic Dispersion Compensation of a 10 Gbit/s OOK Signal Over 4×124 km Field-Installed Single-Mode Fibre," *Lightwave Technology, Journal of*, vol. 27, no. 23, pp. 5327–5335, 2009.

[81] S. J. Savory, G. Gavioli, R. I. Killey, and P. Bayvel, "Electronic compensation of chromatic dispersion using a digital coherent receiver," *Optics Express*, vol. 15, no. 5, pp. 2120–2126, 2007.

[82] A. C. Singer, N. R. Shanbhag, and B. Hyeon-Min, "Electronic dispersion compensation," *Signal Processing Magazine, IEEE*, vol. 25, no. 6, pp. 110–130, 2008.

[83] J. H. Winters and R. D. Gitlin, "Electrical signal processing techniques in long-haul, fiber-optic systems," in *Communications, 1990. ICC '90, Including Supercomm Technical Sessions. SUPERCOMM/ICC '90. Conference Record., IEEE International Conference on*, pp. 397–403 vol.2.

[84] D. Nesset, D. Payne, R. Davey, and T. Gilfedder, "Demonstration of Enhanced Reach and Split of a GPON System Using Semiconductor Optical Amplifiers," in *Optical Communications, 2006. ECOC 2006. European Conference on*, pp. 1–2.

[85] S. V. Pato, R. Meleiro, D. Fonseca, P. Andre, P. Monteiro, and H. Silva, "All-Optical Burst-Mode Power Equalizer Based on Cascaded SOAs for 10-Gb/s EPONs," *Photonics Technology Letters, IEEE*, vol. 20, no. 24, pp. 2078–2080, 2008.

[86] B. Cao and J. E. Mitchell, "Modelling optical burst equalisation in next generation access network," in *Transparent Optical Networks (ICTON), 2010 12th International Conference on*, pp. 1–4.

[87] C. Antony, G. Talli, and P. D. Townsend, "SOA based upstream packet equalizer in 10Gb/s extended-reach PONs," in *Optical Fiber Communication - incudes post deadline papers, 2009. OFC 2009. Conference on*, pp. 1–3.

References

[88] R. J. Manning and D. A. O. Davies, "Three-wavelength device for all-optical signalprocessing," *Optics Letters*, vol. 19, no. 12, pp. 889–891, 1994.

[89] H. A. Haus, "The noise figure of optical amplifiers," *Photonics Technology Letters, IEEE*, vol. 10, no. 11, pp. 1602–1604, 1998.

[90] E. Rotem and D. Sadot, "Performance analysis of AC-coupled burst-mode receiver for fiber-optic burst switching networks," *Communications, IEEE Transactions on*, vol. 53, no. 5, pp. 899–904, 2005.

[91] MaximInc, "NRZ Bandwidth - LF Cutoff and Baseline Wander ," *APPLICATION NOTE 1738, HFAN-09.0.4*, Nov 2002.

[92] J. G. Proakis, *Digital communications*. Boston: McGraw-Hill, 5th ed. ed., 2008.

[93] R. Lopez-Valcarce, "Realizable linear and decision feedback equalizers: properties and connections," *Signal Processing, IEEE Transactions on*, vol. 52, no. 3, pp. 757–773, 2004.

[94] S. U. H. Qureshi, "Adaptive equalization," *Proceedings of the IEEE*, vol. 73, no. 9, pp. 1349–1387, 1985.

[95] U.-V. Koc, "Adaptive Electronic Dispersion Compensator for Chromatic and Polarization-Mode Dispersions in Optical Communication Systems," *EURASIP Journal on Advances in Signal Processing*, vol. 2005, no. 10, p. 164123, 2005.

[96] *The digital signal processing handbook*. Electrical engineering handbook series, Boca Raton, Fla.: CRC Press, 1998.

[97] A. F. Elrefaie, R. E. Wagner, D. A. Atlas, and D. G. Daut, "Chromatic dispersion limitations in coherent lightwave transmission systems," *Lightwave Technology, Journal of*, vol. 6, no. 5, pp. 704–709, 1988.

[98] W. P. Ng, W. Loedhammacakra, Z. Ghassemlooy, and R. A. Cryan, "Characterisation of a parallel optical all pass filter for chromatic dispersion equalisation in 10 Gb/s system," *Circuits, Devices & Systems, IET*, vol. 2, no. 1, pp. 112–118, 2008.

[99] X. Chunmin and W. Rosenkranz, "Nonlinear Electrical Equalization for Different Modulation Formats With Optical Filtering," *Lightwave Technology, Journal of*, vol. 25, no. 4, pp. 996–1001, 2007.

[100] S. S. Haykin, *Adaptive filter theory.* Prentice Hall information and system sciences series, Upper Saddle River, N.J.: Prentice-Hall, 3rd ed. ed., 1996.

[101] R. D. Gitlin and S. B. Weinstein, "Fractionally-Spaced Equalization: An Improved Digital Transversal Equalizer," *Bell System Technical Journal*, vol. 60, no. 2, pp. 275–296, 1981.

[102] J. M. Cioffi, *Equalization.* Chapter 3, Lecture notes, Stanford University, CA, http://www.stanford.edu/group/cioffi/book/chap3.pdf.

[103] I. P. Kaminow, T. Li, and A. E. Willner, *Optical Fiber Telecommunications V (A&B).* Academic Press, 2008.

[104] J. H. Winters, R. D. Gitlin, and S. Kasturia, "Reducing the effects of transmission impairments in digital fiber optic systems," *Communications Magazine, IEEE*, vol. 31, no. 6, pp. 68–76, 1993.

[105] J. G. Proakis, "Adaptive equalization for TDMA digital mobile radio," *Vehicular Technology, IEEE Transactions on*, vol. 40, no. 2, pp. 333–341, 1991.

[106] S. Porto, C. Antony, G. Talli, P. Ossieur, and P. D. Townsend, "Requirements for adaptive electronic dispersion compensation in burst-mode systems," in *Optical Fiber Communication Conference and Exposition and the National Fiber Optic Engineers Conference (OFC/NFOEC), 2013*, pp. 1–3, 2013.

[107] S. Porto, C. Antony, G. Talli, D. Carey, P. Ossieur, and P. Townsend, "Demonstration of 10Gb/s burst-mode transmission using a linear burst-mode receiver and burst-mode electronic equalization," in *Optical Fiber Communication Conference*, OSA Technical Digest (online), p. M3I.5, Optical Society of America, 2014.

[108] J. Johnson, R., P. Schniter, T. J. Endres, J. D. Behm, D. R. Brown, and R. A. Casas, "Blind equalization using the constant modulus criterion: a review," *Proceedings of the IEEE*, vol. 86, no. 10, pp. 1927–1950, 1998.

[109] T. Lang and D. Liu, "Blind predictive decision-feedback equalization via the constant modulus algorithm," in *Acoustics, Speech, and Signal Processing, 1997. ICASSP-97., 1997 IEEE International Conference on*, vol. 5, pp. 3901–3904 vol.5.

[110] J. Redd and C. Lyon, "Spectrum content of NRZ test patterns," *EDN magazine*, (MaximIntegratedCircuits) September 2, 2004.

[111] A. H. Sayed, *Adaptive filters.* Hoboken, N.J.: IEEE Press, 2008.

[112] J. Mathews and S. Douglas, *Adaptive Filters.* Prentice Hall PTR, 2001.

[113] P. Diniz, *Adaptive Filtering: Algorithms and Practical Implementation.* Springer, 2008.

[114] F. Hong and M. Mayeri, "On error surfaces of sufficient order adaptive IIR filters: proofs and counterexamples to a unimodality conjecture," *Acoustics, Speech and Signal Processing, IEEE Transactions on*, vol. 37, no. 9, pp. 1436–1442, 1989.

[115] D. Dasgupta and Z. Michalewicz, *Evolutionary Algorithms in Engineering Applications.* U.S. Government Printing Office, 1997.

[116] C. Hansen and S. Snyder, *Active Control of Noise and Vibration.* Taylor & Francis, 1996.

[117] B. W. Hoff and M.E., "Adaptive Switching Circuits," *IRE WESCON Convention Record, Part IV*, pp. pp. 96–104, August 1960.

[118] ITU-T, "10-Gigabit-capable passive optical networks (XG-PON): Physical media dependent (PMD) layer specification," *Recommendation ITU-T G.987.2*, 2010.

[119] IEEE, "Physical Layer Specifications and Management Parameters for 10 Gb/s Passive Optical Networks," *IEEE Std 802.3av-2009*, 2009.

[120] G. Kanter, A. Samal, O. Coskun, and A. Gandhi, "Electronic equalization for enabling communications at OC-192 rates using OC-48 components," *Optics Express*, vol. 11, no. 17, pp. 2019–2029, 2003.

[121] M. Kuznetsov, N. M. Froberg, S. R. Henion, and K. A. Rauschenbach, "Power penalty for optical signals due to dispersion slope in WDM filter cascades," *Photonics Technology Letters, IEEE*, vol. 11, no. 11, pp. 1411–1413, 1999.

[122] R. J. Nuyts, L. D. Tzeng, O. Mizuhara, and P. Gallion, "Effect of transmitter speed and receiver bandwidth on the eye margin performance of a 10-Gb/s optical fiber transmission system," *Photonics Technology Letters, IEEE*, vol. 9, no. 4, pp. 532–534, 1997.

[123] E. Sackinger, *Broadband circuits for optical fiber communication*. Hoboken, N.J.: Wiley, 2005.

[124] MindspeedTechnologies, "NRZ Bandwidth (-3db HF Cutoff vs SNR) How Much Bandwidth is Enough?," *White Paper*, 2003.

[125] O. E. Agazzi, M. R. Hueda, H. S. Carrer, and D. E. Crivelli, "Maximum-likelihood sequence estimation in dispersive optical channels," *Lightwave Technology, Journal of*, vol. 23, no. 2, pp. 749–763, 2005.

[126] D. Marcuse, "Calculation of bit-error probability for a lightwave system with optical amplifiers and post-detection Gaussian noise," *Lightwave Technology, Journal of*, vol. 9, no. 4, pp. 505–513, 1991.

[127] S. Porto, C. Antony, P. Ossieur, and P. D. Townsend, "An upstream reach-extender for 10Gb/s PON applications based on an optimized semiconductor amplifier cascade," *Optics Express*, vol. 20, no. 1, pp. 186–191, 2012.

[128] G. Talli, A. Naughton, S. Porto, C. Antony, P. Ossieur, and P. D. Townsend, "Advantageous Effects of Gain Saturation in Semiconductor Optical Amplifier-Based Integrated Reflective Modulators," *Lightwave Technology, Journal of*, vol. 32, no. 3, pp. 392–401, 2014.

[129] J. Baliga, R. Ayre, W. V. Sorin, K. Hinton, and R. S. Tucker, "Energy Consumption in Access Networks," in *Optical Fiber communication/National Fiber Optic Engineers Conference, 2008. OFC/NFOEC 2008. Conference on*, pp. 1–3.

[130] S. Nishihara, S. Kimura, T. Yoshida, M. Nakamura, J. Terada, K. Nishimura, K. Kishine, K. Kato, Y. Ohtomo, N. Yoshimoto, T. Imai, and M. Tsubokawa, "A Burst-Mode 3R Receiver for 10-Gbit/s PON Systems With High Sensitivity, Wide Dynamic Range, and Fast Response," *Lightwave Technology, Journal of*, vol. 26, no. 1, pp. 99–107, 2008.

[131] P. Ossieur, T. De Ridder, J. Bauwelinck, C. Melange, B. Baekelandt, Q. Xing-Zhi, J. Vandewege, G. Talli, C. Antony, P. Townsend, and C. Ford, "A 10 Gb/s burst-mode receiver with automatic reset generation and burst detection for extended reach PONs," in *Optical Fiber Communication - incudes post deadline papers, 2009. OFC 2009. Conference on*, pp. 1–3.

[132] Y. Xin, J. Put, J. Verbrugghe, J. Gillis, Q. Xing-Zhi, J. Bauwelinck, J. Vandewege, H. G. Krimmel, and M. Achouche, "A 10Gb/s burst-mode TIA with on-chip reset/lock CM signaling detection and limiting amplifier with a 75ns settling time," in *Solid-State Circuits Conference Digest of Technical Papers (ISSCC), 2012 IEEE International*, pp. 416–418.

[133] M. Nogawa, Y. Ohtomo, S. Kimura, K. Nishimura, T. Kawamura, and M. Togashi, "A 10Gb/s burst-mode adaptive gain select limiting amplifier in 0.13/spl mu/m CMOS," in *Solid-State Circuits Conference, 2006. ISSCC 2006. Digest of Technical Papers. IEEE International*, pp. 940–949.

[134] P. Ossieur, C. Antony, A. Naughton, S. Porto, N. A. Quadir, A. M. Clarke, and P. D. Townsend, "Hybrid DWDM-TDMA PONs for next generation access," in *Optical Fiber Communication Conference and Exposition (OFC/NFOEC), 2012 and the National Fiber Optic Engineers Conference*, pp. 1–3.

[135] P. Ossieur, N. A. Quadir, S. Porto, M. Rensing, C. Antony, W. Han, P. O'Brien, Y. Chang, and P. D. Townsend, "A 10G linear burst-mode receiver supporting electronic dispersion compensation for extended-reach optical links," *Optics Express*, vol. 19, no. 26, pp. B604–B610, 2011.

[136] P. Ossieur, N. A. Quadir, S. Porto, M. Rensing, C. Antony, W. Han, P. O'Brien, Y. Chang, and P. D. Townsend, "A 10G linear burst-mode receiver supporting electronic dispersion compensation for extended-reach

optical links," in *Optical Communication (ECOC), 2011 37th European Conference and Exhibition on*, pp. 1–3.

[137] C. Knochenhauer, B. Sedighi, and F. Ellinger, "40 Gbit/s transimpedance amplifier with high linearity range in 0.13 μm SiGe BiCMOS," *Electronics Letters*, vol. 47, no. 10, pp. 605–606, 2011.

[138] OIF, "Implementation Agreement for Integrated Dual Polarization Intradyne Coherent Receivers," *Optical Internetworking Forum*, vol. IA OIF-DPC-RX-01.0, Apr. 2010.

[139] C. Melange, B. Baekelandt, J. Bauwelinck, P. Ossieur, T. De Ridder, X.-Z. Qiu, and J. Vandewege, "Burst-Mode CDR Performance in Long-Reach High-Split Passive Optical Networks," *Journal of Lightwave Technology*, vol. 27, no. 17, pp. 3837–3844, 2009. Times Cited: 0.